EXPERIMENTAL VALIDATION OF TURBOMACHINERY BLADE VIBRATION PREDICTIONS

A thesis submitted to the University of London
for the degree of Doctor of Philosophy

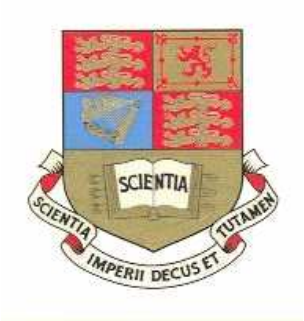

By
İbrahim Ata SEVER

Department of Mechanical Engineering
Imperial College London

March, 2004

To my dear mother
Şerife SEVER

Abstract

Bladed disk vibration amplitudes are known to be seriously amplified and varied from blade to blade due to the scatter in the blade geometry or due to variations in material properties. The phenomenon of having non-identical blades due to these variations is called *mistuning*. Since mistuning can lead to forced response amplitudes which are much larger than those predicted for a tuned assembly, additional dissipation elements (e.g., friction dampers) are sometimes integrated into the bladed disk assembly.

The problem of controlling and predicting the vibration amplitudes of bladed disks has been a primary concern of many research studies. As a result several numerical models have been developed to represent the bladed disk assemblies to facilitate prediction of the relevant behaviour. Since so much depends on the reliability of these components, however, manufacturers are disinclined to use these models, however complicated, in their designs unless or until they are proved to be accurate representations of the real behaviour. In other words, the model proposed must demonstrably be capable of predicting the response of the real bladed disk within the tolerances set by the manufacturer. The process of achieving this situation is called "validation". Since it is an expensive and difficult process, generally it has been largely ignored and a combination of over conservative designs and "fire fighting" procedures in service has been the practice.

This study aims to validate the numerical models developed for blade vibration response predictions at Imperial College via a carefully designed and well-controlled test rig. Using such an experimental facility, it is made sure that the experiments are carried out in the presence of physical phenomena accounted for in predictions and none other. Two integral bladed disks (blisks), one for mistuning and one for damping investigations, are designed and used in a specially designed test rig. Non-contacting measurement (LDV) and excitation (magnetic) techniques are employed so as not to modify the dynamics of the blisks. A method of measuring blade vibration under rotation, regardless of rotational speed is presented. A comprehensive test design is carried out prior to real tests using updated blisk models to maximise the efficiency of the measurements. Through an extensive test campaign, the ability of numerical models to predict forced response of the blisks for several mistuning patterns and when fitted with friction dampers, is demonstrated in a systematic series of tests. The sensitivity of the forced response to various ways of blisk tuning and variations in forcing filed are also studied in this project.

Acknowledgements

I would like to express my gratitude to my supervisor, Professor David J. Ewins, for giving me the opportunity to study at Imperial College. I acknowledge his advice and direction, as well as his patience and great efforts to explain things clearly and simply. Also, the valued input of Mr. D. Robb is highly appreciated.

I am particularly grateful to Mr A. B. Stanbridge for his guidance and teaching in experimental dynamics. John, Sooty and Margaret are remembered for their invaluable support, all in their own ways. I am indebted to many of my colleagues at Dynamics Section, particularly to Dr. E. Petrov and Dr. C. Gan, for at times heated but always fruitful discussions. Dr. Drew Feiner of Carnegie Melon University is thanked for kindly providing their mistuning identification software. Also, I thank my past and present colleagues, Goetz, Anatawit, Enrique, Suresh, Philip and many more who shared their knowledge so willingly at times when it was needed most.

This research was funded by the European Union within the project "Aeromechanical Design of Turbine Blades II" (ADTurB II), contract number G4RD-CT2000-00189. I thank all the project partners for their support and useful exchanges at various stages.

Special thanks are due to all members of my family. Their support and appreciation have been tremendous throughout my life. I hope this study somehow acknowledges their effort and determination in confronting all the hardship they faced while bring me to this level.

Finally, I would like to thank my beloved wife, Meltem, for all we shared in the past ten years, and the future we have created for much to be shared. She sacrificed a lot to keep me on track in completing this study. Without her understanding and encouragement my PhD attempt would have been a short-lived adventure.

Nomenclature

x, y, z	Translational degrees of freedom/coordinates
t	Time
ω	Frequency of vibration, in rad/s
ω_n	Natural frequency of the nth mode
N	Number of nodal diameters
n	Number of modes
k	Order of shaft speed
E	Young's Modules of materials
ρ	Mass density of materials
ζ	Critical damping ratio
η	Structural damping
$[\ ]$	Two dimensional matrix
$\{\ \}$	Column vector
$[M]$	Mass matrix
$[K]$	Stiffness matrix
$\lceil \cdot \lambda \cdot \rceil$	Eigenvalue matrix
$[\phi]$	Mode shape/eigenvector matrix
θ	Circumferential position
Ω	Rotational speed
V	Vibration velocity

Abbreviations

C-R	Cottage roof
DAQ	Data Acquisition
DOF(s)	Degree(s)-of-freedom
EO	Engine order
exp.	Experimental
FE	Finite element
FFT	Fast Fourier Transform
FRF	Frequency response function
LDV	Laser Doppler Velocimeter
HCF	High Cycle Fatigue
SLDV	Scanning LDV
CSLDV	Continuous SLDV
MAC	Modal assurance criterion
*n*ND	Nodal diametral mode of the *nth* family order
ODS	Operating deflection shape
SBM	Single blade mistuning
$S8\theta$	$Sin(8\cdot\theta)$

Contents

List of figures

List of tables

CHAPTER 1

INTRODUCTION

1.1 Overview

There are a few components, such as turbomachinery bladed disks, that have drawn a great deal of attention from researchers in the field of structural dynamics for more than half a century. Given their extensive use and the crucial role they play in applications, such as aeroplane jet engines, this is only understandable. Figure 1.1 shows pictures of a jet engine cross-section and some bladed disks used in real applications.

Figure 1.1 (a) Cross-section of Pratt & Whitney JT9D-7J engine powering Boeing 747, (b) Typical bladed disks (from www.mtu.de)

Bladed disk vibration amplitudes are known to be seriously amplified and varied from blade to blade due to scatter in blade geometry or due to variations in material properties. The phenomenon of having non-identical blades due to these kinds of variation is called *mistuning* and the distribution of the variation across the bladed disk is called a *mistuning pattern*. This pattern is generally

random and unknown to the manufacturer or user. Since mistuning can lead to forced response amplitudes which are much grater than those predicted for a tuned assembly (i.e. one having identical blades), additional dissipation elements (i.e. dampers) are sometimes integrated into the bladed disk assemblies in order to control the vibration amplitudes. Often so-called *friction dampers* are used for this purpose. As the name implies, energy is dissipated via rubbing of the damper and blade surfaces against each other.

1.2. Definition of problem

Due to the crucial role they play during the operation of gas turbine engines, blades and bladed disks require special attention and very careful design. As so much is dependent on the reliability of these components, manufacturers are always keen to be on the safe side of their products' limitations. This, however, generally leads to an over-designed and therefore inefficient product.

In order to optimise the design of bladed disks, many research studies have addressed the problems associated with the vibration behaviour of these components. The engine manufacturer's main concern is to control the resonant response levels of the blades, and therefore the peak resonant stresses in the engine blading. This is one of the major problems in the design of bladed disks since the vibration response of gas turbine blades that occur in practice is very sensitive to mistuning. When the inherent dissipation mechanisms are not sufficient (i.e. when the damping present is low), blade vibration amplitudes can reach higher than the acceptable levels. To avoid the risk of catastrophic failure due to such large amplitude vibrations, inter-blade friction dampers are often incorporated into the bladed disks. However, before implementing such friction dampers, the damping level needed to control the vibration should be predicted and the dampers should be designed accordingly. Therefore, the primary concern for many studies has been to seek an understanding of (i) what the least and the most severe consequences of mistuning are, and (ii) how they can be

controlled. These concerns have been the subject of several studies carried out at Imperial College and elsewhere in the past. As a result, several Finite Element (FE) model-based computer codes have been developed. With the aid of these codes, it is now possible to predict the response of a bladed disk for any mistuning pattern with integrated friction dampers. It is also possible to determine the worst mistuning pattern which leads to extreme blade vibration amplitudes. Nevertheless, developing codes – no matter how complicated - does not necessarily guarantee their accuracy and predictability. Since these codes are not yet validated against real structures and the realistic conditions they simulate, manufacturers are reluctant to incorporate them in their production chain.

In order to make these codes effective in the design and production of bladed disks, an extensive validation study is essential. This study must aim to identify possible sources of mismatch between the real and simulated data and to guide the codes in any necessary corrections to produce acceptable and reliable estimates.

In general, discrepancies between computer model predictions and actual system responses are due either, to inaccurate modelling of some aspects of the dynamics of the system, or to not modelling them at all. When there is a disagreement between the experimental results and numerical simulations, generally the numerical models are believed to be inefficient or not capable of handling the problem. However, this may not be the case all the time. Given the advanced state of the FE modelling, it can be said that mass and stiffness distributions of the components being analysed can be estimated fairly accurately. However the mistuning distribution and the incorporated damping model are, in general, much less certain and are often responsible for the poor predictions that are often obtained. For example, depending on whether the mistuning is due to the dimensional variations or variations in the material properties, the numerical model will be different and so will the predicted

behaviour. Similarly, assumptions inevitably involved in the damping model used may well describe a damping mechanism which is different from the one which exists in the real structure.

The ultimate way of making sure that these phenomena are modelled correctly is to check the numerical predictions against experimental measurements. However, validating a model which is used to predict the mistuned vibration response of a bladed disk on a real gas turbine engine would be extremely difficult. This is because in the engine there are several other components apart from the bladed disk itself, which affect the vibration response of the blades and yet remain unconsidered in the model. Even the bladed disk assembly alone may be so complicated (i.e. due to joints, etc.) that it cannot be handled properly by the model. Moreover, in most cases there will not be enough room to incorporate a measurement system to acquire the necessary data in a real engine measurement. As the numerical model is only as accurate as the input data, these measurements should be made on a carefully-constructed experimental setup, which exhibit only the phenomena under investigation.

Once the numerical models are demonstrated to be accurate representations of the experimental test cases, and the assumptions involved in the modelling are justified, they can be confidently used to predict the vibration responses of real bladed disks and to optimise their design.

1.3. Objectives of the study

The main objectives of the presented work are to design and conduct tests to validate

- the tuned and mistuned vibration response predictions of integral turbomachinery bladed disks (blisks) and to do so with the application of various mistuning patterns both statically and under rotation, and

- the undamped and friction damper damped blade vibration forced response predictions under rotation.

Additional goals in fulfilment of abovementioned objectives are:

- To devise and commission a vibration measurement technique which comprises non-contacting measurement (based on the LDV) and excitation (magnetic) techniques, and functions under rotation and independent of rotational speed
- To build a well-controlled rig and carefully-designed test pieces which only exhibit the phenomena considered in the predictions
- To study bladed disk tuning through individual blade frequencies and the translation of frequency mistuning into physical mistuning
- To study the effects of variations in Engine Order (EO) force amplitudes, applied on individual blades, on vibration response.

1.4 Overview of the thesis

This thesis presents experimental work comprising systematic and well-planned tests in an attempt to validate the predictions of mistuned (i.e. linear) and friction damped (i.e. non-linear) forced response predictions of turbomachinery bladed disks. The presentation of the work is structured in the following way:

Chapter 2, starting with the introduction of basic definitions and terminology related to bladed disks, summarises the relevant literature on validation of vibration response predictions, and mistuned and damped bladed disk studies. The focus is on experimental studies. Nonetheless, the main areas of research on mistuned and/or damped bladed disks are also outlined. Finally, a review of the use of Laser Doppler Velocimeter (LDV) transducers on rotating bladed disks is presented.

Chapter 3 concentrates on the design and instrumentation aspects of test pieces and the rig used in measurements. The objectives of the intended rig, and the

desired and achieved characteristics of the test pieces are presented. Details of the excitation and measurement techniques are given and the hardware and software employed in measurements are introduced. The processing of LDV vibration output to obtain frequency forced response and Operating Deflection Shapes (ODSs) is presented. Advantages and limitations of LDV transducers are also discussed in this chapter

Chapter 4 presents the attempts made at maximising the efficiency of the measurements through careful test planning based on properly updated test piece FE models. The actual characteristics of the blisks are identified and improvement to their symmetry (i.e. tuning) is sought when necessary. The sensitivity of the blisk dynamic properties to various ways of tuning is investigated through a discrete bladed disk model. The blisk models are updated, based on the measured characteristics using the employed updating methods. Using these updated models, a comprehensive test plan is designed.

Validation of undamped tuned and mistuned bladed disk forced response predictions, both at rest and rotating, are given in Chapter 5. The prediction tool used in computations is presented. The results obtained from rotating tuned, and sinusoidally and randomly mistuned blisk are presented. Obtained predictions are correlated to these results and the degree of success and the sources of possible deviations are discussed.

Chapter 6 is devoted to the assessment of friction damped bladed disk forced response measurements and predictions. However, first the undamped blisk response is considered to assess the degree of correlation in the absence of non-linearity. The non-linear forced response prediction tool is introduced. The effects of different ways of modelling frequency mistuning in terms of physical mistuning on forced response are analysed. Also in this chapter, the consequences of EO excitation errors are discussed and the effects are shown in the Blisk-1 FE model.

The overall conclusions are summarised in Chapter 7. The degree of success in achieving the task undertaken is discussed and some recommendations in the furthering of the work performed here are presented.

CHAPTER 2

The TERMINOLOGY of BLADED DISK VIBRATION PHENOMENA and LITERATURE SURVEY

2.1 Overview

In this chapter the relevant literature on mistuned and damped bladed disk vibration studies will be reviewed. The chapter will be divided into three parts. In the first part basic definitions and terminology related to bladed disk vibration phenomena will be given. Then, in the second part, relevant studies carried out on bladed disk vibration will be presented. The focus will be on the experimental studies although the main areas of research on mistuned and/or damped bladed disks will also be outlined. Finally in the last part, a review of the use of Laser Doppler Velocimeter (LDV) transducers on rotating components, such as bladed disks, will be presented.

2.2 Basic definitions and terminology

Over the years, bladed disks, especially those used in aircraft jet engines have been the subject matter of a wide range of studies. Given the environment they work in, and the role they play on the safety of aircraft, this is only understandable. As a result a highly specific terminology regarding these structures is generated. A thorough explanation of mentioned terminology can be found in several references such as [1]. However, a brief summary of certain terms and definitions is thought useful before the literature on the subject is reviewed. The mentioned reference is made use of in preparation of following.

A bladed disk - as the name implies - consists of a disk with a number of blades arranged around its circumference. When the blades are an integral part of a bladed disk, it is generally referred to as a *blisk*. Bladed disks are mostly cyclically-periodic structures (those having non-identical blades or some of their blades grouped are clearly not cyclically-periodic) where a pattern repeats itself 360° about an axis. Each of these repeating patterns are called a *cyclic-symmetric sector* - see Figure 2.1 (a). By exploiting this repetitive symmetric nature, dynamic characteristics of an entire bladed disk can be obtained using a single sector thus enabling more detailed modelling and/or shorter computational times.

Depending on the application, blades can be assembled in various ways around the disk. Figure 2.1 shows some configurations with and without shrouds. Here shrouds are introduced to increase blade stiffness and also provide so called *inter-blade coupling*. For blisks without shrouds, blades are still coupled through disk and the degree of which is determined by the flexibility of the disk.

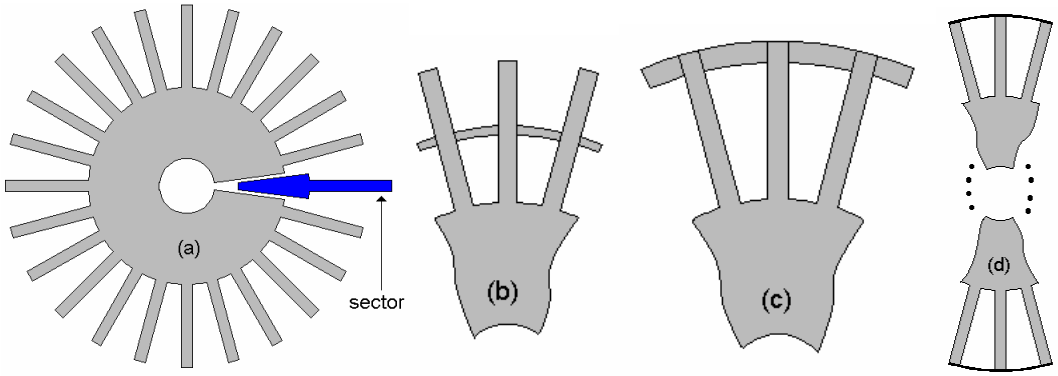

Figure 2.1 (a) an un-shrouded bladed disk and a cyclic symmetric sector, bladed disks with (b) mid-blade shroud, (c) tip-shroud, and (d) grouped blades.

Cyclically symmetric assemblies exhibit well-defined vibration modes. These modes occur either as double modes (two modes having identical frequencies and similar mode shapes) or single modes and can be defined as sinusoidal variations of circumferential displacements around the bladed disk. A double mode is defined by $Sin(n\theta)$ and $Cos(n\theta)$ variations of the circumferential displacement where sinusoidal order n is the number of lines of zero

displacement across the assembly or, as is generally know, the number of *nodal diameters* and θ is the angular separation of two adjacent blades. Note that in case of bladed disks, patterns formed by zero displacements are slightly more complicated than simple lines due to finite number of blades – see Figure 2.2 (b). For a bladed disk with N blades, the number of nodal lines is limited to $N/2$ if N is even and $(N-1)/2$ if N is odd. However, for a continuous disk when its circumferential motion is not described only by some discreet points, nodal diameters higher than $N/2$ are possible. Here the modes with $n=0$ and $n=N/2$ (only when N is even) are single modes in which all the blades experience the same amplitude, in phase when $n=0$ and out-of-phase with neighbouring blades when $n=N/2$. All the other modes occur in pairs. For a given natural frequency, ω_n, for which a double mode exists, the overall mode shape or rather *Operating Deflection Shape* (ODS) is a combination of both of the modes and is in the form of $Cos(n\theta+\varphi)$, where φ is a phase angle. The implication of this is that, a natural frequency can be associated with a particular nodal diameter, n, regardless of radial section's displacement shape. However, for a perfectly tuned bladed disk the angular orientation of these nodal diameter lines is not fixed and they can be anywhere on the structure. Figure 2.2 (a) shows the first 72 natural frequencies of a bladed disk with 24 blades plotted against the nodal diameter numbers with which they are associated.

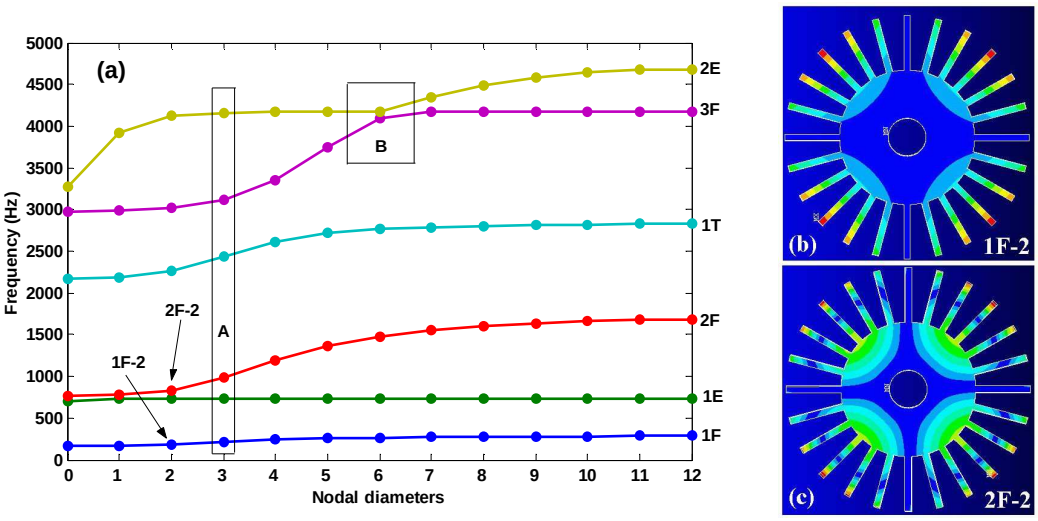

Figure 2.2 (a) Natural frequencies of a 24-bladed bladed disk, and mode shapes for modes (b) 1F-2 and (c) 2F-2.

It is seen from Figure 2.2 (a) that the natural frequencies are grouped into several distinct *families.* As the number of nodal diameters, n, increases the natural frequencies in each family asymptotically approach one of the clamped, blade-alone frequencies (i.e., the natural frequencies of a blade when it is grounded at the boundary where it joins the disk). These families of modes are generally described by the mode shape of the blade mode they converge to. Some of these blade-alone mode shapes are shown in Figure 2.3 for a simple blade model. Note that these mode shapes are usually more complicated (generally a combination of given basic shapes) for real blades with complex geometries and a classification of this kind may not strictly apply.

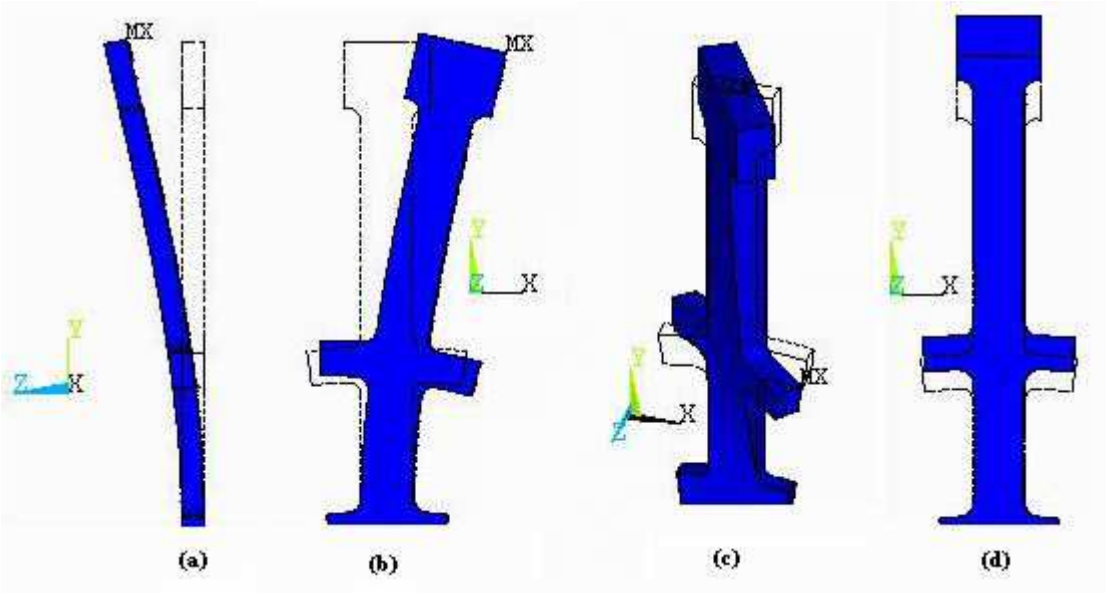

Figure 2.3 Clamped-free blade-alone modes : (a) Flexing mode-F, (b) Edgewise mode-E, (c) Torsional mode-T and (d) Extension mode

When the mode shapes corresponding to natural frequencies associated with the same nodal diameter number, such as those enclosed in region A in Figure 2.2 (a), are investigated, it is observed that, depending on the family of modes they are in, they may possess nodal points in the radial direction in addition to the nodal diameter lines they have in a circumferential direction. These points form

circles around the bladed disk and therefore are called *nodal circles*. See Figure 2.2 (c) for 2 ND mode of 2nd flex (2F) family for a bladed disk with 24 blades.

A bladed disk is said to be *tuned* when all its sectors are identical. However, in reality, making sure that all the sectors are identical is quite difficult. Inevitable variations due to manufacturing tolerances, material variations, damage, or operational wear cause the symmetry to be disturbed. A bladed disk with these variations is said to be *mistuned* or *detuned* and some of its forced response amplitudes are known to be amplified considerably as a result of these variations. As a result, a substantial research effort has been devoted to understanding this problem. It is now well known that mistuning causes mode localisation in which vibration energy of a mode is confined to only a blade or a few blades, resulting in large forced response amplitude magnifications compared to those of a reference tuned case. Moreover, the sensitivity of the forced response to mistuning is shown to be significantly affected in the presence of so called *frequency veering* or *curve veering* [9] which refers to the interaction between different families of modes and manifests itself by a veering in the natural frequencies when they are plotted against the number of nodal diameters. A curve veering region is indicated by region B in Figure 2.2 (a). As the resulting large vibration amplitudes, in turn, cause high cycle fatigue (HCF) problems, they need to be eliminated. One way of doing this is to specify very strict tolerances in manufacture to make sure that these variations are minimal. However, even if it was possible to make a perfectly tuned bladed disk, maintaining this status throughout the operational life is almost impossible due to irregular wear patterns. Besides, tight tolerances will eventually increase production costs. Another way of tackling this problem is to employ additional energy dissipation elements (i.e., in addition to structural damping which is generally quite low and aerodynamic damping). For this purpose friction dampers of various types are most commonly used. These dampers are placed between neighbouring blades and energy is dissipated by interfacial rubbing of

the blade-damper contact surfaces due to relative motion of the adjacent blades. Some friction damper configurations are given in Figure 2.4.

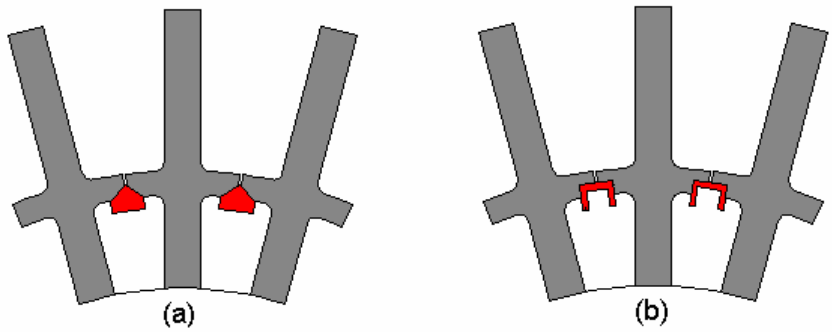

Figure 2.4 Examples of under-platform friction dampers: (a) cottage-roof damper, (b) thin-plate damper.

In addition, some novel techniques, such as those which seek to reduce the sensitivity of the bladed disk to mistuning by intentionally mistuning it in a certain way (based on the fact that after a certain degree, additional mistuning reduces forced response amplitudes, [43]), are also being considered to reduce the sensitivity to mistuning hence reduce the forced response amplitudes.

Bladed disks are mostly subjected to a special form of excitation known as *engine order (EO)* excitation where the bladed assembly rotates past a static pressure or force field. The blades of an assembly facing such an excitation are excited in a way which is periodic in time and varies only in phase from blade to blade. For a steady force/pressure field with a sinusoidal variation, the force experienced by a particular blade, j, at a given time t and for a rotational speed Ω is given by [1] $f_j = F\,Cos(k\Omega t + j\phi)$. Where F is the amplitude of the force and k is the engine order, or the number of excitation cycles a blade experiences in a full rotation of bladed disk (i.e., number of stationary excitation sources equally spaced in the flow field). Inter blade phase angle, ϕ, in this case is given by $\phi = 2\pi k / N$ where N is the number of blades. The implication of this is that, an EO excitation of kth order can only excite those modes with k nodal diameters for a perfectly tuned bladed disk or modes having k-diameter components in

their mode shapes in the case of a mistuned bladed disk. EO forced response characteristics are best demonstrated on a Campbell or interference diagram where frequencies are plotted against rotational speed. A sample Campbell diagram constructed using a lumped parameter model of a perfectly tuned 24-bladed bladed disk is given in Figure 2.5 (note that not all the order lines are plotted for clarity).

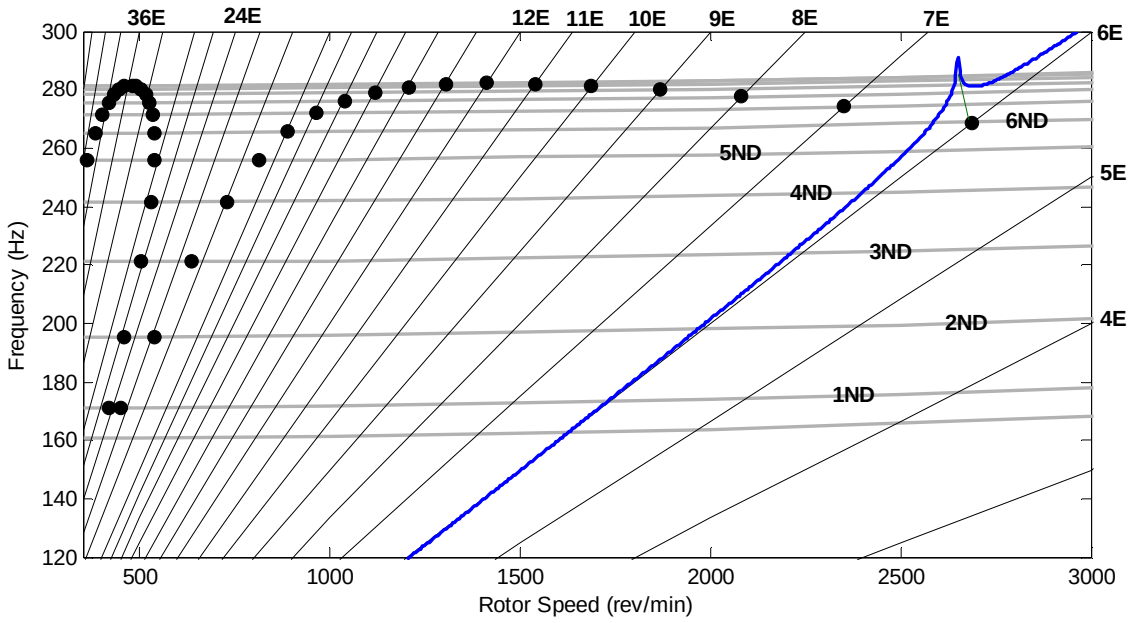

Figure 2.5 A sample Campbell diagram for a 24-blade bladed disk

Here the 3rd dimension, as shown by the sample blue curve, is the vibration amplitude. Although a particular EO line crosses many frequency lines, a resonance occurs only when the *kth* EO line intersects a natural frequency line of a k-ND mode and this is indicated by a solid circle on the diagram. No resonant response is produced for all the other crossings since for a resonance to occur the shapes as well as the frequencies of the force and structural mode should match. Note that due to spatial aliasing k- ND modes will be excited by k-, $(N+k)$-, $(N-k)$- etc. EOs and this is clearly observed from the given Campbell diagram.

2.3 Literature survey on bladed disk vibration

2.3.1 Classification of bladed disk research areas

A huge amount of research has been generated in the area of damped and mistuned bladed disk vibration predictions and a review of all the relevant literature is beyond the scope of this study. The interested reader is directed to major survey papers such as [2-4] and the references given therein. However, at this stage it is worth giving a classification of the research in these areas. Some of the recent references are given below. The research on mistuned bladed disks is mainly collected under a few groups;

(i) identification of the most sensitive parameters influencing mistuning such as blade-disk coupling, rotational speed, modal density, mistuning amplitude, frequency veering, damping variation etc. [5-9, 41],

(ii) reduction of model size to have computationally efficient yet representative models to carry out parametric studies as well as reducing prediction times [10-15],

(iii) probabilistic analysis of mistuned bladed disks to determine forced response statistics [6,16, 17],

(iv) maximum/minimum response amplitude predictions using numerical/analytical [20], optimisation [18,19] or statistical techniques [21],

(v) use of intentional mistuning to minimise the adverse effects of inherent random mistuning [22-24],

(vi) mistuning identification based on experimental data to assess the suitability of the bladed disk for operational use [25-29], and

(vii) experimental investigations aiming at validation of models developed for above-mentioned phenomena [44, 46, 49-50, 54-59]

Research on last two items is reviewed in separate sections (2.3.2, 2.3.3.1) below due to their relevance to this study.

A similar breakdown of research areas can be given for damped bladed disk studies as well. There are three main damping mechanisms concerning bladed disk analyses; inherent material damping, aerodynamic damping and external mechanical damping. In the following list, the studies concentrated on external mechanical damping, friction in particular, introduced at the contact interfaces are mentioned. Most of the research in this area is directed mainly towards

(i) the identification (mainly experimental) of friction contact parameters such as coefficient of friction and contact stiffness, to provide the prediction tools with realistic data [30-32],

(ii) the development of realistic friction damping and contact models or modelling of friction/contact interfaces [33-38],

(iii) non-linear forced response predictions of assemblies fitted with friction dampers [39-40], and

Again, for more references, a survey paper such as [42] and references given in the references mentioned above can be consulted. Similarly, some of the experimental works in these areas are reviewed in section 2.3.3.2. Detailed explanations of prediction tools [14, 39-40] used in this study can also be found in chapters 5 and 6.

2.3.2 Identification of individual blade variation

When predictions of a specific numerical code are to be compared with experimental data collected, the degree of correlation depends not only on the prediction tool's capabilities to capture the dynamic characteristics of the structure but also on how well the structure is described to the prediction tool. Mistuning response prediction tools are no exception to this. When validating these codes, special attention should be given to identification of the true mistuning parameters. Moreover, inherent mistuning identification may benefit the research efforts seeking to reduce the sensitivity to mistuning by introducing suitable intentional mistuning. Therefore it is thought appropriate to report some of the proposed methods on mistuning identification.

Mignolet et. al. and Rivas-Guerra et. al. [25-26] focused on estimations of blade-to-blade variations of masses and stiffnesses in a two part investigation. They used measured lowest frequencies of the isolated blades to recover variations in mass and stiffness properties. Two methods are presented. The first one assumes the mass matrix's variation to be negligible and associates mistuning to stiffness variations only. However this way it is found that significant errors are introduced in estimations of forced response. In the second method, maximum likelihood (ML) strategy is employed in which a simple Gaussian distribution of mass and stiffness matrices is assumed and all the structural parameters are estimated. However, this technique is only applicable to bladed disks with separate blades and it is assumed that individual blades behave in the same way when they are assembled.

A mistuning identification method which predicts individual blade stiffness variations from measurements on an entire bladed disk is given by Judge et. al. [27]. This method, unlike the above, can be applied to blisks. A highly reduced order model [10] is used in which blade modal stiffnesses are isolated. The variations of these stiffnesses then are calculated based on measurement data to assess the degree of deviation from a tuned reference. The capabilities of the method are demonstrated on an experimental bladed disk. Although the variation of intentional mistuning imposed on experimental test piece is predicted reasonably well, significant deviations are observed in quantification of mistuning.

Feiner and Griffin proposed a completely experimental mistuning identification method [28-29] which requires only a set of measured bladed disk modes and works out mistuning as a sector-to-sector frequency deviation relative to corresponding tuned reference. Unlike the method proposed by Judge et. al. it only works for an isolated family of modes. However, the model reduction methodology involved is less complicated and requires less analytically

generated input data. Their method is based on the so called Fundamental Mistuning Model (FMM) [13] in which a highly-reduced 1 DOF per sector model of a bladed disk is used to predict the vibratory response in an isolated family of modes. The effectiveness of the method is experimentally demonstrated on a test specimen. Very good agreement between applied, predicted and identified mistuning, both in terms of shape and magnitude is obtained. However the fact that it can only be applied to an isolated family of modes and uses a rather simple sector model limits its applicability wherever these assumptions are not valid. This method is partly used in mistuning identification of test pieces investigated in the presented study. For a more detailed explanation on the method refer to Chapter 4.

2.3.3 Experimental studies on bladed disks

Compared with the large number of theoretical studies on mistuning and damping in bladed disks, experimental investigations of these structures, particularly under rotation, for the validation of predictions of the mentioned phenomena are rather rare. This is mainly because of the difficulties involved in the required measurement and excitation techniques as well as precise and well-controlled test setups. In the case of mistuning the task is further complicated by the fact that the test application is expected to capture the variations in response due to small changes in the test structure. On the other hand, when damping elements like friction dampers are present, the non-linear nature of the structure makes testing even more challenging. In particular, when mistuning is investigated, the use of conventional excitation and response measurement techniques which require placement of transducers and exciters on the test structure, can modify original mistuning significantly.

In the following sections, experimental studies reported in the area of bladed disks will be reviewed. This review is divided into two areas namely, (i) mistuning studies, and (ii) damping studies.

2.3.3.1 Mistuning studies

One of the earliest thorough experimental investigations of mistuned bladed disks was carried out by Ewins in 1970s [43-45]. Tests were conducted on an integral bladed disk (blisk) having 24 blades. Inherent mistuning in the blisk was accounted for by the addition of small bolts and washers to the blade tips to get a tuned reference for mistuning analysis. Intentional mistuning was introduced the same way on top of this reference case. In order to eliminate the effects of aerodynamic forces tests were carried out in an evacuated chamber. Measurements here were taken on a rotating blisk which allowed the inclusion of centrifugal effects. Strain gauges were used to measure blade tip responses and excitation was performed via carefully arranged air jets close to blade tips. The number of jets could be adjusted to obtain the desired EO excitation. However the fact that air jets were used to excite the system subsequently led to deterioration of the vacuum and introduced variability in damping, and also brought up significant variations in force amplitudes. Nevertheless, satisfactory qualitative agreement between theory and measurements is demonstrated for several mistuning patterns thus validating the theory. Ewins observed, through measurements and was also able to simulate through predictions, the formation of rather complex, irregular modes in which some blades experienced much higher vibration amplitudes and no longer could be described by nodal diameter shapes. These modes were later identified as localised modes and the mechanism behind them was explained by Wei and Pierre [47-48].

Fabunmi [46] reported an experimental study in early 80s where a 23-bladed axial compressor rotor was used. Experiments were carried out on the stationary rotor to acquire modal data which were subsequently used with a semi-empirical method to calculate vibration response of the rotor. Here the blades were driven by piezoelectric actuators placed at the blade roots, and response was measured using a time-averaged holographic technique. The phase and amplitude for each actuator was controlled independently to generate EO-like excitations. Amplitude variations and departures from the regular ND modes

were observed for the detuned rotor. The effect of coupling through the disk was also investigated. However the agreement between the predictions and measurements was rather qualitative.

In a series of papers Kruse and Pierre reported on an elaborate experimental investigation of vibration localisation in bladed disks. They performed tests for free [49] and forced [50] response analyses. They examined two 12-blade bladed disks, one nominally tuned and one corresponding mistuned blisk. Tests were deliberately carried out at rest to eliminate aerodynamic forces and centrifugal effects. However, the latter was known to have a significant effect on blisks exhibiting curve veering phenomena [51], which was also investigated in their work. Non-contacting measurement (a proximity probe) and excitation (electromagnets) techniques were employed so as not to disturb the symmetry of the blisk. A special arrangement of two electromagnets was used as shown in Figure 2.6 to generate pure harmonic forcing.

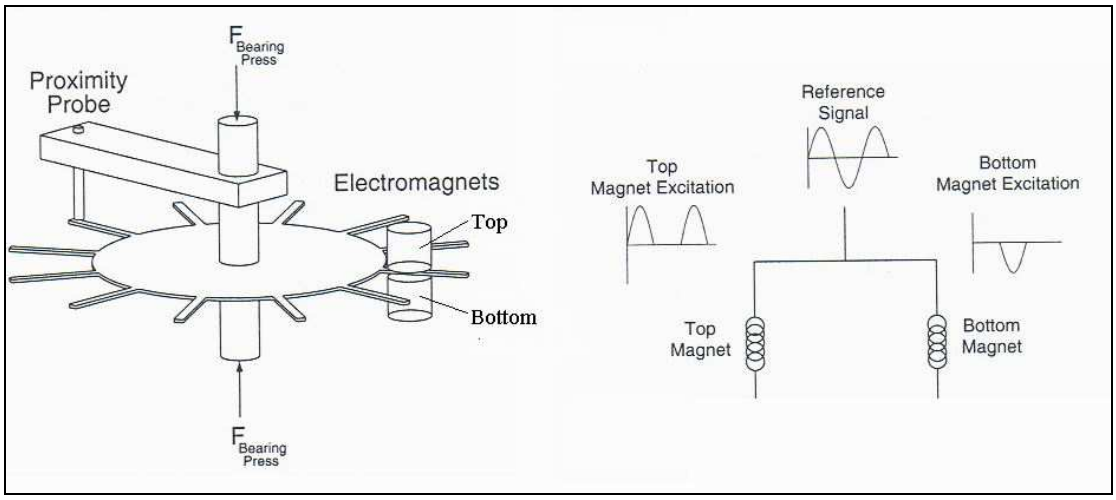

Figure 2.6 Pure harmonic excitation setup used in [49] (Taken from [49])

They used experimental results to validate component mode-based, reduced-order models [52-53] as well as demonstrating mode localisation. Their results show the sensitivity of blade-dominated modes to mistuning in the regions with high modal density and, equally, insensitivity of disk-dominated modes where

modes are reasonably separated. In-plane modes, in particular, are found to be very sensitive to mistuning due to their high modal density. Though the qualitative distortion to vibration modes due to mistuning was captured by their reduced order model, reduction was achieved at the expense of loss of accuracy in quantification of these changes.

In a later study Kruse and Pierre [50] abandoned the use of electromagnets due to collapse of magnetic fields at high frequencies and replaced them with piezo-electrical actuators which in turn contributed to the mistuning of the blisks. Forced response measurements and corresponding full FE and reduced-order model predictions in the frequency regions with high modal density are given. It is demonstrated that in the presence of curve veering with high modal density, in-plane modes in particular, experience vibration amplitudes of up to 240% higher than those of perfectly tuned blisk. Though in general good correlation is established between measured and predicted forced responses, the deviation of predictions is notably significant for some engine order excitations in the presence of high modal density.

Jude *et al* [54] used the same 12-bladed disk used by Kruse and Pierre in [49-50] to investigate mode localisation and forced response amplitude amplification due to mistuning. Unlike Kruse and Pierre though, they focused on a frequency range containing modes with lower modal density but exhibiting strong coupling between blade and disk motion. Another departure from the earlier study was the way they introduced mistuning. Investigation of separately manufactured bladed disks (one nominally tuned and one deliberately mistuned) in the previous study is believed to be the main source of poor correlation in forced response comparisons as the manufacturing tolerances are inevitably different for both blisks. As a result, mistuning was introduced by means of gluing various masses to blade tips. However this meant that they could only add masses, a process which led to a different mean natural frequency for tuned and mistuned cases. Their experimental results

demonstrated that localisation did not occur in the veering regions where strong coupling between disk and blades was present as the vibration energy was distributed throughout the structure through strong coupling, but outside the veering region where coupling was weaker. Qualitative agreement is demonstrated by direct comparison of measured and predicted response curves but degree of similarity is not quantified in anyway. The fact that the blisk they used was inherently mistuned to some degree and no attempt was made to account for this fact in analysis, and errors introduced in reducing the model order might be possible reasons for poor correlation.

Another experimental investigation studying forced response localisation and amplitude amplification due to mistuning was given by Jones and Cross [55]. The bladed disks in this study too were stationary and therefore the effects of rotation were not accounted for. They designed a travelling wave excitation setup which was able to produce magnetic and acoustic excitation as well as being capable of testing different size bladed disks at rest for various engine order excitations. A laser vibrometer was used to measure blade tip responses and mode shapes were observed by laser holography. The study mainly focused on developing and validating the experimental setup and so the results obtained were not correlated with any predictions. An important feature of their study was the demonstration of the effects of excitation errors on amplitude amplification and mode localisation. They experimentally showed that compared to mistuning, excitation errors introduced little variations in vibration response. Though not as dramatic as mistuning, acoustic excitation errors in particular caused slightly larger appearances of other modes than magnetic excitation errors did in blade responses. However, their attempt to quantify the effects of these errors against deliberate mistuning was not realistic as unaccounted inherent mistuning in the bladed disk is also responsible for the introduction of more response peaks and amplitude amplifications.

A similar experimental work to that of Jones and Cross was carried out by Judge et. al. [56]. Measurements were, similarly, conducted on a non-rotating bladed disk. They applied a non-contacting acoustic excitation by means of a series of speakers and used a non-contacting optical measurement technique to investigate bladed disk dynamics. Using reduced-order models [10], they obtained similar response patterns with measurements at various resonance peaks but no quantification is given to asses the degree of accuracy of predictions to provide conclusive evidence on validation of these models.

Kenyon and Griffin [57] performed experiments to demonstrate the theory of the method presented in [20] which predicts maximum amplification due to mistuning. Since their bladed disk was not rotating, a travelling wave excitation setup, the one developed in [55], was used. A single point laser vibrometer was employed to measure blade responses. Two cases are investigated; a nominally tuned configuration and a mistuned configuration which was optimised to maximise forced response. The fact that damping was non-linear in second case due to clamped boundary conditions violated their assumption in the theory that forcing in second case had to be adjusted to have the same damping for both cases. Using optimised mistuning pattern they managed to obtain a very close amplification factor to that predicted by the theory. Later, this mistuning pattern was altered by extra small-amplitude random patterns to investigate the robustness of attained amplitude. It was observed that this amplitude did not change significantly with small perturbations.

Shu and Cutts [58] presented a paper in which they extracted modal properties of a bladed disk using time domain strain signals measured on a rotating bladed disk. A time domain curve fitting technique was used to identify damping and an FFT spectrum interpolation technique was used to obtain frequency, amplitude and phase information. Another experimental study targeting modal parameter identification of bladed disks was given by Hollkamp and Gordon [59]. Extrapolating from their experience with an 8-bladed rotor, they concluded

that modal parameter identification for a real bladed disk under operating conditions was practically impossible and simplifying assumptions were inevitable.

2.3.3.2. Damping studies

Jaiswal and Bhave [60] studied the effectiveness of different damping mechanisms on a rotating experimental bladed disk. Eight evenly-spaced electromagnets were used to simulate engine order excitations. Blades were grouped into two groups of seven blades located opposite each other, each group covering 90 degrees. Several configurations of damping pins, lacing wires and damping wire were among the damping mechanisms they investigated. Damping values at the first bladed disk resonance were investigated both by analysing decay curves and frequency response functions. Their study showed that with loose and tight pins and lacing wire, damping decreased with rotational speed due to inadequate friction between the interfaces. Friction damping with damping wire is found to be most effective. However the way blades were arranged and fixed to the blisk did not allow the effect of coupling between blades on the damping characteristics of overall bladed disk to be observed. In addition, due to the same reason, simulation of engine order excitation was not realistic.

Berruti et al [32] designed a test rig via which friction damping effects on a stator low pressure stage blade segments could be investigated. Friction damping was introduced through contact of neighbouring surfaces. Later experimental results were published in [61] in which they aimed at quantifying the amount of energy dissipation and its relation with normal force. Also they sought to identify the contact behaviour so that Harmonic Balance Method (HBM) based numerical prediction tools could be provided with realistic empirical models. Their attempts to relate interlocking force with physical parameters of the contact such as contact stiffness and friction coefficient did not yield any meaningful

correlation. They concluded that Fourier expansion of tangential force could be related to total displacement range and showed that this relation formed curves in which interlocking force was the main parameter.

Sextro [31] published a paper in which he presented a contact model for shrouded blades with friction contact and experimentally demonstrated its effectiveness. The model included roughness of the contact surface and normal pressure distribution due to it, the stiffnesses in normal and tangential directions and friction damping. A blade with two non-Hertzian contact surfaces (for there are two shrouds) was used in experiments and normal contact force was simulated by dead weights. Generally good agreement between predicted and measured frequency response curves for different normal loads was obtained however deviations in amplitude and resonance frequencies were also evident. The nonlinearity of contact stiffnesses and normal force due to roughness of the contact surfaces were demonstrated experimentally. A numerical investigation on a bladed disk for variable contact force was also given.

Hollkamp and Gordon, [59, 62] carried out an experimental work to identify damping in jet engine blades. They showed that the common test practice of damping only a few of blades in a bladed disk and keeping the remaining ones undamped in identification of damping values was valid only if the damped blades' response was localised (i.e. they were sufficiently mistuned) to prevent coupling with the other blades. They concluded that in cases where this coupling was effective damping estimates of mixed assembly would depart from the one in which all the blades were damped considerably.

Sanliturk et. al. [35] presented a paper in which they sought to predict the vibration response of under-platform dampers for turbine blades. The experimental data was acquired initially on a test setup comprising 2 beams representing blades and a damper in between. Afterwards the measurements were repeated by replacing the beams with two industrial turbine blades. The

blades/beams were clamped at the root. Tests were performed at rest and the damper loads were simulated through mass loading by hanging dead weights to the damper. The system was excited at damper level by a shaker and the response was measured at blade/beam tips utilising an accelerometer. Friction contact parameters (friction coefficient and contact stiffness) were obtained using the test setup described in [30]. One of the main observations they reported was the occurrence of so-called rolling motion. They found that when subjected to in-phase bending vibrations, the damper was forced to rotate due to radial blade motion, leading to loss of contact with adjacent platform faces thus reducing the effective damping. However, the same was not observed for out-of-phase mode. Big discrepancies were evident from their comparisons, particularly for in-phase mode as the rolling motion was not included in the model. The correlation was improved through a correction factor though the authors too acknowledged that a better model was needed.

Besides studies seeking to understand the mechanisms of additional mechanical damping, some are aimed at measuring available blade damping (structural damping). An experimental study on measurement of blade damping was given by Jeffers et. al. [63]. Here they used a piezoelectric actuator embedded in blade geometry to excite blades at various vibration modes and strain gauges to measure the responses. Both stationary and rotating blades are considered. Several damping measurement techniques are employed and consistent results are reported. However, the use of intrusive measurement and excitation techniques modified both damping and natural frequencies of the system. Additionally, the use of a SDOF curve fitting technique did not allow realistic damping estimates for systems having closely spaced modes such as bladed disks.

An experimental study focused on identification of gas turbine under-platform friction damper properties at high temperatures was conducted by Stanbridge et. al. [30]. Two specimens loaded by dead weights were used. Temperatures up

to 1000 C were reached and response near the contact area was measured via an LDV. Based on linear asperity contact theory by Burdekin et. al. [64] they devised a simple model and experimentally demonstrated that just one hysteresis loop was enough to characterise the contact. They showed that the coefficient of friction and the micro-slip parameter were sufficient to represent the contact in non-linear analysis.

2.4 LDV measurement techniques on bladed disks

The area of non-intrusive measurement techniques is a very broad one and it is not intended here to review all the work in the area. However, it is worth mentioning the developments, especially the ones concerning the use of LDVs on rotating bladed disks, which have somehow shaped and led to the techniques used in this study.

Although in most of the above-mentioned experimental studies, LDVs are used to measure the response due to benefit of their non-intrusive nature, almost all are concentrated on stationary test objects. When the test object is moving, either the test setup or data processing technique, and in some cases both are more complicated. One of the earliest studies on the subject dates back to 1970s [65] where Kulczyk used an LDV to measure moving turbine blade vibration. The approach used there was very simple. Figure 2.7 shows the basic principle where a laser beam is directed at a fixed point in space and the response is measured as the structure passes this point. Since then the use of the optical sensor has been primary objective of many vibration measurement studies through 1970s [66-67] and 1980s [68-71] just to mention a few. Kulczyk's approach is used in many researches such as by Rothberg, [72] where it is adopted for torsional measurements and by Bucher [73] where it is used for radial vibration measurements on shafts.

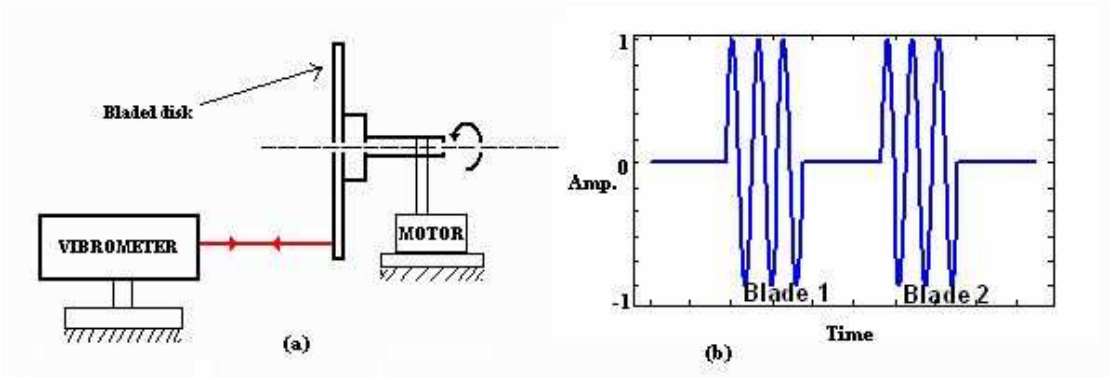

Figure 2.7 (a) A fixed-in-space measurement point diagram, and (b) a typical vibrometer output

Reinhardt et. al. [74] presented an application of Kulczyk's method. Here, as the blade responses were measured during the time in which they passed the laser beam, the length of signal was not long enough to perform a conventional spectrum analysis. Instead, measured time signals were curve fitted using a least squares approach. However this meant that the speeds at which the method could be applied were limited as this technique required at least two full cycles of vibration to be captured. Use of a modal filter was proposed to overcome this difficulty.

Disadvantages associated with the use of a fixed measurement point LDV, such as very short measurement times and speckle noise, are sought to be overcome by using a measurement beam which tracks the desired location on the rotating structure. This is mainly tried to be achieved by a set of mirrors in the laser vibrometer's head to direct the laser beam. These mirrors are driven by sine waves at the same frequency but out of phase with each other so as to track a circle. Then, the motion of the beam and rotating structure can be synchronised so that the same point on the structure is followed at all times. The use of this technique is reported by Bucher [73] and Castellini et. al. [75]. Nevertheless, this technique also can only be used for a limited speed range as the mirrors cannot manage to track the measurement location at above certain rotational speeds. Here it is necessary to note that speckle noise can be a problem in tracking measurements as well as in fixed point measurements. However in the former

case the risk can be reduced significantly by appropriate selection of measurement location as this location is not going to change (provided that misalignment is completely eliminated and in-plane motion of the measurement point is small) during the measurement session.

A way of solving problems associated with speed limitations in tracking a point on a rotating structure is to use a so called self-tracking system. This was first reported in a work by Lomenzo et. al [76]. wherein it is stated to have been suggested by Maddux, G. E. via personal correspondence with the authors. In their technique they proposed using a set of plane mirrors, one on the rotating structure and one stationary in front of the structure. A schematic of the proposed self-tracking system is given in Figure 2.8.

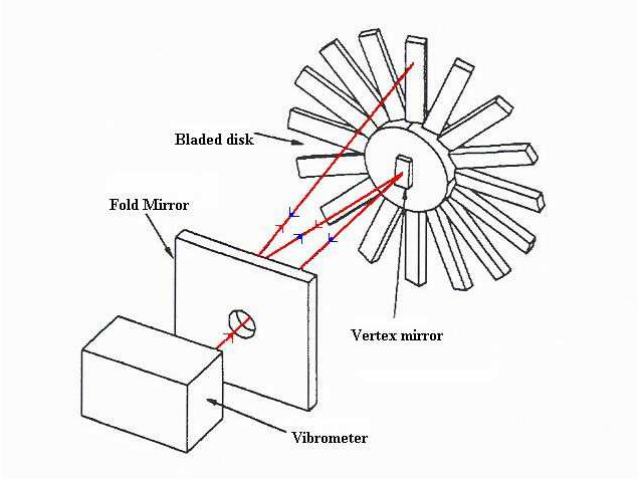

Figure 2.8 Schematic of the self-tracking system (Taken from [76])

In this arrangement the laser beam passes through the fold mirror and lands on the vertex mirror rotating with the structure. The beam is then directed back to the fold mirror and from there to a particular point on the bladed disk. The beam follows back the same path to the laser head. Although limitations on rotational speed are eliminated via this technique, misalignment of the bladed disk relative to the stationary mirror and vibrometer introduces errors in velocity measurements and in location of measurement point. While a method to eliminate the misalignment problem is given by the authors, removing the effect completely in practice is a challenging one. The vibration measurement

techniques used in the presented study is based on this idea but considerably modified. For a detailed explanation of the technique refer to Chapter 3.

While tracking is a useful tool to acquire vibration response of a single point, it is often desirable to measure multiple points on a structure to get information about mode shapes or operating deflection shapes (ODS). In this case the ability to direct the laser beam to any desired location is made use of through a scanning mechanism to observe the vibration response of a series of points in quick successions. A device capable of scanning in steps is often referred to as a Scanning Laser Doppler Velocimeter or SLDV and, similarly, a device capable of scanning in a prescribed continuous manner is called as a Continuous Scanning Laser Doppler Velocimeter or CSLDV. Although measurements can be completed faster in this way, there are certain limitations on the speed of measurements such as the time required to stay at a point to characterise its behaviour and the time required to overcome the inertia of the scanning mirrors in displacing them [83]. Stanbridge and Ewins [77] presented detailed work which described a number of ODS measurement techniques using SLDV and CSLDV. The ODSs were measured for straight line scan, circular scan where structure was scanned at a given radius and area scan where mirrors were controlled in a way to cover a rectangular area on the structure. Methods of extracting mode shapes in each case were given. A small diameter circular scan was used to measure angular vibration of the structure. Also presented in their paper was a way of measuring translational vibration using a short-focus lens at the point of focus. The application of these techniques on a stationary and rotating bladed disks was demonstrated in [78]. Some of the techniques proposed here are also used at various stages of the presented study and more details on how they work can be found in Chapter 3.

2.5 Summary

In this chapter, studies on bladed disk vibration and the use of LDV on rotating components such as bladed disks are reviewed. A general review of terminology

and basic definitions regarding these structures are given. The focus of the survey has been the experimental studies concerning the effects of mistuning and damping on bladed disks however some applications dealing with mistuning identification in particular are also reviewed. Together with an increased understanding of physics behind the problems related to these structures, and advances in technology, a noticeable increase in the number of complicated experimental works is observed. However, majority of the studies used stationary bladed disks in the analyses. Most of these experimental works dealt with effects of mistuning. Where bladed disks integrated with friction dampers were investigated, studies were limited to small scale test setups consisting of a few blades at most.

Finally, in the last part of the chapter, the use of non-intrusive response measurement transducers, and the LDV in particular, on rotating blade assemblies is reviewed. So far, tracking of a single point on a rotating bladed disk using external mirror arrangements has been possible with a certain degree of success. All other techniques controlling LDV mirrors for tracking have been restricted to certain speed limits (frequencies) due to inability of mirrors to operate at higher frequencies, generally much lower than typical operational speeds.

CHAPTER 3

BLISKS and TEST RIG: DESIGN and INSTRUMENTATION

3.1 Overview

This chapter focuses on the design and instrumentation details of the bladed disks and the test rig accommodating them. The design and manufacture of two bladed disks, one to be used in mistuning analysis (Blisk-2) and the other to be used in damping tests[1] (Blisk-1) are given. Test rig design requirements and justifications for the selected configurations are stated. Excitation and measurement techniques are introduced. The LDV transducer used in measurements alongside the rest of the data acquisition hardware and software is given. The processing of the LDV output to obtain forced response and ODSs is presented. Advantages and limitations of LDV transducers are stated

3.2 Bladed disk (blisk) design

Originally, it was decided to have only one blisk made which in turn could be used in both mistuning and damping tests. However, as will be explained in Chapter 4, the first manufactured blisk (Blisk-1) was not adequate to be used for mistuning investigations. As a result, a second blisk (Blisk-2) was manufactured for this purpose.

[1] Throughout this document, unless otherwise stated, the following terminology applies
Tuned tests: Tests on Blisk-2 as manufactured
Mistuned tests: Tests on Blisk-2 with applied deliberate mistuning
Undamped tests: Tests on Blisk-1 after tuning, and
Damping tests: Tests on Blisk-1 with integrated friction dampers.

3.2.1 Blisk-1

When designing an experimental bladed disk to validate a prediction capability, it is important that its characteristics are specified to reflect those of a blisk used in a real application and at the same time to eliminate uncertainties in the computations. It has been noticed through the literature reviewed in Chapter 2 that some parameters are particularly important in forced response predictions of the bladed disks. Naturally, it is preferable to design the test pieces such that these effects can be observed and consequently predicted for validation purposes. The design specifications for Blisk-1, therefore, are listed as follows:

- the bladed disk should be manufactured as an integral piece to eliminate uncertainties introduced through contact regions of the disk and blades;
- the natural frequencies of the first (1F) family of modes should be sufficiently well separated that tuned modes could be clearly identified
- it should be possible to excite most of these natural frequencies by steady-state EO forcing at speeds which are achievable under laboratory conditions (preferably, less than 5000 rev/min)
- the testpiece should be capable of accepting inter-blade, under-platform friction dampers, and preferably of various types, for dynamic testing.
- blades should be capable of being tuned and mistuned in specific patterns
- blades should also be staggered, so that the bending mode vibration has roughly similar components both in the plane of the disc (to give reasonably realistic relative under-platform damper motion) and out-of-plane (to give sufficient blade-disc modal coupling); and
- the disk portion of the blisk should be sufficiently flexible that disk-blade coupling can be cleanly observed.

The design of the blisk is based on the one used in reference [45] but modified in many ways to meet all the criteria mentioned above; most notably, the accommodation of platform dampers and improved blisk dynamic properties. Additionally, the current blisk has enlarged blade tip areas to allow magnetic tip forcing. An initial FE model was prepared and through systematic modifications, the final blisk characteristics were obtained. A picture of the

machined test piece and an FE model of a single bladed sector are shown in Figure 3.1. The technical drawings of the blisk are also given in Appendix A.

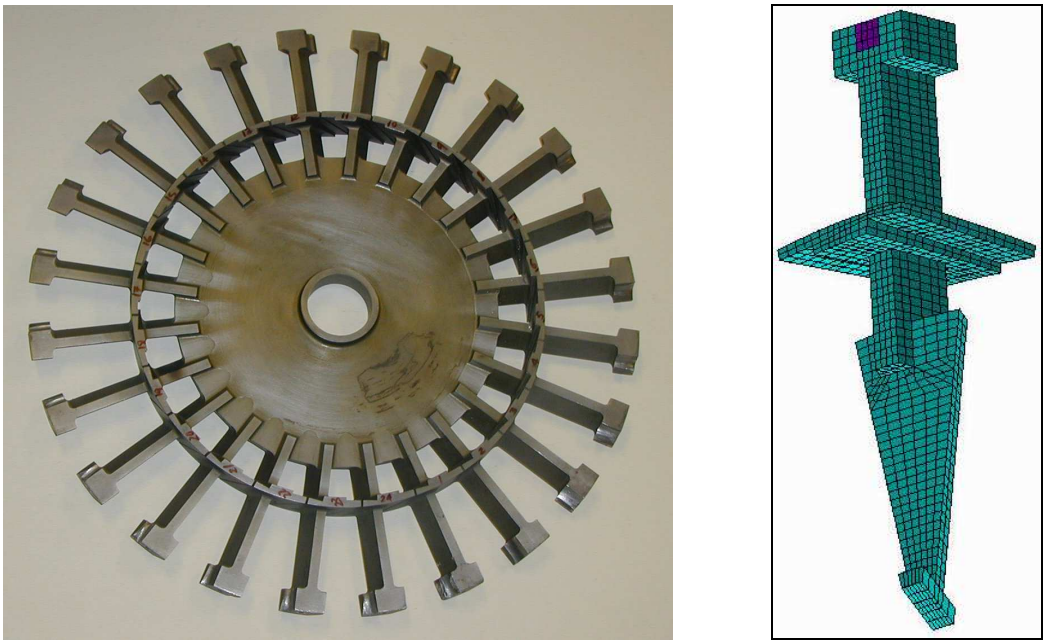

Figure 3.1 a) Blisk-1 (as received), and (b) FE model of a cyclic sector

Although Blisk-1 was designed to be an integral piece, blade inserts which accommodate and retain the friction dampers in place were made separately. Attempts at making them integral with the blisk would have complicated manufacturing considerably, thus making it very costly. Separate machining of these pieces does not introduce any uncertainty for mistuning analyses, as their integration was not needed until the damping tests. Hence, initial static tests and the blisk tuning process given in Chapter 4 were carried out in their absence. A photograph of a pair of blisk inserts is given in Figure 3.2.

Figure 3.2 Blade inserts

The disk and blade thicknesses are set at 5 mm and the blades are staggered at 40° with respect to the axis of rotation. This allows the centring of the under-platform damper forces. The first six families of modes for the designed blisk at rest are plotted against nodal diameter index in Figure 3.3. In this study, only the first family of modes will be investigated experimentally. As it is seen from Figure 3.3 (b), the modes of the first family with 7 to 12 ND are clearly blade-dominated while the 2-6ND modes exhibit blade-disk coupling, as they were intended to. Note that due to fixing of the blisk, the strain energy in the 0 ND mode could be higher than that of 1 ND mode (these two modes have very different mode shapes) and that would result in the 0 ND mode natural frequency being higher that that of 1ND mode. Most of the first family modes are reasonably well separated in accordance with the design requirements and are given in tabular form in Table 3.1.

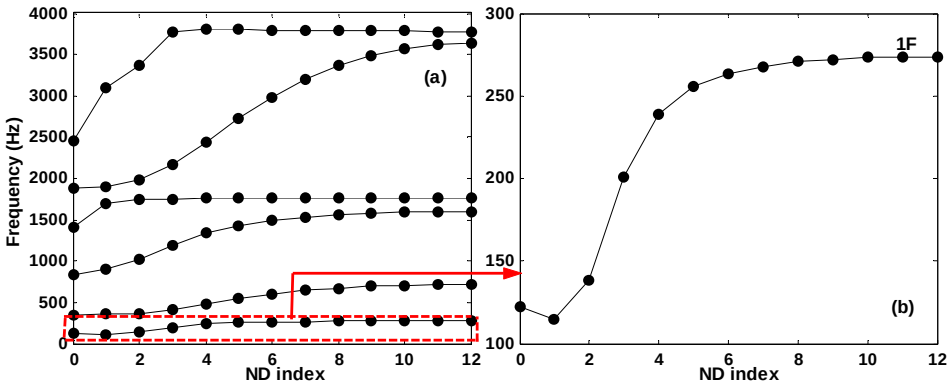

Figure 3.3 Natural frequencies of Blisk-1 at rest (from FE)

ND #	0	1	2	3	4	5	6
Freq (Hz)	122.22	114.983	138.762	201.181	238.752	255.45	263.516
$ND_n - ND_{n-1}$	—	-7.237	23.779	62.419	37.571	16.698	8.066
ND #	7	8	9	10	11	12	—
Freq (Hz)	267.896	270.473	272.047	272.996	273.507	273.669	—
$ND_n - ND_{n-1}$	4.38	2.577	1.574	0.949	0.511	0.162	—

Table 3.1 Separation of Blisk-1 first family modes (from FE)

It was stated in the design requirements that most of the 1F family modes should be excitable by rotor speeds attainable under laboratory conditions. The natural

frequencies at various rotational speeds needed to be calculated so that an interference (Campbell) diagram could be constructed to map out the primary forced response characteristics of the blisk (ideally calculations at two speeds are enough since natural frequencies vary with the square of rotational speed). At the time of design, an electric motor previously used at speeds up to 5000 rev/min (max 6000 rev/min) was readily available and it was decided to make use of it. Therefore, a speed range up to 6000 rev/min was considered. The constructed Campbell diagram showing the resonances corresponding to 1F family of modes is given in Figure 3.4. In the light of earlier experience with the motor planned to be used and also for safety issues speed limit was identified as 4000 rev/min. Therefore, based on given Campbell diagram, it was anticipated that 4D and above modes could be excited during tests. The exclusion of lower ND modes is not a drawback as they can be excited at lower speeds due to spatial aliasing.

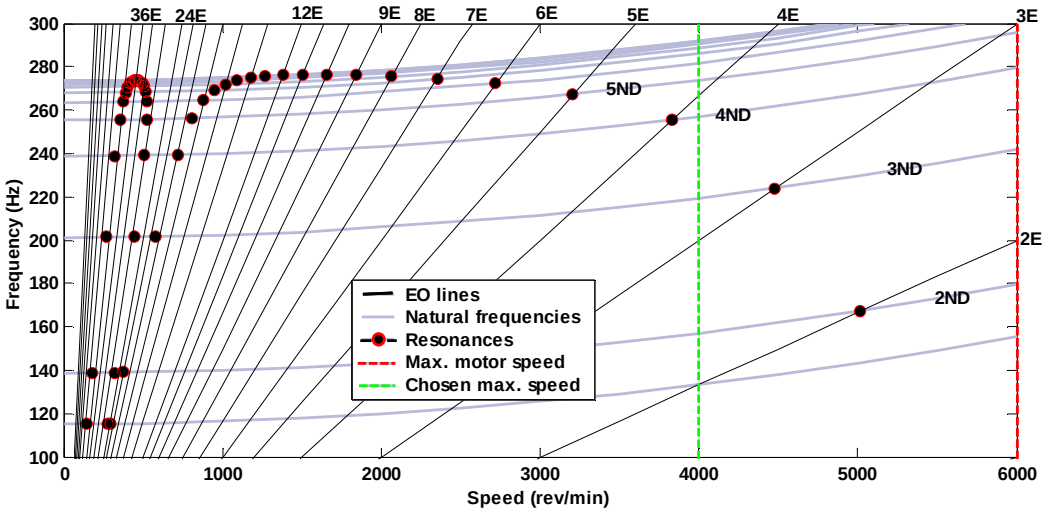

Figure 3.4 Blisk-1 Campbell diagram (from FE)

3.2.2 Blisk-2

The second blisk (Blisk-2) was designed to be used in mistuning investigations only and therefore did not have to be as complicated as Blisk-1. However, the overall dimensions had to be consistent as it was going to be used in the same rig. Based on the experience gained in the manufacture of Blisk-1, it was decided

to have a fairly simple geometry for this second blisk so that a near-perfect symmetry could be achieved, thus eliminating the need for tuning. Most of the design requirements listed for Blisk-1 still apply, and so: Blisk-2 must be an integral piece, most of 1F family modes to be excited by rig speeds, 1F modes to be reasonably separated, it should be excited by magnets, and should allow tuning and deliberate mistuning of the blades. Again, an FE model was prepared to match these requirements. The blisk was wire cut from a uniform 5mm thick steel plate. A picture of the manufactured blisk together with a cyclic sector of its FE model are given in Figure 3.5. Again, the technical drawings of the blisk are given in Appendix A.

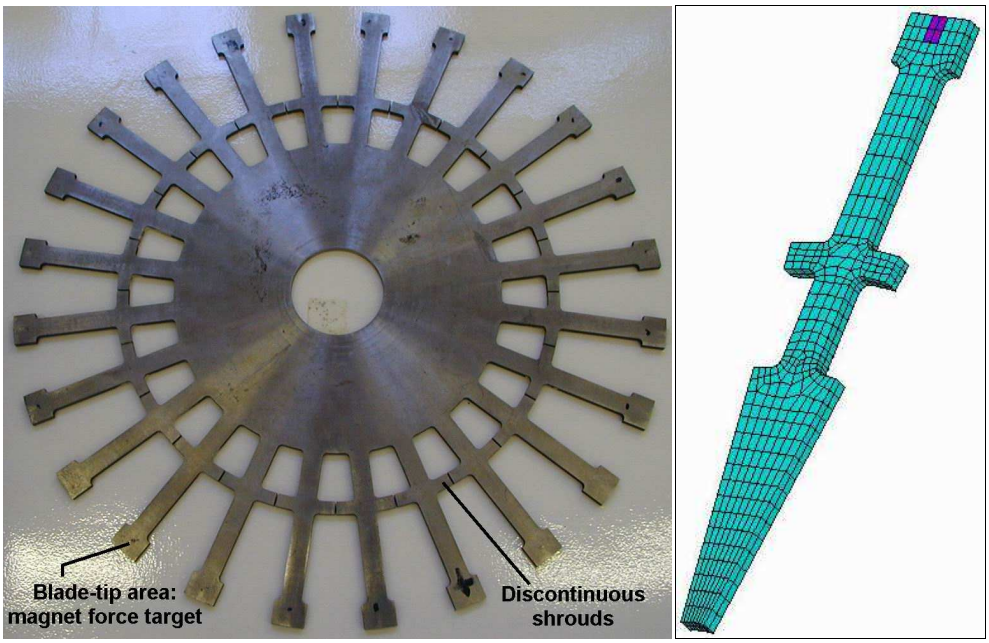

Figure 3.5 a) Blisk-2, and (b) FE model of a cyclic sector

Although the dampers would not be used with this blisk, the discontinuous shrouds were kept as they provided a near continuous and sufficiently vibrating path for LDV circular scanning of 1F assembly modes. Natural frequencies of the blisk obtained at rest from FE analysis are given in Figure 3.6. The blisk was clamped in the centre, in accordance with actual boundary conditions. Given the simple geometry of Blisk-2, it has been possible to obtain better 1F characteristics in terms of design requirements. As it is observed from Table 3.2, almost all the modes in this family are sufficiently separated

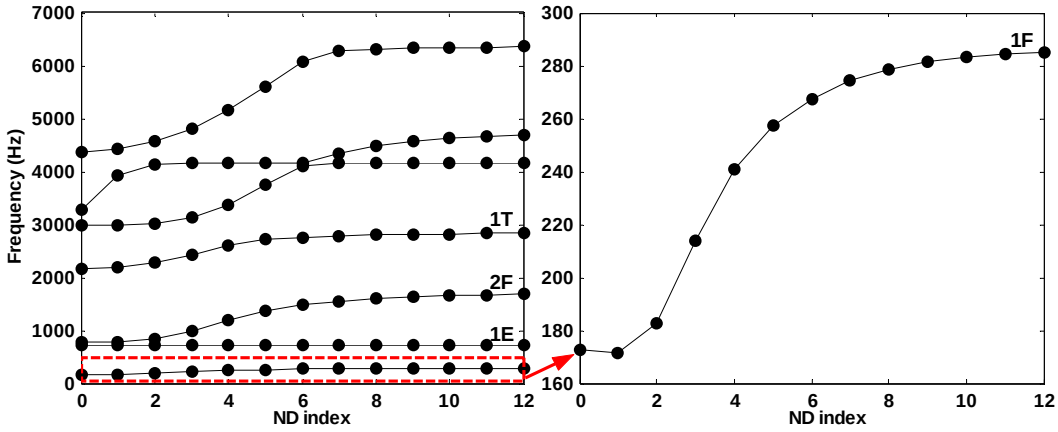

Figure 3.6 Natural frequencies of Blisk-2 at rest (from FE)

ND #	0	1	2	3	4	5	6
Freq (Hz)	172.563	171.549	182.584	213.734	240.715	257.331	267.536
$ND_n - ND_{n-1}$	—	-1.014	11.035	31.15	26.981	16.616	10.205
ND #	7	8	9	10	11	12	—
Freq (Hz)	267.536	274.126	278.523	281.465	283.355	284.414	—
$ND_n - ND_{n-1}$	6.59	4.397	2.942	1.89	1.059	0.342	—

Table 3.2 Separation of Blisk-2 1F family modes (from FE)

A Campbell diagram similar to that for Blisk-1 was constructed in the same way and shown in Figure 3.7. Based on the chosen maximum speed value of 4000 rev/min, the 4D and above modes are expected to be excited successfully, similarly to Blisk-1.

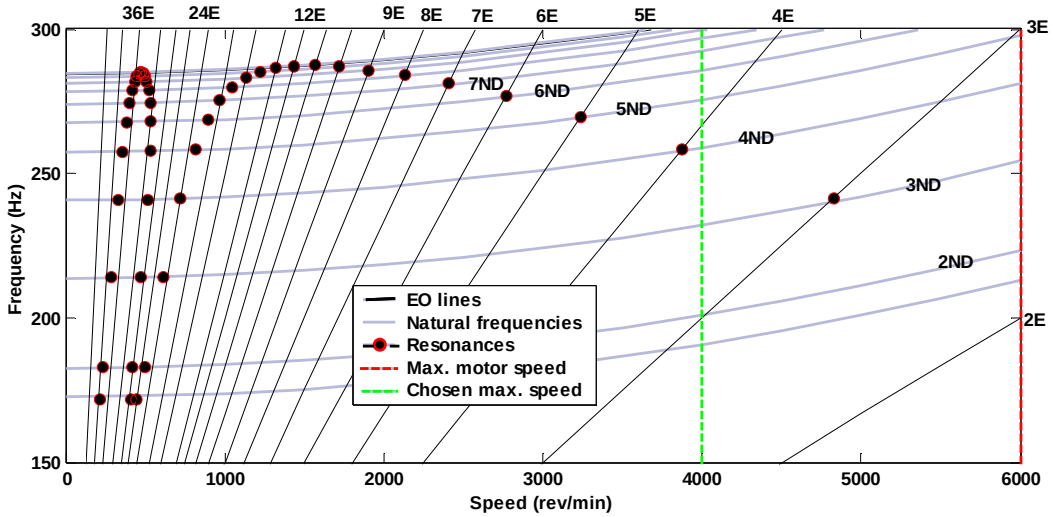

Figure 3.7 Blisk-2 Campbell diagram (from FE)

3.3 Rig Design

3.3.1 Design requirements

Experimental investigation of the sensitivity of a gas turbine bladed disk to a particular phenomenon such as mistuning alone in its normal operation is extremely complicated. This is not only because of the difficulties due to instrumentation but also due to the practical near-impossibility of isolating that particular phenomenon from the others. Aerodynamic effects, and the existence of other components etc., inevitably contribute to the overall response yet distinguishing their participation may not be possible. Therefore, it is important that all phenomena but the one being investigated are eliminated in testing. This generally requires well-controlled and precise test setups in which only the effects due to investigated features are highlighted.

In this study, as the response predictions of the mistuned and damped bladed disks subjected to steady (engine-order, EO) excitation are sought to be validated, the design requirements for the test rig are identified as follows:

- The test pieces must be operated in a vacuum so that aerodynamic effects can be eliminated;
- The operational speed range must be broad enough to enable excitation of most of the first family of modes of the test blisks by EO forcing;
- Excitation and measurement techniques must be non-intrusive so as not to introduce additional mistuning or damping;
- Accommodation of several exciters must be possible to increase the force, if necessary, and also to cancel out specific EO inputs if needed;
- It must be possible to measure vibration response on a point on a rotating blade regardless of the rotational speed;
- It should be possible to measure the response from various blades without interrupting the operation of the rig.

Eventually, the hardware of the test rig consists of a base support-block upon which the rig is mounted, a chamber accommodating the test pieces, a back plate providing support for various parts, a tracking mirror arrangement enabling tracking of a given point, an indexing mechanism switching the LDV beam from blade to blade, magnetic exciter holding and positioning mechanisms and a safety cage which encloses the entire test rig. Pictures of the front and rear views of the rig are given in Figure 3.8. The technical drawings of all the parts of the test rig can be found in Appendix A.

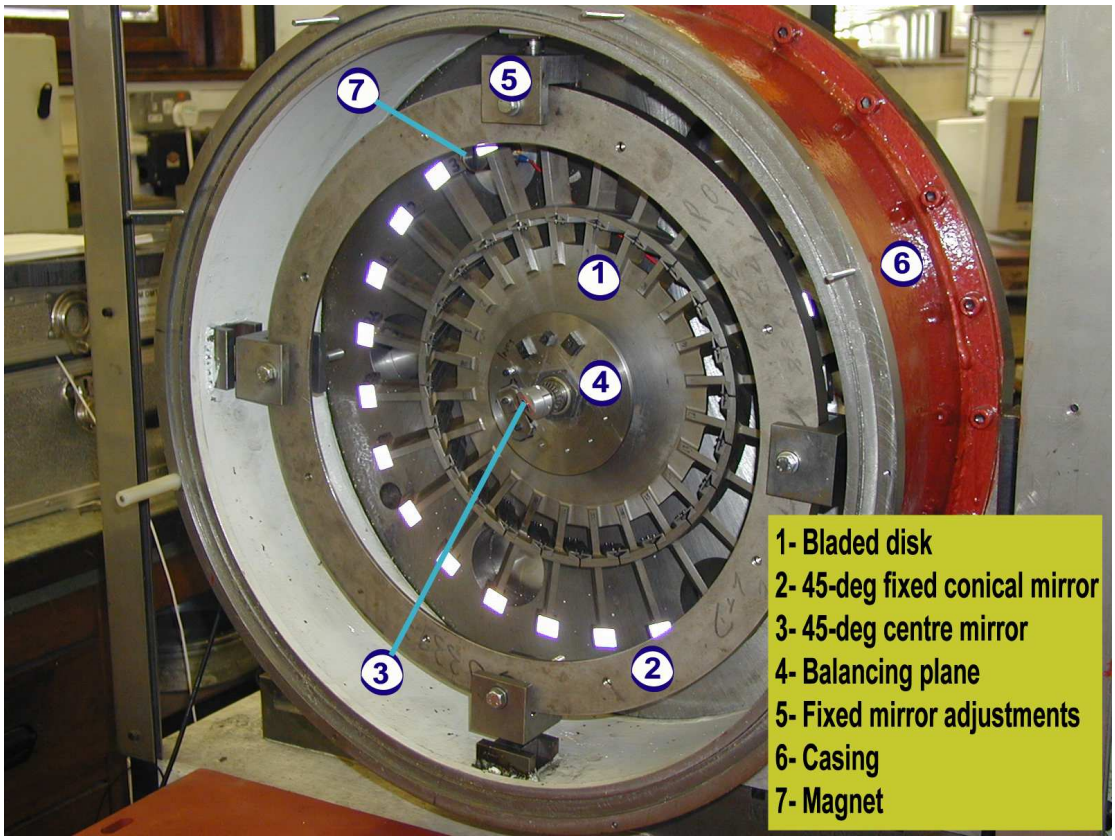

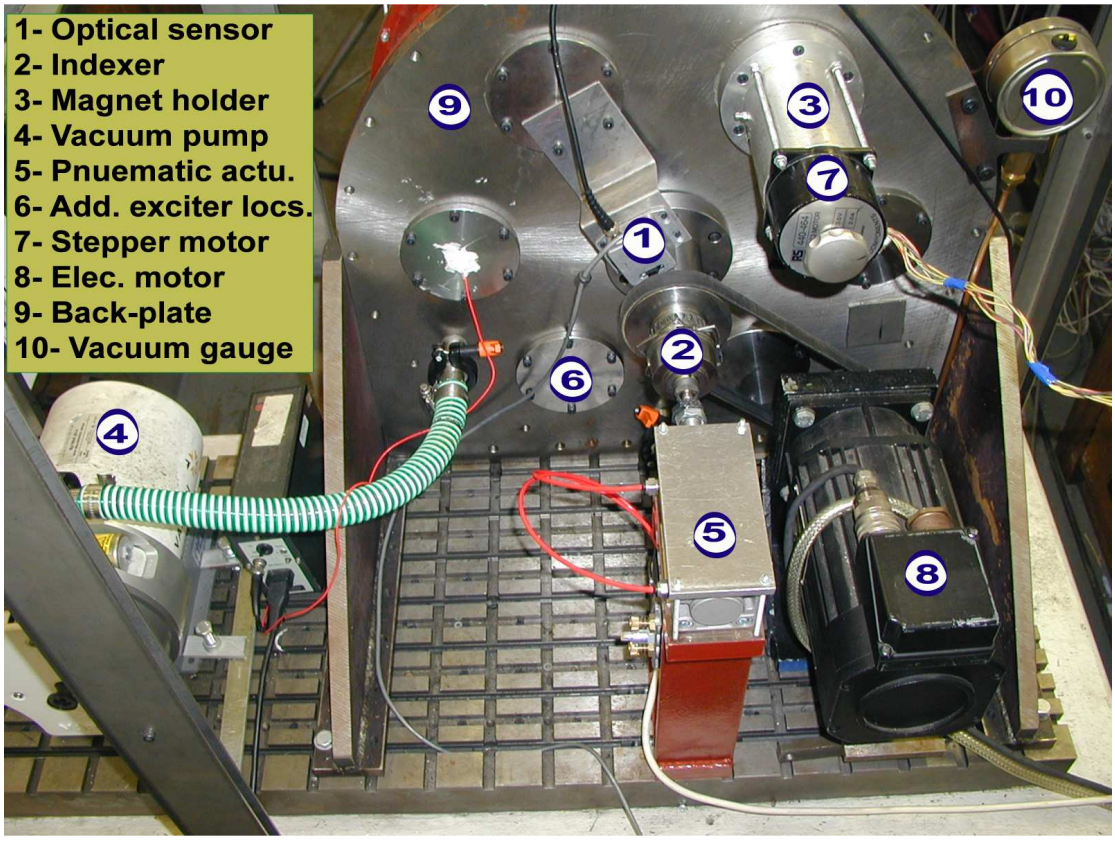

Figure 3.8 Mistuning and damping test rig

3.3.2 Test chamber

The test chamber consists of a back plate and a cylindrical part, which are made of steel, and a polycarbonate front cover. This polycarbonate front cover is interchangeable with a transparent glass window to allow various measurement techniques that are also explained in this chapter. Since the rig runs in vacuum, all the joints and mountings are sealed. Other than sealing of bearing housing where lip seals are more appropriate, O-rings have mostly been used for the sealing. The casing is secured to a concrete block with slotted steel inserts, which eases mounting of the rig to the base.

An air-free 0.37 kW Varian SH100 vacuum pump is used to evacuate the air in the chamber. This way, additional complications such as aerodynamic damping, blade coupling through fluid motion, blisk heating are prevented. Therefore, a high standard vacuum is not needed. A relatively crude vacuum gauge with 0.02

bar pressure increments is used to observe the vacuum. The air leakage, if there was any, was less than the gauge could successfully measure.

As the chamber is evacuated, the front cover, back plate and cylindrical parts are all subjected to atmospheric pressure. Moreover, the cylindrical steel part is required to be strong enough to withstand impact loads in the event of a catastrophic failure such as blade loss under rotation. An FE model of the chamber is prepared and analysed under the mentioned loading to verify the design. The force resulting from a blade loss is modelled as a steady, static force. The FE model and results are given in Figure 3.9. The maximum equivalent Von Mises stress was calculated as 200 MPa for a yield strength of 420 MPa, resulting in an adequate safety factor of 2.1.

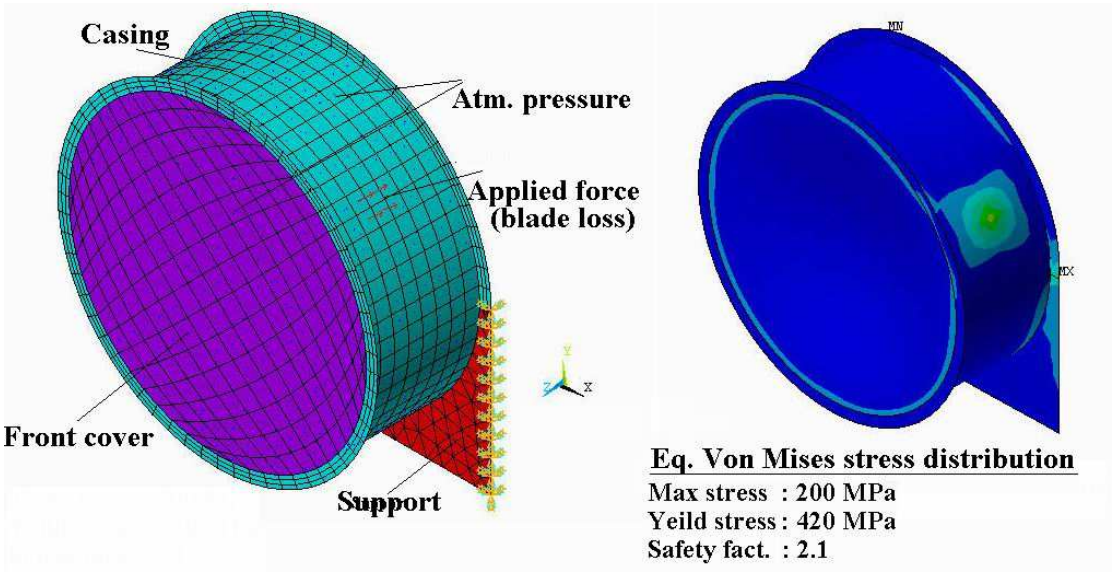

Figure 3.9 FE model of the casing and analysis results

3.3.3 Drive system

The operating speed limit was decided to be 4000 rev/min in Section 3.2. As the entire speed range (0-4000 rev/min) is to be swept in measurements, the drive shaft should be designed such that its critical speeds occur outside this range. An FE based critical speed calculation code RotFE [84] was used to calculate

shaft critical speeds. Here the bladed disk is modelled as a rigid disk. The FE model and the calculated critical speed values are given in Figure 3.10.

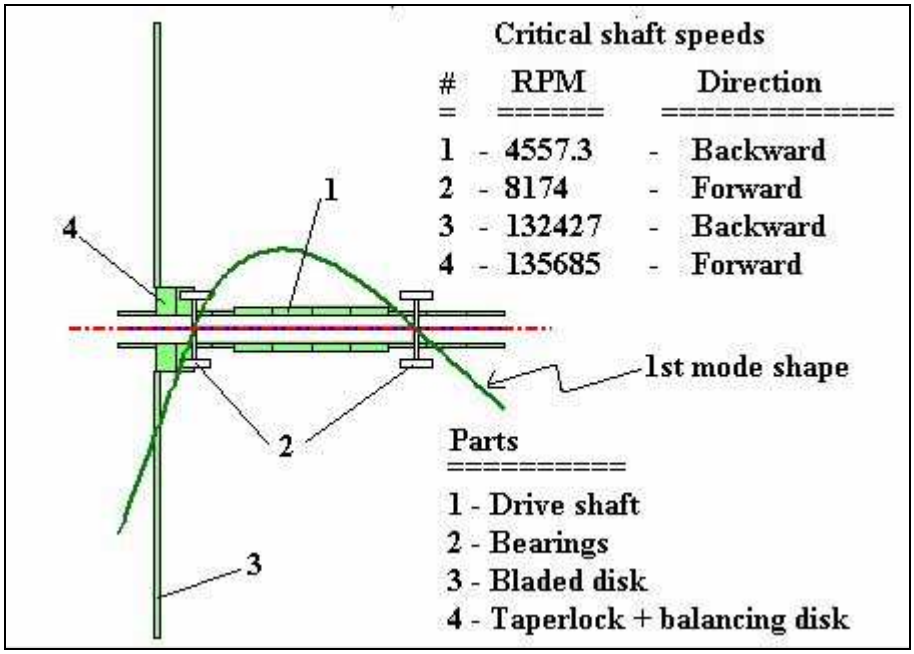

Figure 3.10 Shaft FE model and critical speeds for the final design.

The test rig is driven by an SEM, type HD142C6-88 electric motor. The maximum speed achievable with this motor, as mentioned earlier, is 6000 rev/min and it is capable of delivering a continuous stall torque of 11.3 Nm. Motor output is transmitted to the drive shaft via a 1:1 ratio transmission system with a V-ribbed drive belt. The motor is operated by a Drive2000/4000 controller supplied by IRT-SA for this particular model. Communication with the controller is achieved through one of the RS232 communication ports of the Data AcQuisition (DAQ) control PC. For this purpose a Matlab based software is written via which speed and torque can individually be set.

The encoder installed on the motor provides 1024 pulses per rev and as a result gives precise speed and position information. Assuming that no slippage occurs in the drive belt, the actual speed values can be taken from the motor's encoder. However, no slippage assumption has to be verified. In order to measure the rotor's speed independently, a 1/rev signal is acquired on the drive shaft by

means of an optical sensor. It must be noted that this 1/rev signal is also necessary for phase measurements as it provides a reliable trigger signal for the vibration measurements. For this purpose a high-reflectivity small mirror is glued to one of the flanges on the drive shaft and the optical sensor is secured to a fixed base and at a prescribed distance to the small mirror. Each time the mirror rotates past the optical sensor, a pulse is generated. Created pulses then are fed into a simple circuit where the analogue signals are converted to digital TTL pulses. By counting the number pulses in a given period of time, the rotational speed is calculated. However, the accuracy of this kind of measurement depends on the sampling frequency of the acquisition board, and especially when precise speed measurements are required, very high sampling frequencies are needed. As the vibration, force and 1/rev signals are acquired via the same DAQ board and a few seconds worth of vibration signal is necessary for proper signal processing, using high sampling frequencies is quite costly since the same sampling frequency is dictated for all channels by the DAQ board. As a result, some tests are carried out with very high (up to 200 kHz) sampling rates to find out the amount of variation between rotor and motor side speed values. The summary of performed tests is given in Table 3.3. It is clear from this table that as the speed increases so does the deviation. This can be attributed to the decrease in number of points acquired per rotation as the speed increases since the same (maximum available) sampling frequency is used for all measurements. Based on this evidence the difference is attributed to inadequate sampling frequency rather than the slippage in the belt and therefore the measurements taken on the motor side are regarded as the true speed values.

Nominal	120	300	600	1200	1800	2400
Motor encoder	120.01	299.93	600.1	1199.95	1800.05	2399.91
1/rev signal	120.04	300.21	600.5	1200.7	1801.1	2401.9
% difference	0.02	0.04	0.07	0.07	0.07	0.08

Table 3.3 Comparison of speed values on motor and rotor side (all speed values in rev/min)

The balancing of the blisks under rotation had also to be addressed. Note that even if they are perfectly symmetrical, depending on the mistuning pattern used, balancing might still be needed. To this end, a balancing plane is used and is mounted on a taper-lock used to secure the blisk to drive shaft. Single-plane, static balancing is found adequate and is done by attaching masses of various magnitudes to the balancing plane at required angular positions.

3.3.4 Excitation system

The excitation system is required to simulate EO type excitations, as this is the case in most of the practical situations, and by means of non-contacting exciters. There are a number of ways in which this can be achieved. One of the options is to hold the test piece and the exciters (electromagnets or speakers) stationary and to change the phases of the signals sent to exciters accordingly [49,55]. However, in this approach one has to have as many exciters as there are blades. Bearing in mind the size of these exciters, for bladed disks having large numbers of blades there may not be enough room to accommodate them circumferentially. Another option is, again, to hold the testpiece stationary but to mount the exciter(s) on a rotating fixture. In this way realistic phased pulses will be generated but since the test piece is not rotating the effects of centrifugal forces on the forced response will not be observed. The option which eliminates all these disadvantages, and the one which is used in this study, is to spin the test piece in vacuum and to use stationary exciters [45]. The evacuated environment will eliminate the unwanted effects of aerodynamic forces and the rotation of test piece will enable realistic forcing and inclusion of centrifugal effects.

Throughout the rotating tests, permanent magnets of various sizes were used to excite the bladed disks. That is to say, the frequency of excitation was determined by the rotational speed. Ideally, the use of electromagnets would be

preferable as the frequency of excitation could be varied independently of rotational speed. However, the force produced via these magnets was so small that the required magnitudes could only be generated when they were placed at very close proximity of the blisks. This was considered unsafe under rotating conditions that the use of electromagnets was confined only to the static measurements. Almost all of the tests (although for some friction-damped tests 2 magnets were used briefly) were carried out by using only one magnet. The permanent magnet is secured to a holding and positioning mechanism such that the magnetic force is exerted on the blade tips. The magnet and the holding system are connected via a force transducer which measures the magnet's reaction in the presence of a passing blade, and the holding mechanism is secured to the back plate. The magnet's proximity to the bladed disks is adjusted via a stepper motor which can be controlled from the DAQ PC through a code written in Matlab. The gap can also be adjusted manually using a knob. A cross section of the excitation system is given in Figure 3.11.

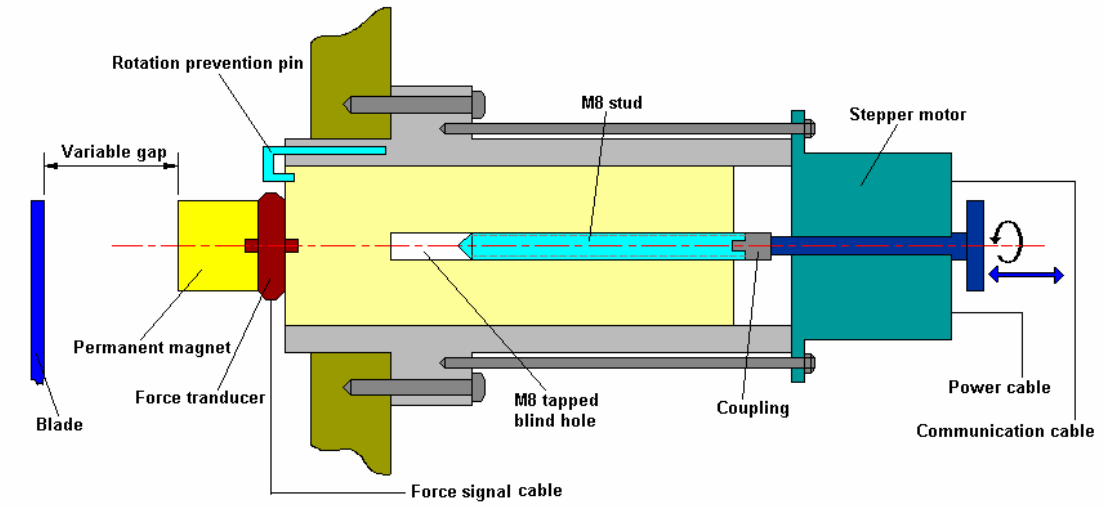

Figure 3.11 Excitation system

Mainly two different types of permanent magnets supplied by MagnetSales company (http://www.magnetsales.co.uk/) are used. For mistuning tests on Blisk-2 a Samarium deep-pot magnet (SMDP-00163, ∅20) with 25 kg maximum pull force is used. Whereas for tests with friction dampers on Blisk-1 a magnet of

the same type but having a 40 kg maximum pull force (SMDP-00105, ∅25) is used. This is necessary, as higher forces are required to make dampers work effectively.

3.3.5 Vibration measurement system

As stated in the design requirements, the response measurement transducer must be a non-contacting one so as not to perturb the tested structure's dynamics. That is to say, traditional techniques such as strain gauge—slip ring or telemetry arrangements cannot be employed. As a non-contacting measurement technique, "tip-timing" has been used with considerable success for turbomachinery blade vibration measurements where an electromagnetic or optical probe attached to the turbomachine casing is used to measure the blade tip arrival times as they rotate past this probe. In the presence of vibration, each blade passes the probe earlier or at a later time compared to non-vibrating case, depending on the phase of their vibration at the time of arrival. Further processing these arrival times, the vibration in the tangential direction is obtained. This implies that the technique cannot be used with Blisk-2 as no vibration in this direction for the family of modes of interest is produced. Additionally, the use of this technique requires particular expertise, and high-standard equipment and positioning tolerances to resolve the required information.

As a result, it was decided to use an LDV transducer. Besides being a non-contacting device, the LDV offers acquisition of spatially dense measurements in fairly short times as well as providing easier instrumentation. Two vibration measurement techniques; one using a tracking LDV and another using a scanning LDV are used. Most of the rotating vibration measurements are performed using the first, so called the self-tracking system. Several techniques using scanning LDV are also used, mainly on stationary blisks, to measure radial and circumferential deflection shapes and the direction of vibration.

3.3.5.1 The LDV transducer

The LDV transducer, as the name implies, works on the basis of Doppler effect, which states that light from moving objects will appear to have different wavelengths depending on the relative motion of the source (vibrating test object) and the observer (LDV transducer); longer when the object is moving away from the observer (a red-shift), and shorter when it is approaching to the observer (a blue-shift). The principle behind the operation of an LDV transducer can be explained simply as follows: light produced by a laser source is split into two beams of the same amplitude by a beam splitter, one directed to a fixed reference and the other to the vibrating target. Following the same path back, the beams are combined by the same splitter and send to a photodetector. Since the light from the target is optically mixed with an equally coherent reference beam and heterodyned on the photodetector surface, the resolution of the sign of the vibration velocity is achieved by pre-shifting the reference beam's frequency by a known amount. The signal received by the photodetector is then frequency demodulated by a suitable Doppler processor and the vibration velocity of the target is worked out. The LDV transducer used in measurements was a single-beam OMETRON VPI Sensor and its working principle is shown schematically in Figure 3.12.

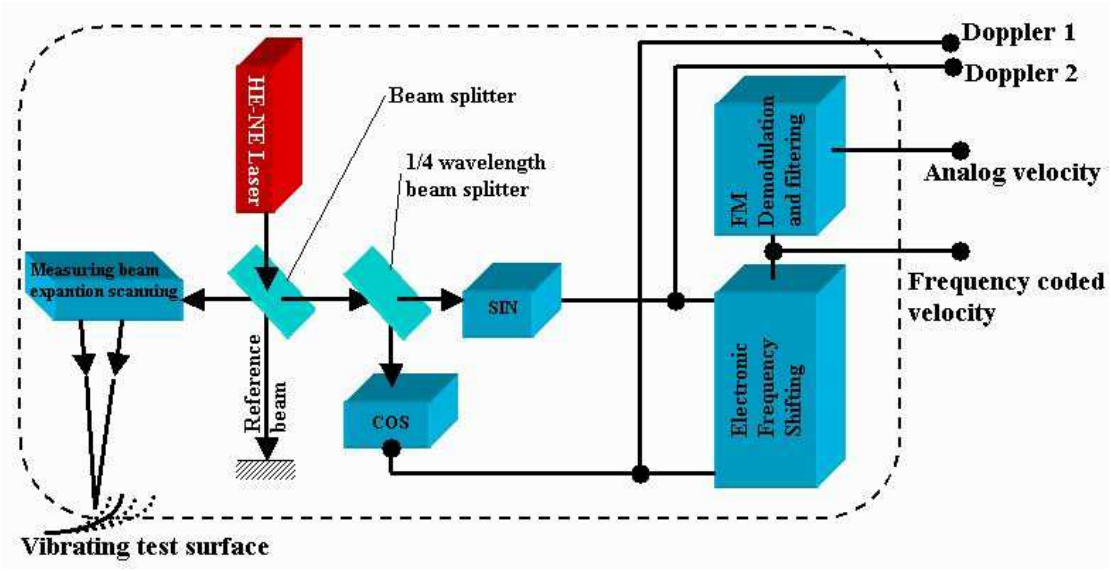

Figure 3.12 Working principle of OMETRON VPI Sensor (Adapted from [80])

The transducer consists of one optical and one power supply units. The generated laser beam is positioned via two deflection mirrors (X *and* Y) in the optical unit. These mirrors can be driven by external signals through the power supply unit. The transducer has a frequency range of $DC-300\ kHz$ and can measure velocities from $\pm 1\mu m/s$ up to $\pm 1000mm/s$. The velocity signal is output either via a $\pm 10V$ BNC coaxial socket or $\pm 1V$ BNO twinaxial (differential) socket. Signals outside these ranges are truncated. There sensitivity options, (low, medium and high) with corresponding $1000\,mV/(mm/s)$, $100\,mV/(mm/s)$ and $10\,mV/(mm/s)$ sensitivity values are provided for the BNC socket. Additionally, 4 frequency ranges labelled from 1 to 4 are available, each applying a low-pass filter to the analogue velocity signal with different cut-off frequencies. For the measurements of this study HIGH-1 ($10\,mV/(mm/s)$ - $500\,Hz$) and MED-3 ($100\,mV/(mm/s)$ - $5\,kHz$) options are found suitable.

3.3.5.2 The self-tracking measurement system

Ideally, the deflection mirrors of the LDV transducer can be driven at frequencies up to 80 Hz. However, due to inertia of the mirrors and the rotors driving them, the laser beam does not move in phase with the input signal but is delayed by a certain amount resulting in a phase shift. As the frequency is increased, this phase shift becomes significant (in fact, it is an almost linear function of frequency [79]) and the amplitudes at which the mirrors can be driven get significantly reduced. With the implementation of proper phase correction algorithms, frequencies up to 30 Hz have been successfully applied in the past. However, this value is well under the maximum speed value of 4000 rev/min (~66.7 Hz) and therefore the tracking of a given point on the rotating bladed disks cannot be achieved utilising these mirrors. Thus, a system of measuring vibration response on a given point on the bladed disks, independent of rotational speed is designed. This so-called the self-tracking technique is based on the idea proposed by Lomenzo et.al. in [76] but is considerably

modified. Here most notably the fold mirror of [76] is replaced by a fixed annular conical mirror. This way laser beam can be sent to the blade tips at a right angle. Additionally a means of switching measurements from blade to blade is introduced. The devised tracking system is given in Figure 3.13.

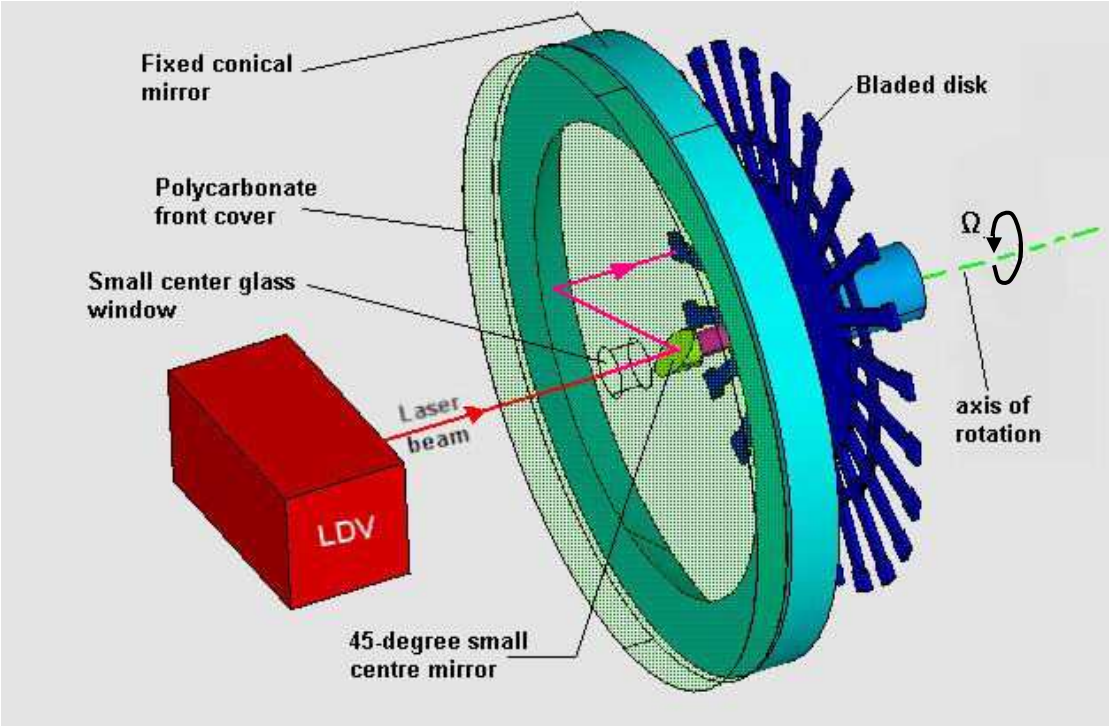

Figure 3.13 The self-tracking system

In Figure 3.13, the laser beam passes through the small centre glass window in the centre of the polycarbonate front cover and lands on the central 45-degree small mirror rotating with the bladed disk. It then is directed to the fixed 45-degree conical mirror before it finally arrives at a particular blade tip. The central small mirror is mounted on a spring-loaded push rod which runs all the way through the drive shaft to the rear end of the rig where it is fitted with a slotted mechanical indexing device. The push rod is integrated with 3 pins at 120 degrees which sit on a 24-tooth bevel gear fixed to the drive shaft thus enabling their engagement. When the pneumatic actuator is powered, it moves the push rod forward consequently disengaging it from the drive shaft. Since the indexing device moves with the push road, guided pins in the slots of indexing device force the push rod to be rotated as well as moving forward, precisely by 15

degrees at each push. When the pneumatic actuator is released, the now compressed spring moves the push road straight back without rotating it. Since the angle between two neighbouring blades is 15 degrees, the laser beam is now directed to the next blade. With the release of pneumatic actuator the pins on push rod sit back on the bevel gear only shifted by 15 degrees. Details of indexing mechanism can be seen in Figure 3.14. As this process can be performed during the operation of the rig, all the blade responses can be measured without interrupting the measurement session.

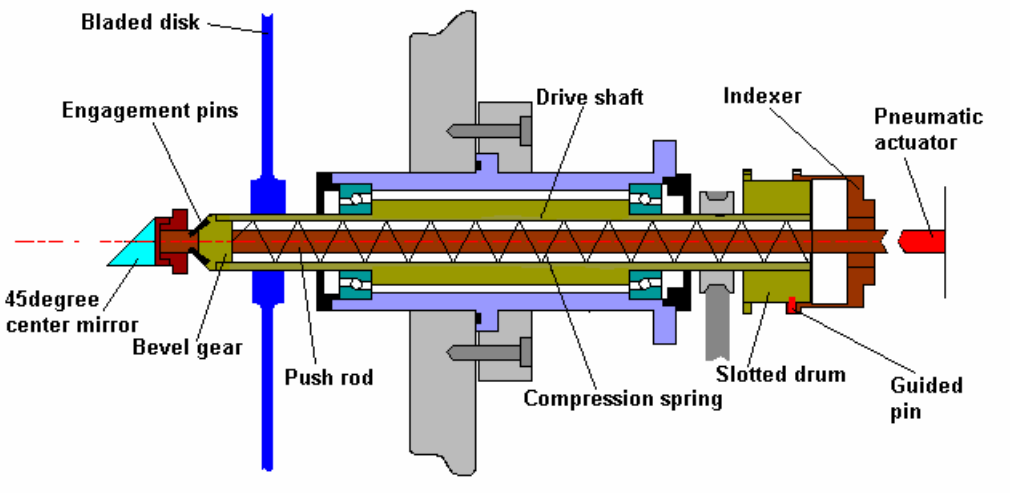

Figure 3.14 Indexing mechanism

The indexing mechanism described above requires the operator to push a button each time a new blade is to be measured. However this process can easily be automated by designing a simple circuit in combination with a timer/counter card or a simple chip capable of processing commands sent via RS232. As a result the laser beam can be automatically switched to the next blade once the measurements on the current blade are completed. This can save considerable time when the measurements are to be carried out for various speed values (see Section 3.4.2).

3.3.5.3 Scanning system

Mainly two scanning techniques are used Conical Circular Scanning and Line Scanning, which are both shown in Figure 3.15 (a) and (b) respectively. In case of circular scan the external mirrors (fixed conical and small centre mirrors) and mechanical indexing are not used and polycarbonate front cover is replaced by a fully transparent, hardened glass window to enable optical access. The blisks then can be scanned at a frequency Ω in a circle, by applying suitable $Sin(\Omega \cdot t + \alpha)$, and $Cos(\Omega \cdot t + \beta)$, waves to the LDV-integral beam-deflection mirrors. Here the arbitrary phase angles α and β are introduced to account for phase correction due to mirror delay. Since the bladed disks are discontinuous at the blade tips, measurements in this system are taken at the near-continuous platform edges and circumferential ODSs are extracted. In case of line scan the blisks are scanned along the blade lengths to measure radial ODSs. This is used in static measurements only and the blisks are oriented such that the blade measured is vertical so that one mirror can be used for scanning. Both techniques when applied to stationary blisks are excited by an electromagnet at desired frequencies.

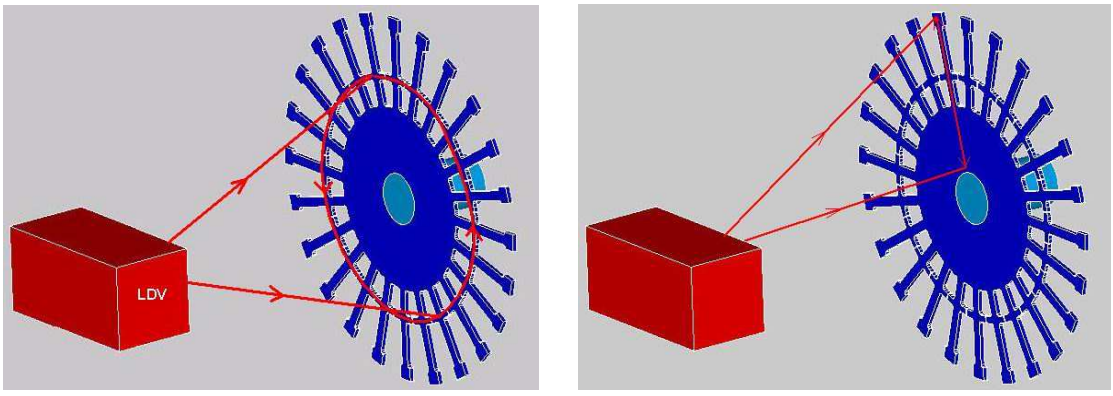

Figure 3.15 (a) Conical Circular Scan, (b) Line Scan

3.3.5.4 LDV alignment

Despite its major advantage of working regardless of rotational speed, the self-tracking system is prone to misalignment problems, as indeed all other LDV

measurement techniques are. In an ideal arrangement, the laser beam is normal to the plane of rotation of the test piece. The deviations from this plane will result in errors in the position of the laser beam as well as in the measured vibration velocity. Misalignment errors in this particular test setup are mainly introduced in either because (i) the laser beam is not aligned with the axis of rotation (Figure 3.16 (a)), and/or (ii) fixed conical mirror's position is not properly adjusted with respect to the test piece (Figure 3.16 (b)). In a misaligned setup, the LDV signal will contain a proportion of the blade rotation velocity, at rig rotation frequency, as demonstrated in Figure 3.16 (c).

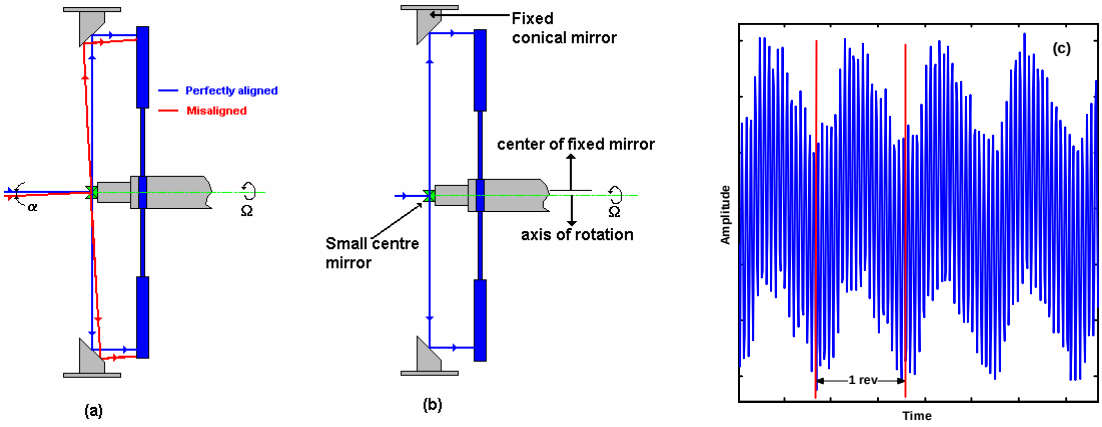

Figure 3.16 Sources of misalignment (a, b) and its reflection on velocity signal (c).

As it is evident from Figure 3.16 (c), misalignment introduces slow frequency oscillations (1 per rev in this case) on top of normal vibration frequency. Though this can be eliminated by applying a high pass filter, it has been observed that in some cases misalignment causes DAQ board to overload for signals it would not if the alignment was perfect. This happens because peak-to-peak amplitude of the signal is increased (see Figure 3.16 (c)). Additionally, misalignment may vary the measurement spot with respect to the test piece introducing measurement uncertainties. In order to alleviate these effects, the position of LDV head and orientation of the fixed conical mirror should be checked and properly adjusted, if necessary, before a measurement session is started. In order to achieve this, the LDV head is placed on a milling machine traverse which enables precise

horizontal and vertical adjustments. In addition, an adjustable 4–leg platform is placed between the LDV and the milling machine which provides a means to tilt the LDV head. Horizontal rotation of the head is done by the operator. The correction of the fixed conical mirror's orientation is done via an adjustment mechanism in which in-plane translation and out-of-plane rotation of the mirror can be controlled. Details of both the LDV head and fixed mirror adjustment configurations are shown in Figure 3.17.

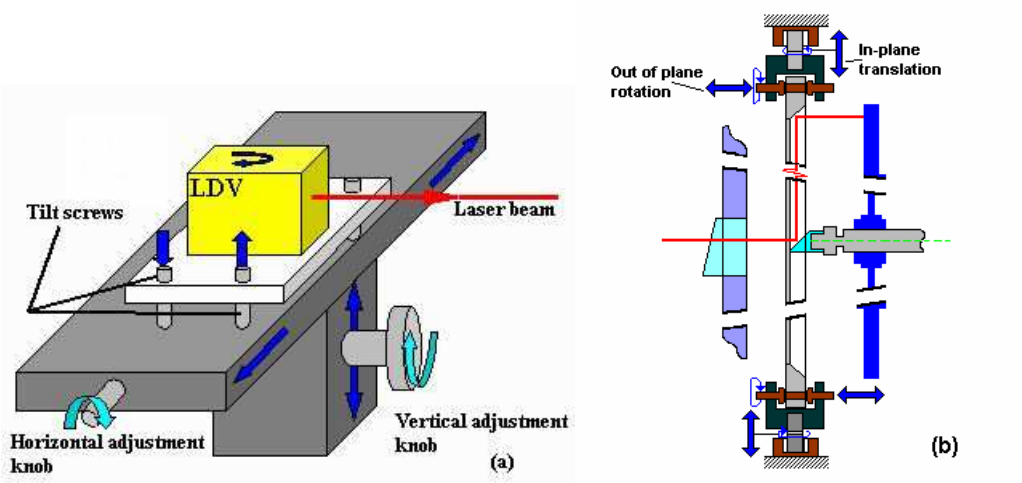

Figure 3.17 (a) The LDV head and (b) the fixed mirror positioning details

A practical and quick way of achieving the LDV alignment by utilising the adjustments shown in Figure 4.14 is given in Figure 3.18. Here the 45-degree small centre mirror is replaced by a flat one but tilted by a few degrees. The LDV beam is fired though a small hole, barely the size of laser beam, in the middle of the suspended plate and onto the centre of tilted mirror (i.e., the centre of drive shaft). When the mirror is rotated at a very slow speed, the reflected LDV beam tracks a circle on the plate. By making use of the adjustment controls, the LDV beam can be forced to follow one of the concentric circles on the plate. This, assuming that the axis of rotation is normal to the suspended plate, will sucessfuly align the LDV beam with the axis of rotation.

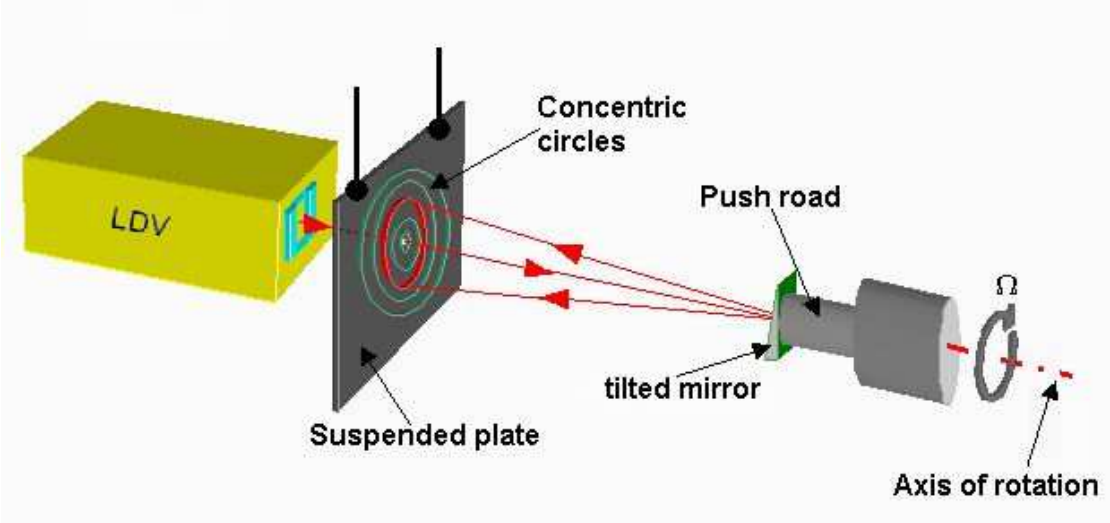

Figure 3.18 LDV alignment technique

When the laser beam is close to normal to the glass window, such that the reflection off the glass window surface falls into the LDV aperture, no vibration response will be measured since the beam coming from a non-vibrating source (the glass window) is processed to work out the velocity (Figure 3.19 (a)). Thus, the small glass window in the centre of the front cover is tilted as shown in Figure 3.19 (b). This way the reflected beam is prevented from coming back into the LDV interferometer. Note that this is not a problem with circular and line scanning techniques (see Figure 3.15) as the laser beam is never normal to the glass window.

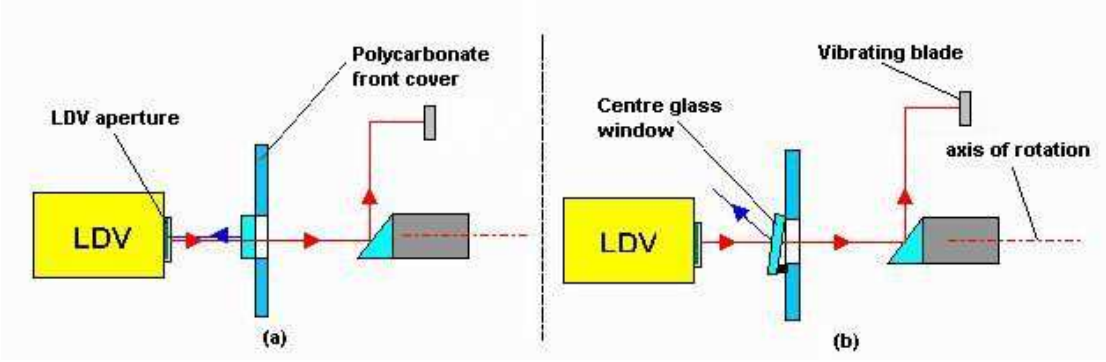

Figure 3.19 (a) No vibration response is measured; (b) true vibration response is measured.

3.3.5.5 On the limitations of LDV transducers

While intrusive measurement techniques are not suitable for the current study, the LDV transducers are not without their own complications. Since these are optical devices, line of sight is a necessity which may not always be the case, especially when some internal components are of interest. Moreover, though not a problem for the self-tracking system, the application of scanning LDV to a rotating structure is limited to relatively low speeds. This together with the strict alignment requirements mean that the in-situ use of these transducers on realistic structures such as turbine jet engines is still a remote possibility. Furthermore, despite some attempts made at applying them to impact modal testing [81], their application has been mostly confined to measuring one frequency at a time.

One of the most important problems in LDV measurements is the sudden sharp jumps, or dropouts, in velocity signal due to so called speckle noise and demands a closer look as it limits the accuracy of the measurements, typically to 1% [79]. The speckle noise is a phenomenon related to speckle pattern which is formed when surface roughness of the test object is comparable with the wavelength of the laser light. In most of the real applications the test surface is comparably rough and the light reflected back from the LDV has a granular appearance referred to as speckle pattern. This pattern changes as the location of the laser beam changes on the test surface and tends to get coarser as the laser beam spot gets smaller. Therefore for a correctly focused laser beam the intensity of light collected by the LDV fluctuates strongly as the laser beam moves on the test surface. When the Doppler signal amplitude is lower than a threshold value, the demodulation circuit in LDV cannot function properly and results in “dropouts” in velocity signal [80]. This impairs the quality of the measurements and limits the performance of the measurement system

For the self tracking measurements, once the laser beam is focused and a proper velocity signal is received, assuming that this spot does not change in time, the

speckle noise will not be a problem. However this requires that the amplitude of vibration is not large enough to cause the measurement spot to change and that the LDV beam to be perfectly aligned with the axis of the rotation of the test structure. In practice, though it can be eliminated to a great extend (see previous section), misalignment cannot be removed completely and causes the laser spot to move across the test piece, making the velocity signal more susceptible to speckle noise. The same effect can be observed when the large vibration amplitudes are present. A typical example demonstrating the coupled effect of both the misalignment and large vibration amplitudes is given in Figure 3.20. In Figure 3.20 (a) tracking measurement on a particular blade under rotation is given. Here a frequency modulation due to misalignment and amplitude modulation due to dropouts caused by speckle noise are observed. Note that the dropouts are periodic (see point A in Figure 3.20 (a)), occurring at the same locations on the structure. When the amplitude of input force is reduced, Figure 3.20 (b), thus reducing the vibration amplitude, the dropouts and consequently the amplitude modulation is eliminated. However, the misalignment remains unaffected. The reflection of these dropouts in the frequency spectrum is in the form additional pseudo-frequency components, Figure 3.20 (c) which are not present otherwise, Figure 3.20 (d). When EO response is to be extracted, the presence of speckle noise does not introduce errors in the frequency but may slightly modify the amplitudes. However, when for example, a z-mod plot is to be constructed using frequency spectra alike, one has to pay attention, as these pseudo-components will appear as resonances.

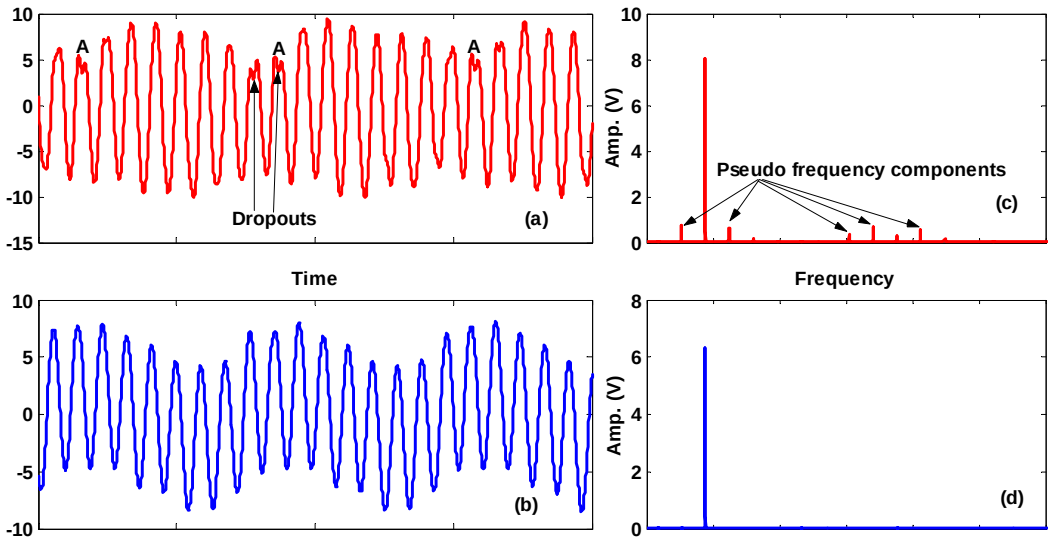

Figure 3.20 Velocity signals with (a), and without (b) dropouts, and the corresponding frequency spectra, (c) and (d).

The adverse effects of speckle noise, however, may be minimised by using a proper working distance, applying reflective coating on the measurement surface, properly focusing the laser beam and using a suitable sensitivity range as all these precautions will increase the intensity of the light collected by the LDV and make the signal strong enough to exceed the mentioned threshold. By paying attention to above-mentioned precautions, in general, it has been possible to acquire satisfactory velocity signals, both for tracking and scanning measurements in this study, though there have been cases such as the one shown in Figure 3.20. However, this meant that H-1 (i.e., minimum frequency range) sensitivity level had to be used. Fortunately, the frequencies of interest were within the range covered by this sensitivity option.

3.3.6 Safety provisions

It is demonstrated through FE analysis (Section 3.3.2) that the test chamber is strong enough to withstand forces which may result due to failures such as blade-loss. However in the event of bearing failure or sudden vacuum loss, the blisks may come loose and the front covers used in the tests may be detached or

broken. In order to confine any flying object in the event of such failure a safety cage enclosing the test chamber is designed and manufactured, Figure 3.21. The rest of rig is also encircled by transparent polycarbonate screens to retain any parts should they come off under rotation. An emergency shut-down is provided for the motor drive, to remove power, allowing the rotor to coast down to zero speed.

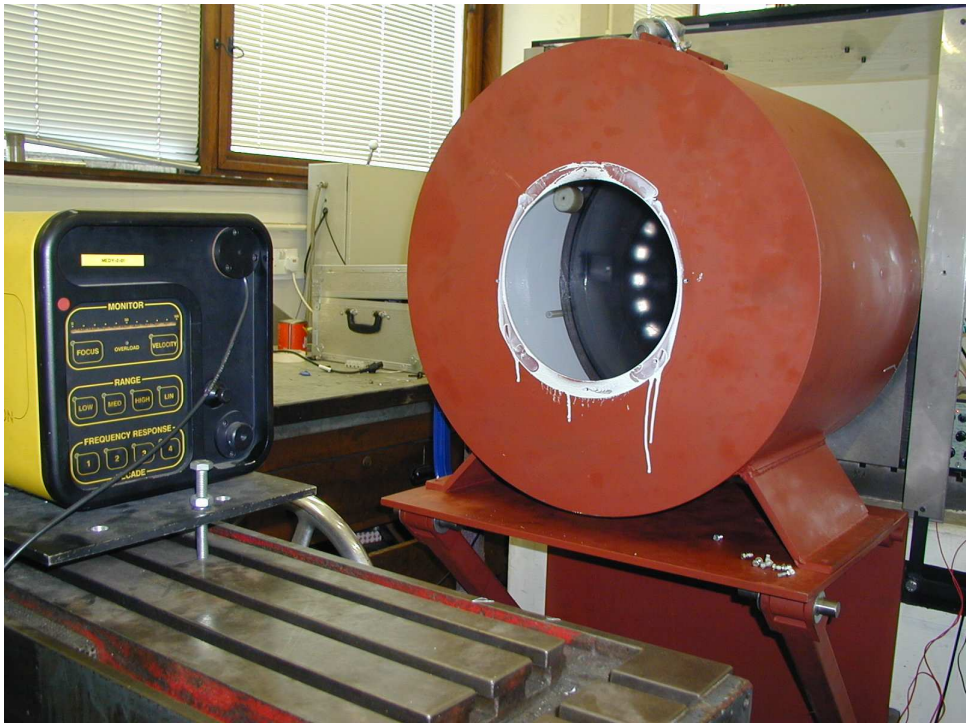

Figure 3.21 Containment Enclosure (set up for conical LDV scanning, with the Small-Aperture Cover removed).

3.4 Data acquisition and processing

3.4.1 Hardware

The data acquisition hardware consists of a DAQ PC as mentioned above, an HP VXI (a high-spec standard DAQ system-based DAQ frame, an LDV, a force transducer, an optical sensor, and BNC and RS232 cables. In addition to these a general purpose National Instrument (NI) DAQ card, PCI-6024E, is used in friction damped rotating test in parallel with the VXI frame. The layout of DAQ system is given in Figure 3.22.

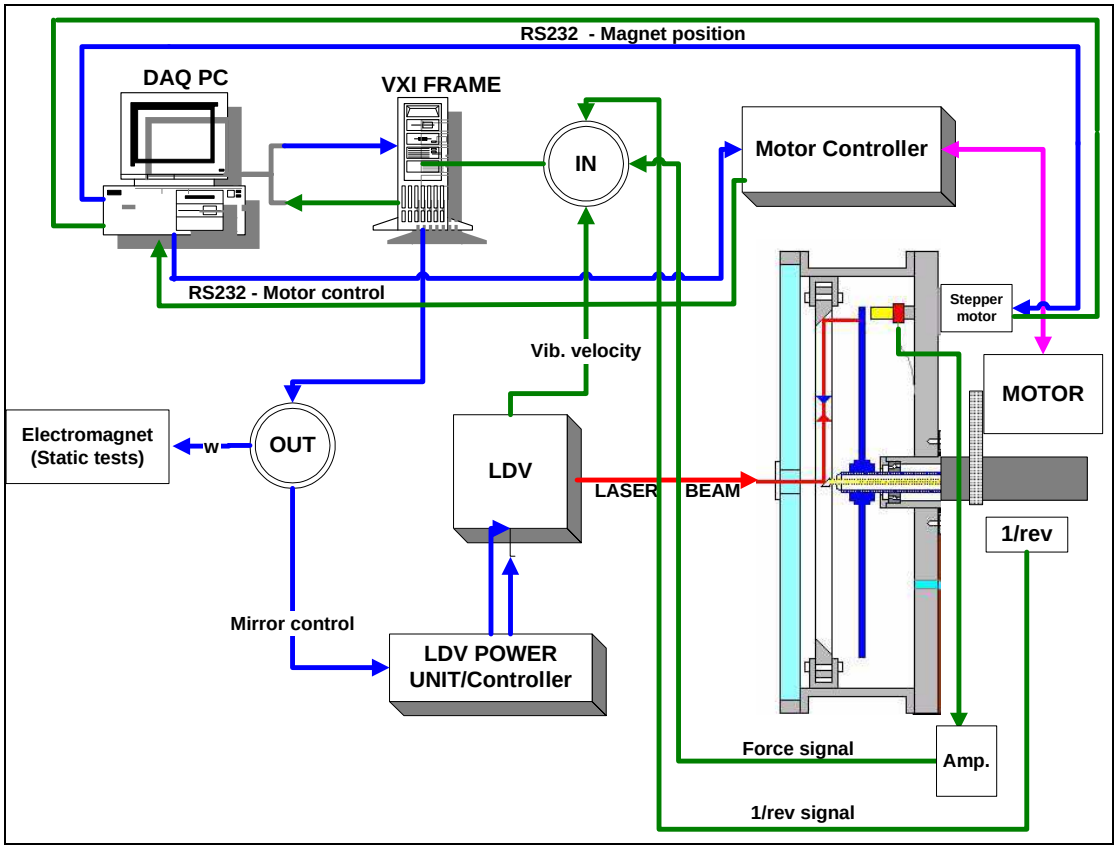

Figure 3.22 Data acquisition layout (—output, —input)

The VXI system is connected to the DAQ PC via a FireWire bus (IEEE 1394). It comprises a controller (HP E 8491A), a digitiser (HP E 1432A) and a generator (HP E 1434A). The digitiser's specs are: 16 input channels, 16bit A/D converter per channel, 32MB memory. With this board it is possible to store 8 million samples on-board at a precision of 32bit. The generator's specs are: 4 output channels, 16-20bit A/D converter per channel, 32 MB memory, and built-in sine, step, square, arbitrary and random wave forms. The maximum sampling frequency, $f_{s\max}$, with the digitiser is 51.2 kHz and the valid sampling frequencies, f_s, are given as $f_{s\max}$ divided by powers of two, and $f_{s\max}$ divided by five and by powers of two. There is an on-board anti-aliasing filter which is set at $f_s/2.56$. The NI card has 12 input and 4 output channels and can be used as a timer/counter card as well. The sampling frequency range with this card is 0-200 kHz.

In the long-run stepped-speed rotating measurements (i.e., measurement sessions in which a given speed range is measured at given steps), sampling frequencies of 800 Hz and 1280 Hz are mostly used depending on the max. frequency of interest. The use of relatively small sampling rates has the advantage of storing long data samples to carry out proper signal processing at low costs. However when the phase information is to be extracted satisfactorily, which is especially of interest in friction damper tests, these sampling frequencies do not provide the necessary resolution. Since the same sampling rates has to be used for all the channels of the VXI system, it has been decided to use a second DAQ card, NI-PCI-6024E, to measure short samples at a relatively high sampling rate to obtain accurate phase information. This way, using both of the DAQ boards, the necessary information is collected while the data lengths are kept manageable.

3.4.2 Data acquisition

High-level instrument control and data acquisition is done via a visual code written in MATLAB The low-level drivers controlling the DAQ board are provided by the manufacturer. The code consists of a main panel via which appropriate input and output DAQ boards, channels and their attributes can be specified; a motor control tool which sets and controls the motor speed, range and steps; a magnet position tool which controls the stepper motor to adjust the magnet-blade gap; an indexer tool which switches the laser beam from blade to blade, and various processing tools to design band-pass filters, display/compare ODSs etc. All the mentioned tools can be combined to complete a measurement session automatically without user intervention. More details on the code and snapshots of the user interface can be found in Appendix B.

Since a single static excitation source is used, frequency response curves for various EO excitations are measured by changing the rotational speed. For an

nEO response, a rotational speed range around the $nND - nEO$ lines crossing is selected. Note that this location is fairly accurately estimated via FE models in the test planning phase of the measurements. Then the discrete speed values at which the response is acquired are decided. Generally, speed values are clustered around resonances and coarser step sizes are used away from resonances. The minimum speed change which can be achieved (i.e., the minimum change in speed which makes sure that the new speed is higher or lower than the previous value depending on the direction of sweep) is 1 to 2 rev/min (0.017-0.033 Hz) depending on the speed range used (see Table 3.3). Then the motor speed is varied through this range and the vibration reponse together with the force and 1/rev signal are streamed from the DAQ board for each value in the range. The bladed disks used here are extremely lightly damped when not fitted with external damping elements. In order to make sure that the steady-state vibration levels are reached, it is necessary to wait up to one minute each time the speed is changed to a new value. Assuming that k seconds worth of data are to be acquired, and p seconds pause is necessary between each speed change, the time it takes to complete a measurement session of N speed points for all blades can be estimated as $N \cdot (k + p + \Delta) \cdot 24$ seconds, where Δ is a computer-dependent value (time needed to stream and store the data, and generally around 1 second). For a measurement session of 100 speed points where 5 seconds worth of data is collected, and a minute's pause is introduced between each successive speed change, assuming $\Delta = 1\,\text{second}$, the required time to measure 24 blades is 44 hours! In a situation where the indexing is automated and assuming that indexing the laser beam from blade to blade takes 10 seconds, this time can be reduced to 12 hours. With implementation of a proper timer/counter card, indexing time can be reduced to less than 5 seconds, thus bringing the measurement time for this particular example under 10 hours.

3.4.3 Data processing

The methods of processing the force transducer and tachometer signals have been given in previous sections. Here the processing of measured velocity signal will be given. A flowchart explaining the various stages of frequency response calculations is given in Figure 3.23. Note that since the excitation frequency is varied by means of changing the rotor speed, this loop is repeated for all speed values and engine orders, albeit in a computationally efficient way. Three ways of calculating the EO frequency response are considered. In all cases, vibration data are first low-pass filtered (anti-aliasing filter) and then flat-top windowed.

In the first option, the signal is band-pass filtered with a pass-band covering a small range around the desired vibration frequency (i.e., $EO \cdot \Omega - \delta < EO \cdot \Omega < EO \cdot \Omega + \delta$, where Ω is rot. speed and δ is a small value such that only a few frequency bins are covered). Then an FFT is applied and the maximum amplitude of the output spectrum is recorded as the amplitude of vibration at that particular speed value. In the second option, the FFT is applied and the amplitude of the desired frequency is retrieved by finding the maximum amplitude in the spectrum, in a frequency range similar to the one given above. In the third option, assuming that the rotational speed is known reasonably accurately, only the frequency bins at the frequency of vibration ($EO * \Omega$) are calculated to obtain the frequency response.

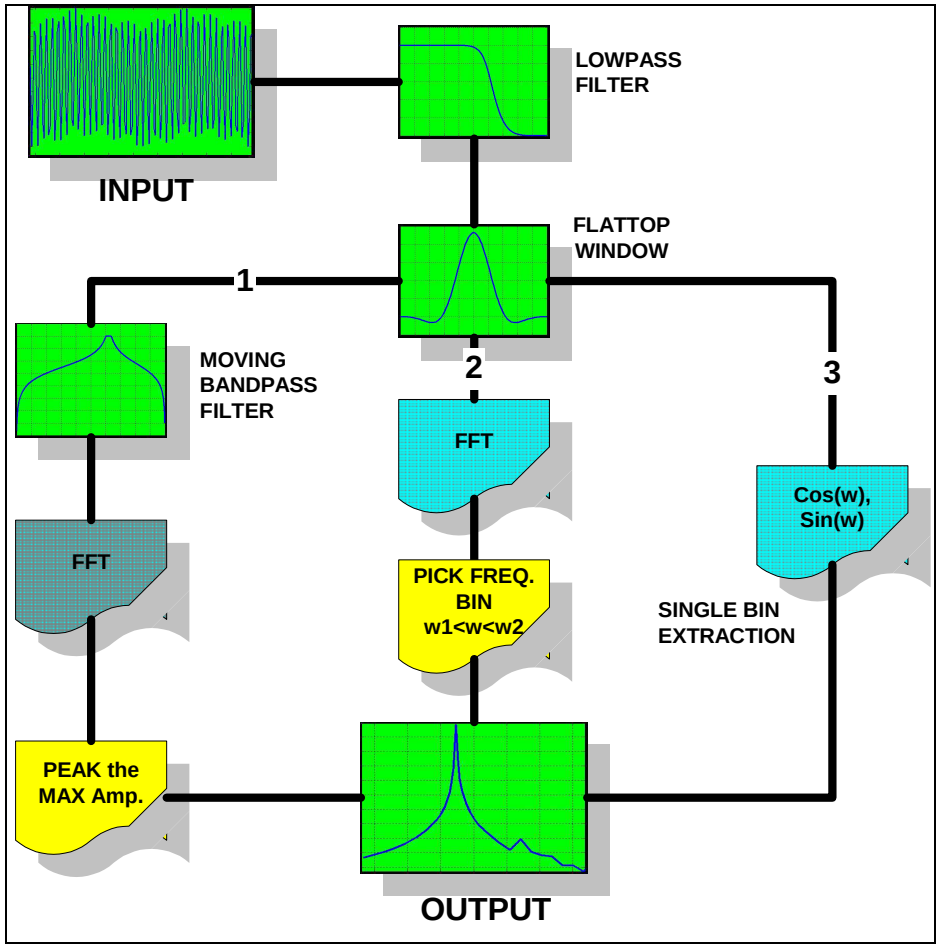

Figure 3.23 Process of EO response calculation

In theory, all these options provide the same information. However, the first one takes a considerable time to run since filtering is a computationally expensive process. The last option is particularly useful, and especially so in phase extraction, when only short data samples are available.

3.5 ODS measurements using CSLDV

As mentioned before, throughout the measurements several LDV scanning techniques are made use of: line scan and circular scan for ODS measurements in radial and circumferential directions respectively, and conical scan for direction of vibration measurements. For the details of these techniques, references [77] and [79] can be consulted. However, the circular scanning technique is particularly of interest in the current study and is extensively used in stationary

blisk measurements as well as in some rotating ones. Thus, a brief explanation of the theory and application is thought appropriate. An electromagnet is used to excite the blisks to recover these ODSs under stationary conditions and a note on the application of this kind of forcing is warranted.

3.5.1 Electromagnetic excitation

In fact, a.c magnet excitation is always attractive such that when driven by a sinusoidal signal at ω_n, the excitation experienced by the structure is modified and is at $2\omega_n$. However in the present case, it has been possible to excite the blisks at a natural frequency, ω_n, by driving the magnet at the same frequency, ω_n. In practice, when the blisks vibrate at frequency ω_n, the magnet-blade gap is modulated at this frequency. Given the fact that the magnetic force is related to the gap by an inverse square rule, a force input at frequency ω_n is generated via this modulation. And it is this component that maintains the vibration. Naturally, the degree of this effect depends on the modulation at the drive point, which is maximised at natural frequencies. To understand this better consider the sketch given in Figure 3.24. Assuming that the blade shown vibrates at frequency, ω, the clearance between the magnet and the blade can be given by

$$x(t) = \delta - aSin(\omega t)\,. \qquad (4.3)$$

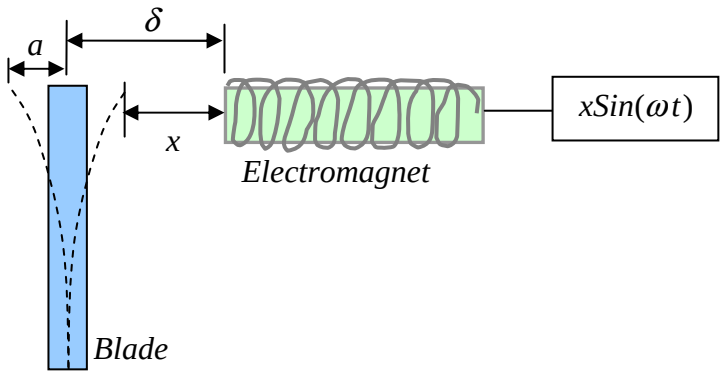

Figure 3.24 Electromagnetic excitation on a stationary blade

Suppose that the magnet is driven at the same frequency, ω, in the form

$$f(t) = bSin(\omega t), \tag{4.4}$$

and recalling that the magnet force is always positive, the force experienced by the blade may be related to the gap and the input force as follows

$$F(t) \rightarrow \left| \frac{1}{(\delta - aSin(\omega \ t))^2} bSin(\omega \ t) \right| \tag{4.5}$$

Assuming above relation to be an exact representation of force, a typical force signal calculated for a relatively small vibration amplitude, a (i.e. stiff blade or large gap) is given in
Figure **3.25** (a). The corresponding frequency spectrum is also given in
Figure **3.25** (b) in which a dominant frequency component at 2ω is evident and no force is produced at frequency ω. However, when the vibration amplitude, a, is comparable to magnet-blade gap, δ, (i.e. flexible disk or small gap), the forcing function takes the form given in
Figure **3.25** (c). In this case, the main frequency component is obtained at input frequency ω (
Figure **3.25** (d)), as well as some other comparable components at its integer multiples. The blisks used in this study are fairly flexible. Additionally the magnet needed to be positioned reasonably close to the blade so that enough force could be produced. Thus, the magnet blade gap was significantly modulated, and especially at resonances, that blisks were excited by driving the electromagnet at natural frequencies.

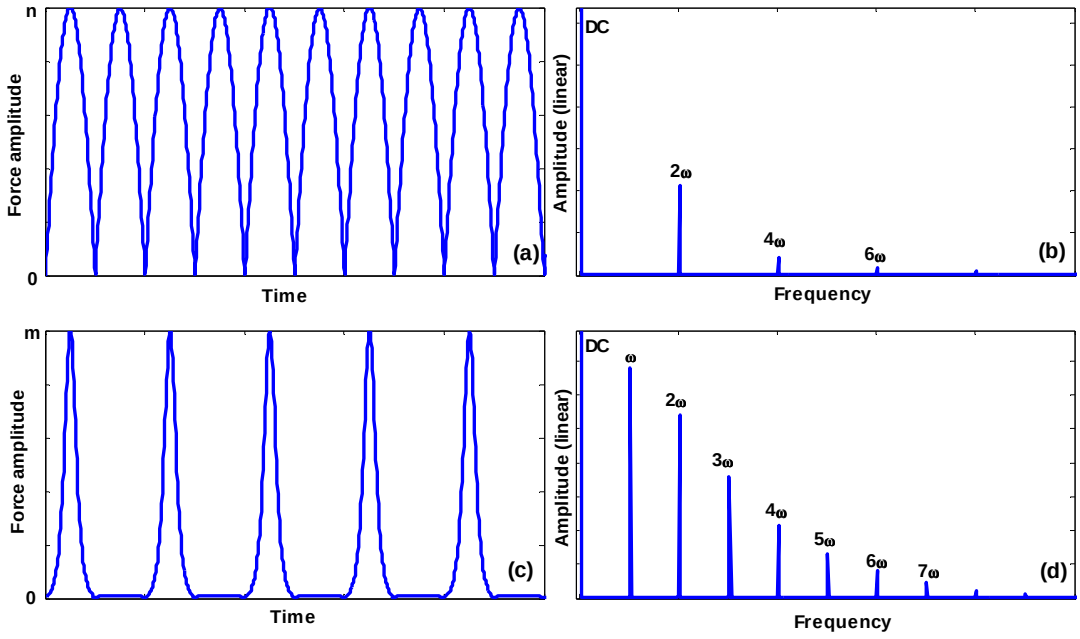

Figure 3.25 Electromagnet force experienced by a blade (a) large gap and (b) frequency spectrum. (c) Small gap and (d) frequency spectrum

3.5.2 ODS by circular scanning

Assuming sinusoidal vibrations at a frequency of ω, the out-of-plane sinusoidal vibration velocity, V_z, of a circular structure, such as a disc, can be written as:

$$V_z(t,\theta) = V_a(\theta)Cos(\omega t) + V_b(\theta)Sin(\omega t) \qquad (4.6)$$

where $\theta = \Omega t$ is the angular position around a scan circle at a given radius for a scan frequency of Ω. For a given n ND mode, $V_a(\theta)$ and $V_b(\theta)$ are the amplitude distributions of the spatially orthogonal cosine and sine modes in the circumferential direction. For a constant scan frequency, V_z is a function of time only. In this case the ODS can be obtained by demodulating the CSLDV output. The most common way of doing this is simply to multiply Equation (4.6) by $Cos(\omega t)$ and $Sin(\omega t)$, which yields:

$$\frac{1}{2}V_a(\Omega t) + \frac{1}{2}V_a(\Omega t)Cos(2\omega t) + \frac{1}{2}V_b(\Omega t)Sin(2\omega t) \qquad (4.7)$$

$$\frac{1}{2}V_b(\Omega t) + \frac{1}{2}V_a(\Omega t)Sin(2\omega t) - \frac{1}{2}V_b(\Omega t)Cos(2\omega t)\,. \qquad (4.8)$$

If a sufficiently slow scan frequency is used, the frequency components at around 2ω in Equations (4.7) and (4.8) can be removed by applying a low-pass filter. Following that these equations yield real and imaginary parts of the ODS.

The LDV output from a sample circular scan session on Blisk-1 is given in Figure 3.26 (a). The blisk is scanned at platform level using a scan frequency of 0.5 Hz while being excited by an a.c. magnet at a natural frequency. The individual blade responses are clearly identifiable from the given circular scan output but better demonstrated in Figure 3.26 (b). Note that dropouts occur in-between blades since the platforms are discontinuous, and within a blade due to speckle noise. The ODS obtained by demodulation is also given in Figure 3.27, in 3D and 2D form. The 2D option will be used from now on, as it is easier to visualise. The number of nodal points and therefore the number nodal diameters is clearly demonstrated, indicating a mostly real, smooth 4-ND mode. However, a non-trivial imaginary part, in quadrature with the real, is also present. With this technique, the identification of number of NDs in a given mode barely takes a few seconds as demodulation can be carried out straight after the acquisition.

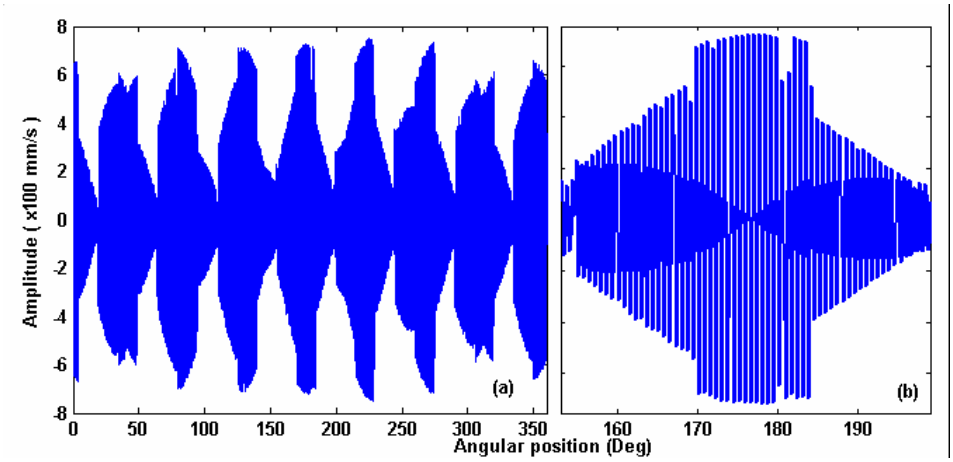

Figure 3.26 Slow circular scan LDV output

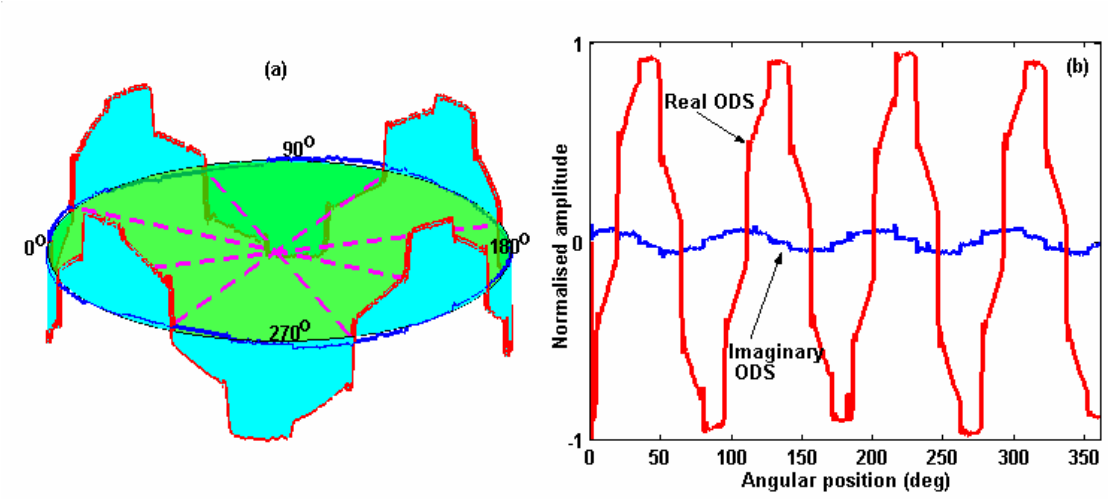

Figure 3.27 Real and imaginary parts of circumferential ODS

Assuming the blisk vibration to be at an n ND mode and substituting $V_{Rn}Cos(\theta)$ for $V_a(\theta)$, and $V_{In}Sin(\theta)$ for $V_b(\theta)$, the expansion of Equation (4.6) gives:

$$V_z(t) = V_{Ro}Cos(\omega\ \ t) + V_{Io}Sin(\omega\ \ t) + \frac{V_{Rn}+V_{In}}{2}Cos(\omega - n\Omega)t + \frac{V_{Rn}-V_{In}}{2}Cos(\omega + n\Omega)t \qquad (4.9)$$

The vibration velocity described by the above equation has frequency components at $(\omega \pm n\Omega)$. The spectrum, therefore, will have sidebands spaced at $\pm n\Omega$ about the vibration frequency, ω. Some important properties can be observed from Equation (4.9):

- When the mode being measured is purely real, the V_I terms are all zero and sidebands are of equal amplitude, indicating a pure standing wave in the blisk
- When V_R and V_I are equal there exists only one sideband at $(\omega - n\Omega)$, indicating a pure travelling wave, and finally
- When V_R and V_I are different than each other, the deflection shape will be a combination of standing and travelling waves, the degree of which being decided by the relative amplitudes of the sidebands (the difference will indicate the travelling wave portion).

The LDV output of the same mode given in Figure 3.28, scanned at Ω=5Hz , together with the corresponding frequency spectrum is given in Figure 4.25. Since the sidebands are separated by $2n\Omega$, the identification of the number of NDs, n, is straightforward: 40/(2*5)=4. Note that the frequency spectrum contains additional, relatively small, amplitude sidebands, again centred about the vibration frequency, indicating the existence of other ND mode components in the deflection shape. Here the mode observed is mainly a standing wave with slight difference in sideband amplitudes, thus hinting at the presence of some travelling wave portion as well (inline with the findings in Figure 3.27). Even then, the amplitude at the frequency of vibration, ω, is indistinguishable from the noise floor.

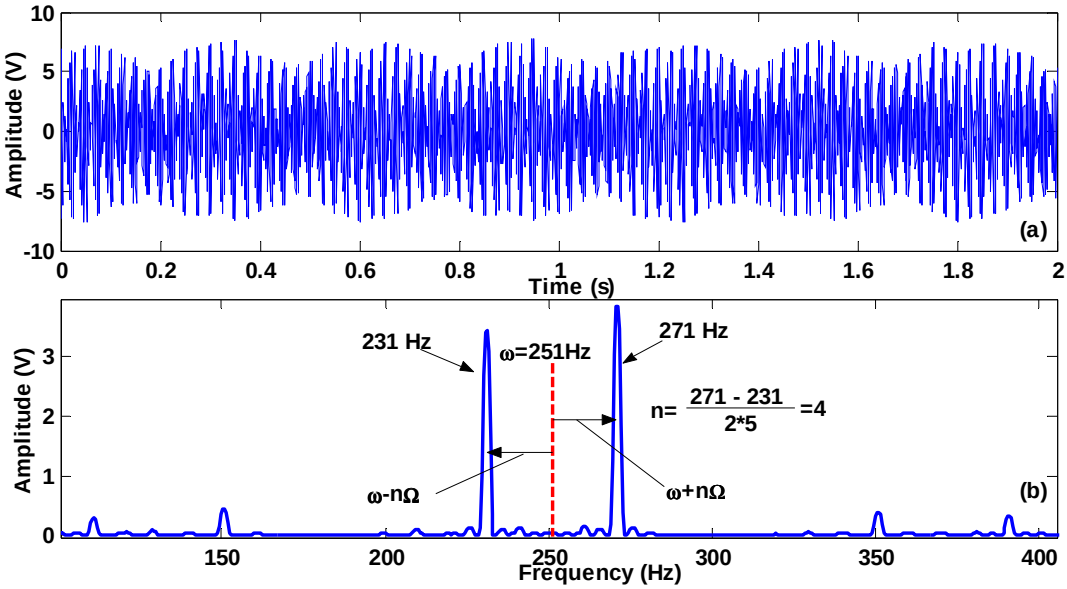

Figure 3.28 (a) Circular scan LDV output, and (b) the frequency spectrum

3.6. Validation of measurement setup

The vibration and force measurement setups need to be validated against independent alternative techniques in the way the speed measurements were validated in Section 4.2.3. Here the calibration of the transducers used in the alternative measurements is not given as standard procedures are followed in ensuring this.

3.6.1 Vibration measurement setup validation

The use of the LDV transducer with circular and line scanning methods was validated against traditional response measurement techniques in [79], and good qualitative and quantitative agreements were obtained. However, the same needs to be repeated for the self-tracking system as well. To this end, a B&K accelerometer is used to measure the vibration on a blade. Note that the instrumentation in this case dictates the bladed disk to be tested at rest. Impact response at a particular blade tip is measured by the LDV transducer and the accelerometer simultaneously so that the response to the same force input can be measured. The comparison of the acquired impact responses covering a frequency range mostly used in tests are given in Figure 3.29. Note that the LDV measures velocity therefore the corresponding signal is differentiated once to get the acceleration so that it can be compared to the accelerometer's output. The excellent agreement between both measurements confirms the validation of vibration measurement setup.

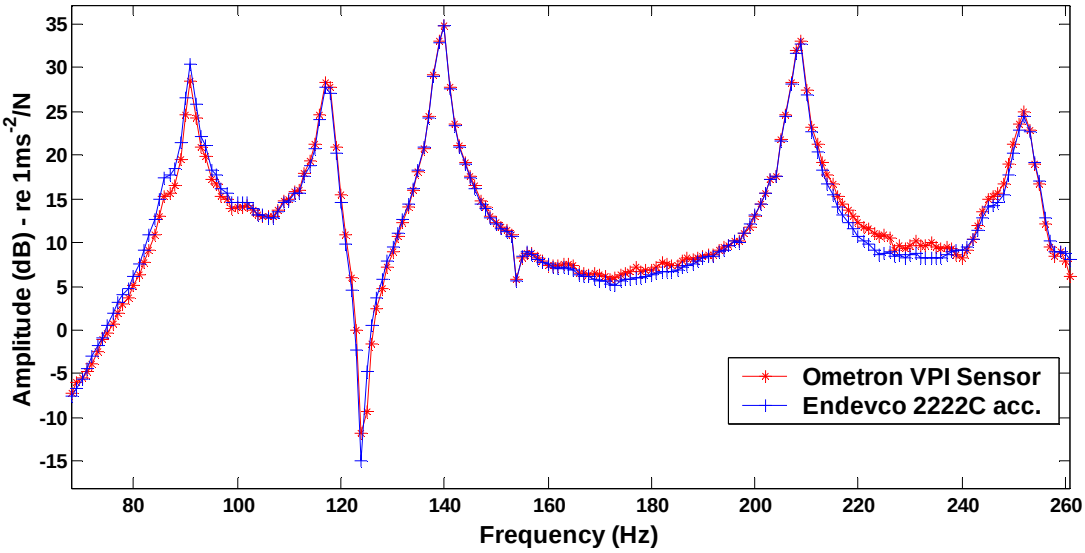

Figure 3.29 Comparison of LDV and accelerometer outputs

3.6.2 Force measurement setup validation

The validation of excitation system requires an elaborate setup compared to vibration setup. Here the validation is carried out in two steps. In the first step, the static deflection of a blade is measured for various force values using a non-contacting proximity probe (Bently Nevada). The forces are applied via a pulley system by utilising the tapped hole in the tip of the blade. Metal pieces of known quantity are hung by a string, which eventually is tied to a bolt screwed into the tapped hole in the tip of the blade. This way the force is applied normal to the blade simulating the magnetic force. The proximity probe is brought near to the unloaded blade and the measured value is taken as the reference zero. Than relative readings are recorded as the payload is increased. In the second step, again, the blade position relative to the probe is first measured in the absence of magnetic force by retracting the magnet. In this case, no force is registered by the force transducer. It is made sure that the same reference value is achieved by adjusting the blade-probe distance. Then the magnet is advanced to close proximity of the blade in precise increments by controlling the stepper motor via the DAQ PC. The relative readings are again recorded at various blade-magnet gaps. Later, the force transducer signals at exactly the same stations where the probe measurements were taken are acquired. The variation of the proximity probe's output with increasing payload is given in Figure 3.30 (a). A perfectly linear relation, as expected, is obtained. Later, using this relation, the relative readings of magnet-imposed deflections are converted into corresponding force values and are compared to the force transducer's readings. This comparison is given in Figure 3.30 (b). The range of applied magnetic forces covers the typical values used in the experiments. Overall, a good match is obtained between the estimated and force transducer measured magnet forces with an error less than 3.6%.

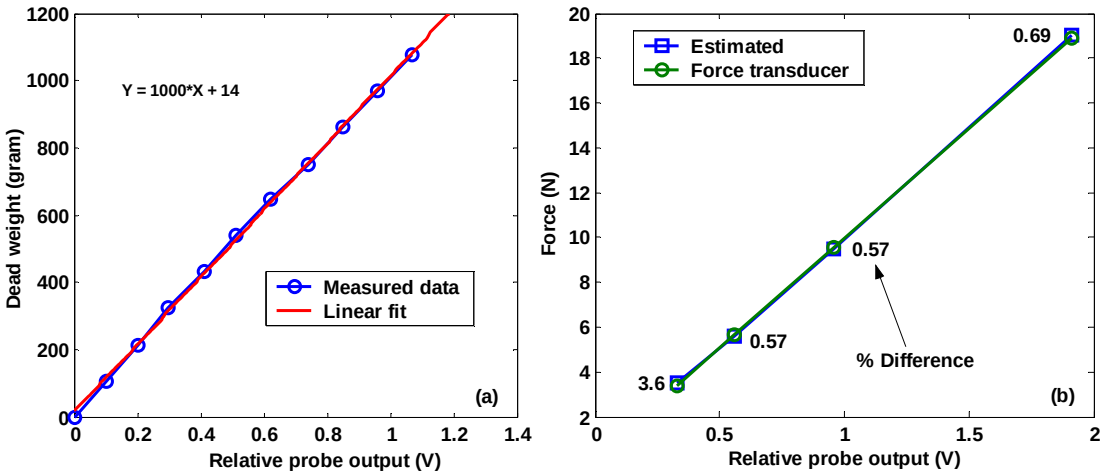

Figure 3.30 Force measurement setup validation

3.7 Summary

In this chapter the design and manufacture of blisks to be used in mistuned and friction damped vibration response measurements is given. Through FE analyses, the blisks are designed to reflect the design requirements. Based on the computed Campbell diagrams, a maximum speed limit is chosen to be 4000 rev/min, covering most of the resonances (i.e., 4D and above) corresponding to the 1F family of modes for both blisks.

The design and instrumentation details of a rig to be used in the tests have also been presented. The rig runs in a vacuum so that unwanted aerodynamic effects are excluded. Through FE analyses, the test enclosure and drive shaft were designed to withstand possible operational forces. Speed and phase measurement methods are introduced. A variable-gap permanent magnet excitation mechanism is implemented. The rig design allows the use of up to six exciters. A special mirror arrangement and indexing mechanism were designed to address the need to track a point on a rotating structure. This so-called self-tracking system works independently of rotation speed.

The employed LDV transducer is introduced. Two measurement techniques are described: one using tracking LDV to measure blade tip vibration responses, and

another using scanning LDV to measure ODSs in radial and circumferential directions. The steps which need to be taken to align the LDV with the axis of rotation are explained. The limitations, as well as the advantages, of LDV measurements are stated. The effect of speckle noise on measurement quality and its minimisation through improved surface reflectivity and alignment is shown.

The DAQ hardware components and their connectivity are presented. The software controlling the instrumentation and DAQ is also mentioned. Different ways of data processing in obtaining EO frequency response curves are given. The use of CSLDV in circumferential ODS recovery is presented through some real measurements.

Finally, the used vibration and force measurement setups are validated through independent measurements.

CHAPTER 4

BLISK TUNING, MODEL UPDATING and TEST DESIGN

4.1 Overview

So far we have concentrated on the design and development of the blisk testpieces and the test rig, and have reported on the measurement tools and techniques to be used in preparation of the real tests. However, before we go about testing, there are a number of crucial steps which need to be taken in order to make the test campaign time-efficient and to make sure that only useful data are acquired. It is also necessary to ensure that the blisk models to be used in predictions are good representations of the real ones. In this chapter, first, the tuned states of blisks designed in Chapter 3 are identified and the blisks are tuned when the tuning is deemed to be necessary. The sensitivity of a blisk's dynamic properties to various ways of tuning is investigated through a lumped parameter model. Methods to be used in model updating are then introduced, and based on the preliminary measurements on stationary blisks, the blisk models are updated. Using these updated models, a comprehensive test plan is designed and the selected configurations are justified through appropriate FE analyses.

4.2 Tuning of blisks

The manufacture of blisks and their designed characteristics were given in the previous chapter. However, before testing it is necessary to measure the actual

characteristics on the real test pieces in order to gauge their adequacy for intended studies, and to improve them if needed.

4.2.1 Blisk-1

The machined blisk, received from the manufacturer, had two damaged blades; one cut-in—Figure 4.1 (a)—, and one bent and straightened—Figure 4.1 (b). Additionally, geometric imperfections were present on various locations across the blisk as shown in Figure 4.1 (c). Preliminary experiments in the form of measuring 1F family natural frequencies demonstrated considerable splits in 1F several ND modes. At the time this was attributed to the blemished blade shown in Figure 4.1 (a). The fault was corrected by filling with weld metal. The blade was re-machined and re-straightened to correct thermal distortion.

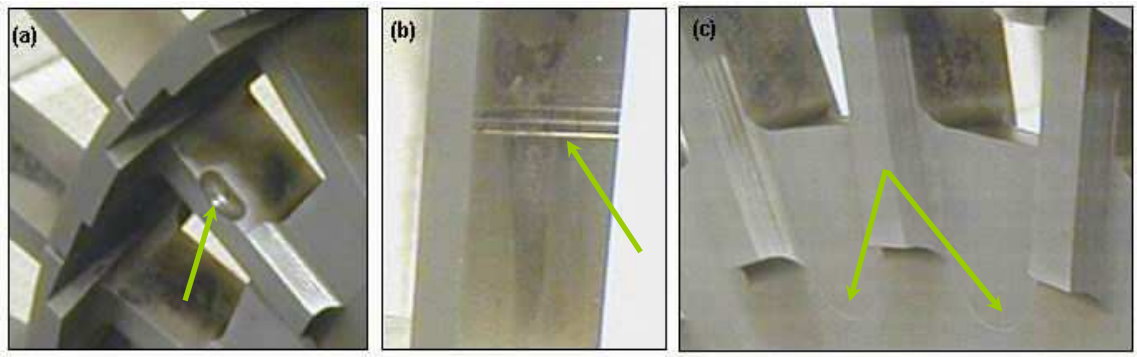

Figure 4.1 Damaged areas on Blisk-1

1F family blisk natural frequencies were re-measured after repair. Although the splits in the ND mode natural frequencies were considerably reduced, the blisk was still significantly mistuned such that it could not serve as an acceptable tuned reference to be compared with deliberately-mistuned configurations. In order to improve the symmetry of the blisk, a tuning process was undertaken. Initially, it was decided to attach appropriate masses to blade tips via tapped holes in the blade tips to equalise individual blade frequencies. However, the blisk was so grossly mistuned that if these holes were to be used for tuning, no room would be left for deliberate mistuning masses. Thus, the method used to

adjust the state of tune of the blisk was to remove metal from the mass at the end of each blade in turn, so that all the first family of natural frequencies were as near identical as possible. In this way, all blade natural frequencies were to be brought up the level of the highest-frequency blade. This process required individual blades to be isolated so that their natural frequencies could be measured, uninfluenced by the other blades on the blisk. To this end, the disc was clamped between two massive blocks, up to the blade roots, and all blades, apart from the one being tested, were interconnected – initially by modelling clay ('Plasticene') and later with annular metal clamps, with a gap for the test blade. Figure 4.2 shows the later test arrangement. The 'Plasticene' technique was easier to use, but was found to be insufficiently consistent, and was abandoned after the first check on the damaged blisk.

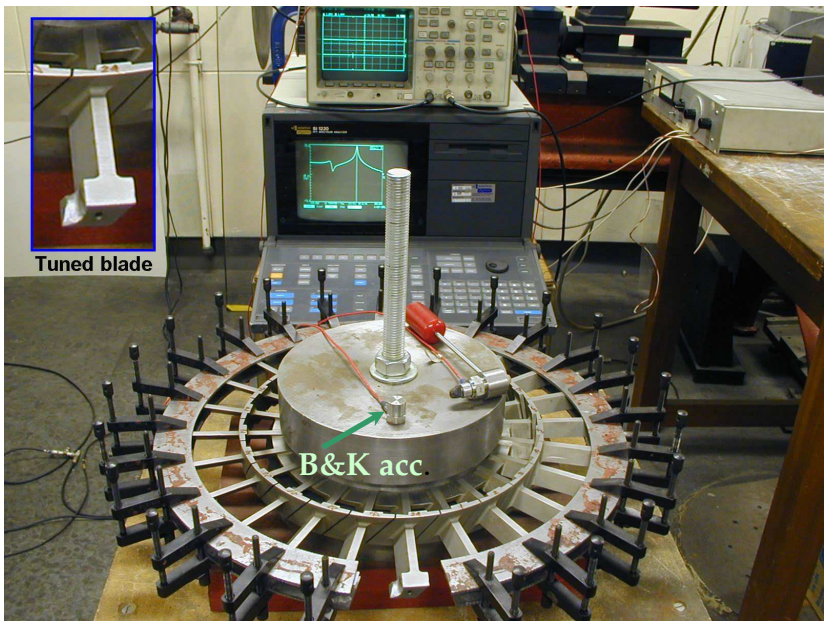

Figure 4.2 Test Arrangement used for measuring individual blade frequencies

Only the first natural frequencies for the isolated blades were tuned. The variation of blade-alone frequencies for the blisk before repairs, after repairs and after tuning are given in Figure 4.3 and statistics of these variations are given in Table 4.1.

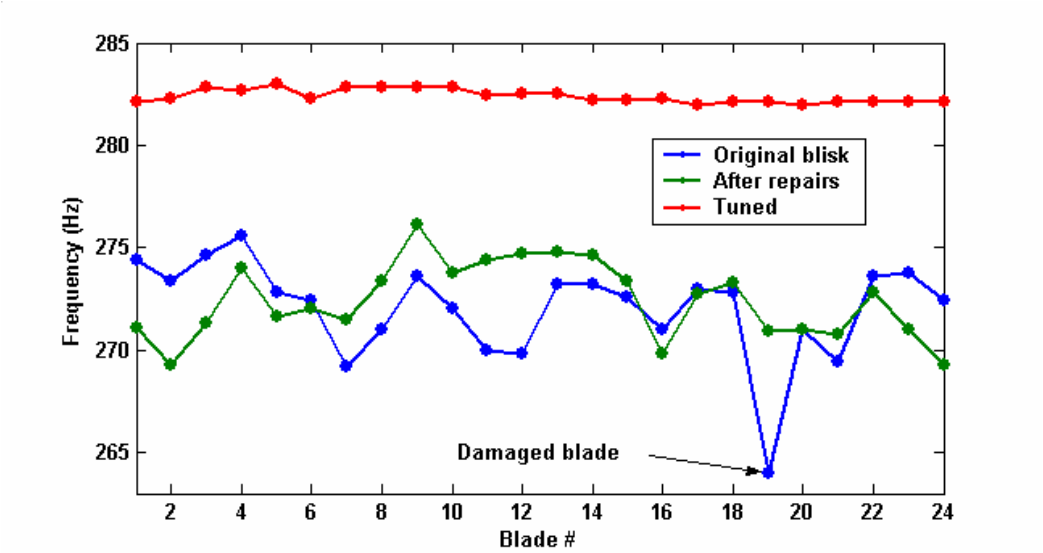

Figure 4.3 Variation of blade-alone natural frequencies

	Min (Hz)	Max (Hz)	Mean (Hz)	Std dev	Max % dev. from mean
Original blisk	264.0	275.6	272.03	2.39	2.95
After Repairs	269.3	276.1	272.40	1.87	1.36
Tuned Blisk	282.0	283.0	282.38	0.32	0.22

Table 4.1 Statistics of blade-alone natural frequencies

Since the disk portion could not be fully clamped, due to disk-blade blend geometry (see Figure 4.1), it was not possible to decouple the blades completely. Although low-amplitude, non-trivial vibration signals were measured on the clamped blades. In fact, since the blades were tuned in turn, as metal was removed from the blade being tuned, the frequencies of other blades were shifted, due to the non-negligible inter-blade coupling, to values which were different to those they had at the time of the first measurement. As a result, it was necessary to go round the blisk a few times to make sure that all the blade frequencies were sufficiently close. Gross inherent mistuning in the blisk (mainly due to poor manufacture) together with this iterative procedure, resulted, unfortunately, in large masses being removed from blade tips (see the inset of Figure 4.2). The "Original" and "After repairs" blade-alone measurements were made by sticking a small accelerometer (0.5 gm Endevco 2222C) to blade tips

whereas for the "Tuned" case measurements, a high sensitivity B&K accelerometer was attached on a mounting block, see Figure 4.2. This situation caused an upward shift in the tuned case mean blade frequency, as can be seen in Figure 4.3 (note that as the accelerometer affects all the blades in the same way in the former two cases, the relative blade frequencies are still valid).

The 1F family of modes of the blisk after tuning were measured by applying an impact to one blade, and measuring the response of another. The blisk was clamped to a shaft via a tapered-lock device. An LDV transducer, parallel to the blisk central axis, was used to measure the response on the blade tips. Since the damping of the blisk was low, the transient response continued long enough to allow the use of a 10 Hz bandwidth, 500-point zoom FFT transform via which the blisk natural frequencies could be identified to within 0.02 Hz i.e. to around 0.01%. On this scale of accuracy, the natural frequencies were not absolutely consistent, variations of around +0.1 Hz were noted, day to day, probably due to ambient temperature variation.

The blisk was also excited at the natural frequencies obtained using an electromagnet, as described in Chapter 3, and circumferential Operation Deflection Shapes (ODS) were measured using circular scanning of the LDV at platform level so that the ND index and smoothness of the modes could be identified. Measured ODSs were found to be regular deflection shapes for simple ND mode shapes up to 7, as would be expected from a tuned blisk. However, they became distorted then onwards, eventually becoming highly localised for 9 to 12 ND modes. Sample circular scan spectra and corresponding ODSs are given in Figure 4.4. Here, the mode given in (a) is a tuned mode with a clear single ND index. A clear pair of sidebands centred about the frequency of the mode is seen from the given frequency spectra. For the one marked with a single question mark (b), the ODS contains a dominant component, although some other non-negligible components also exist. This fact is clearly demonstrated by the frequency spectra given for this mode. Two question marks

are used for the mode which is highly localised, (c), that modal diameter representation is no more valid. In these cases, circular scan spectra contain many equally strong components.

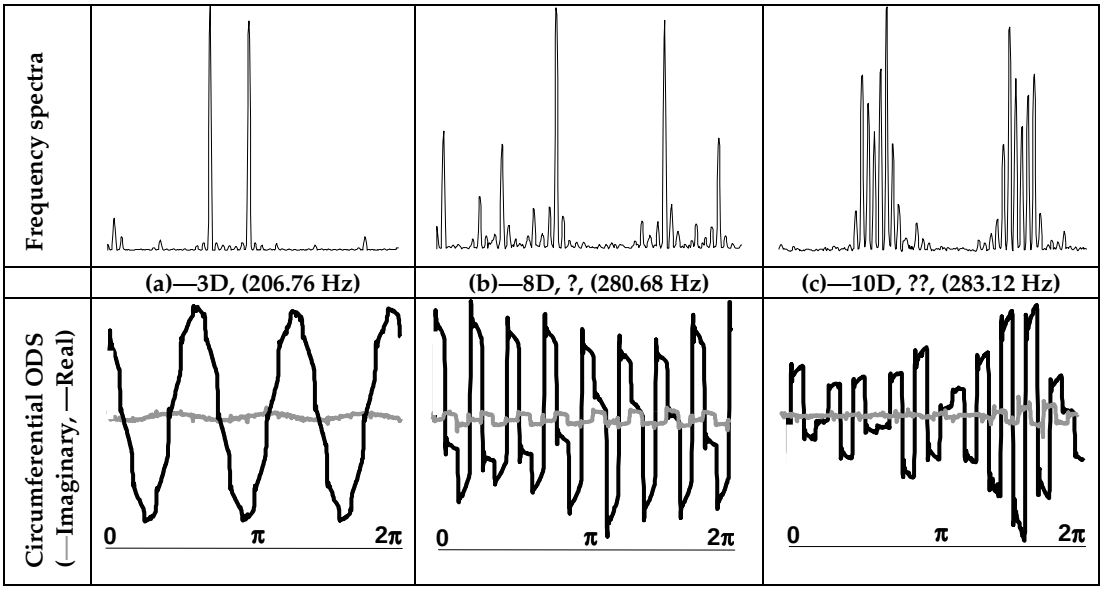

Figure 4.4 Circular scan spectra and ODSs for the identified first family modes of Blisk-1

The list of ND mode natural frequencies and percentage splits in identified double modes is also given in Table 4.2. The ND index is labelled as explained in the previous paragraph.

	Before tuning				After tuning			
ND	Freq.(1) Hz	Freq.(2) Hz	Split Hz	% split	Freq.(1) Hz	Freq.(2) Hz	Split Hz	% split
2	134.8	135.4	0.60	0.44	141.64	141.74	0.1	0.07
3	206.76	206.9	0.14	0.07	209.5	209.7	0.2	0.10
4	247.32	247.4	0.08	0.03	250.88		0	0.00
5	265.0	265.34	0.34	0.13	269.1		0	0.00
6	275.56	273.66	0.10	0.04	277.8		0	0.00
7?	277.7	278.6	0.9	0.32	282.44	282.6	0.16	0.06
8?	280.68	281.06	0.38	0.14	285.2	285.26	0.06	0.02
9??	282.28	282.62	0.34	0.12	286.7	287.08	0.38	0.13
10??	283.12	283.72	0.60	0.21	287.78	287.88	0.1	0.03
11??	284.24	284.44	0.20	0.07	288.4		0	0.00
12??								

Table 4.2 1F ND modes of Blisk-1 before and after tuning.

Judging from Table 4.2, the tuned state of Blisk-1 has been reasonably improved, compared with the "before tuning" state, with mode splits of less than 0.13%. However, this has not been sufficient to yield regular (i.e., tuned) assembly modes for the entire 1F family. Various aspects of tuning through individual blades are explored through a systematic study on a lumped-parameter model in Section 4.2.3 to find out the reasons behind this failure and to asses whether a better tuned state could have been achieved.

In order to quantify the effects of an applied mistuning pattern, the reference case to which the obtained results could be related must be known fairly accurately. Since the inherent and significant mistuning present in the blisk was not known, it was concluded that it would not serve as a suitable reference for mistuning investigations. As a result, it was decided to have another blisk made to be used for mistuning studies. Blisk-1, nevertheless, could be used in friction damping experiments if the present mistuning was reasonably identified.

4.2.2 Blisk-2

Based on the experience gained with Blisk-1, the geometry of Blisk-2 was kept simple and the manufacture was tightly controlled. Blisk-2 1F modes natural frequencies were measured in the same way as for Blisk-1, and the measured frequencies and identified ND numbers are given in Table 4.3. The impact response spectra from which these frequencies were extracted are also given in Figure 4.5. Despite the use of a considerably high frequency resolution (0.02 Hz), only 2 and 11 ND modes are found to be split, by 0.3% and 0.02% respectively. For all other modes, the separation in repeated modes could not be identified. The double modes given in Table 4.3 could only be identified in different impact tests (i.e., changing the input force location), therefore they are not apparent from Figure 4.5.

ND #	2	3	4	5	6	7	8	9	10	11	12
Freq 1	172.34	212.44	240.98	257.58	267.7	274.18	278.52	281.42	283.3	284.32	284.68
Freq 2	172.84	—	—	—	—	—	—	—	—	384.38	—
% split	0.3	0	0	0	0	0	0	0	0	0.02	0

Table 4.3 Measured 1F Blisk-2 frequencies.

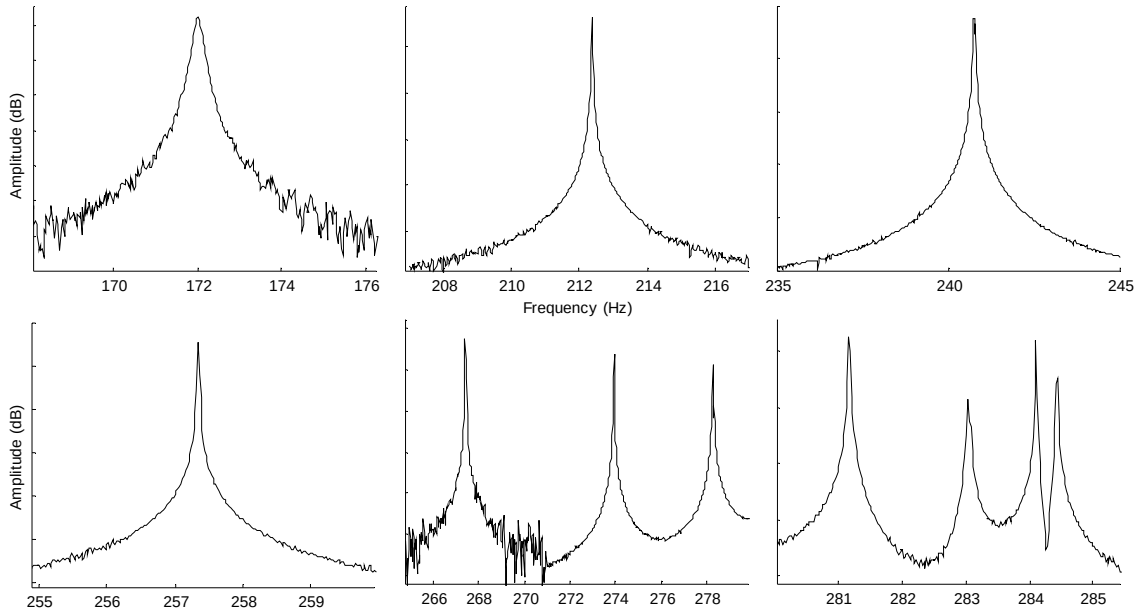

Figure 4.5 Blisk-2 impact response spectra

Based on the circumferential ODSs, the as-delivered tuned state of Blisk-2 was significantly superior to that of Blisk-1. However, the sensitivity of the applied mistuning to present inherent mistuning, however small, needed to be investigated so that the exact state of tune of Blisk-2 could be validated. To this end, a test setup is devised in which a random mistuning pattern was applied to the blisk and the ODS at platform level was measured by circular scanning LDV. Then, this pattern was shifted around the blisk by three blades (45°) and the ODSs are re-measured. The applied mistuning patterns are given in Table 4.4.

Blade #	Pattern 1 (gr)	Pattern 2 (gr)	Blade #	Pattern 1 (gr)	Pattern 2 (gr)
1	0.87	2.01	**13**	1.80	2.24
2	1.87	2.23	**14**	1.80	2.77
3	0.87	2.65	**15**	1.74	0.87
4	2.37	0.87	**16**	2.58	1.80
5	1.85	1.87	**17**	2.51	1.80
6	1.87	0.87	**18**	2.62	1.74
7	2.72	2.37	**19**	1.50	2.58

8	0.87	1.85	**20**	0.87	2.51
9	2.13	1.87	**21**	1.49	2.62
10	2.24	2.72	**22**	2.01	1.50
11	2.77	0.87	**23**	2.23	0.87
12	0.87	2.13	**24**	2.65	1.49

Table 4.4 Random mistuning patterns

In a perfectly tuned blisk, one would expect to get the same ODSs in both cases since shifting the mistuning pattern practically corresponds to rotation of the blisk, with applied mistuning pattern, by 45°. However, if the blisk is inherently mistuned, the measured ODSs will depart from each other, depending on the degree of this mistuning. Some of the measured ODSs for Blisk-2 for both orientations are plotted on top of each other and given in Figure 4.6.

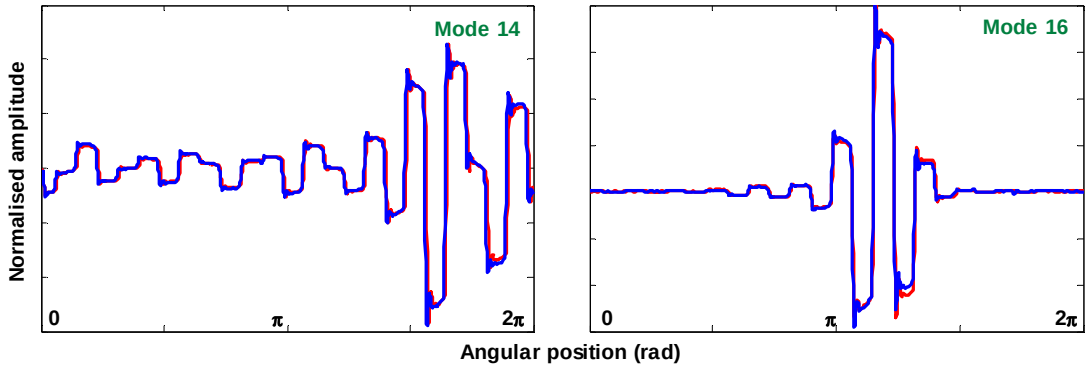

Figure 4.6 ODS comparisons for shifted random mistuning patterns (—1st pattern, —2nd pattern)

The plotted ODSs are almost indistinguishable. The quality of the match is quantified in Table 4.5 where the degree of correlation for all measured ODSs is given. Note that as the modes are significantly disturbed, an ND description is not applicable. The minimum correlation coefficient was found to be 98%. These results gratifyingly demonstrated the state of tune of Blisk-2 such that no tuning was needed and it would serve as a suitable tuned reference for mistuning tests. The amplitude of applied random mistuning pattern was smaller than the one planned for the rotating tests. This implies that, however small, the effect of inherent mistuning will be even less significant on the rotating tests. The same

test was applied to Blisk-1 as well, where considerable deviations in corresponding ODSs from pattern to pattern were observed, as expected.

Mode #	Freq (Hz) Pattern 1	Freq (Hz) Pattern 2	% freq. change	% corr. coef.
1	165.22	165.60	0.23	99.46
2	167.20	166.90	-0.18	99.82
3	202.94	202.92	-0.01	99.40
4	203.86	203.86	0.00	99.39
5	229.32	229.32	0.00	99.16
6	230.16	230.18	0.01	98.83
7	243.72	243.70	-0.01	98.73
8	245.90	245.96	0.02	98.39
9	259.22	259.18	-0.02	99.44
10	260.90	260.90	0.00	98.55
11	262.82	262.86	0.02	99.16
12	265.34	265.34	0.00	98.72
13	266.50	266.60	0.04	98.19
14	267.14	267.18	0.01	99.70
15	271.34	271.34	0.00	99.75
16	273.18	273.24	0.02	99.23

Table 4.5 Correlation of randomly mistuned Blisk-2 ODSs

The percentage changes in the frequencies of first two modes given in Table 4.5 are an order of magnitude larger than those of the other modes. This might be explained by the sensitivity of these frequencies to disk fixing, more than the degree of inherent mistuning, as the ODSs correlate excellently.

4.2.3 On blisk tuning through individual blade frequencies

The experience with Blisk-1 demonstrated that the common practice of tuning 1F blade-alone natural frequencies was not enough even to tune the 1F assembly modes of the blisk satisfactorily. Although the 1F blade-alone natural frequencies were matched to a degree, it is certain that the symmetry of the system would have been improved had more than one blade-alone natural frequencies been made identical. There are a number of reasons for this. First, it is anticipated that the way in which changes were made to tune the 1F blade-alone natural frequencies plays an important role. Considering an isolated blade as a single DOF system represented by a lumped mass, m, and a stiffness, k,

there exist an infinity of combinations of m and k which give the same natural frequency, ω_0. However, for each such combination, the mass and stiffness distributions of the assembly are different, yielding different natural frequencies and forced response characteristics. Secondly, in this way of tuning, it is inherently assumed that the mistuning is confined to blades only. Depending on the flexibility of the disk portion, the effects of disk mistuning may play an important role on not only the lower ND modes (1D, 2D), but also the higher ones as well. Given the poor state of manufacture of the blisk, especially around blade roots (Figure 4.1 (c)), mistuning in the disk portion is believed to have contributed to the failure of the tuning process. If individual sectors, rather than blades, were isolated, this fact could have been taken into consideration. However, prospects of achieving this in practice are very limited and require complicated fixtures.

At this stage it is desirable to make some simulations to investigate whether tuning through 1F blade-alone modes could have been improved if the different parts of the blisk were modified and whether the presence of disk mistuning was significant. These simulations will also be useful in identifying important parameters on the blisk modes under investigation (1F family), since this information will provide a valuable input when mistuning patterns are applied to FE models of the next two chapters, especially in damped tests with Blisk-1. As will be explained in subsequent sections of this chapter, the inherent mistuning in Blisk-1 was identified as a sector-to-sector frequency deviation. However, in order to use this deviation in the FE model, it has to be translated into physical parameters to be applied on individual blades. The sensitivity analysis through these simulations, therefore, will provide important clues as which parameters should be used in this process to best represent the measured mistuning pattern.

To this end, a discrete bladed disk model of 3DOF per sector was used in which a blade was represented by 2 DOFs and the disk portion by a single DOF.

Oversimplified models of this kind are not suitable for design or quantitative prediction purposes, but, they have been often used in the literature as they provide computational efficiency in qualitative investigations. The model used is shown in Figure 4.7.

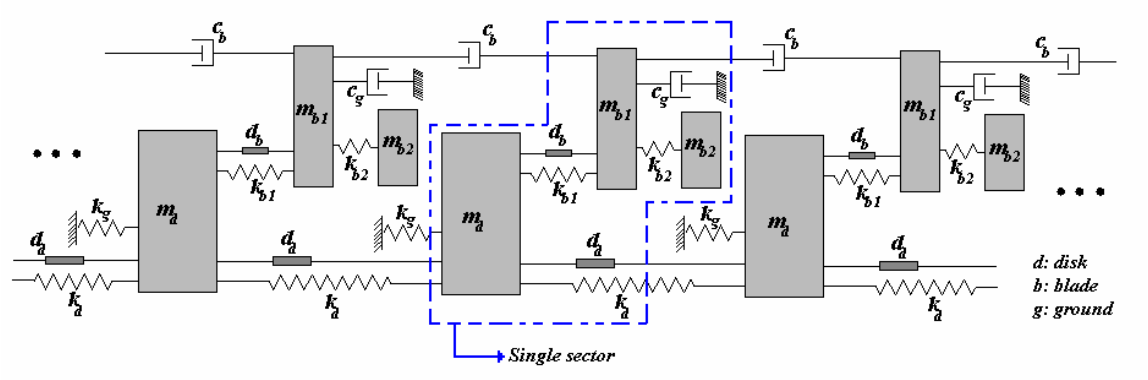

Figure 4.7 Lumped parameter bladed disk model

The equations of motion for this system can easily be derived and therefore are not given here. It must be noted that the model is circular (i.e., the last sector connects to the first one) and a total of 24 sectors are present. The values of masses and stiffnesses in this system were fine-tuned so as to obtain 1F natural frequencies as near to those of the full FE models (Blisk-1 and Blisk-2) as possible. By doing so, the intention was to ensure that realistic values were used in the analysis. The 1F family of natural frequencies of the full FE Blisk-2 and lumped parameter models are compared in Figure 4.8.

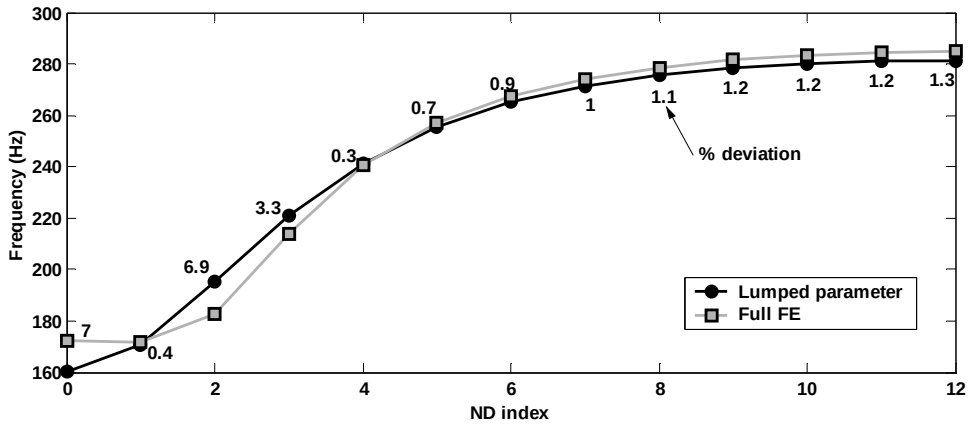

Figure 4.8 Comparison of full FE and discrete Blisk-2 1F frequencies

4.2.3.1 Simulation of Blisk-1 tuning

As mentioned before the as-delivered mistuned state of Blisk-1 was mainly the result of stiffness deviations whereas the tuning was accomplished via mass removal. Inspections on the real blisk revealed that the thicknesses at the blade-disk junction showed significant variability. Although not on the same scale, some variations were also observed in the disk thicknesses as well. Therefore, the blisk was mistuned via k_{b1} and k_d stiffness terms in the simulations and then tuned through mass m_{b2} using an isolated blade model. A 2 DOF lumped parameter model was manageably small enough to be manipulated parametrically in a symbolic solver such as Maple. Therefore, deriving equations for the eigenvalues and solving them for certain parameters yielded the desired accuracy for cases where convergence was achieved. Here a maximum of 0.35% deviation in 1F blade frequencies was sought as this was the accuracy achieved in Blisk-1 tuning. The results given in Figure 4.9 (a) show a general trend of reduction in mode splitting, indicating an improved state of tune. However, the split in ND modes does not automatically signify an irregularity of the mode shapes. Particularly for lower ND modes, the shapes may remain regular despite significant natural frequency splits in double modes since the modal density is relatively low around these modes. The regularity of the mode shapes was checked by Fourier analysis. The harmonic contents of a few tuned and mistuned modes are given in Figure 4.9 (b) to (f). For a regular n ND mode of an N-bladed blisk, Fourier analysis will yield significant n, $N-n$, $N+n$ etc harmonics and negligible amplitudes for the rest (note that the amplitudes of these harmonics will not necessarily be zero since the mode shape is defined by only 24 discrete points). However, when the modes are irregular (i.e., mistuned), additional non-trivial harmonics will show up depending on the degree of irregularity. In this particular case, 7 ND and higher modes are clearly mistuned as is evident from Figure 4.9. The irregularities in the modes with up to 8ND are reasonably removed by adjusting the blade tip masses. However, as for the Blisk-1 case, the higher ND modes were less regular and exhibited mode

localisation which manifested itself in the form of non-trivial additional harmonics.

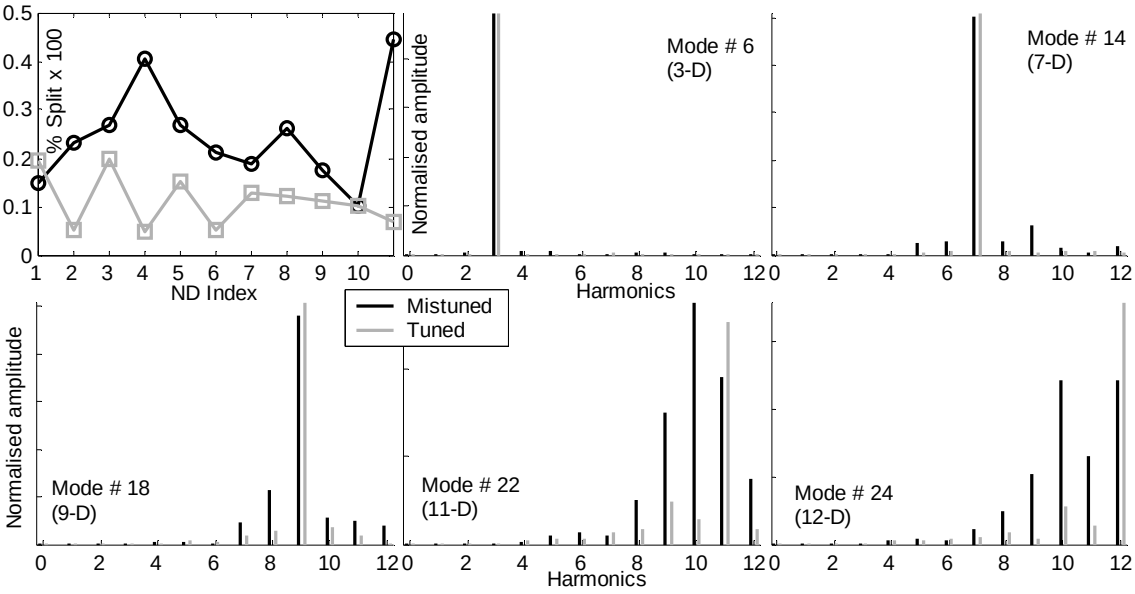

Figure 4.9 Blisk-1 tuning simulation

In the tuning process illustrated in Figure 4.9, all the individual 1F blade frequencies were brought up to the level of the highest frequency blade as this was the case in the real tuning of Blisk-1. However, aiming at the mean value of the frequencies would be preferred, whenever possible. Simulations with this particular model showed that, although not significantly different, a better state of tune can be achieved this way. Also, it is desirable as it causes the least disruption to individual blades.

The target error for blade-alone natural frequencies is reduced systematically down to 0.0001% to see whether an improved tuned state was possible if blade-alone frequencies were literally identical. The performed simulations showed an overall decreasing split in some of the modes although no clear correlation between increasing accuracy and the split in modes was evident. Fourier analysis of the mode shapes showed similar results for the irregularity of the modes. The results obtained for the 12ND mode are given in Figure 4.10 (note

that only the 7-12 harmonics are shown as the 0-6 harmonics are almost zero). Despite the drastic enhancement of the accuracy, the gain in terms of increased tuned state has not been significant.

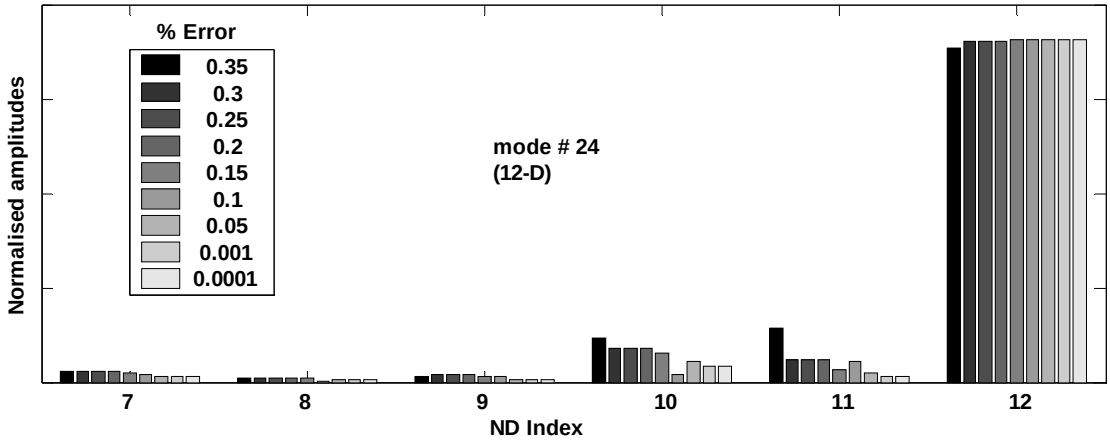

Figure 4.10 12ND mode's harmonics variation with increased accuracy in 1F blade alone modes

The same procedure was repeated for a case in which the disk portion was "perfectly" tuned (i.e., mistuned via k_{b1} and tuned via m_{b2}) to demonstrate the effect of disk mistuning. The accuracy of matching individual blade frequencies was again set at 0.35%. Significantly better results are obtained for lower ND modes, as expected, in terms of mode splits. Despite slight improvement, however, the existence of irregularities in higher modes has not been possible to eliminate.

In the light of the findings of the above analysis, it can be concluded that, although the minimisation of variation in 1F blade-alone frequencies and the inclusion of the effects of the disk portion's mistuning might have resulted in a better tuned state in Blisk-1, it would not be possible to tune the blisk satisfactorily even if the adverse consequences of these effects were minimised.

4.2.3.2 Tuning through various parameters

In this section simulations are presented where various parameters are used for mistuning and subsequently tuning of the blisk. By doing so it is aimed at identification of the sensitivity of the blisk tuning to various parameters and also to see if, for a given mistuning pattern, a better combination for tuning of the blisk existed when 1F blade alone frequencies were matched. Initially, mistuning was introduced via k_{b1} stiffness element. Later, some other cases in which mass mistuning and tuning through several parameters were also considered. The list of cases studied is given in Table 4.6.

	Mistuned via						Tuned via					
Case	k_{b1}	k_{b2}	k_d	m_{b1}	m_{b2}	m_d	k_{b1}	k_{b2}	k_d	m_{b1}	m_{b2}	m_d
1												
2												
3												
4												
5												
6												
7												
8												
9												
10												

Table 4.6 Mistuning/tuning test configuration

In all these cases, the 1F blade-alone frequencies are set to the same value of 300 Hz with an error of less than 0.0001%. The results, in the form of the natural frequency split in the double modes corresponding to first four cases, are given in Figure 4.11.

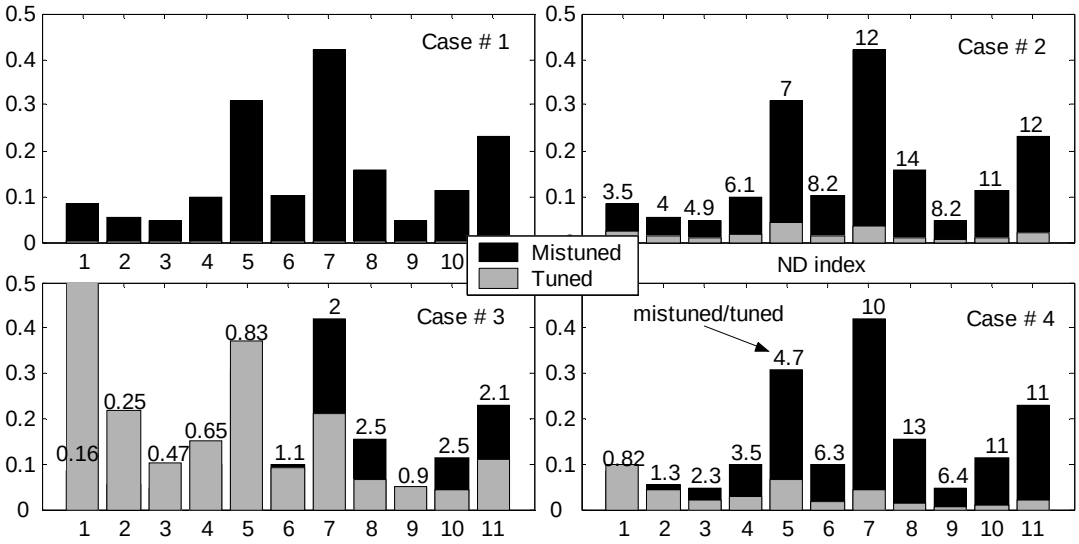

Figure 4.11 Cases 1 to 4: Split in 1-11 ND modes

Case 1 in the above figure is included to demonstrate the validity of the algorithm used in the tuning process. In this case the blisk is mistuned and then tuned using the same parameter and the tuned case is restored successfully. Although the individual blade frequencies are tuned to the same value in all four cases, significant variations are obtained depending on the tuning parameter. The minimum split in the ND modes is achieved in case 2 where the mistuning introduced via a stiffness element is corrected through another stiffness element. The 1F family of modes of the blisk were found to be the least sensitive to changes in mid-blade mass and this is evident from the results for case 3 where a little improvement is achieved in the higher modes whereas most of the lower ND modes got worse. It is seen from cases 3 and 4 that the frequency split in the lower ND modes (disk dominated modes) cannot be reduced by modifying mass parameters. However, as the ND index increases (blade dominated modes), the tuning becomes more effective.

An alternative study was carried out, covering cases 5-10 of Table 4.6, to study the case of mass mistuning. Here, the mass elements, m_{b2}, (cases 5-7) and m_{b1}

(cases 8-10) were mistuned in turn. The results for these cases are given in Figure 4.12.

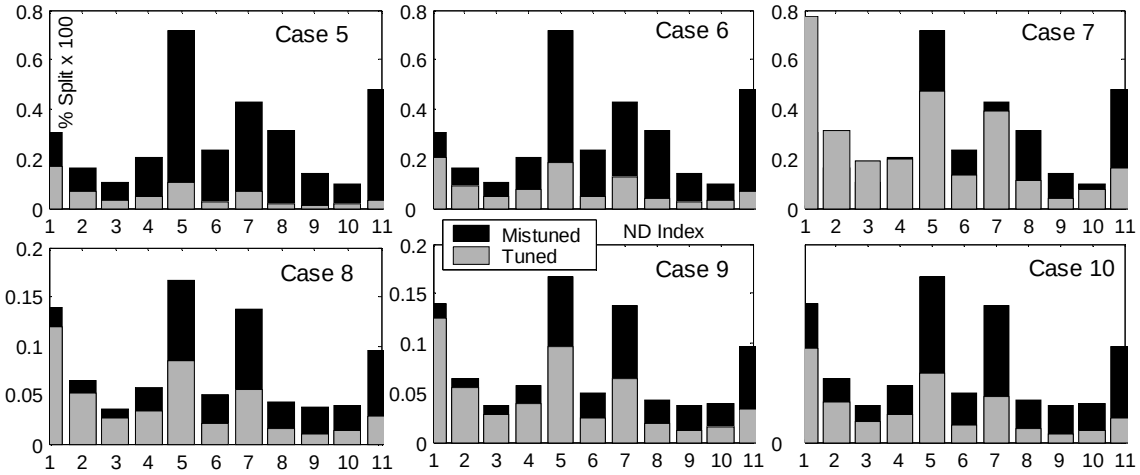

Figure 4.12 Mass mistuning corrected through mass and stiffness elements

In all presented cases, 1F blade frequencies were brought to the same value and in all cases the blisk characteristics achieved were different. Despite improvements in some cases, none of the configurations were effective enough to tune all the modes in the 1F family. In fact, there are a large number of combinations of the stiffness and mass elements of an isolated blade which give the same 1F frequency. Therefore, matching only this natural frequency will result in different stiffness and mass distributions across the blisk, producing the variability obtained in the above analysis. In order to improve the tuned state of a blisk satisfactorily, a number of blade-alone natural frequencies may have to be matched. This will limit the mass-stiffness combinations yielding these natural frequencies. The efficiency of matching more than one blade alone frequency is discussed in the next section. However, in cases where only one natural frequency is to be matched, efforts should be made to identify the most sensitive parameters so that the effectiveness of the tuning can be maximised. In an ideal case, when the mistuning distribution is known precisely, corrections through mistuned parameters will yield the desired tuned state. However, in general, the mistuning patterns are not known. Additionally, it may not be possible to modify those which are parameters responsible for mistuning in the direction

required. In such cases the tuning will have to be done using other parameters and therefore it is important that the sensitive parameters are identified.

4.2.3.3 Tuning by matching two natural frequencies

In cases where both of the blade-alone frequencies of the lumped parameter model used are to be matched, the appropriate combinations of tuning parameters (note that tuning has to be performed through more than one parameter) leading to these frequencies are limited. For realistic ranges of parameters, in fact, this combination is mostly unique. Figure 4.13 presents two plots which show the variation of penalty function sought to be minimised (i.e., $J = \lambda_{calculated} - \lambda_{target}$) by appropriate values of the tuning parameters. In (a), only the first frequency of the isolated blade is considered and the values of tuning parameters yielding a solution are indicated by a red contour line at 0 level. When two frequencies are to be matched, (b), the intersection of the 0 contours produces only two points, shown in red. One of these points suggests that a mass parameter to be increased by 300% and this is clearly not realistic. Thus, a unique solution is obtained.

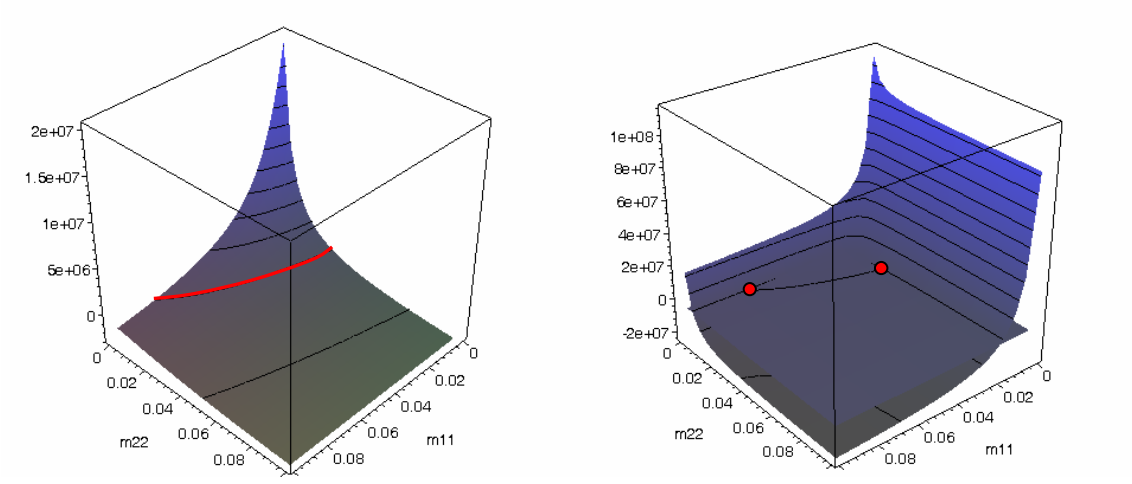

Figure 4.13 Valid combinations of tuning parameters when (a) one frequency, and (b) two frequencies are matched

A table of cases analysed is given in Table 4.7. The blade root stiffness was mistuned in all cases and the same blade mistuning pattern was maintained. In the first three cases, the first blade-alone frequency was tuned to be compared with the cases 3-6 where both of the blade-alone natural frequencies were tuned. All the frequencies were brought literally to the same level (matched up to 12 significant digits).

	Mistuned through				Tuned through				# of matched frequencies
Case	k_{b1}	k_{b2}	m_{b1}	m_{b2}	k_{b1}	k_{b2}	m_{b1}	m_{b2}	
1									1
2									1
3									1
4									2
5									2
6									2

Table 4.7 Mistuning/tuning test configuration

The results obtained are shown in Figure 4.14. Depending on the combination of parameters used to match both of the blade alone frequencies, significantly different results were obtained. The best tuned reference case was achieved in case 5 where the split in all ND modes was substantially reduced. The harmonic content of the modes of this case exhibited clear components, corresponding to the ND indices. Cases involving tuning through mid-blade mass m_{b1} yielded the poorest results. Interestingly, the cases 1 and 3, where only the first blade-alone natural frequencies were matched, produced, in general, relatively better results compared to the cases 4 and 6 where both of the blade-alone natural frequencies were matched.

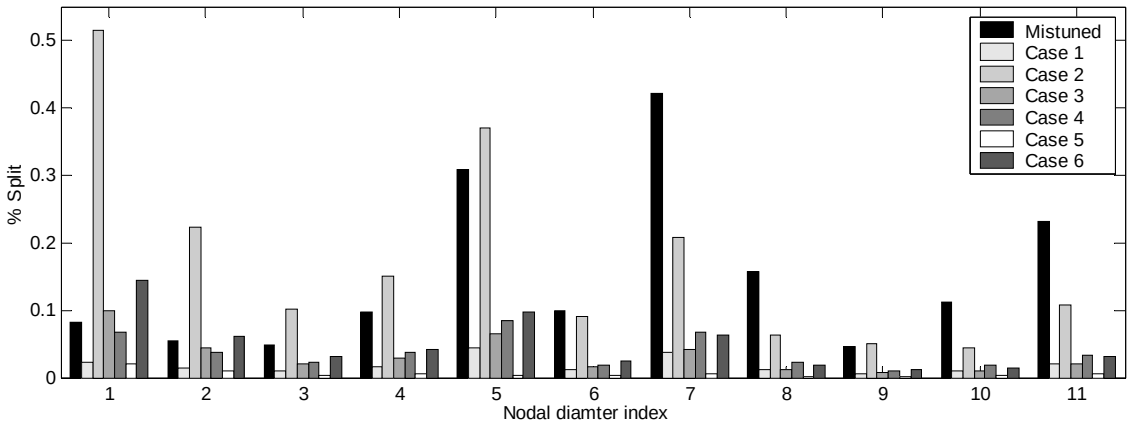

Figure 4.14 The comparison of cases given in Table 4.7.

4.2.3.4 Concluding remarks

It has been demonstrated through various virtual tests that the tuned state of a blisk obtained by adjusting 1F blade-alone natural frequencies, no matter how accurate the frequencies are matched, cannot be improved beyond a certain accuracy. However, depending on the desired level of accuracy, some parameters give substantially better results than others. In fact, the simulations showed that, tuning through some parameters might even worsen the tuned state. Therefore, before a tuning process is undertaken, it is useful to perform preliminary simulations on a numerical model to identify the most effective parameters.

The tuned state of the blisk has been sought to be improved by matching the natural frequencies of the both, in-phase and out-of-phase, blade-alone modes of the model used. With proper selection of tuning parameters it has been possible to obtain a substantially better tune state compared to the cases where only 1F blade frequencies were matched. However, it has been demonstrated that matching both of the frequencies does not automatically produce the desired tuned case. Though both blade frequencies were matched, some cases produced inferior results. Therefore, the selection of proper tuning parameters is as effective a factor as the number of matching frequencies. In fact, in a tuning

process, attempts are made to enhance the dynamic properties of an assembly by using a sub model of smaller size (e.g. an isolated blade) and different boundary conditions. When the sensitivities of the natural frequencies of the sub model to the tuning parameter are considerably different to those of the assembly frequencies of interest, the tuning process may not lead to an improved tuned state.

4.3 Model Updating

Up to this point, we have presented computed and measured blisk characteristics separately. In a given design-to-manufacture process, though, the characteristics of a machined test piece are inevitably different from those of the design model. This might be either due to variations in dimensions resulting from manufacturing tolerances or different material properties, or, in general, due to both. The bladed disks introduced in the previous section are no exception and a systematic approach is needed to reconcile the measured and predicted properties. For this purpose, two techniques, inverse eigensensitivity (IES) and so-called Fundamental Mode of Mistuning-Identification (FMM ID) methods, have been used at various stages of updating of Blisk-1 and Blisk-2 FE models.

4.3.1 Inverse eigensensitivity method

The inverse eigensensitivity method, [85-86], is one of the most commonly-used FE model updating techniques in which either eigenvalues and/or eigenvectors of the system are sought to be brought closer to the reference values (generally measured data) by making appropriate changes to the updating parameters based on the sensitivity of the system mass and stiffness matricies to these updating parameters. The method employed in this study uses only the eigenvalues in the updating process and therefore the Inverse Eigenvalue Sensitivity (IES) method is employed.

The ultimate goal of this method is to minimise the distance between the measured and current model eigenvalues. Often an objective function of the following form is used for the minimisation process:

$$J(p) = \Delta z^2 \tag{4.1}$$

Where $\Delta z = \left(\lambda^{FE} - \lambda^{ref}\right)$, and λ^{ref} represents the vector of measured eigenvalues and λ^{FE} the current values of the corresponding estimated eigenvalues. As the penalty functions are generally nonlinear functions of updating parameters, they are usually represented by truncated Taylor series. Representing λ^{FE} as a function of updating parameters, p, and expanding with respect to linearisation point $p = p_0$ and keeping only the 1st term gives

$$J(p) \cong \left(\Delta z^0 + S_0 \delta p\right)^2 \tag{4.2}$$

where the first term in the brackets represents the difference between measured and calculated eigenvalues at the linearisation point, $S_0 = \dfrac{\partial \lambda^{FE}}{\partial p}$ is the vector containing the sensitivities of the eigenvalues to updating parameters and δp is the vector of increments to updating parameters which the updating process seeks to obtain. The values of updating parameters can be found by partial differentiation and then equating Equation (4.2) to zero. After some manipulations, the updating equation in matrix form can be found as follows:

$$[S_\lambda]\{\delta p\} = \{\Delta z^0\} \tag{4.3}$$

Here, $\{\delta p\}$ is the vector of changes in updating parameters to be calculated and $[S_\lambda]$ is the sensitivity matrix containing first derivatives of the eigenvalues with respect to updating parameters. These sensitivities are calculated from the structural eigenvalue problem of the form;

$$[K]\{\phi_r\} = \lambda_r [M]\{\phi_r\}, \qquad r = 1..m \tag{4.4}$$

where K and M are the system stiffness and mass matricies. λ_r and $\{\phi_r\}$ are the eigenvalue and mass normalised eigenvector of the *rth* mode. Differentiating Equation (4.4) with respect to an updating parameter, p_r, yields;

$$\frac{\partial[K]}{\partial p_r}\{\phi_r\}+[K]\frac{\partial\{\phi_r\}}{\partial p_r}-\frac{\partial\lambda_r}{\partial p_r}[M]\{\phi_r\}-\lambda_r\frac{\partial[M]}{\partial p_r}\{\phi_r\}-\lambda_r[M]\frac{\partial\{\phi_r\}}{\partial p_r}=0 \qquad (4.5)$$

Premultiplying Equation (4.5) by $\{\phi_r\}^T$, rearranging and substituting $\{\phi_r\}^T[M]\{\phi_r\}=1$ and $\{\phi_r\}^T[K]-\lambda_r\{\phi_r\}^T[M]=0$, the formula for eigenvalue sensitivity can be obtained as,

$$\frac{\partial\lambda_r}{\partial p_r}=\{\phi_r\}^T\left(\frac{\partial[K]}{\partial p_r}-\lambda_r\frac{\partial[M]}{\partial p_r}\right)\{\phi_r\}. \qquad (4.6)$$

Therefore sensitivity of an eigenvalue to updating parameters can be calculated from that eigenvalue and the corresponding eigenvector. Applying Equation (4.6) for all updating parameters, the sensitivity matrix $[S_\lambda]$ of equation (4.3) can be formed. Generally the penalty functions are non-linear function of updating parameters therefore the solution of these equations require an iterative process to be employed. In general the computed eigenvalues of the updating process are weighted by some weighting factors to reflect the variation in the accuracy of their measurements. In this case the data known to be more accurate is given more weight in calculations.

4.3.2 FMM ID method

The Fundamental Mistuning Model– Identification (FMM ID) is a method of mistuning identification proposed in [28]. It is based on the Fundamental Mistuning Model (FMM) given in [13] where a highly reduced, 1 DOF per sector, model of a bladed disk is used to predict the forced response for an isolated family of modes. The FMM ID uses vibratory response measurements of a whole bladed disk to work out existing mistuning on a sector to sector frequency deviation basis. As it uses system modes and natural frequencies in analysis, means that it is particularly suitable for integrally machined bladed disks (i.e.

blisks). The fact that mistuning is identified for a cyclically symmetric sector, disk mistuning as well as blade mistuning can be accounted for. This feature is of particular importance for Blisk-1 since the inherent mistuning in this test piece is not known and non-negligible. Meaningful predictions using this blisk will only be obtained once the asymmetry is accounted for.

Details of the theory of the method can be found in abovementioned references. A brief description of the underlying equations is summarised as follows. The FMM modal equation upon which the theory of FMM ID is based, is given in [28] as:

$$\left([\Omega]_T^2 + 2[\Omega]_T \lceil \bar{\Omega} \rceil [\Omega]_T\right)\{\mathrm{B}\}_j = \omega_j^2 \{\mathrm{B}\}_j \tag{4.7}$$

where $[\Omega]_T$ is a diagonal matrix of tuned system frequencies, $\lceil \bar{\Omega} \rceil$ is a matrix containing the discrete Fourier transforms of the sector frequency deviations, each row of which is identical but shifted circularly. The eigenvector of Equation (4.7), $\{\mathrm{B}\}_j$, contains the weighting factors that describe a mistuned mode as a sum of tuned system modes in the form $\varphi_j = \sum_{m=0}^{N-1} \mathrm{B}_{j_m} \phi_m^T$ where ϕ_m^T is the *mth* tuned mode shape and B_{j_m} is the corresponding weighting factor.

In Equation (4.7) the mistuning pattern is provided and the resulting mistuned mode shapes and frequencies are calculated. The main idea of FMM ID is to invert the FMM equation such that when mistuned modes and frequencies are known, the individual blade mistuning pattern could be extracted as the deviation of sector frequencies. The sector frequency of a particular sector used here is calculated by mistuning all the sectors of the bladed disk in the same way (i.e. by obtaining a new tuned system) and then calculating the mean ND mode (i.e., 6ND mode in the case of a 24-blade bladed disk) of this system. The same is repeated for all the mistuned sectors and the deviation of calculated mean ND modes is taken as the mistuning pattern and defined as sector frequency deviation.

Two mistuning identification methods are proposed:

(i) basic FMM ID: where information of tuned mode shapes and frequencies is expected to be provided (usually from FE). The mistuning identification in this case is carried out through following equation:

$$\bar{\omega} = \left(2[\Omega]_T [\Gamma]_j\right)^{-1} \left(\omega_j^2 [I] - [\Omega]_T^2\right) \{B\}_j \tag{4.8}$$

Where the inverse DFT of vector $\bar{\omega}$ gives the sector frequency deviation (i.e., mistuning), matrix $[\Gamma]_j$ is formed by scaling the weighting factors given in $\{B\}_j$ by corresponding eigenvalues given in Ω_T on an element by element basis. Each row of this matrix is again identical but circularly shifted by one element in each row. Equation (4.8) requires only one mode and the corresponding natural frequency to work out the mistuning. Therefore errors in the measurements are directly reflected on the identified mistuning pattern. In order to minimise the effects of measurement errors, this equation is formed for several measured modes for the modes of the family of interest and the resulting assembly of equations is solved via a least squares fit as it cannot be solved by direct inverse due to its over-determined nature.

(ii) advanced FMM ID: where only the experimentally-identified mistuned natural frequencies and mode shapes of the bladed disk are needed. In this case an estimation of the tuned bladed disk natural frequencies, as well as the mistuning pattern, is returned. The equation of mistuning identification in this case is given as:

$$\left[[P]_j \quad 2[\Omega]_T [\Gamma]_j\right] \begin{bmatrix} \lambda \\ \bar{\omega} \end{bmatrix} = \omega_j^2 \{B\}_j \text{ where } P_j = \begin{bmatrix} B_{j0} & & & \\ & B_{j1} & & \\ & & \ddots & \\ & & & B_{jn} \\ B_{j1} & & & \end{bmatrix} \tag{4.9}$$

Here, the given $[P]_j$ matrix is formed for a bladed disk with an even number of blades. A similar one can be constructed when this number is odd. λ is the vector of natural frequencies corresponding to identified tune case and, again,

the inverse DFT of $\bar{\omega}$ yields the sector frequency mistuning. In order to obtain a unique solution for the tuned bladed disk frequencies it is assumed that the mean value of the mistuning is zero. Similarly, Equation (4.9) is constructed for several modes to minimise the measurement errors. Unlike Equation (4.8), Equation (4.9) cannot be solved by the least-squares fit method as the tuned natural frequencies in $[\Omega]_T$ in this case are not known. Solution of this non-linear equation, therefore, is obtained through an iterative process.

4.3.3 Updating of Blisk-2

Although Blisk-2 was shown to be sufficiently tuned, the measured frequencies were inevitably different from those of the design model. Therefore a model updating step needed to be taken before this model could be used in predictions. The frequencies of the first 4 families of modes (1F, 1E, 2F and 3F) were measured via impact testing. The response was measured from the tip of each blade by using an LDV transducer. The correlation of measured and computed 1F natural frequencies of the Blisk-2 at the beginning of updating process is given in Table 4.8. Some of the measured ND modes were found to be slightly split. In this table the mean values of the split natural frequencies are given for convenience.

ND	0	1	2	3	4	5	6	7	8	9	10	11	12
Exp.	-	121.62	172.34	212.44	240.98	257.58	267.7	274.18	278.52	281.42	283.3	284.38	284.68
FE	169.73	169.09	180.21	210.29	236.35	252.42	262.28	268.65	272.9	275.74	277.57	278.59	278.92
% diff.	-	28.07	4.36	-1.02	-1.96	-2.04	-2.07	-2.06	-2.06	-2.06	-2.06	-2.08	-2.07

Table 4.8 Initial correlation of measured and computed Blisk-2 1F frequencies (all frequencies in Hz)

In the FE model, the degrees of freedom at the bore of the central hole were fully fixed (i.e. the flexibility of the shaft was ignored), as this is the general approach in bladed-disk analyses. However, achieving the same condition in the test setup was not practically possible and the eventual blisk-shaft coupling possessed

some degree of flexibility. The effect of this, was predominantly reflected on the 0-4ND mode frequencies, the 0 and 1 ND frequencies being particularly affected. The contribution of the flexibility of the shaft on bladed-disk modes was studied in [11] and similar findings were reported. However, as the lower ND modes were not considered in the present study, the shaft flexibility was not included in the FE analyses.

For most of the higher modes, the computed frequencies differed uniformly from the measured ones by about 2%. Therefore, choosing an updating method such as IES and including only these modes, the FE model could easily be corrected to be a better representation of the real blisk. The mode shapes were not included in the updating process as the blisk was found to be reasonably tuned (i.e., having regular diametral mode shapes). Therefore, in theory, selecting the material properties as updating parameters would suffice to reconcile measured and computed frequencies. During the design phase, material properties, density and modulus of elasticity, were taken to be $\rho = 7800\,kg/m^3$ and $E = 210\,GPa$ respectively. Only the modes with 5ND and higher were included in the updating process as the lower ones were less reliable due to the abovementioned reason. After a number of iterations, the IES method converged to a reasonably tuned FE model with its 1F frequencies fluctuating within ±0.1% (mostly around ±0.03%) of the measured values as shown in Table 4.9. The correlations of 1E, 2F and 3F family natural frequencies are also given in this table for which the deviations are less than 1%, 0.15% and 2.2%, respectively. Final density and modulus of elasticity values were obtained as $\rho = 7594.3\,kg/m^3$ and $E = 207\,GPa$.

	1F			1E			2F			3F		
ND	Exp	FE	% Diff	Exp	FE	% Diff	Exp	FE	% Diff	Exp	FE	% Diff
5	257.58	257.33	0.10	722.82	729.37	-0.91	1359.60	1357.50	0.15	2774.50	2713.76	2.19
6	267.70	267.54	0.06	723.18	728.74	-0.77	1477.40	1475.18	0.15	2802.50	2762.80	1.42
7	274.18	274.13	0.02	723.30	728.22	-0.68	1555.00	1553.16	0.12	2819.30	2789.31	1.06

8	278.52	278.52	0.00	723.68	727.78	-0.57	1606.40	1604.90	0.09	2819.60	2805.64	0.50
9	281.42	281.47	-0.02	723.82	727.43	-0.50	1640.20	1639.03	0.07	2830.40	2816.28	0.50
10	283.30	283.36	-0.02	724.30	727.18	-0.40	1661.60	1660.66	0.06	2830.70	2823.11	0.27
11	284.38	284.41	-0.01	724.40	727.03	-0.36	1673.80	1672.65	0.07	2873.80	2826.95	1.63
12	284.68	284.76	-0.03	725.00	726.98	-0.27	1677.40	1676.50	0.05	2841.20	2828.19	0.46

Table 4.9 Blisk-2, 5-12ND 1F, 1E, 2F and 3F family natural frequencies, measured and updated (all frequencies in Hz)

The ODSs of the stationary Blisk-2 for the modes included in updating process were also measured in the way described in Chapter 3 so that they could be correlated with the updated FE model. Some of the 1F family modes are compared in Figure 4.15. Spikes seen on experimental curves were due to discontinuities at platform level (where the LDV signal drops to zero). Excellent agreement was obtained not only for the lower ND modes but also for the higher ones where the modes are very sensitive to mistuning due to the high modal density. Based on the quality of correlation between measured and calculated frequencies and ODSs, the Blisk-2 FE model was assumed to be updated and could be used for prediction purposes.

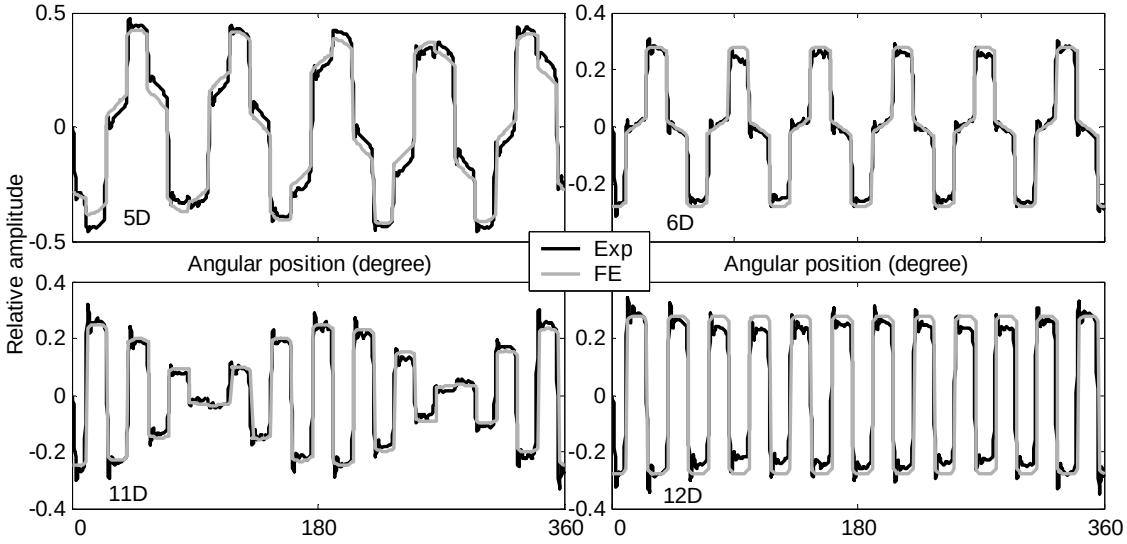

Figure 4.15 Correlation of measured and computed ODSs for 5, 6, 11 and 12D, 1F family modes

4.3.4 Updating of Blisk-1

Poor dimensional consistency of Blisk-1 made it difficult to specify a realistic set of updating parameters such that a suitable model could be constructed to reproduce the measured blisk characteristics. Thus it was decided to identify the inherent mistuning in the blisk by measuring the FRFs corresponding to modes of the family of interest and then using the FMM ID method. As this method gives mistuning in terms of sector natural frequency deviation, it could then be translated to physical mistuning using point masses at suitable locations as identified in Section 4.2.3**.** Although computational, and to a degree experimental, validation of the method has been given in [29], the FMM ID method needed to be validated independently against a real blisk so that it could be used confidently.

4.3.4.1 Experimental validation of FMM ID method

The blisk to be used in this process needed to be reasonably well tuned such that the intentional mistuning applied could be treated as the only mistuning source. For this purpose Blisk-2 was used as it has been shown to have a near perfect tuned state.

The validation was carried out in the following way: First, Blisk-2 was deliberately mistuned. Then, the FRFs at all blade tips were measured for a frequency range covering the 1F family of blisk modes. Later, these FRFs were processed in ICATS (Imperial College's Modal Analysis Software) and the modal data obtained was fed into the FMM ID equations to get the mistuning. For this purpose two mistuning patterns were used: (i) regular mistuning: sinusoidal circumferential mistuning, $Sin(8\theta)$ and (ii) random mistuning. Blades were mistuned by attaching lumped masses to the blade tips via screws through tapped holes machined for this purpose. The FMM ID method requires that the natural frequencies and corresponding mode shapes be measured for a few modes of the family of interest. During this validation work almost all of the 1F

family modes were measured so that the applicability of the method could be checked when various combinations of measured modes were used. The FRFs were measured by applying a pseudo-random excitation through an electromagnet and measuring the response at blade tips using an LDV beam normal to the plane of the blisk. Since the FMM ID operated on the relative amplitudes of response measurement locations at a given resonance, the measured mode shapes did not need to be normalised by the actual applied force magnitude but they were divided by the voltage input generated by the power unit driving the electromagnet (Note that here it is assumed that the force generated is proportional to the input voltage). Each mode shape contained 24 measurement points corresponding to deflections at the 24 blade tip locations.

As will be explained in the next chapter, the response prediction tools used required that the mistuning pattern be expressed in terms of the frequency variation of a sub-model, such as a blade clamped at the root. The applied mass mistuning, therefore, was converted to blade frequency deviation so that a consistent mistuning definition could be used. This was done by modelling a single blade of Blisk-2. The geometry and the weight of the mistuning masses were modelled as closely as possible and the 1F frequencies of all the blades clamped at the root were computed. The percentage deviations of these frequencies from those of the perfectly tuned blade were calculated to obtain the actual frequency mistuning. Bearing in mind that the FMM ID method expresses mistuning as sector frequency deviation (see Section 4.3.2 for the definition of the sector frequency), further processing of the obtained mistuning is necessary to get comparable results. Assuming the mistuning is confined to the blade, which in this case it is, a sector frequency deviation simply differs from a blade frequency deviation by a scaling factor. To obtain the appropriate scaling factor, N/4 ND mode frequency (i.e., the reference ND mode FMM ID uses in computations), N being the total number of sectors, of the perfectly tuned Blisk-2 was computed. Then, the blade modulus was changed uniformly to increase it's frequency by 1%. Using this modulus for all blades N/4 ND mode frequency of

the blisk was recalculated. The inverse of the percentage change in N/4 frequency in both cases, therefore, gave the scaling factor to obtain the blade frequency deviation from the sector frequency deviation. The scaling factor for Blisk-2 was found to be 1.11 so the output of FMM ID was multiplied by this factor to obtain the blade frequency deviations.

The correlation between the applied mistuning pattern and the one identified through the FMM ID Basic method is given in Figure 4.16. The tuned blisk frequencies provided for mistuning identification were those of the updated model given in the previous section. Overall, a very good match is obtained between the two patterns with a correlation coefficient of 98.8%. The only significant deviation observed was for blades 7 to 10. Here it must be noted that the effectiveness of the mistuning prediction method relies totally on the accuracy of the provided modal data. Since they possess repeated modes, providing reliable modal data could be difficult for symmetric structures such as bladed disks. In the case of these double modes being slightly split, identification of mode shapes and frequencies requires very high frequency resolution which may not be achievable, depending on the analyser used. Here, the prominent deviations observed from Figure 4.16 are thought to be associated with this feature of the blisk rather than the inefficiency of the identification tool. Note that although mistuned, the blisk in this case is still symmetric and most of its double modes (in fact, all but 8 and 4 ND modes) are only slightly split if at all.

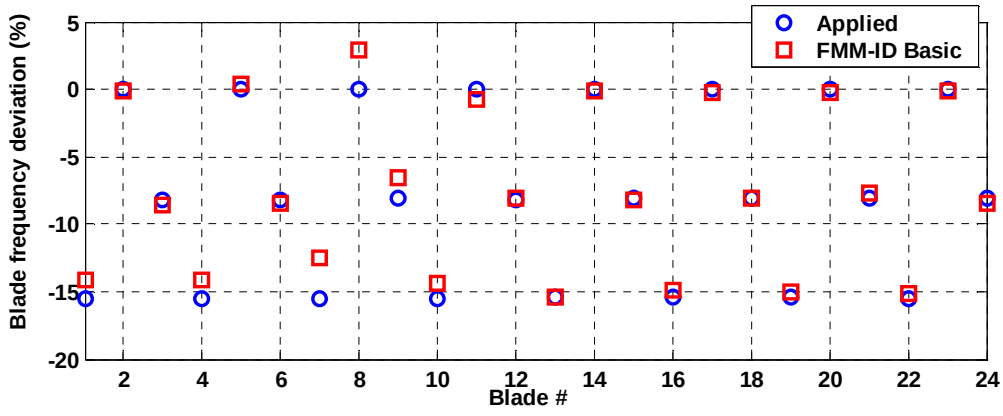

Figure 4.16 Correlation of applied and identified mistuning patterns - $Sin(8\theta)$

The same analysis was carried out for a random mistuning pattern. The mistuning masses used were those of the previous case but were reshuffled randomly. The results of this case are given in Figure 4.17.

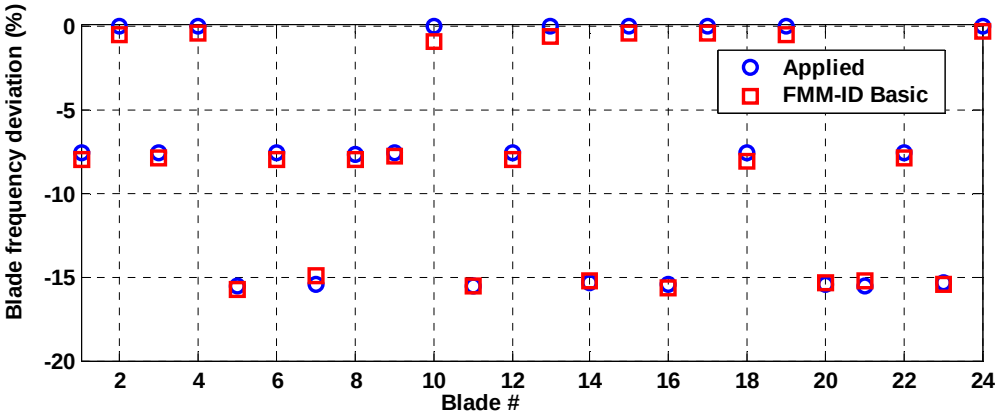

Figure 4.17 Correlation between applied and identified mistuning patterns - Random

In the random mistuning case, all the double modes of the 1F family of modes of the blisk were sufficiently split that the natural frequencies and the corresponding mode shapes could be measured more accurately. As a result, better estimates were obtained, as seen from Figure 4.17. Although small, some deviations are still observed between the identified and applied mistuning patterns. This may be due to two reasons: first, the blisk may not have been perfectly tuned, as is assumed in the FE calculations, and this combined with deliberate mistuning might have produced the variation obtained. Second, the results labelled as "applied" are, as mentioned, obtained from an FE analysis by modelling the mistuning masses. Errors introduced through the modelling process might have led to slightly different variations than the actual.

4.3.4.2 Identification of the mistuned state of Blisk-1

The FMM ID method uses the frequencies and mode shapes of a blisk measured at its blade tips. However, ODSs measured at platform levels were also made available to assess the quality of the updated model. The FRFs of the blisk, after

it was subjected to the tuning process given in Section 4.2.1, were measured in the same way as the Blisk-2 measurements were conducted for FMM ID validation. The blisk was clamped in the centre in the same way as it was to be clamped in the rig. The natural frequencies and mode shapes were extracted from measured FRFs by using ICATS software. The correlation between the natural frequencies of the initial design and the measurements is given in Table 4.10. A sufficiently fine frequency resolution (0.008 Hz) was used in order to make sure that split ND modes were identified accurately. AutoMAC between the measured mode shapes was also checked and excellent orthogonality was observed, as given in Table 4.10.

1F ND	Experimental		Computed	% Difference	AutoMAC
	Freq1 (Hz)	FE (Hz)	Freq 2 (Hz)		
0	102.58	NA	133.503	-30.15	
1	29.42	29.802	117.474	-296.72	
2	136.72	136.831	110.607	19.13	
3	204.32	204.540	195.522	4.36	
4	247.25	247.345	234.527	5.16	
5	266.56	266.658	252.078	5.45	
6	275.74	275.772	260.519	5.53	
7	280.53	280.730	265.078	5.54	
8	283.41	283.487	267.748	5.54	
9	284.94	285.354	269.375	5.53	
10	286.097	286.186	270.354	5.52	
11	286.716	286.937	270.881	5.56	
12	287.535	NA	271.048	5.73	

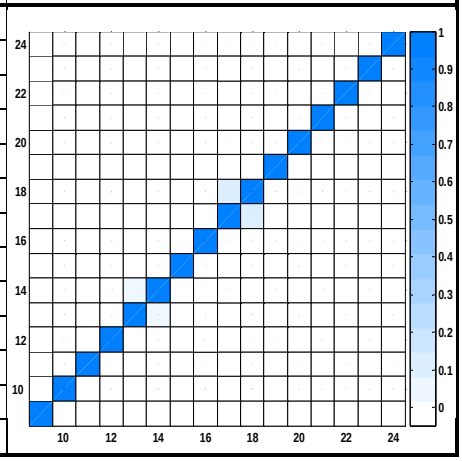

Table 4.10 Correlation between initial FE and measured frequencies (-- Frequencies used in IES method, --: modes used in mistuning identification)

Note that the experimental values given in this table are slightly different from those given in Table 4.2. This is due to the integration of blade inserts. The frequencies, in general, are lower. However, the split in the mode pairs and the distortion of the mode shapes were unchanged. In fact, during the integration of the blade inserts, efforts were made to improve the tuned state of the blisk by arranging the blade inserts appropriately. However, little, if at all, improvement was achieved. In the light of findings presented in Section 4.2.3, this was not

surprising, since the assembly modes were found to be not very sensitive to mass changes at the locations where the inserts were mounted.

As for the Blisk-2 case, the natural frequencies of the 0, 1 and 2-ND modes were significantly lower than the predicted ones due to different boundary conditions in the real test setup and the FE model. As for the 3-ND and higher modes, a steady deviation of 4-6% was apparent. The fact that the deviation for these modes was in the same direction (i.e., experimental frequencies were higher than FE predicted ones), indicated that the overall material properties needed to be adjusted. At first, it was sought to change the material properties such that the percentage difference between the measured and computed frequencies oscillated around zero. This could be done either through modifying the density or elasticity modulus, or both, using the IES method.

When designing Blisk-1, the material properties, density and modulus of elasticity, were assumed to be $\rho = 7800\,kg/m^3$ and $E = 210\,GPa$, respectively. These were used as updating parameters in the IES updating method. The 5ND and higher modes were taken into account in the analysis as the lower modes were known to be less accurate for other reasons. The reference frequency value aimed at for each ND mode was the mean value of the corresponding split pair measured. At the end of the updating process, the density and elastic modulus were found to be; $\rho = 7130\,kg/m^3$ and $E = 215\,GPa$. Using these values, the 1F blisk natural frequencies (those with 5ND and higher) were brought within 0.6% of the reference (i.e. measured) natural frequencies, as given in Table 4.11.

ND #	5	6	7	8	9	10	11	12
FE	266.78	275.71	280.53	283.36	285.08	286.12	286.68	286.85
Exp. (mean.)	266.61	275.76	280.63	283.45	285.15	286.14	286.83	287.54
% Difference	-0.06	0.02	0.03	0.03	0.02	0.01	0.05	0.24

Table 4.11 Blisk-1 FE frequencies after updating via IES method

Now that the 1F natural frequencies of the FE model were brought closer to the actual values, the FMM ID Basic method could be used to identify the inherent mistuning as a deviation from this tuned FE model. Again, only 5ND and higher modes were used in the analysis. The mistuning pattern, obtained as a set of sector frequency deviations, was again converted such that it could be expressed in terms of the frequency deviation of the sub-model used. In the case of Blisk-1, a cyclic sector is used as a sub-model and is clamped at the cyclic boundary faces (faces on which cyclic symmetry boundary conditions are applied). The reason for this was that the sector model would have the disc portion as well as the blade and therefore it would be possible to include the effect of disc mistuning too. The FE model calculations revealed that a scaling factor of 1.14 (i.e. 1.14xNat. Frequencies) needed to be used in the conversion. The deviation of the clamped sector-alone 1F natural frequencies obtained using this scaling factor is given in Figure 4.18.

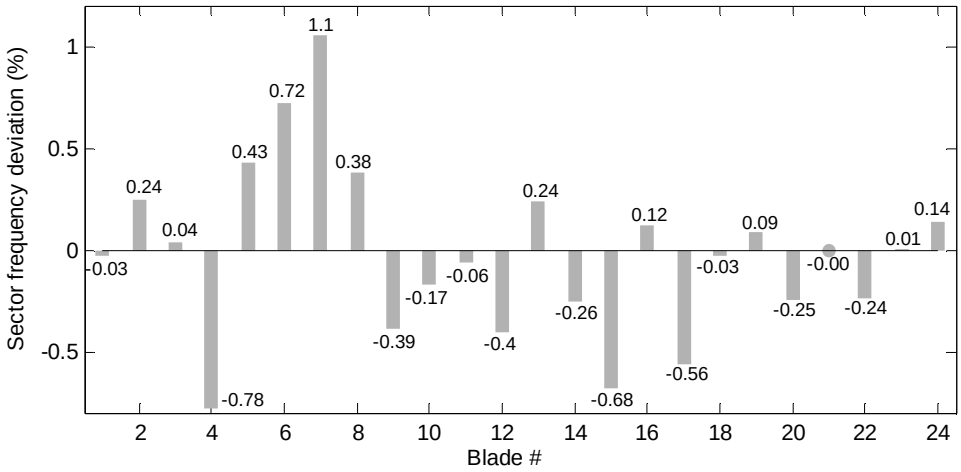

Figure 4.18 Identified Blisk-1 mistuning in terms of clamped, sector-alone frequency deviation

4.3.4.3 Verification of the mistuning pattern identified

The accuracy of the mistuned natural frequencies and the mode shapes calculated using the pattern identified had to be checked against the measured counterparts. This, eventually, would have to be done using the full Blisk-1 FE model but some preliminary checks could be performed by using the 1 DOF

sector model of the FMM method. To this end, the mistuning pattern was used in Equation (4.7) and the mistuned mode shapes of the blisk were recalculated. The correlation between the measured and calculated mode shapes is given in Figure 4.19 (a). Another useful check was to use the FMM ID Advanced Method (i.e. no tuned FE model data provided) to calculate the natural frequencies of the tuned reference state from the mistuned mode shapes and frequencies. The closeness of these tuned frequencies to the FE model frequencies used in the FMM ID Basic Method would provide further confidence in the obtained result. This comparison is given in Figure 4.19 (b). It is seen that the estimates for the 0-4D modes are significantly higher. This can be explained by the fact that only the 5D and higher modes were included in the identification process. In this case, the estimates for the excluded modes were worked out based on the amplitudes of the components corresponding to these modes (i.e. spatial Fourier harmonics) in the included ones. Better estimates for the natural frequencies of these modes could be obtained by inclusion of their mode shapes in the process. Note that the mistuning identification is not affected by the exclusion of these modes. A very close match is obtained for included modes (i.e. 5D and up) indicating that the mistuning obtained is reasonably accurate.

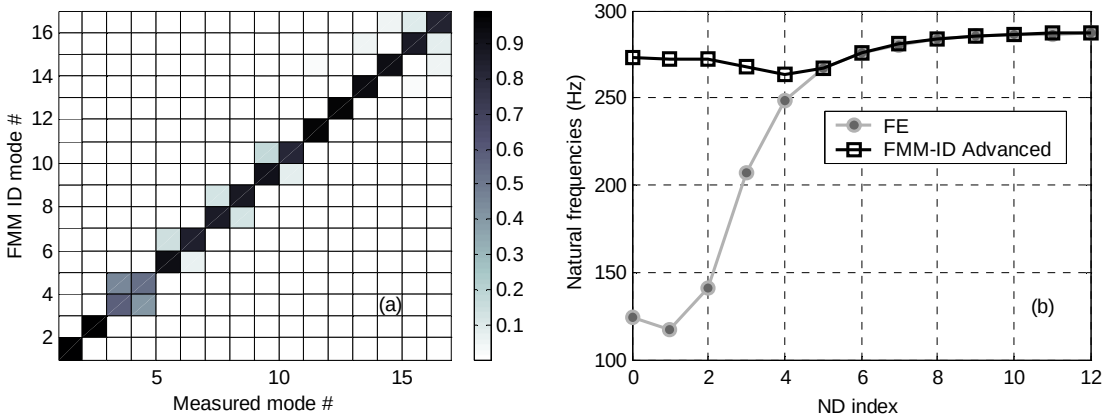

Figure 4.19 (a) Correlation between measured and FMM calculated mistuned modes, (b) Full FE model tuned frequencies vs. FMM ID Advance estimates

Good initial correlation obtained using the 1 DOF per sector model of the FMM method was tested with the FE model of Blisk-1, as this model would be used in

the analyses. The prediction tool to be used, which is to be validated in the course of this study, was intended for response calculations only and did not provide mode shapes. As a result, the mode shapes of Blisk-1 with applied mistuning pattern needed to be calculated using a commercial FE package, such as ANSYS. Since the cyclic sector analysis in this package was not applicable to mistuned assemblies, a full FE model needed to be prepared so that the mistuning could be applied. The easiest and most convenient way of converting the identified frequency mistuning into physical mistuning was to modify each sector's Young's modulus according to its frequency deviation. For example, if a sector's frequency deviation is +1%, one needs to multiply the Young's modulus of that sector by $1.01^2 \cong 1.02$. The fact that the mistuning identification method operates on a 1 DOF sector model, means that representing the mistuning in this way (i.e. uniform variation of a single parameter for each sector) yields a very good approximation. Thus, the results obtained by this can be used as a benchmark for the aptness of the model to be used in the prediction tool, in which mistuning is required to be implemented by way of local mass and stiffness adjustments. The correlation of the mode shapes of the full FE model and those obtained from measurements is given in Figure 4.20 (a). The mean value of MAC for the modes included in the mistuning identification was 86.5%, indicating a successfully updated model. The natural frequencies of the full FE model were also correlated with the measured ones. A maximum error of 0.7% was observed for modes 8 and 9. However, in general, the calculated frequencies were within 0.3% of the measured ones, as shown in Figure 4.20 (b). The larger deviations in the lower natural frequencies, as mentioned, were due to the flexibility of the disc clamping during measurements.

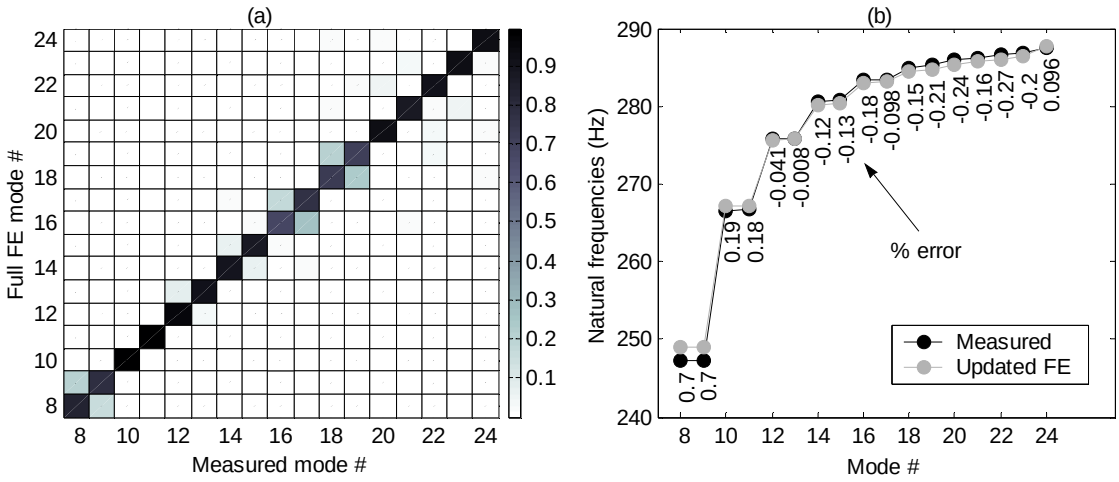

Figure 4.20 (a) Correlation of the measured Blisk-1 modes with updated Blisk-1 FE model, (b) measured and computed Blisk-1 frequencies for 1F modes (8-24).

4.4 Test design

In a study seeking validation of numerical predictions, the selection of the appropriate test configurations carries utmost importance in ensuring the effectiveness and the usefulness of the measured data. This requires that a test design phase be undertaken by performing a series of simulations in the computer environment before any real tests are performed. The test design, or test planning process in the classical modal analysis sense (i.e., drive/measurement point selection, suspension location etc.), is not applicable in this study as the information of interest is either obvious (i.e. drive/measurement points) or not applicable (i.e. suspension location). Nevertheless, depending on the nature of the phenomena being validated, there are a number of decisions the experimentalist is expected make, as explained in following sections. The test planning presented here is oriented towards the identification of test configurations (i.e. which EOs to measure, which mistuning patterns to apply etc.). Although efforts are made to draw a definitive test plan (including rotational speed ranges, necessary excitation forces, testing time etc.), adjustments to these will inevitably be necessary in practice.

4.4.1 Tuned and mistuned tests on Blisk-2

Validation of the mistuned bladed disk predictions were to be performed by using the measurement results obtained on Blisk-2. It was decided from the outset that only the 1F family of modes of the blisk should be considered. This was thought appropriate since the employed LDV measurement technique allowed only out-of-plane vibrations to be measured. It was also favourable from the data acquisition point of view as lower sampling frequencies could be used, thereby allowing manageably longer samples to be acquired for optimum signal processing.

First, the tests to be conducted on the tuned blisk were planned. When testing a bladed disk, it is necessary to map out the dynamic characteristics of the test object (i.e. the locations of resonances). Experimentally, this is done through construction of so-called *z-mod* plots. A z-mod plot is a surface plot, the height of which (i.e. z-axis, hence the name z-mod) is determined by the vibration response amplitude measured at a given point while x and y axes are defined by the rotational speed and the vibration frequency, respectively. The colouring of this surface is proportional to the height (i.e. vibration amplitude), so that the resonances are easily observable. In order to make sure that such an experimental graph is constructed as accurately as possible, the rig can be run for the entire speed range with uniform and very small speed increments and the vibration signal recorded at each speed step. However, using very small step sizes is certainly not efficient as the valuable information and the need for fine step sizes will only be necessary at around resonances. Therefore, having a prior knowledge of the resonance map for the speed range of interest will be of immense help in reducing the measurement time and data size without compromising the completeness of the data. Based on the Campbell diagram of Blisk-2 given in Chapter 3, and the reliable and safe working limits, the operating speed limit of the test rig was chosen to be 4000 rev/min. A new Campbell diagram using the updated Blisk-2 model was constructed for this

speed range to find more accurate locations for the resonances. The constructed diagram is shown in Figure 4.21.

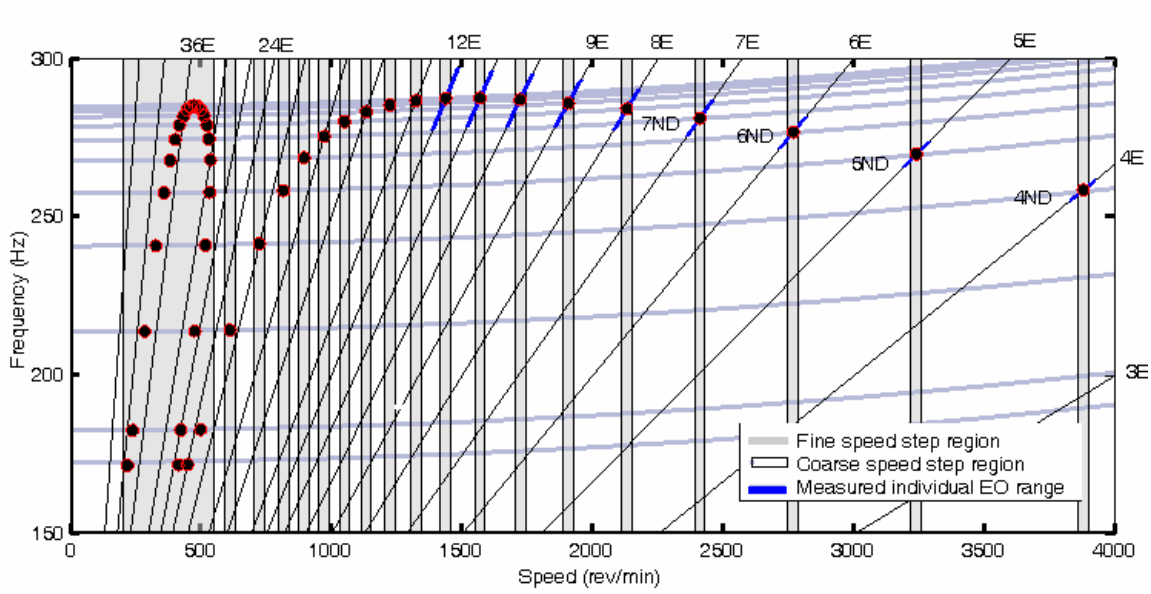

Figure 4.21 Updated Campbell diagram with identified fine and coarse speed step regions for Blisk-2

The regions at the diagram where finer speed steps are to be used are shown by grey bands. Some preliminary forced response calculations were carried out to decide on the speed step size and the width of the fine speed step ranges around each resonance. The damping values used in these computations were obtained from the modal analysis performed on the FRFs acquired for the model updating process given in previous sections. All the modes measured possessed 0.01% structural damping. With such low damping values, the resonance peaks were very sharp. It was seen that only a range of 10-15 rev/min needed to be covered for the resonance to be accurately captured. Thus, it was decided that the width of each fine-step speed band shown in Figure 4.21 (apart from the initial band where the resonance density is very high and partitioning is not worthwhile), would be 20 rev/min to allow for errors in computations and measurements. Z-mod plots would be prepared to provide a snapshot of the overall blisk characteristics. To this end, the speed step size used did not have to be very

small but fine enough to make sure that the resonances were captured. Therefore, it was decided that 6-7 points should be measured for each fine-step speed range. Thus, the fine speed step size was chosen to be 3 rev/min and all other ranges were to be step-swept at 10 rev/min.

In practice the vibration response due to a particular EO excitation (or in some cases a few) is generally of interest. In this study, however, it was decided to measure the vibration response for all 1F family of modes excited within the operating speed range of the rig (i.e. response to 4-12 EO excitations). Such a wide range of measurements for a tuned blisk was affordable since measuring only one blade for a particular EO excitation would suffice (i.e., in theory all blades of a tuned blisk have the same vibration response). The lower end of the EO range would, therefore, provide vibration data at relatively high rotational speeds and the higher end of range would make vibration data at a relatively high modal density region available. Unlike the z-mod plot measurements, EO responses were to be measured for quantified comparisons with predictions. Therefore, it was important that fine enough speed increments were used to acquire accurate response curves. Recalling from Chapter 3, the minimum attainable speed step with the motor controller employed was 1 rev/min. However, preliminary response predictions using measured damping values showed that in the immediate neighbourhood of resonance peaks, a step size of 0.05 rev/min would be needed to measure the resonance amplitudes accurately. Achieving such fine speed increments would be very difficult in practice, if indeed possible at all, and extremely expensive. Instead of comparing the whole resonance curve, on the other hand, off-resonance regions (i.e. rising and falling flanks of response curves), which could be constructed accurately using the minimum achievable increment of 1 rev/min, could be used to correlate the measurements and predictions. This is demonstrated on a computed response curve shown in Figure 4.22. The red dots shown here represent likely measurement points. It is seen that, bar the "region of uncertainty", the response curves can be measured reasonably well by using 1 rev/min steps. Based on

Figure 4.22, a speed range of 100 rev/min, centred about the corresponding resonance (EO-ND crossing), was chosen for each response curve, as indicated by the blue portions of EO lines given in Figure 4.21.

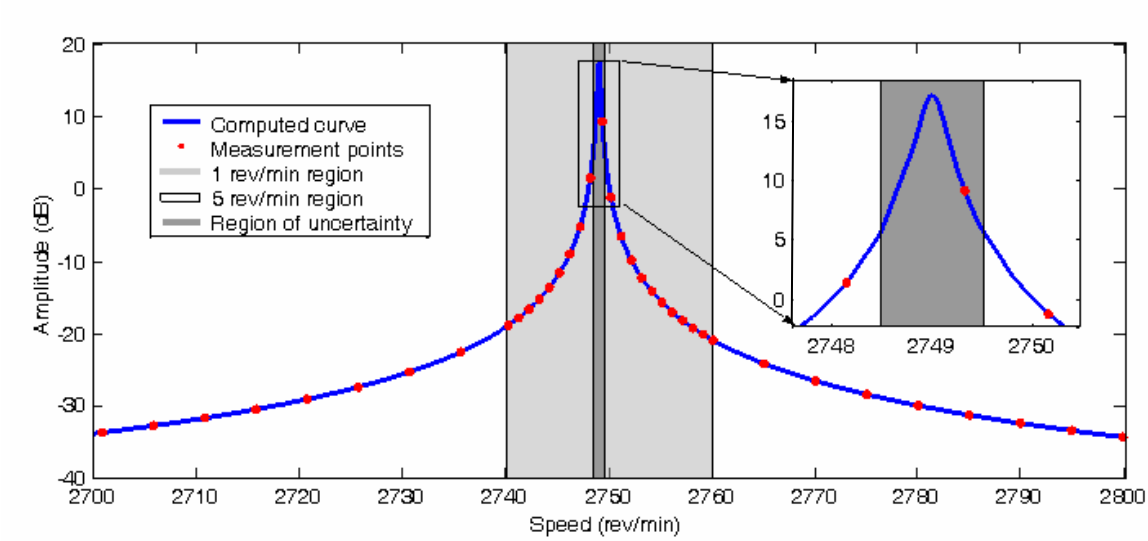

Figure 4.22 Measurement plan for a particular EO response curve

With the completion of the test plan for tuned measurements, a mistuning test programme was attempted next. To this end, the shapes and corresponding amplitudes of mistuning patterns to be applied needed to be defined. Two different sets of tests (stationary and rotating) were planned with a number of mistuning patterns applied.

The purpose of the stationary tests was to experimentally determine the effect of various types of mistuning patterns on blisk frequencies and mode shapes (or more precisely, ODSs). The results of these tests would also provide preliminary measurement data to assess the suitability of the FE model and the capabilities of the prediction tool when the results are not yet complicated by the effects of rotation. For this purpose, 3 mistuning patterns were chosen to be tested: (i) single blade mistuning (SBM), which would cause all ND modes to split, (ii) regular pattern mistuning, introducing a sinusoidal variation of blade frequencies in the circumferential direction, which would result in only particular modes splitting (see Section 2.2), and (iii) irregular (random) mistuning, which would simulate a real case scenario. Mistuning was to be

introduced using small masses attached to the blade tips. The amplitude of the largest mass to be attached was chosen such that it would cause large enough splits in the modes that they could be measured easily. Computations showed that a mass of 1.7 gram would introduce a minimum frequency spit (SBM case) of 0.2 Hz which could easily be measured with a 10Hz-span, 500-line zoom FFT. The regular pattern was selected to be $Sin(12\cdot\theta)$, which required every other blade to be mistuned by the same amount.

For the rotating mistuned tests, it was decided to use only two mistuning patterns: regular and random. The SBM was not used as it would make the blisk unbalanced and necessitate a balancing plane to be incorporated. It was thought advisable to use the same mistuning masses for both patterns so as to minimise the effort of preparing new ones. The regular pattern for the stationary tests was clearly not suitable for this purpose as it contained masses of the same amplitude. As a result, a $Sin(8\cdot\theta)$ regular mistuning pattern was chosen to be used. Fourier analysis performed on this pattern revealed the presence of strong 0^{th}, 8^{th}, 16^{th}, and 24^{th} harmonics which, recalling from Chapter 2, would cause the 0, 4, 8 and 12 ND modes to split. Noting that the 0 and 12 ND modes do not occur in pairs, only the 4 and 8 ND mode pairs would split and the corresponding resonances would be excited within the test rig's working speed range (0-4000 rev/min). Additionally, such a pattern contained 3 different blade configurations. These would provide a sufficiently random mistuning variation when shuffled arbitrarily and would require only 16 masses to be prepared out of maximum of 24.

The amplitude of the mistuning patterns was also chosen to be sufficiently large to cause considerable modal overlap, with, in consequence, noticeably irregular mode shapes – to form an interesting case for numerical predictions. After some preliminary FE analyses, the maximum blade tip mistuning was fixed at 6 grams. Since the frequencies of the blisk were reasonably separated, the mass had to be large enough to cause the desired modal overlap. The identified

regular and random mistuning patterns are given in Figure 4.23. The random pattern, as mentioned, was obtained by using the same masses as used for the $Sin(8\cdot\theta)$ mistuning, but rearranged irregularly in such a way that no significant imbalance was imposed on the blisk.

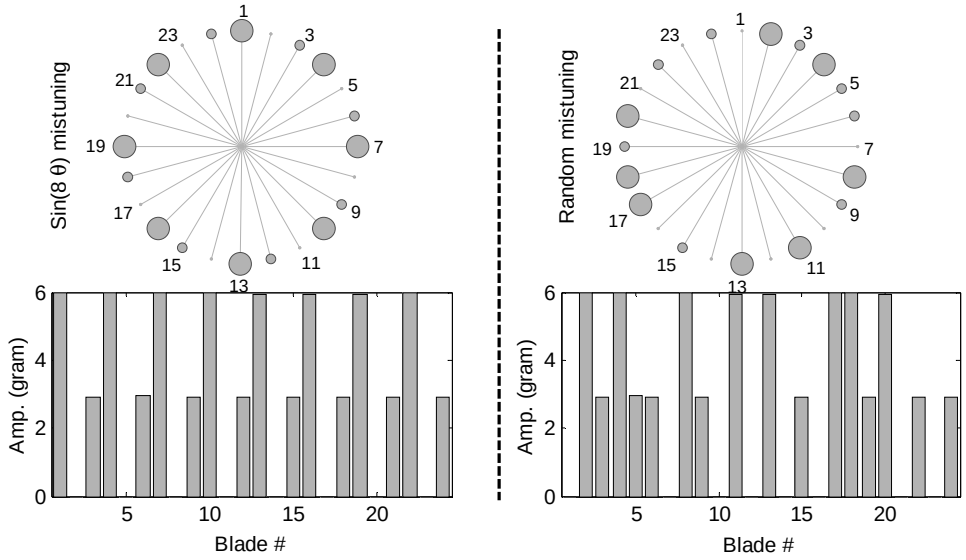

Figure 4.23 Regular and random mistuning patterns to be used in rotating (Blisk-2 tests)

A test plan similar to that for the tuned Blisk-2 tests needed to be prepared for the mistuned rotating tests. First, the $Sin(8\cdot\theta)$ case was considered and the mistuned bladed disk model was prepared. For test planning purposes, the mistuning masses were modelled as point masses. In order to find out the locations of resonances, a Campbell diagram was constructed. Only the 4-12EO lines were taken into consideration as tuned tests were also planned for this range of EOs. However, the Campbell diagram for the mistuned blisk could not be constructed in the same way as the tuned one. For the tuned blisk, the variation of natural frequencies with rotational speed was obtained by calculating the natural frequencies at various speeds. The intersection of the k-EO line with k-ND line was marked as a resonance, knowing that no other resonance will occur at the intersection of the k EO line with all other ND lines. For the mistuned system, however, a particular EO line, the kth, may exhibit more than one resonance depending on the magnitude of the kth harmonic

contained in the mistuned modes. Therefore, in order to construct the Campbell diagram for a mistuned blisk, one needs to compute the necessary EO responses (in this case 4-12 EOs) for the desired frequency (i.e. operating speed) range. The Campbell diagram computed in this way for the sinusoidal mistuning pattern is given in Figure 4.24.

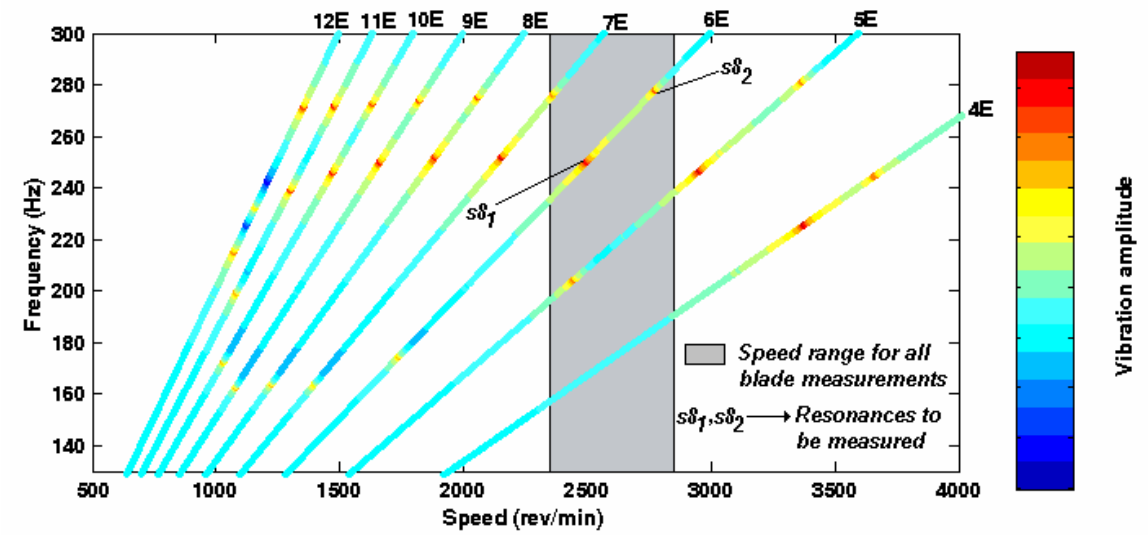

Figure 4.24 Computed Campbell diagram for $Sin(8\cdot\theta)$ mistuned Blisk-2, blade 18 (red spots indicate resonances).

The prediction tool used in the preparation of the data presented in Figure 4.24 (see Chapter 5 for more details) operated on tuned mode shapes and the natural frequencies of the blisk when calculating the mistuned response to a particular EO excitation. For this purpose, the tuned mode shapes and natural frequencies of the blisk were calculated at a particular speed and then fed into the prediction tool. As a result, the changes in the natural frequencies and mode shapes due to rotational speed were not accounted for when responses at different frequencies (i.e. rotational speeds) were calculated. When the variation of natural frequencies with rotational speed is known, more accurate locations of the new frequencies under rotation can be calculated by using this relation. So far as the data presented in the Campbell diagram of Figure 4.24 is concerned, this correction should suffice as far as the locations of resonances are of interest. The resonances shown in this diagram were shifted with respect to the rotational speed-natural frequency relation used in the preparation of the tuned Campbell

diagram. However, when response data are to be compared, the changes in the mode shapes should also be considered. A way of doing this is presented in the next chapter where the experimental and computed results are correlated.

As expected the Campbell diagram of Figure 4.24 was completely different to that of the tuned blisk Figure 4.21. In particular, an interesting formation of two distinct groups of resonances was evident where a persistent resonance at around 280 Hz seemed to be excited by all EOs. To help explain this behaviour, the mode shapes of the 1F family of modes needed to be calculated and analysed. Accordingly, a full blisk model, complete with applied sinusoidal mistuning pattern, was prepared and the first 24 modes (1F family) were calculated. To make this model compatible with the measurements, the mode shapes extracted from the FE analysis were represented by 24 points, each corresponding to a blade tip location. Fourier analysis was performed on each mistuned mode shape to determine the strong harmonics contained. A chart, mapping the 4-12 spatial harmonics of the mode shapes of the 1F family of modes is given in Figure 4.25.

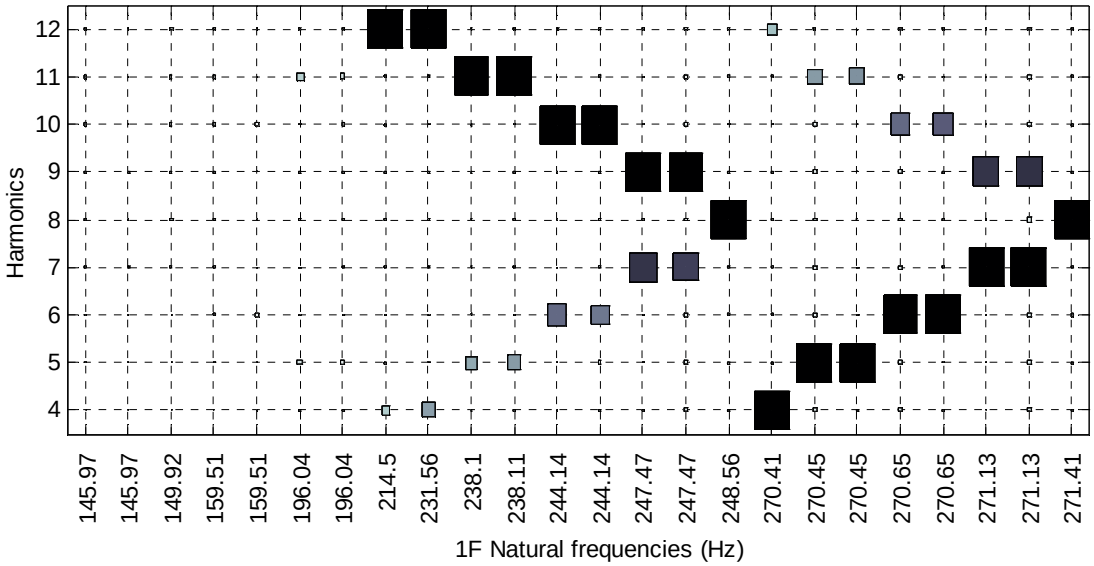

Figure 4.25 Normalised amplitude spectrum of the first 12 spatial harmonics for the first 24 Blisk 2 modes, with applied $Sin(8\cdot\theta)$ mistuning.

The harmonics map shown in Figure 4.25 correlates excellently with the Campbell diagram of Figure 4.24, where darker colours indicate stronger harmonics. For example, it is seen that three groups of modes at reasonably well separated frequencies have significant 5 nodal diameter components, and would therefore be strongly excited by 5EO. In fact, this is reflected in the Campbell diagram as three resonances appearing on the 5EO line. The primary harmonics contained in the first 16 modes were in ascending order. For modes 17 and higher, this order was reversed with a primarily 8D mode being the highest in frequency thus providing the expected modal overlap. Another interesting revelation from the harmonics map was that it clearly indicated the number of modes participating in a given resonance shown in Figure 4.24, which could not be inferred from the response curves.

The FE analysis showed that there was not one but eight modes at around 270 Hz. Different engine orders excited different modes from this group, depending on their harmonic content, but their frequencies were too close to be differentiated visually in the Campbell diagram. Although many resonances appeared in Figure 4.24, each was accounted for thanks to Fourier analysis.

Now that the resonance map of the regularly mistuned assembly was constructed, a dynamic test plan similar for that of the tuned assembly could be organized. The first step, likewise, was to measure the response on a particular blade (i.e. the corresponding blade to that was used in the construction of the computed Campbell diagram) for the full speed range so that a z-mod plot could be obtained. An optimised speed vector was prepared according to the identified locations of the resonances, similar to the one depicted in Figure 4.21, only with more speed points due to scattered resonances.

As all the blades were now experiencing different vibration amplitudes, due to the deliberate mistuning, measuring only one blade for a particular EO excitation was not enough to account for blade-to-blade response variation.

Therefore, all blades needed to be measured. If the same test plan which was adopted for the tuned assembly was to be followed here (i.e. measuring 4-12EO excitation responses but now for 24 blades), it would not be practical in terms of the measurement times. Besides, most of the data would not add any extra information so far as the validation of the prediction tool was concerned. Thus, it was decided to concentrate on a specific EO excitation response and to explore this in depth. To this end, the 6EO excitation response was chosen for study. Equally, any of the 5-12 EOs could also have been selected. One particular reason for going for the lower end of the EO range was to perform the tests under relatively high rotational speeds. To this end, the 5EO excitation would clearly be a better choice, but the modes it excited had mainly 5ND components and were more affected by boundary conditions than the modes excited by 6EO excitation. Only a limited speed range, covering the higher two resonances (the third resonance was exciting a mainly 2ND mode and the disc fixing would have a significant effect on it, which was not accounted for in the predictions) appearing on the 6EO line was chosen to be swept, as shown by the grey band in Figure 4.24.

The test plan for the random mistuning pattern case was very similar to that of the case of regular mistuning. An interference diagram covering 4-12 EO lines was prepared using the FE model of Blisk-2 with applied random mistuning. This diagram is given in Figure 4.26. It must be noted that, unlike the sinusoidal mistuning case, in the randomly mistuned blisk, considerably different interference diagrams were obtained (depending on which blade's response is used). In selection of measurement speed ranges, the responses of all blades were taken into consideration. Here only the diagram constructed for blade 20 (selected arbitrarily) is given for brevity.

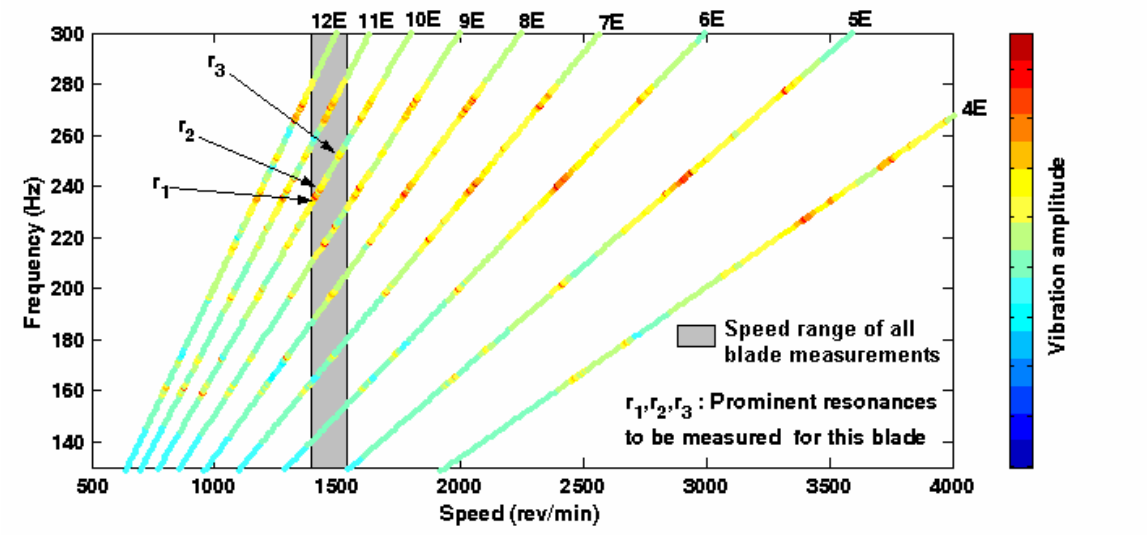

Figure 4.26 Computed Campbell diagram for random mistuned Blisk-2, blade 20

The resonances shown on the diagram, Figure 4.27, are accounted for by the harmonics map of the 1F family of modes, prepared using the same full FE model as used for regular pattern but here with random mistuning applied. Since the random nature of the mistuning caused modes to be more irregular, more resonances were excited by a given EO excitation. Again, a speed vector encompassing the entire range, based on the interference diagram, was constructed for z-mod plot measurements.

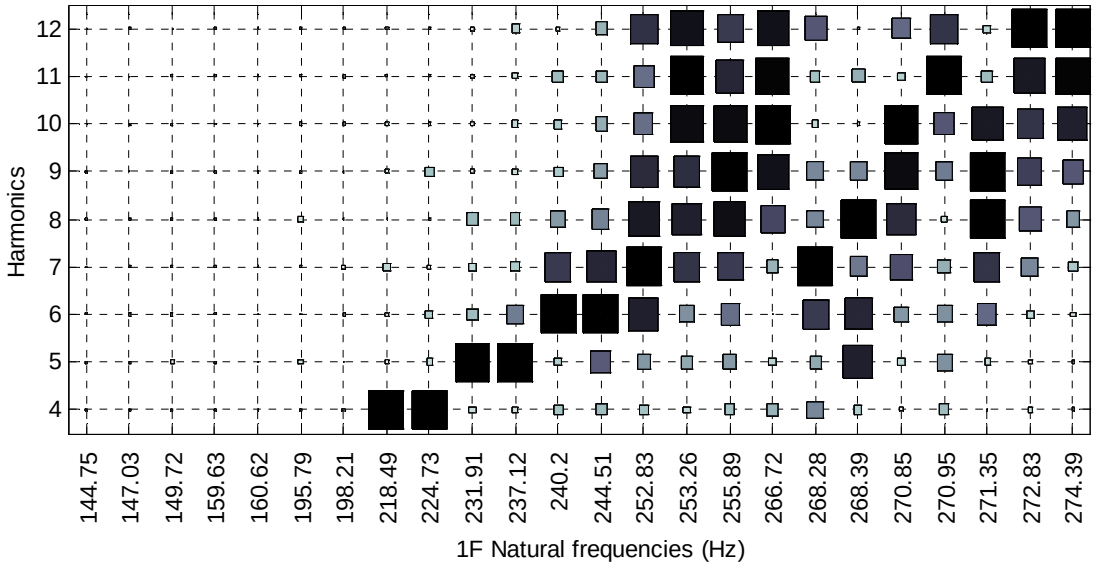

Figure 4.27 Normalised amplitude spectrum of the first 12 spatial harmonics for the first 24 Blisk 2 modes, with applied random mistuning.

All blade measurements in the random mistuning case were chosen for the range shown in grey in Figure 4.26. The choice of 10EO (an EO on the higher end of 4-12EO range) was made because of the high resonance density it provided in a relatively short speed range (there are 5 resonances in this region, only 3 of them strongly excited for the given blade). The predictions for this high density region would therefore set a challenging task for the prediction tool. Equally, other EOs (8, 9, 11 or 12) could also be selected.

4.4.2 Undamped and damped tests on Blisk-1

The planning of the friction damping tests on Blisk-1 with integral dampers followed more or less the same guidelines but was a more challenging task, particularly due to uncertainties brought in with the non-linear nature of the under-platform friction dampers. Moreover, the lack of a tuned reference state of the blisk (though this has been compensated to a degree through model updating and mistuning identification techniques) also complicated the test planning.

The main objective of the friction damped Blisk-1 tests was to validate the predictions of a numerical code through which the forced response of an entire bladed disk can be calculated in the presence of various types of non-linearities, including under-platform friction dampers. More details on the prediction tool can be found in Chapter 6. However, it was though appropriate to measure the corresponding undamped configurations as well, so that: (i) the errors introduced via the FE model could be inferred and, if possible, corrected through less complicated and less uncertain linear forced response computations, thereby limiting the source of uncertainties in the computations to non-linear elements, and (to a lesser extent) (ii) the effectiveness of the dampers could be assessed by comparing damped and undamped responses.

For a linear structure, once a convincing FE model is obtained, it is possible to come up with a reasonably accurate test plan which can be closely followed in practice, even if some minor modifications are often inevitable during implementation. However, with non-linear systems this cannot be taken for granted as modelling of the actual behaviour of the non-linear components is somewhat less certain and the results will vary depending on the modelling of the non-linearity. Besides, even if the model is sufficiently accurate, reliable estimates of the values of non-linear parameters such as friction coefficient and contact stiffness are often not available during the planning phase. Therefore it is important that the test planning is made as flexible as possible so that a range of options can be covered.

One of the most important things in the planning of tests with friction dampers is to determine the speed range in which the dampers will operate successfully. Since a damper always has a finite mass, the centrifugal load exerted on it increases with increasing speed and at a certain point becomes too high, thereby preventing it from functioning properly. Dampers in such a state are said to be locked-up. In this situation, the neighbouring blades are interconnected through dampers which lead to substantial stiffness increases in the assembly, thus resulting in the natural frequencies being raised. Often the shifts in natural frequencies are considerably higher so that exciting the "new" resonances may not be possible within the speed range of the test setup.

In order to reduce the possibility of such a situation, it is essential that certain parameters such as damper mass, excitation forces, operating speed range etc. are determined accordingly. It was decided to use so-called "Cottage-Roof" (CR) dampers in the experiments since they were commonly used in real engines and relatively cheap to manufacture. A rather simple methodology was adopted to calculate a rough estimate for the damper mass. The dampers were considered in their stuck position (i.e. no relative motion between the dampers and blades), so that the system behaved linearly. The idea was to work out the relationship

between the blade tip response amplitudes and the forces exerted on the dampers. Therefore, assuming a blade-tip amplitude response, the mass of a damper which could be made to slip by the created damper forces could be calculated. To this end, a 0.5 mm blade tip amplitude was assumed. The amplitude of the applied harmonic force was adjusted so that the assumed response amplitude could be obtained. The dampers were represented by their equivalent stiffnesses, obtained from FE analysis. As the relation between blade tip amplitude and the force in the stiffness elements (representing the dampers) was of interest, a simple model, such as the one shown in Figure 4.28 (a), could be used. The resultant forces in the springs representing the dampers were then fed into the free body diagram of Figure 4.28 (b) and the forces on the damper faces were balanced.

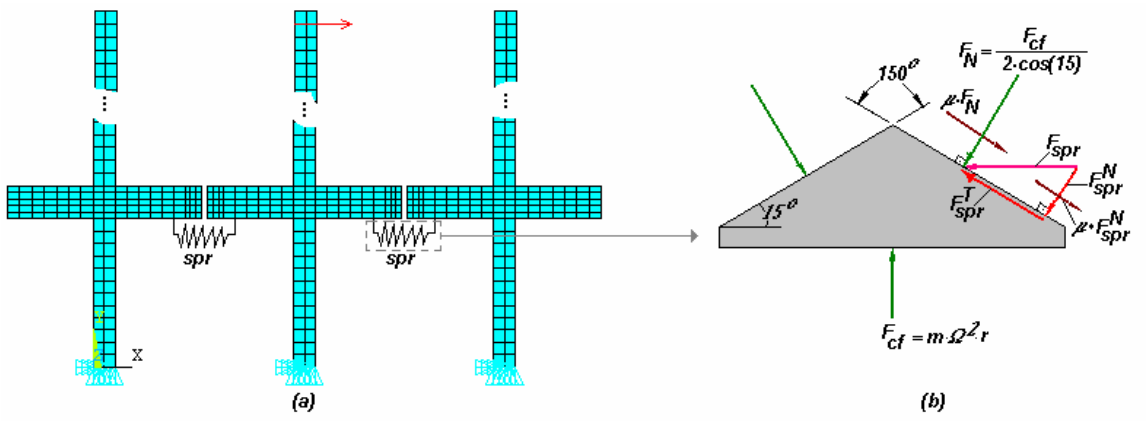

Figure 4.28 (a) Simple FE model used in damper design, (b) free body diagram of a damper

Assuming a friction coefficient of 0.3 and a roof angle of 150° (following a damper from a real application), the mass of the CR damper was calculated as a function of rotational speed, Ω. Calculations showed that for the blade tip amplitude assumed, the damper mass should be less than 4.5 grams at the maximum rig speed of 4000 rev/min. Therefore at lower speed values, the dampers would work for even smaller response amplitudes. Based on this result, a steel damper was designed. The designed damper and the way in which

was integrated into the blisk are given in Figure 4.29. Assuming the density of Steel to be 7800 kg/m^3, the damper mass was found to be 4.2 gram.

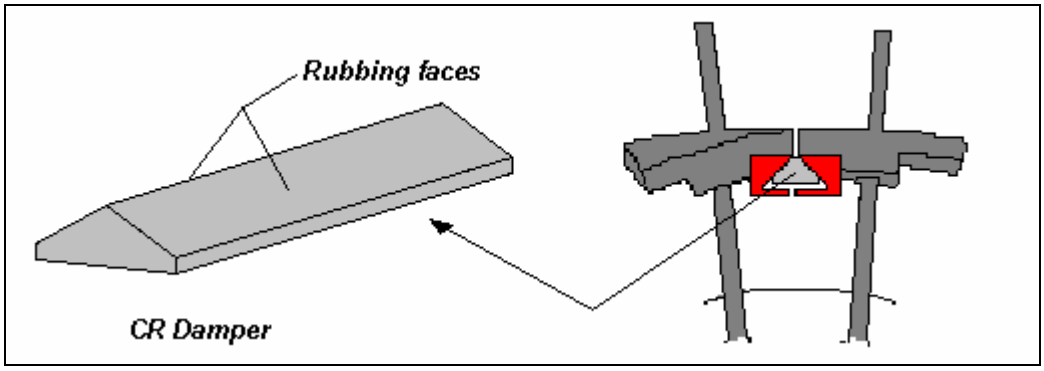

Figure 4.29 Designed damper and its integration

The simplifying assumptions necessitated further measures to be taken to ensure the success of the test campaign. For this purpose it was decided that another set of dampers should be made from a lighter material in case the original ones proved too heavy to be effective. The material for the second set of dampers was chosen to be Titanium which reduced the damper mass to 2.2 grams. Another measure taken was to make the necessary provision so that the excitation force could be increased, should there be need for it, as documented in Chapter 3.

Following the same procedure as used for Blisk-2, first, an FE based interference diagram was constructed for the 1F family of modes of undamped Blisk-1, and is given in Figure 4.30 (necessary forced response calculations were carried out using the prediction tool to be validated. More details on the code are given in Chapter 5 and the way in which the identified mistuning is presented to the code is given in Chapter 6). Based on this diagram, a variable-step speed vector was prepared to measure a single blade for z-mod plots. Both blisks possessed similar damping characteristics, therefore the same number of measurement points as taken around Blisk-2 resonances was chosen for Blisk-1 as well. In order not to complicate the computations further by mistuning, it was considered favourable to measure the response at resonances corresponding to

the lower ND modes as they were known to be sufficiently tuned. However, as lower ND modes were excited at high rig speeds, there was a risk of dampers locking up due to high centrifugal forces. Eventually, it was decided to make arrangements for three speed bands to cover the damped and undamped characteristics of Blisk-1.

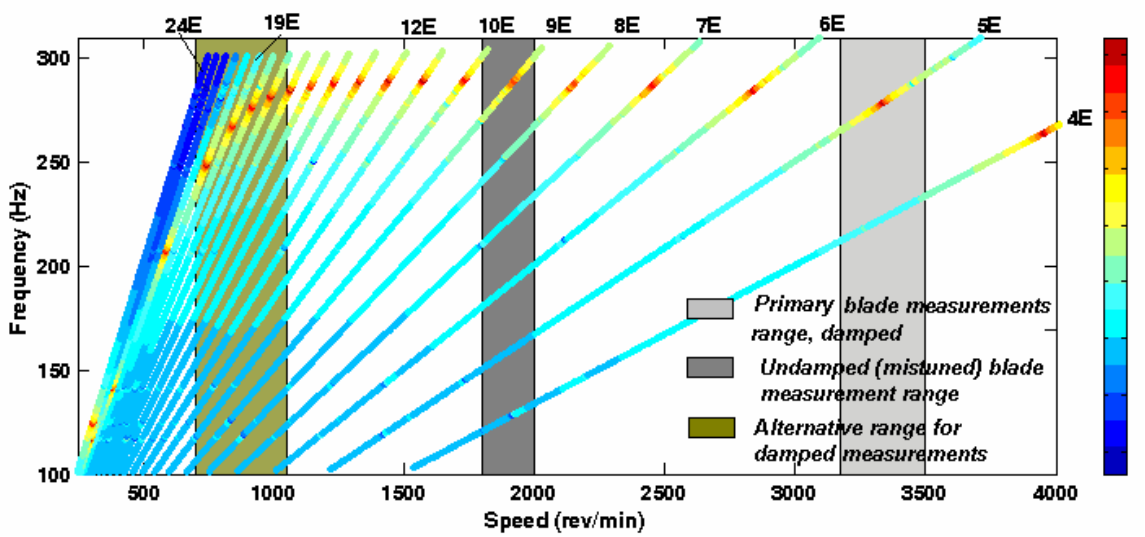

Figure 4.30 Computed Campbell diagram for updated Blisk-1 FE model including inherent mistuning, 4-24 EOs

The first band concentrated around the 5EO-5ND resonance covering a range shown by the light grey band on the computed interference diagram given in Figure 4.30. The 5ND mode was so reasonably tuned that uncertainties in mistuning identified or in its modelling would not have an adverse effect on the predictions. The second band of measurements, shown by a darker grey colour, was intended for undamped tests. A closer inspection of the computed 9EO response curve revealed the occurrence of a number of resonances (note that primarily 9D modes were significantly mistuned even after the tuning process). By then the ability of the numerical code to predict the mistuned response accurately will have been demonstrated via Blisk-2 measurements. Therefore, the measurements around this resonance should provide the necessary data to assess the degree to which the mistuning has been correctly identified or modelled. The third speed band shown in dark green was envisaged as being used in the event of the dampers not working in the first band. It covered the

resonances corresponding to the 4-7 ND modes but this time excited by 20-17 EOs, respectively (i.e. for a bladed disk having 24 blades an n ND mode will be excited by n, $24-n$, $24+n$ etc EOs due to spatial aliasing). Therefore, the first 24 EO excitation responses, as shown in Figure 4.30, needed to be calculated. Since these resonances were excited at relatively low rotational speeds, the chances of the dampers working properly are higher. Also, they corresponded to reasonably tuned ND modes which would reduce the uncertainties in computations. The third band covered a range of resonances. However, the actual measurements were to be conducted for a range covering one or two of them because of testing time considerations.

Ideally, it would be desirable to construct an interference diagram (similar to the one computed for the undamped case) for the blisk with integrated CR dampers. However, doing this would be computationally very expensive, especially bearing in mind that it would have to be repeated several times to improve the design. Moreover, at the time the test design was undertaken, the prediction tool was not yet coded to handle such big assemblies.

4.5 Summary

In this chapter three issues have been addressed: (i) identification of the reference tuned states of the blisks, (ii) updating of their FE models, and (iii) the design of tests in the run up of the real tests and the validation of the predictions, have been addressed.

Through FRF and ODS measurements at rest, Blisk-2 has demonstrated that it can act as a suitable tuned reference for forced response calculations. Blisk-1, on the other hand, has been found to be significantly mistuned. Although a tuning process has been undertaken to improve the tuned state of Blisk-1 (and to a certain degree this has been achieved) it has not been possible to establish a sufficiently reasonable tuned state to provide a suitable reference case. Blisk

tuning has been studied via a lumped parameter blisk model to see if better accuracy could have been obtained had the tuning been performed in different ways. The results have showed that, by matching 1F blade-alone frequencies, the symmetry of the blisk can be improved to a certain extent, but only if modifications are introduced through appropriate parameters. However, it has been concluded that, ultimately, more than one frequency of the blade-alone models will have to be matched, using appropriate parameters, for higher accuracy. These parameters should be identified based on their influence on the assembly properties.

The FE models of the blisks have been updated based on the mode shapes and the natural frequencies measured on the real bladed disks that they are expected to represent. The IES updating method has been used for the FE model of Blisk-2 and a combination of the IES and FMM-ID methods have been used to update the FE model of Blisk-1. The results obtained by employing these models have been demonstrated to correlate closely with measurements. The difference between measured and FE natural frequencies, resulting mainly from dimensional variations in the blisk, has been reduced by using the material properties as updating parameters. As a result, somewhat unrealistic material properties, density in particular, have resulted from the updating process.

Finally, based on the updated FE models of the blisks, a comprehensive test plan has been prepared in an attempt to make the actual testing more efficient. Tuned and mistuned tests with Blisk-2 have been planned. The mistuning shapes and strengths to be applied have been chosen and the resonances to be measured identified. Undamped and damped Blisk-1 tests have also been designed. The damped testpiece test plan, compared with the undamped one, is less reliable due to the uncertainties associated with the friction dampers and may need to be modified during the execution of tests.

CHAPTER 5

VALIDATION of TUNED and MISTUNED BLADE RESPONSE PREDICTIONS

5.1 Overview

Having prepared the necessary ingredients in the previous chapters, it is now time to compare forced response predictions for the tuned and mistuned Blisk-2 with the measurements taken under rotation. To this end, the numerical code to be used in calculations, and therefore the one sought to be validated, is first introduced. Then, starting with the stationary/mistuned tests, following the test plan drawn in the previous chapter, the results obtained from rotating/tuned, and sinusoidally- and randomly-mistuned Blisk-2 are presented. The predictions are correlated with these results and the degree of success and the possible sources of discrepancies are discussed.

5.2 The prediction tool

The existing mistuned bladed disk response prediction tool sought to be validated here exploits an exact relation between the tuned and mistuned assemblies' dynamic properties. The complete derivation of the method is given in [14]: there the main features and the use of the method are summarised.

The main goals of the method for calculation of mistuned forced response are achieved: (i) without inverting a matrix, (ii) by using a cyclic sector (as in the case of tuned calculations), and (iii) by including the contribution of all the

degrees-of-freedom, thus avoiding the errors which can occur in conventional reduction processes.

The application of the method can be summarised as follows: first, the tuned assembly's mode shapes and natural frequencies are calculated for a number of families of modes of interest, using a cyclically symmetric sector FE model. Then the DOFs where the mistuning is to be introduced and response levels are to be calculated are identified. Together with the DOFs where the excitation forces are applied, these coordinates are called "active DOFs" and all the remaining ones are "passive DOFs". They are named in this way because the active DOFs are involved explicitly in the calculations of both tuned and mistuned assemblies, whereas the passive ones are not, being used only in tuned response calculations. A subset of tuned assembly mode shapes is prepared by extracting the values at the identified active DOFs, together with the tuned natural frequencies and applied mistuning, and used in the mistuned computations. With such partitioning, the matricies involved in the mistuned response calculations are reduced to much smaller sizes without loss of accuracy. This provides the ability to calculate the forced response, at the DOFs of interest in much reduced computation times.

Physical mistuning is introduced via so-called "mistuning elements" at desired nodes of the sector FE model. These relatively simple but efficient mistuning elements include: lumped mass, discrete stiffness and damping elements applied between a node and the ground, or between two nodes. Values of the mistuning applied in each coordinate direction at a given node can be different. Although many mistuning patterns can be defined by mistuning elements, mistuning is often expressed in terms of the variation of blade-alone natural frequency or frequencies (i.e. those of a separate or isolated blade). This kind of mistuning is accommodated in the method by establishing a relationship between the known frequency scatter and the properties of a set of mistuning elements defined at certain nodes. In this way, the given frequency mistuning is translated to

physical mistuning, through these mistuning elements, such that the blades with applied mistuning elements exhibit a specified frequency variation.

The method is coded into a computer program, MISTuning RESponse (MISTRES), to perform forced response calculations for a desired EO excitation. The type of excitation and mistuning, response DOFs, frequency range of interest, etc are provided through a general input file. Additionally, another file containing the mode shape data corresponding to DOFs of interest for the included modes of the tuned assembly, and natural frequencies of these modes, is submitted. If the mistuning is defined in terms of natural frequency variation of sub-models (e.g. of isolated blades), then another file, similar to the second one, for each sub-model is also provided. The outputs of the code are: (i) response levels at the desired nodes of the FE model (which can be calculated for all available DOFs separately, or as a total response at those nodes); (ii) maximum responding blade for all the resonances, and (iii) natural frequencies, within the frequency range of analysis. Blade-to-blade amplitude variations at the frequencies corresponding to excited resonances are also output.

5.3. Mistuning analysis on the stationary blisk

In accordance with the test plan prepared in Chapter 4, a number of mistuning patterns were selected and applied to Blisk-2 and the natural frequencies and the mode shapes measured, non-rotating, before the dynamic tests were started. By doing this it would be possible to gauge the ability of the prediction tool to predict the correct natural frequencies and vibration amplitude variations when excited at these frequencies in the absence of rotation. Three mistuning patterns were considered: (i) Single blade mistuning (SBM), (ii) sinusoidal mistuning ($Sin(12\cdot\theta)$), and (iii) random mistuning. The applied mistuning patterns are illustrated in Figure 5.1.

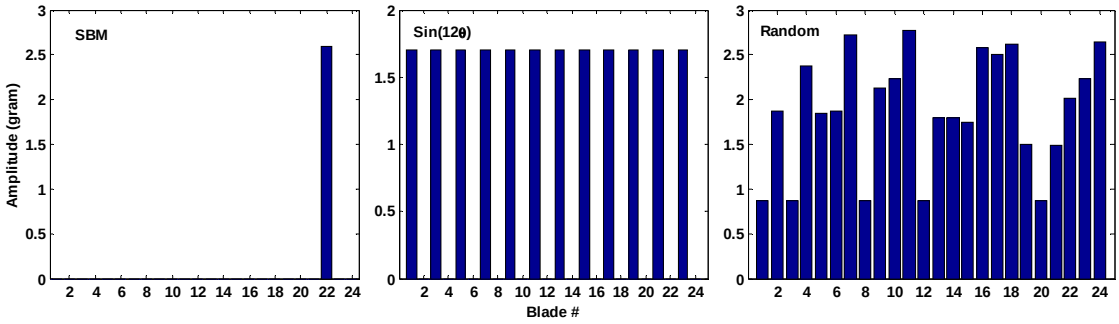

Figure 5.1 Mistuning patterns applied to stationary Blisk-2.

Mistuning of Blisk-2 was achieved by attaching washers via small bolts to the blade tips. Updating of the FE model of Blisk-2 was covered in the previous chapter, where it was demonstrated that it simulated the characteristics of the real blisk satisfactorily. Therefore, it is fair to assume that the degree of correlation of these tests with predictions will depend on the modelling of the applied mistuning. In the FE model, mistuning weights were modelled as point masses, applied in the middle of the blade tip outer surfaces but distributed over a number of nodes. This was reasonable as the centres of mass of these masses laid very close to the mentioned surfaces. The resultant frequency splits (separation of double modes) in 1F family double modes (i.e. 1-11ND) of Blisk-2 are given in Figure 5.2.

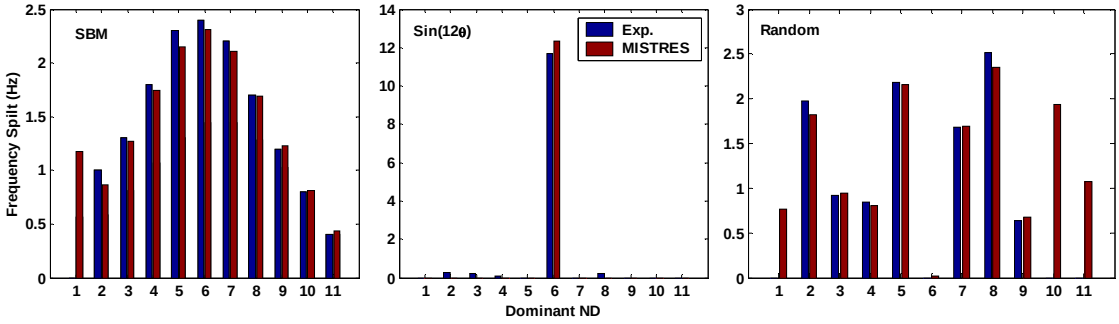

Figure 5.2 Split in 1F family double modes due to applied mistuning patterns

Experimental results corresponding to some of the mode pairs are missing from SBM and random cases given above. This is not necessarily because these modes

do not split, but some of the frequencies, despite several attempts, could not be captured in the experiments. In principle, a mistuning pattern will split an n ND mode only if a $2n$ harmonic is present in its Fourier series representation. Therefore, the SBM mistuning pattern is expected to cause all, and the given random mistuning pattern should cause all but 6ND, modes to split. Similarly only the 6ND mode is expected to be split in case of $Sin(12\cdot\theta)$ mistuning pattern. The predicted results were supported gratifyingly closely by the available measured counterparts, both in terms of split patterns and amplitudes. Individual natural frequency values were predicted with errors less than 0.2%. Nevertheless, some deviations were evident, probably due to errors in mistuning and boundary condition modelling in the FE model.

ODSs corresponding to the "random" case were measured for the 1F family of modes so that they could be compared with the predicted ones. The choice of random case was particularly challenging for the FE prediction model because of the complexity and variability produced in the mode shapes. Circumferential ODS measurements were performed using an SLDV and an electromagnet, as explained in Chapter 3.5. Some of the measured ODSs encompassing natural frequencies from the lower and higher ends of 1F family of modes are compared with the predicted ones in Figure 5.3. Since the modes are distorted by applied mistuning, they are numbered from 1 to 24 rather than using the ND notation which does not apply to all of them. The numerical code used, MISTRES, is intended for the calculation of the forced response amplitudes. As a result, the outputs are not "signed". For clarity of the comparisons, therefore, absolute values as well as signed ODSs of the experiments are given in the presented plots. The measured ODSs were obtained by scanning the blisk continuously at platform level. However, each blade is represented in predictions by a single point in the middle of the blade at platform level. This is appropriate as the out-of-plane flexural modes are of interest. Very good agreement is obtained, not only for regular lower natural frequency modes but also for highly localised higher ones. During the measurements , the electromagnetic force input was not

measured since it required an additional and complicated fixture. The predictions have therefore been normalised by the amplitude of the maximum responding blade in the measurements.

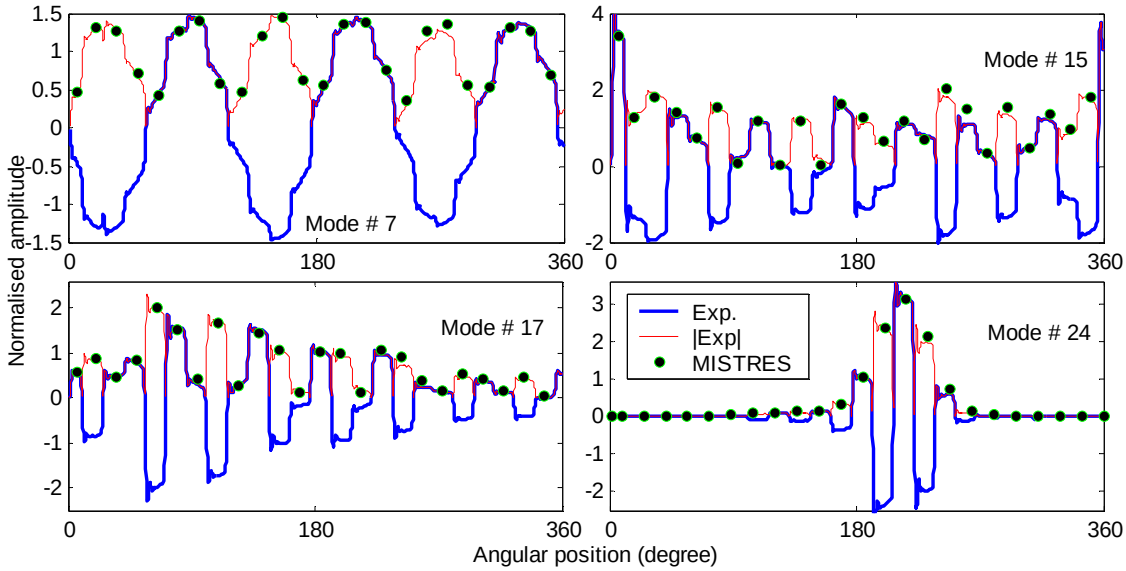

Figure 5.3 Comparison of ODSs for stationary Blisk-2 with applied random mistuning.

5.4 Tuned and mistuned analysis on rotating blisk

In a validation study, it is important that one step is taken at a time so that the contribution of every new feature can be properly interpreted and accounted for. Following this, the rotating tests were conducted in three steps. First, the tuned blisk was tested, to provide a reference set of data, and necessary inputs, such as damping and force magnitudes, for numerical predictions. Then, measurements on regularly and randomly mistuned blisk configurations were executed, according to the agreed test plan.

5.4.1 Repeatability of rotating measurements

Before the rotating tests could begin in earnest, the ability of the rig to reproduce the same data under the same/similar conditions at different times had to be checked. This would provide confidence in the data supplied by the rig,

establishing it as a "well-controlled" environment for precise vibration measurements.

To this end, the technique devised (Chapter 4.2.2) was thought appropriate to check the tuned state of Blisk-2 under stationary conditions. Following the same procedure, a selected mistuning pattern was applied to the blisk and a particular blade's response was measured for a specific speed range. Then the mistune pattern was shifted by a number of blades around the blisk, as shown in Figure 5.4 (a), and the "same" blade was re-measured for the same range. This test, therefore, would not only assess the repeatability of the measurements but would also gauge the effect of any asymmetry (i.e. inherent mistuning) in the blisk, if present, on forced response under rotation. The results obtained for the original and shifted patterns are given in Figure 5.4 (b).

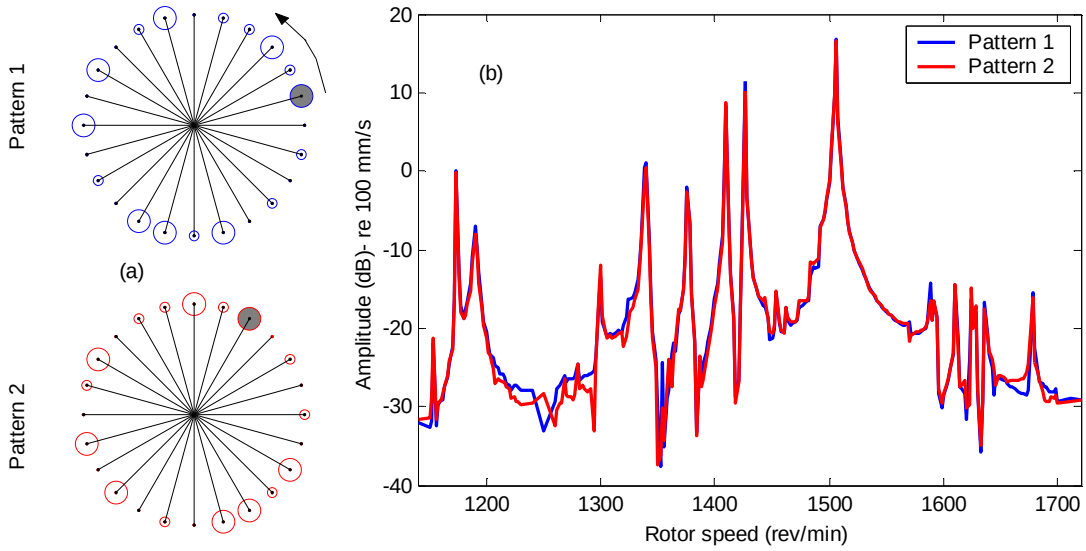

Figure 5.4 (a) Original and shifted mistuning patterns, (b) comparison of 10-EO response curves for both patterns – shaded circles indicate corresponding measurement locations.

The applied mistuning pattern was the one chosen to be used in random mistuning analyses on Blisk-2. Given the complexity of the test rig and the measurement system, the excellent agreement between curves in Figure 5.4

constitutes good evidence of the repeatability of the tests and also the suitability of the blisk as a tuned reference under rotation.

5.4.2. Inclusion of rotation in forced response predictions

The frequency of excitation in measurements varied with rotational speed, thus the natural frequencies and to an extent the mode shapes of the blisk, changed as the speed changed, due to centrifugal stiffening. MISTRES uses the mode shapes and natural frequencies of the tuned system, and once these inputs are provided they remain the same for all frequencies of that forced response calculation session. Therefore, in order to simulate the actual behaviour in the rig precisely, one has to calculate the response at each speed point by using mode shapes and natural frequencies calculated at that particular speed. However, this is extremely time consuming and is not entirely necessary. In terms of natural frequencies, a near exact relationship can be obtained between rotational speed and the frequency shift by calculating frequencies at a few speed values and then fitting a quadratic curve to these values (the change in natural frequencies of the 1F family of modes is proportional to the square of the rotational speed). Therefore, once the forced response calculations for a given set of modal data are complete, the frequency axis can be modified to reflect the effects of rotational speed. As for the mode shapes, and particularly when response is to be calculated in a limited frequency (i.e. rotation speed) range (e.g. a range of 100-300 rev/min), mode shape and natural frequency data calculated at mid-speed range value provide sufficiently accurate results. This is because the mode shapes do not change much with rotation, over such small ranges. An example of this is given in Figure 5.5 where the 6EO response is calculated using mode shapes calculated at both 2500 rev/min and also at a speed corresponding to 1F 6EO-6ND resonance, 2756 rev/min. The green curve represents the results obtained for the former case, before frequency shift. For the blue and red curves, the frequency axes are arranged to reflect the effect of rotation (i.e. in case of the blue curve, all the frequencies corresponding to values higher than 2500

rev/min are shifted to the right in accordance with the speed-frequency shift relation). Resonance frequencies of the red and blue curves were practically the same; response amplitudes showed differences of up to 0.05%. Bearing in mind that the speed ranges of interest are smaller than that of this particular case, thus resulting in smaller deviations, the handling of the effects of rotation in this way is entirely justifiable.

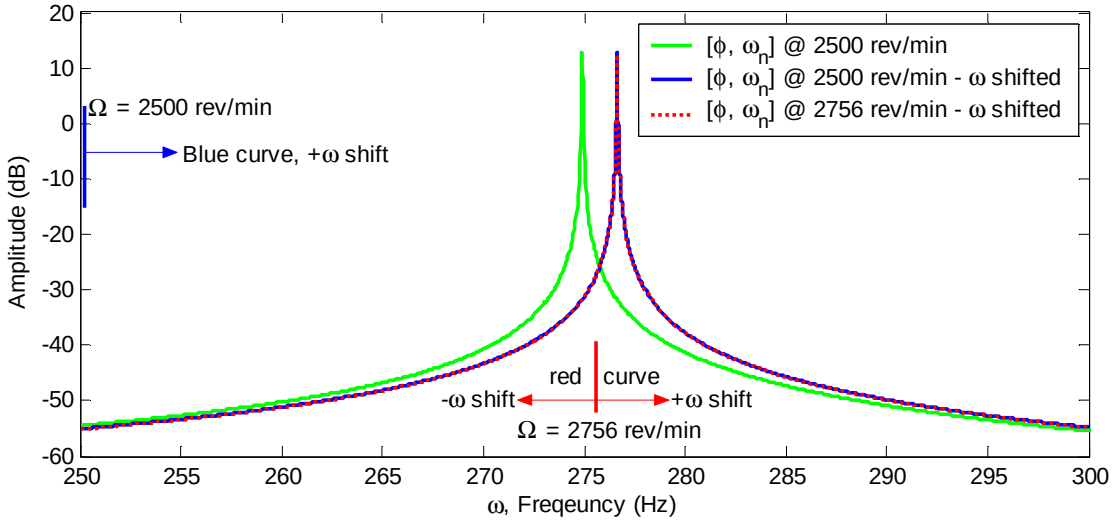

Figure 5.5 Comparison of 6EO excitation response using mode shapes calculated at different speeds.

5.4.3 Evaluation of forcing input

Excitation was achieved through a permanent magnet fixed in space. In their normal operation the bladed disks with this arrangement are being excited by phased pulses generated by the magnet each time a blade rotates past. The excitation force fluctuates from near-zero when the magnet is between blades, to a maximum when the magnet is centred on a blade tip. Note that this type of forcing is different and more realistic than applying harmonically pure phased pulses to a static blisk [55, 49] (i.e., $F_i = A \cdot Sin(\omega \cdot t + i \cdot \theta)$, where A is the amplitude, ω is excitation frequency t is time, θ is inter-blade angle and i is the blade number). In the present case, the magnet only attracts the blades; therefore, all the force values are positive. Hence the forcing consists of, predominantly, a mean level at zero frequency, and a harmonic at the

fundamental forcing frequency (rotational speed X # of blades) as well as some lower amplitude harmonics that appear at integer multiples of the fundamental forcing frequency. A train of typical magnet pulses generated during the operation of the rig with Blisk-2 is given in Figure 5.6. Also shown in this figure is the magnet force applied to a particular blade in one rotation cycle of the blisk (note that only a portion of rotation cycle is given here).

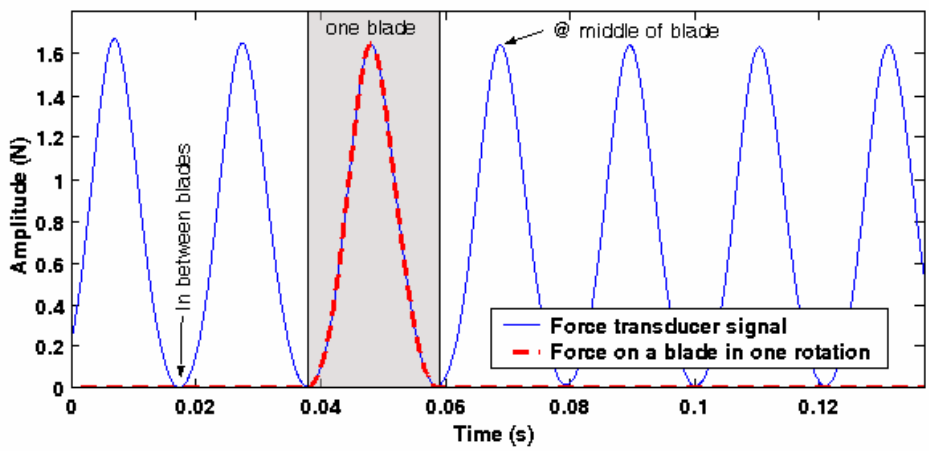

Figure 5.6 A typical train of magnet pulses applied to Blisk-2 @ 120 rev/min.

Given a magnet pulse such as the one given in red in Figure 5.6, the amplitudes of the force exciting different EOs can be calculated by performing a Fourier series analysis. Assuming that the discrete force signal, f, is defined at N time points, $t = t_k$ $(k = 1,2,...,N)$ and is periodic, with a period T, in the form $f(t) = f(t+T)$, it can be represented by a finite series:

$$f_k = \sum_{n=0}^{N-1} X_n e^{2\pi i n k / N} \tag{5.1}$$

where

$$X_n = \frac{1}{N} \sum_{k=0}^{N-1} f_k e^{-2\pi i n k / N} \quad , \quad n = 1,2,...,N \, . \tag{5.2}$$

Here the absolute value of the complex X_n, $|X_n|$, gives the amplitude of the nth harmonic, or the amplitude of the nEO excitation. The first 48 harmonics of a typical magnet pulse together with the reconstructed pulse using these harmonics in (5.1) are given in Figure 5.7.

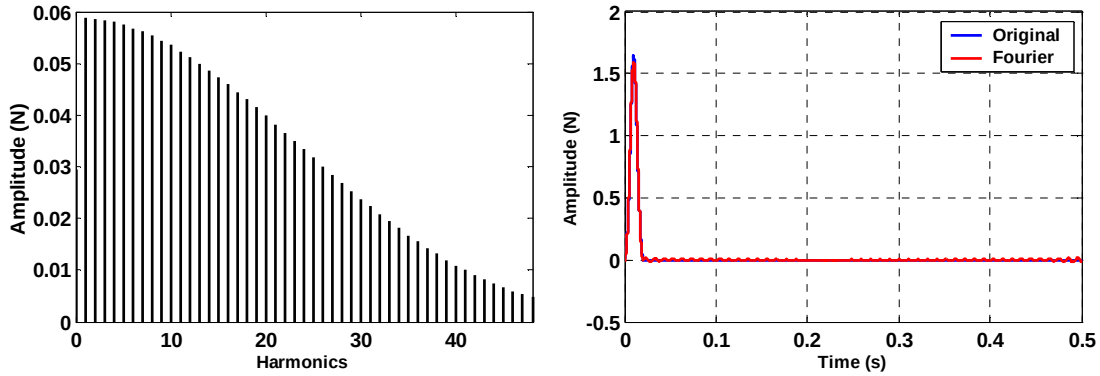

Figure 5.7 Harmonics of a magnet pulse and its reconstruction through these harmonics

5.4.4 Tuned blisk analysis

The first step in the tuned tests was to measure a blade's response for the entire speed range (0-4000 rev/min) to obtain the overall distribution of the resonances. For this purpose the blade tip response of a particular blade (arbitrarily chosen as # 18) was measured at speed values identified in the previous chapter. A z-plot showing the results of these measurements, together with the overlaid predicted resonance locations is given in Figure 5.8 (Note that only 300-4000 rev/min range is given). The z-mod plot contains 1.8 million measurement points and took 6 hours of continuous rig running to acquire.

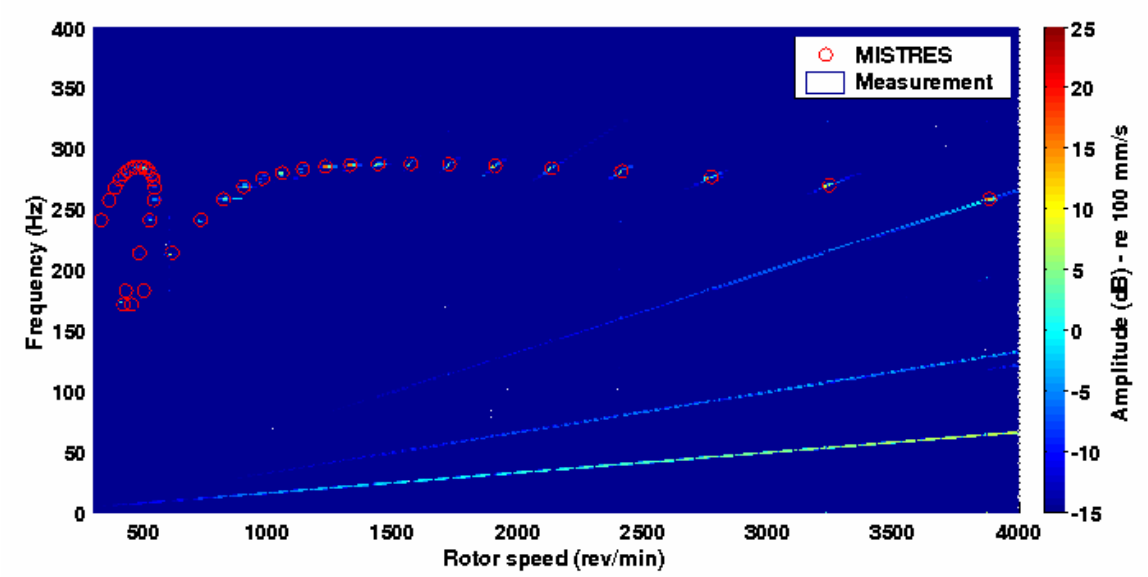

Figure 5.8 Comparison of experimentally and numerically obtained resonances

Some of the EO lines in Figure 5.8 are overemphasised (i.e. 1, 2 and, to an extent, 4 EO lines) by error signals due to the lack of perfect alignment between the rotor and LDV scan rotation axes. This imperfection led to cross-talk errors, largely at 1EO, increasing in proportion to speed. Although significantly improved through rigorous alignment measures, it has not been possible to eliminate the adverse effects of misalignment completely. Fortunately, the consequences of misalignment were confined to the lower EOs and the effects on those of interest have been minimal.

Figure 5.8 shows a very good agreement between predicted and measured resonance spots. The locations of predicted natural frequencies were obtained through speed–frequency relation obtained for Blisk-2. The degree of correlation, therefore, validates the relation used. From the figure it seems that some of the predicted resonances are not captured in measurements as they do not appear. This is due to the fact that all the resonances were excited to different amplitudes. The z-mod colour is set to be proportional to amplitude, and some of them were simply too small to show up.

The comparison shown in Figure 5.8 does not provide enough resolution to assess the degree of correlation precisely. In order to do this, individual EO response curves needed to be measured, and with finer speed steps as planned earlier. This was also necessary so that the actual force and damping values could be measured and identified for absolute response levels. For this purpose the response to 6EO was measured. Measured response amplitude and phase plots are given in Figure 5.9 (a) and (b) respectively. As anticipated in the test design phase, true resonance peak amplitudes could not be measured due to the extremely light damping. Very high vibration amplitudes in the immediate neighbourhood of the resonance frequency led the LDV transducer to overload (despite using the minimum possible sensitivity), resulting in the notch seen on Figure 5.9 (a). Inspection of the time signals (also shown in the figure) around the resonance revealed that overloading occurred in the range between the points marked as "1" and "3", clearly seen from the time signal given for point "2". It was a limitation in the LDV transducer's electronics that it truncated signals larger than 20V p-p. Moreover, with large vibration amplitudes, the measurement point shifted, sometimes, to such positions where speckle noise became significant and disturbed the measured signal grossly, in the form of drop-outs. As this signal was low-pass filtered in the LDV's head, the time signals measured by the DAQ board were much reduced in amplitude and showed some higher harmonics as seen from the time signal corresponding to point "2". This fact should be taken into consideration in the analyses of measured data and their comparison with predictions.

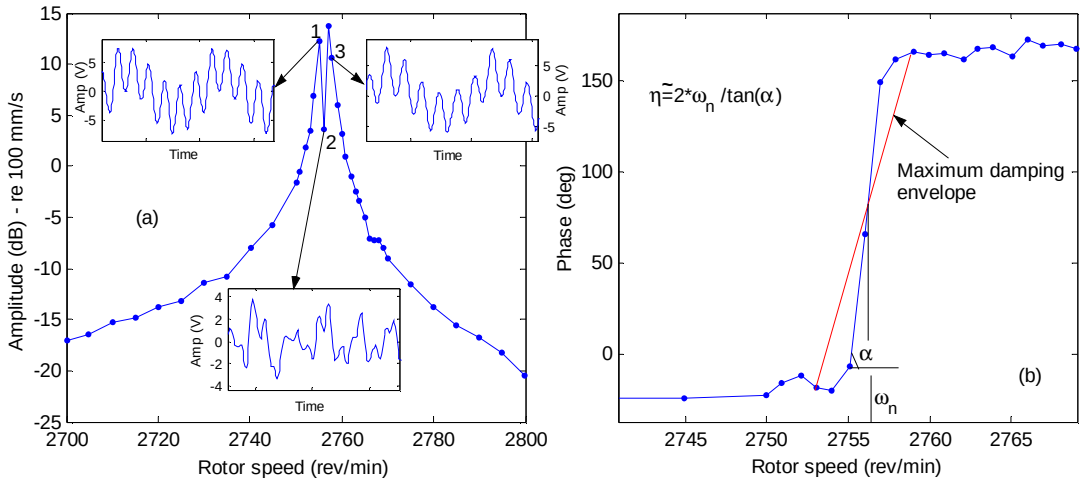

Figure 5.9 (a) Amplitude, and (b) phase plots of 6EO forced response on blade #1.

Frequency response data of Figure 5.9 were analysed in ICATS to find out the damping value to be used in predictions. Discarding the points between "1" and "3", the structural damping loss factor, η, was found to be 0.005%. Unreliable measurements around the resonance made damping identification somewhat uncertain. However, it was possible to define a conservative upper bound for damping value from the phase plot. Assuming an SDOF behaviour around this resonance, the slope of the phase vs. normalised frequency (ω/ω_n) plot gives the inverse of critical damping ratio, ζ. Therefore by considering the slope of the red curve in Figure 5.9 (b), and using $\eta = 2\zeta$ at resonance, a conservative value of the loss factor could be obtained. This calculation gave a loss factor of 0.01%. This result, as an upper bound, was reasonable as the damping value measured at rest and in the presence of air was 0.01%. Therefore, it was decided that a damping value of 0.0075% (mean of 0.005 and 0.01) to be used in the predictions.

Measurements were taken from the mid blade tip area, and therefore FE responses were extracted from the same location. Excitation force, measured in the form of pulses, was decomposed into its harmonics using Fourier analysis as described in the previous section. Predicted and measured responses to only 6, 8 and 12 EO excitations are given in Figure 5.10 for brevity. The magnet-blade gap was different in each case, and, therefore the response amplitudes are similarly

different. Natural frequencies and the mode shapes for these analyses were calculated at 2756, 1965 and 1435 rev/min respectively. Frequency axes of the given plots were rearranged as described previously.

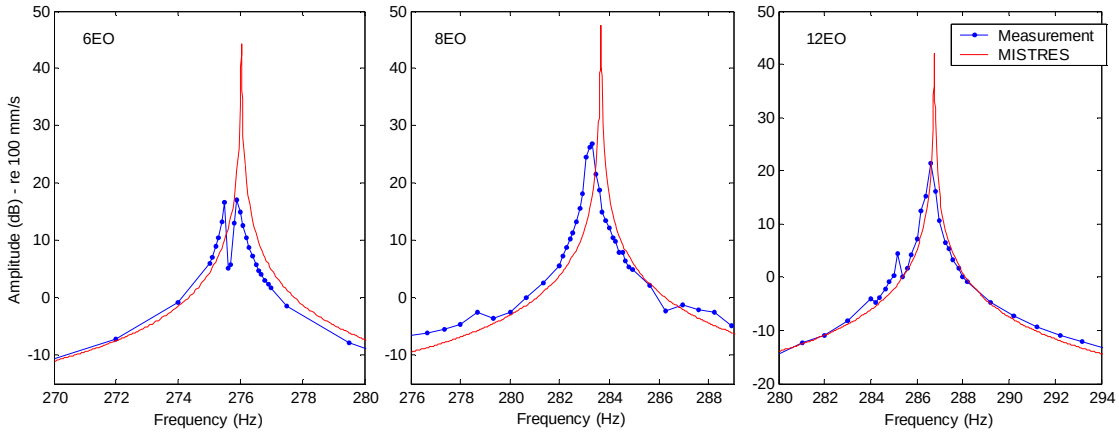

Figure 5.10 Comparison of response measurements for 6, 8 and 12 EO excitations (η=0.000075 in predictions).

Comparison given in Figure 5.10 presents a good match between measurements and predictions. However, some deviations, particularly in terms of frequencies, are evident. Although the variations in frequencies, in general, were around 0.2%, this was an increase compared to maximum stationary frequency deviation of 0.1%. This might be explained by the change of boundary conditions between stationary and rotating cases as well as changes in ambient temperature. Although similar fixtures were used in both configurations, unavoidably different setups had to be employed in rotating and stationary tests (i.e. the static tests were carried out prior the manufacture of the rotating rig). Also, due to the long time span of the testing process, the corresponding tests had to be conducted at somewhat different ambient temperatures. At this level of accuracy, differences of this magnitude due to these effects are not unusual.

The magnet-blade gap was reduced significantly to capture resonance amplitudes more accurately, but to no avail. Therefore, to limit the blade amplitudes the responses of all the blades were measured slightly off-resonance, and compared with the predictions. For this purpose, the exact location of the

resonance was located and the rotational speed increased by 1 rev/min to get reduced amplitudes. With sufficiently large magnet-blade gaps, it has been possible to obtain good signals at such speeds. The results of this comparison are given in Figure 5.11. Predicted values at 1 rev/min away from the resonance are considerably higher than the measured ones. Bearing in mind that the true resonance frequency might not have been captured precisely during testing, predicted values at 1.5 and 2 rev/min away from the resonance are also given. Very close results are obtained for 1.5 rev/min case. It must be also noted that the previously identified damping value might also be lower than during this test, contributing to discrepancy between measured and predicted amplitudes.

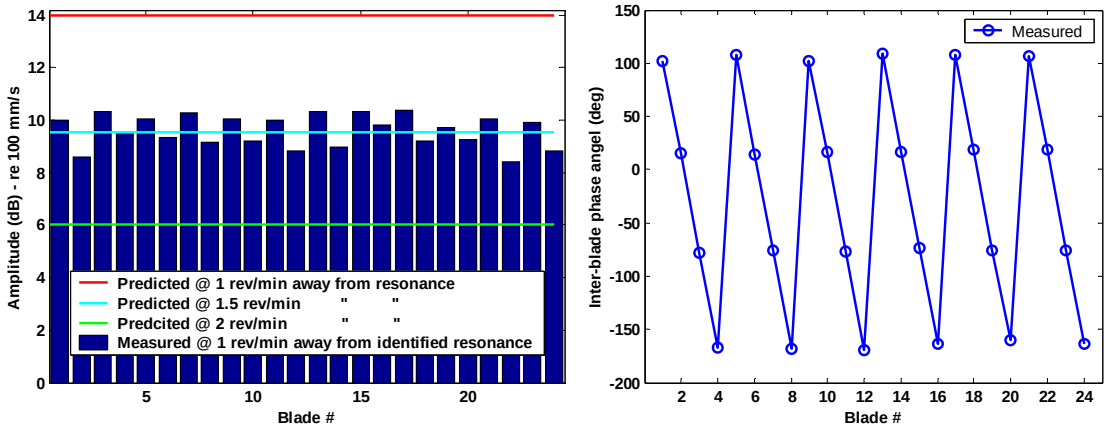

Figure 5.11 Comparison of 6EO response amplitudes away from 6EO-6ND resonance and measured inter-blade phase angles.

Inter-blade phase angles plotted in Figure 5.11 suggest a pure travelling wave in the blisk with constant 90° phase angles between the two adjacent blades. This implies that all the blades experience the same vibration amplitude. Even though a small ripple is apparent, this is backed by the even distribution given in the amplitude plot.

5.4.5 Regularly-mistuned blisk analysis

The selected regular mistuning pattern had a sinusoidal variation ($Sin(8\cdot\theta)$ - $S8\theta$ for brevity-, θ: angular position) in the circumferential direction of the

blisk. The amplitude and distribution of this pattern was given in Chapter 4. Since it was decided to use a large mistuning amplitude (i.e. 6 gram), mistuning masses were relatively big. As a result they protruded from blade tips noticeably as shown in Figure 5.12 (a). Therefore, considering them as point masses would introduce non-negligible errors. It was important that equivalent point mistuning masses were identified. For this purpose, using an isolated blade model and by modelling applied masses as closely as possible, the first blade-alone frequencies were calculated. Then the values of the point masses simulating mistuning weights were adjusted such that the same frequencies were obtained. It must be noted that once the blade-alone frequencies are obtained, the latter is done automatically by the prediction tool. Real mistuning masses could not be modelled physically since the prediction tool uses only one cyclically symmetric sector, thus necessitating the same physical model for all the sectors.

Nodes indicated by blue points in Figure 5.12 (b) are those where the point mistuning masses are applied. Similarly, green points indicate response measurement locations, corresponding to blade tip and platform level measurement locations considered in the real blisk. Forces are applied to the reverse side of the blade in the middle of the enlarged blade tip area.

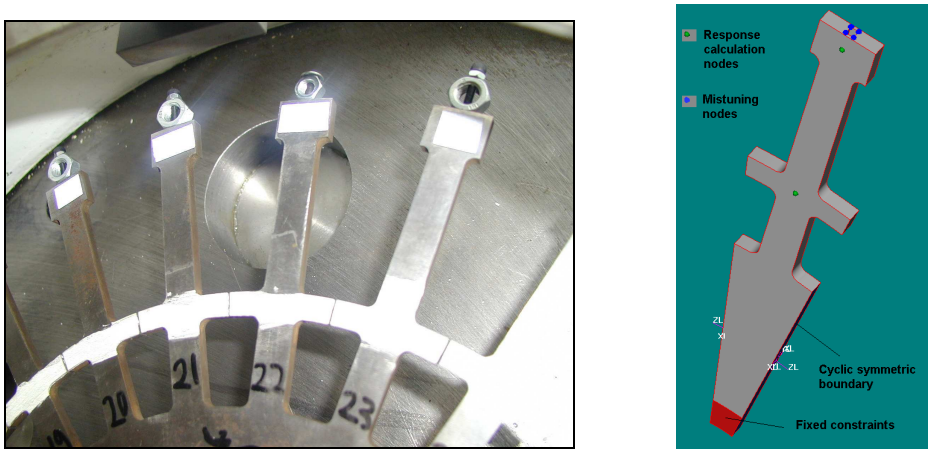

Figure 5.12 (a) Mistuning masses attached to Blisk-2 (picture shows random mistuning pattern), (b) sector model used in MISTRES

Once the mistuned model was constructed, natural frequencies of the 1F family of modes were calculated. These values are compared to the measured ones in Table 5.1. In theory, when a perfect $S8\theta$ mistuning pattern is applied only 15 distinct frequencies, corresponding to 0 and 12 ND single modes, 1, 2, 3, 5, 6, 7, 9, 10 and 11 ND double modes and 4 and 8 ND split modes, will be identified. However, some of the mistuning masses, though intended to be identical, showed some variations and as a result ND modes other than significantly split 4 and 8 ND modes were also split. Only 12 frequencies could be identified in measurements, as given in the following table. Comparisons with the predictions showed that the difference was in general less than 0.2% which is thought to be reasonable.

Mode #	Measured (Hz)	Predicted (Hz)	% diff.	Mode #	Measured (Hz)	Predicted (Hz)	% diff.
1	–	160.71	–	13	–	240.11	–
2	–	159.76	–	14	242.25	242.72	0.19
3	–	159.80	–	15	–	242.72	–
4	161.64	169.36	4.58	16	243.80	244.07	0.11
5	–	169.39	–	17	–	267.08	–
6	194.42	195.45	0.52	18	–	267.20	–
7	–	195.45	–	19	–	267.20	–
8	210.60	210.87	0.13	20	267.66	267.71	0.02
9	229.68	229.79	0.05	21	–	267.71	–
10	234.76	235.06	0.13	22	267.78	268.19	0.15
11	234.88	235.06	0.08	23	–	268.20	–
12	239.90	240.10	0.08	24	268.06	268.46	0.15

Table 5.1 Natural frequencies of the $S8\theta$ mistuned blisk modes, measured and predicted.

In a similar way to the tuned rotating tests, a blade's response was measured for the entire speed range and a z-mod plot demonstrating a resonance map of regularly mistuned Blisk-2 was constructed as given in Figure 5.13 (a). The predicted plot given in (b), is repeated here for ease of comparison.

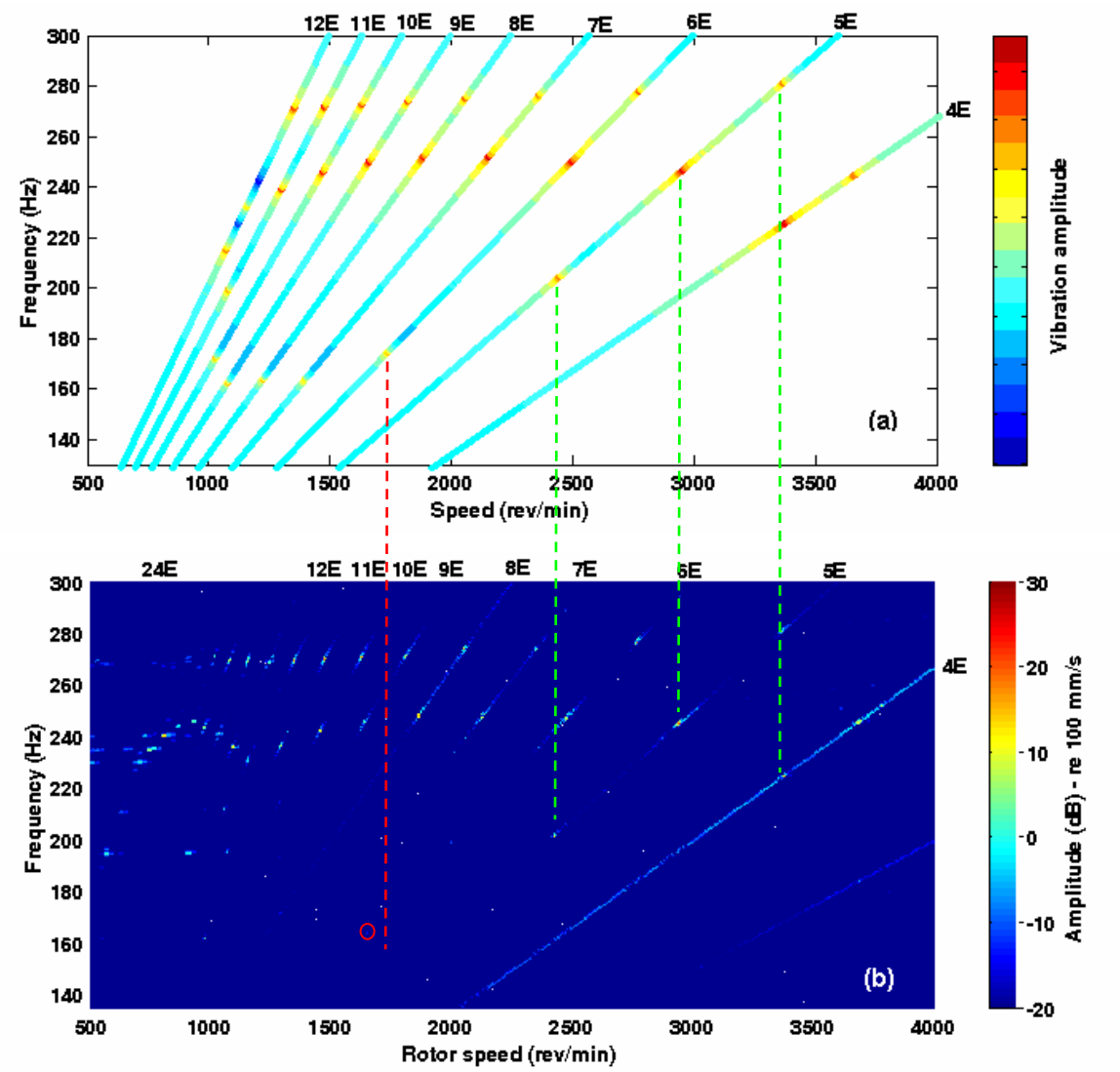

Figure 5.13 (a) Predicted and (b) measured z-mod plots for Blisk-2 with applied $S8\theta$ mistuning

The resonances shown in z-plots given in Figure 5.13 correlate well with predictions as indicated by green dashed lines connecting corresponding spots. The lower group of resonances shown in Figure 5.13 (a) were not excited as strongly as the upper two (and this is apparent from (a) too, but there they are clearly visible thanks to noise-free calculations and individual line colour scaling) and were much closer to the noise floor. As a result, when scaled with respect to the highest amplitude in the given surface, some of them did not show up as clearly as the upper group of resonances. However, their existence was evident from the extracted EO responses. Such a resonance is designated by a

red circle (the lowest resonance on the 6EO line) in Figure 5.13 (b). The red dashed line indicates that this resonance was excited at a lower speed in measurements than it was in predictions. As explained in Chapter 4.4, the 6EO line excited a predominantly 2ND mode at this resonance. Since the blisk fixing in the test rig was not as rigid as the prediction tool assumed it was, the natural frequencies of the modes at the lower end of 1F family of modes were (as they are most affected by the disk boundary conditions) lower and excited at lower speeds. Hence, this resonance was kept out of the speed range of individual blade measurements. Similar to the tuned case, the lack of perfect alignment of the LDV beam with the rotation axis manifested itself on 1, 2 and 4 EO lines (1 and 2 EO lines not shown). Resonances corresponding to the 1F family of modes excited by higher EOs (13 and above), due to spatial aliasing, were also captured in measurements and are clearly demonstrated on the given z-plot. Responses of all blades to 6EO excitation were measured in the speed range of 2350-2850 rev/min, thus covering two prominent resonances shown in z-plots, as decided in the test design phase. The results of these measurements are given in Figure 5.14.

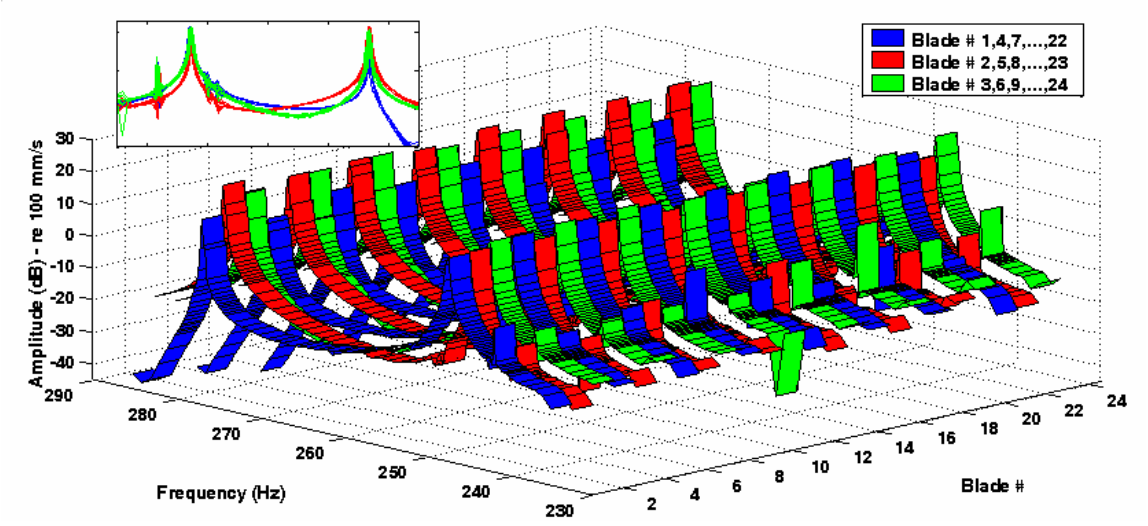

Figure 5.14 Response of Blisk-2 with $S8\theta$ mistuning to 6EO excitation - all blade measurements.

Since a regular mistuning pattern consisting of three different masses was applied (i.e. three masses periodically distributed round the blisk), blades having the same mistuning mass should exhibit the same response. This was demonstrated gratifyingly by the measurements and is more clearly seen from the inset given in Figure 5.14. Although, in theory, measuring only three blades would have sufficed, all blades were measured: (i) to prove that this behaviour was confirmed by real data, and (ii) to have an envelope of variability through multiple measurements of "identical" blades.

Measured individual blade responses given in Figure 5.14 were compared to their predicted counterparts and are given in Figure 5.25.

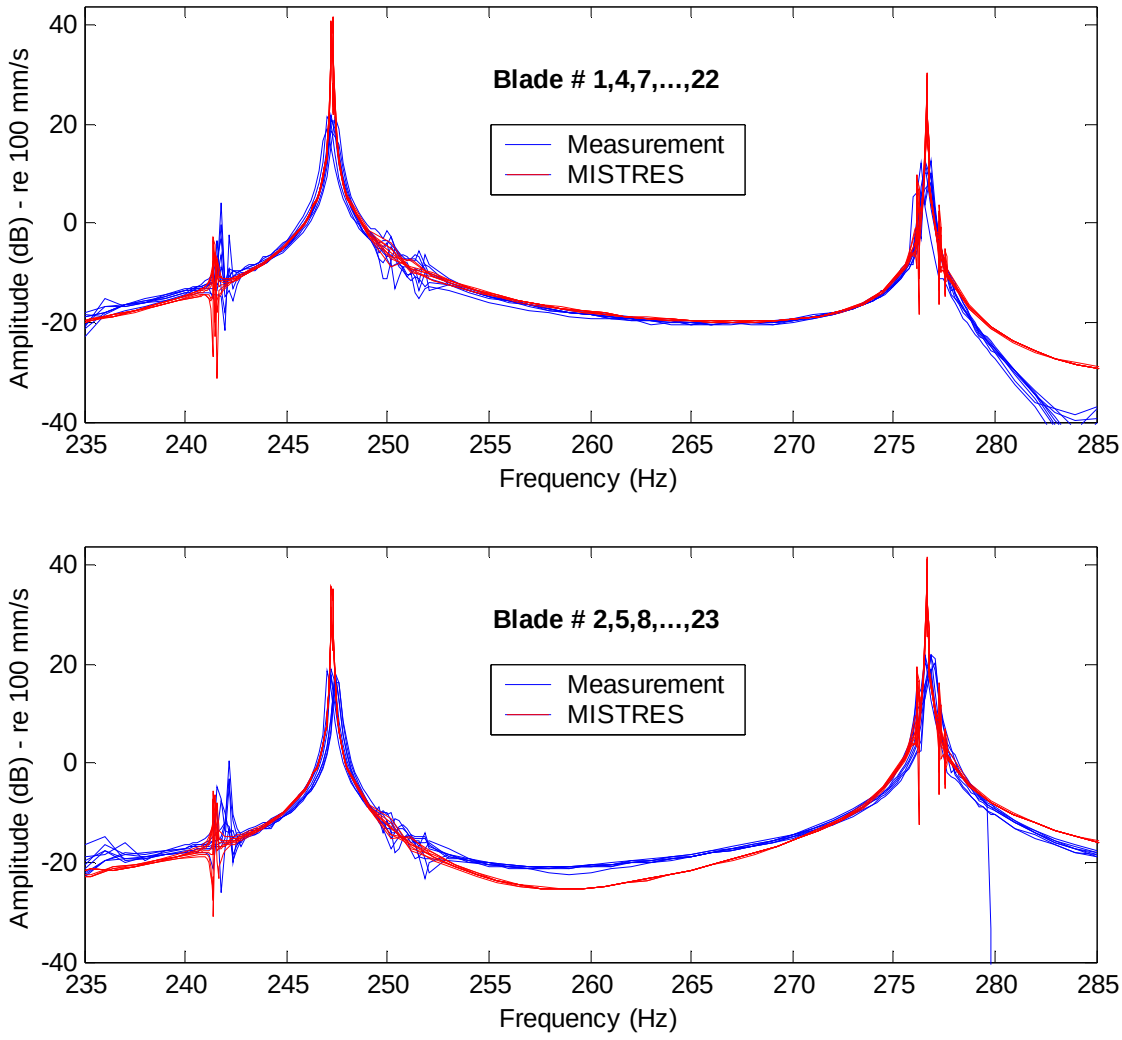

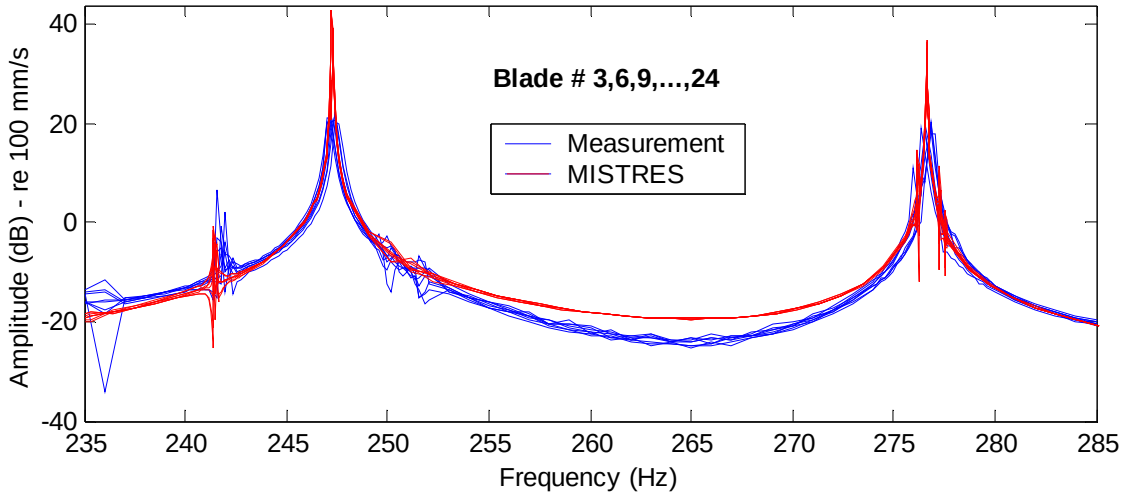

Figure 5.15 Blisk-2 with $S8\theta$ mistuning pattern: Comparison of individual blade responses to 6EO excitation.

Similarly, due to the lightly damped nature of the blisk, the resonance peak amplitudes could not be captured precisely, and were significantly different than those predicted. However, away from the resonance regions the response curves were strikingly similar to those predicted by the numerical model. Figure 5.16 shows close-up views of measured and predicted resonance groups shown in Figure 5.15. As shown in Figure 5.16 (a), it is predicted that two very close modes should be excited. However, this could not be seen from the measured plots, primarily due to insufficient sweep rate (note that the minimum speed increment was 1 rev/min, which meant that the frequency increments for the 6EO response measurements could not be less than 0.1 Hz). The same effect, to an extent, is seen from Figure 5.16 (b) as well, where one of the small-amplitude sharp resonances is not showing on the measured response curve. Also from Figure 5.16 (b), a steady shift in frequency is apparent, though, in general, it is around 0.1% and amplified, in this particular case, because of the narrow frequency range shown. Nevertheless, the predicted response curves, both in Figure 5.16 (a) and (b) are reassuringly followed by the measured data

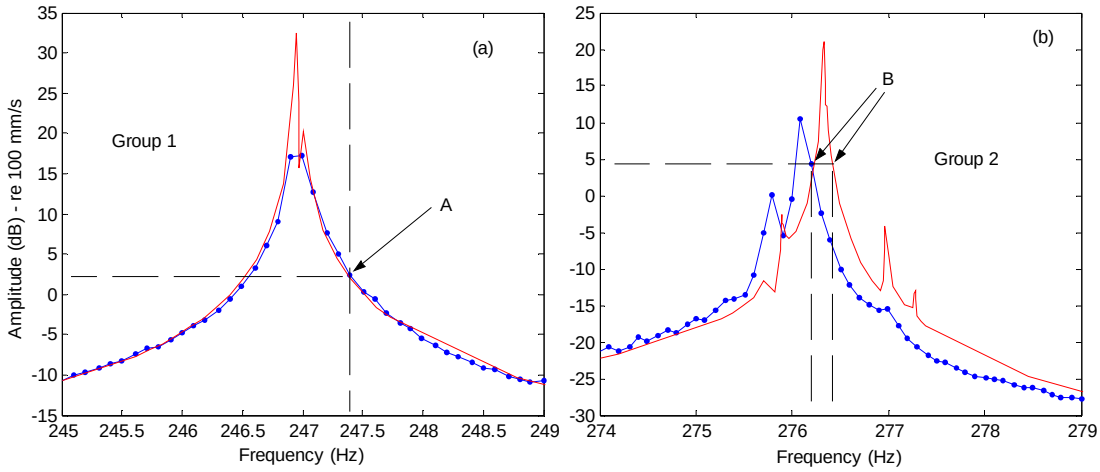

Figure 5.16 Close-up of covered resonance groups Measured and predicted amplitude curves for blade #1.

Blade-to-blade response amplitude patterns for both of the resonance groups were also compared with the predictions as shown in Figure 5.17. For this purpose, using a slow-circular scan at the blade tips, all the blade amplitudes were measured at frequency (speed) points A and B, as shown in Figure 5.16 (a) and (b) respectively. The points A and B were selected as at around the immediate neighbourhood of the resonances, true amplitude peaks could not be measured due to truncated signals. It was demonstrated in Figure 5.11, that uncertainties in the proximity of the selected speed point (e.g. A or B) to the true resonance frequency lead to significant errors in amplitude comparisons. In order to make sure that corresponding data are compared, the predicted amplitude variation is amplitude-scaled such that one of the blade amplitudes matches the measured counterpart. This is appropriate as it is already proved through the given response curves that, away from the resonances, the measured amplitudes are closely predicted in numerical simulations. Despite minor departures, amplitude variation plots show good agreement both in terms of distribution and amplitude. Extracted inter-blade phase angles corresponding to given amplitude variations showed that standing waves were excited at both measurement speeds.

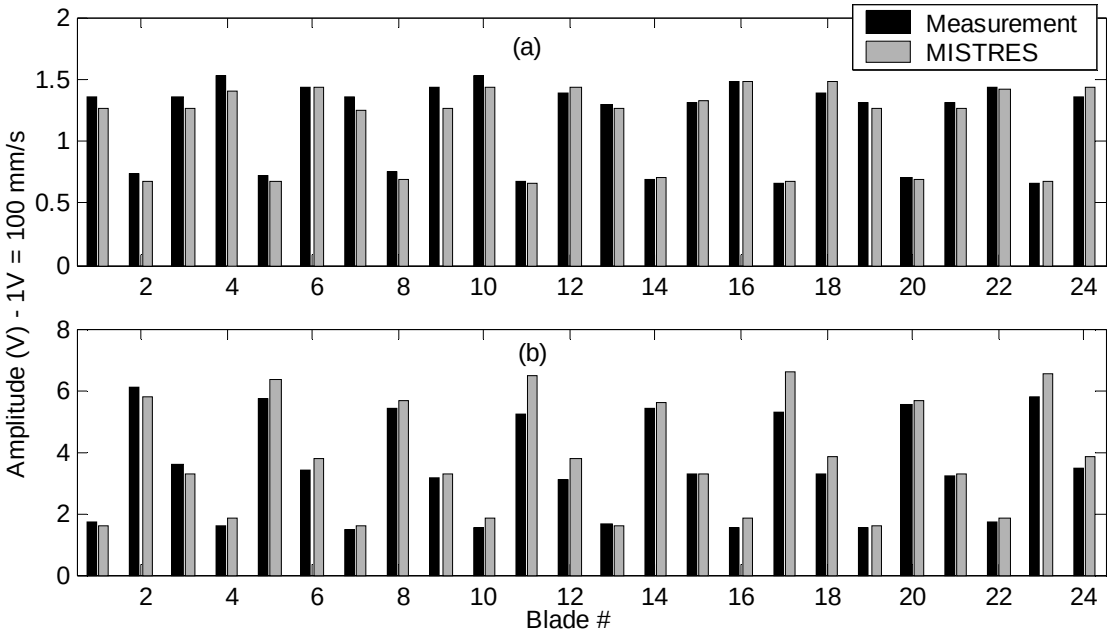

Figure 5.17 Comparison of blade-to-blade amplitude variation at (a) point A, and (b) point B shown in Figure 5.16.

5.4.6 Randomly mistuned blisk analysis

The random mistuning pattern was obtained by "randomly" reshuffling the $S8\theta$ mistuning pattern, as explained in Chapter 4. Therefore, assuming that no significant inherent mistuning existed in the blisk, the randomly-mistuned blisk model to be used in predictions was obtained by simply changing the order of the blades of the $S8\theta$ model. Similarly, first the natural frequencies at rest were measured, and the results are compared with the predictions in Table 5.2.

Mode #	Measured (Hz)	Predicted (Hz)	% diff.	Mode #	Measured (Hz)	Predicted (Hz)	% diff.
1	-	157.97	-	13	239.40	239.80	0.17
2	-	160.08	-	14	248.25	248.73	0.19
3	-	160.85	-	15	248.50	248.82	0.13
4	161.70	169.54	4.63	16	251.80	252.20	0.16
5	162.70	170.97	4.84	17	262.80	263.25	0.17
6	194.05	195.13	0.55	18	265.75	265.40	0.13
7	196.64	197.97	0.67	19	266.10	265.79	0.12
8	214.55	214.97	0.20	20	267.85	267.90	0.02
9	221.20	221.61	0.18	21	268.10	267.92	0.07
10	227.30	227.67	0.16	22	268.40	268.50	0.04
11	232.75	233.11	0.15	23	269.80	269.81	0.00
12	235.40	235.72	0.14	24	271.40	271.45	0.02

Table 5.2 1F family natural frequencies of the randomly mistuned Blisk-2 at rest.

Only 21 out of a possible 24 modes could be detected in the measured data. Although an exceptionally good match was obtained for the natural frequencies at the higher end of the 1F family of modes, the predictions in general departed from measurements by 0.1 to 0.2%. Similar to the tuned and $S8\theta$ cases, relatively larger errors in the lower natural frequencies were probably due to flexibility of the disk clamping in the experiments.

Before comparing individual response curves, it is useful, again, to see the overall correspondence of the measurements and predictions using z-mod plots. Such an experimental plot measured on blade 21 of the blisk and its predicted counterpart are given in Figure 5.18.

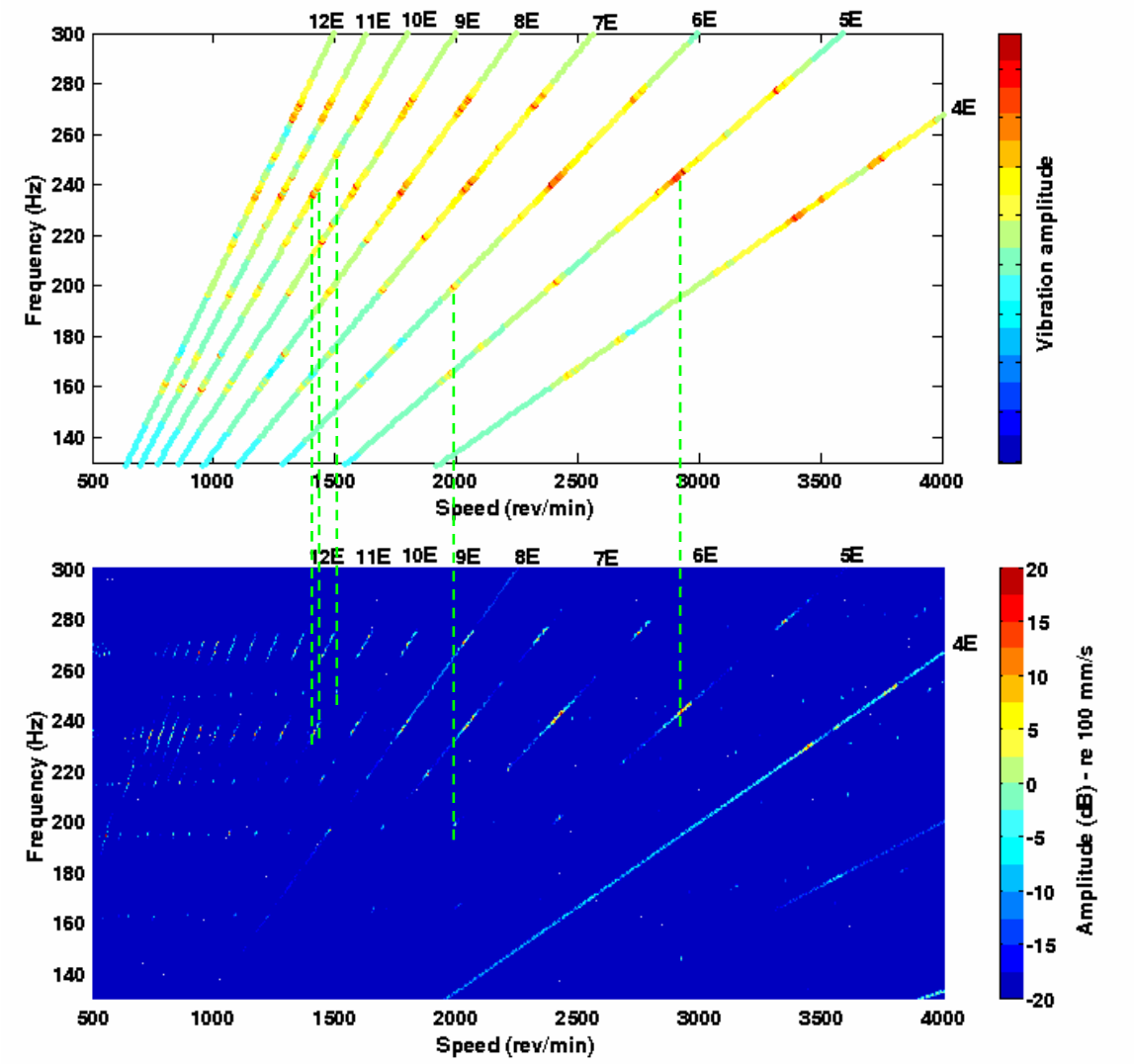

Figure 5.18 Predicted and measured z-mod plots for Blisk-2 with applied random mistuning

The vertical dashed green lines are provided to make the comparisons easier. Overall, a very good correlation is observed between the given diagrams. Again, due to global amplitude-dependent colour scaling in the measured plot, some of the resonances were not seen as clearly as they were in the predicted one. However they were evident on the extracted EO response curves.

Individual blade responses were measured for a speed range of 1400-1540 rev/min. This range covered 5 distinct resonance groups excited by 10EO excitation. Extracted 10EO response curves are compared to the predicted ones for all blades as given in Figure 5.19.

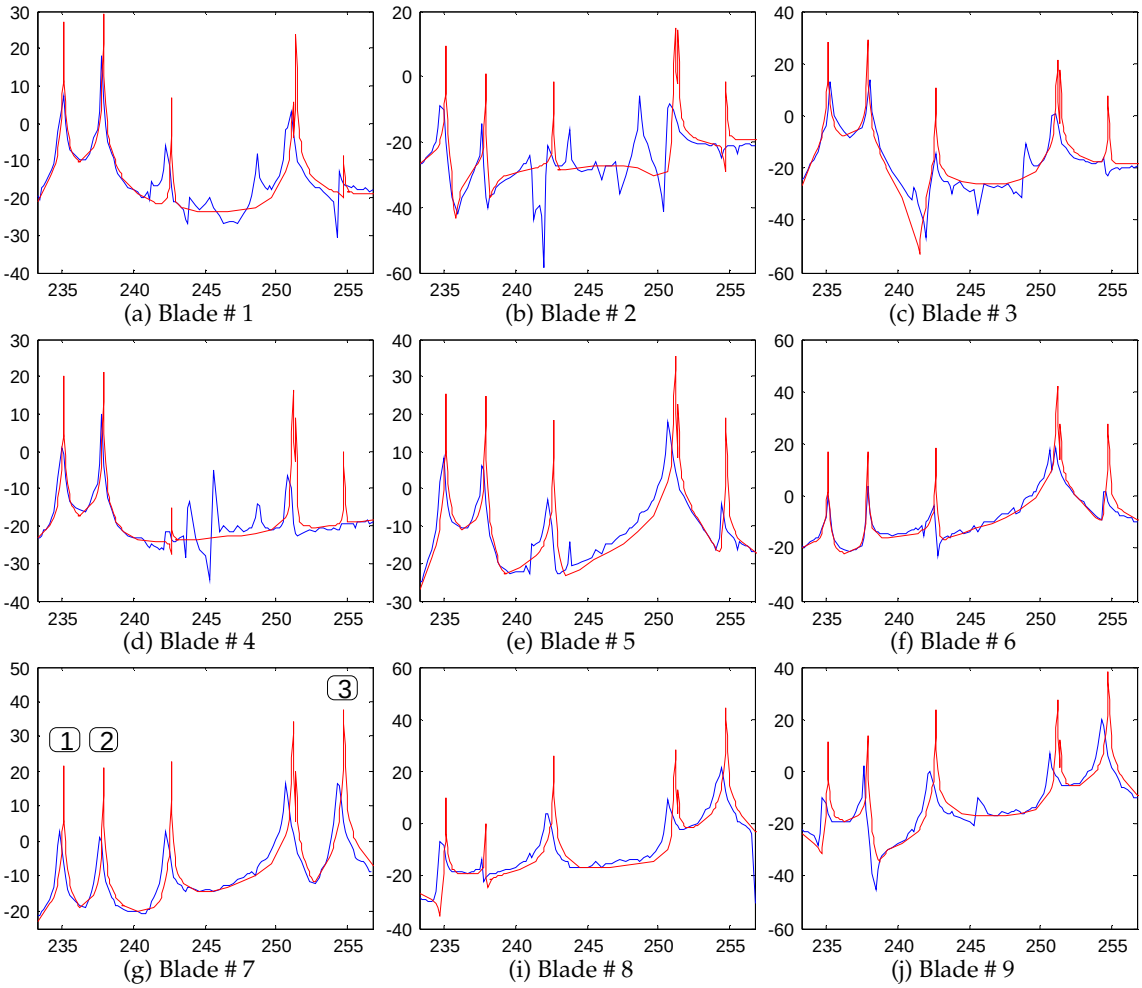

(Continued over…)

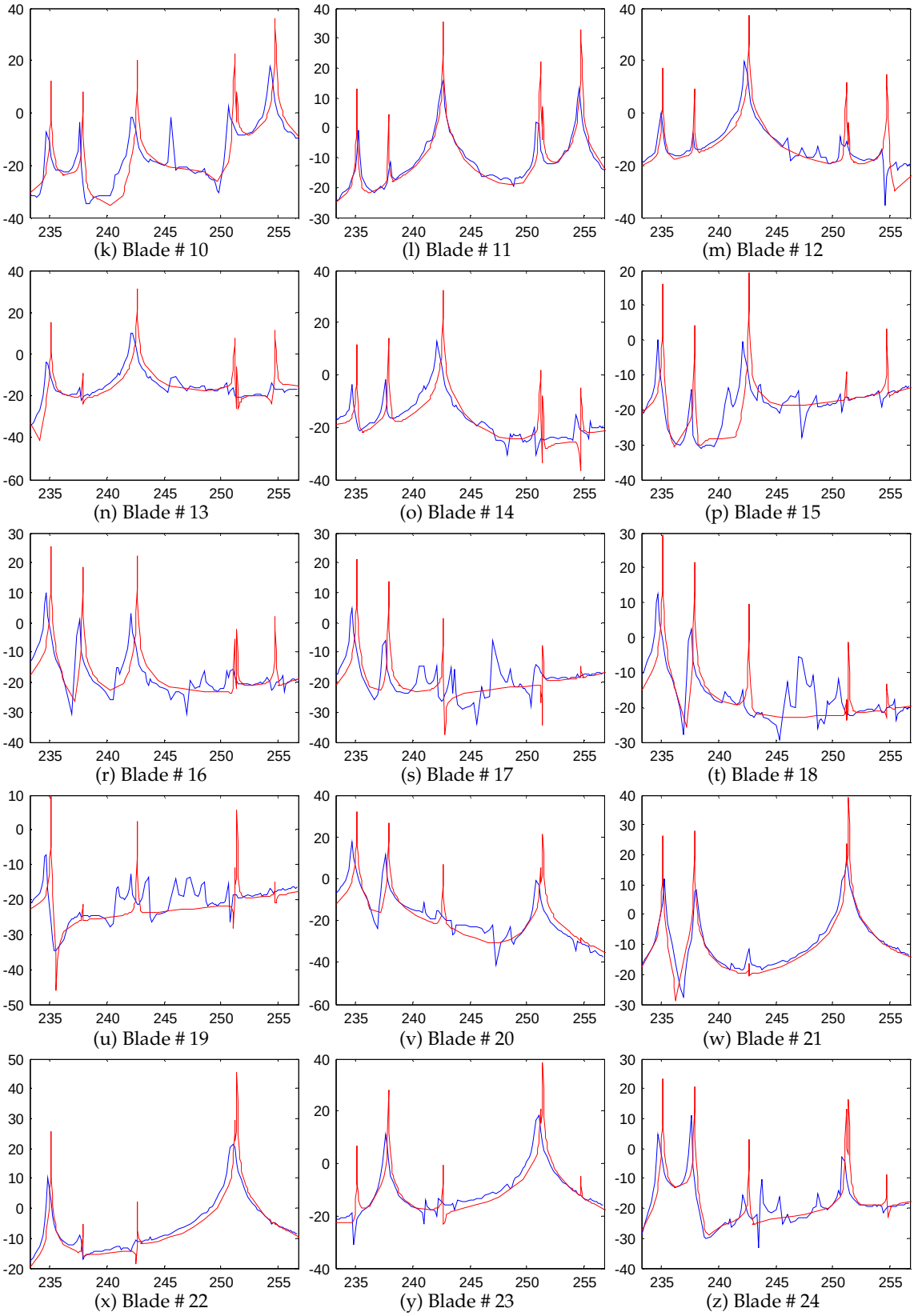

Figure 5.19 Blisk-2 with random mistuning pattern: Comparison of individual blade responses to 10E excitation. —Measured, —Predicted. (x-axes: *Frequency (Hz)*, y-axes: *Amplitude (dB) – re 100 mm/s*)

Forced response comparisons given in Figure 5.19 exhibited a very good match between measurements and predictions. In particular, the degree of correlation well away from resonances, for very low amplitudes, demonstrated the extent of the capability of the self-tracking LDV measurement system as well as the strength of the prediction tool. However, some discrepancies were inevitably present. In general, predicted natural frequencies were found to be slightly higher than the measured ones although there were some cases in which the opposite trend was observed. This variability can probably be attributed to errors introduced through modelling of the mistuning masses. As the mistuning masses were taken into account after the natural frequencies and the mode shapes of the corresponding tuned case were computed, the effect of rotation on these masses is not accounted for. This situation, as a result, contributed to the deviations in the natural frequencies. However, the locations of the natural frequencies identified in measurements also showed slight variability from blade to blade, probably due to minor changes in test conditions as the blades were measured in turn. Nonetheless, the difference in frequencies was in general around 0.2% and therefore in-line with frequencies compared at rest and the results of $S8\theta$ mistuning case. Note that due to the narrow frequency range used (23 Hz), deviations in natural frequencies were emphasised compared with the $S8\theta$ case, where a frequency range of 50 Hz was swept. Similar to previous cases, true resonance peak amplitudes could not be recovered from the measurements. In some cases, such as the ones given in (b), (d) and (p), some of the resonance curves were too sharp that they could not be captured with 0.17 Hz frequency steps (i.e. (1 rev/min)/60*10). As a result, they did not show up on measured response plots.

A 1/rev signal was used to trigger data acquisition so that the vibration phase data could also be worked out. The amplitude and phase measurements for some blades are given in Figure 5.20, which clearly demonstrated that successful phase measurements were achieved.

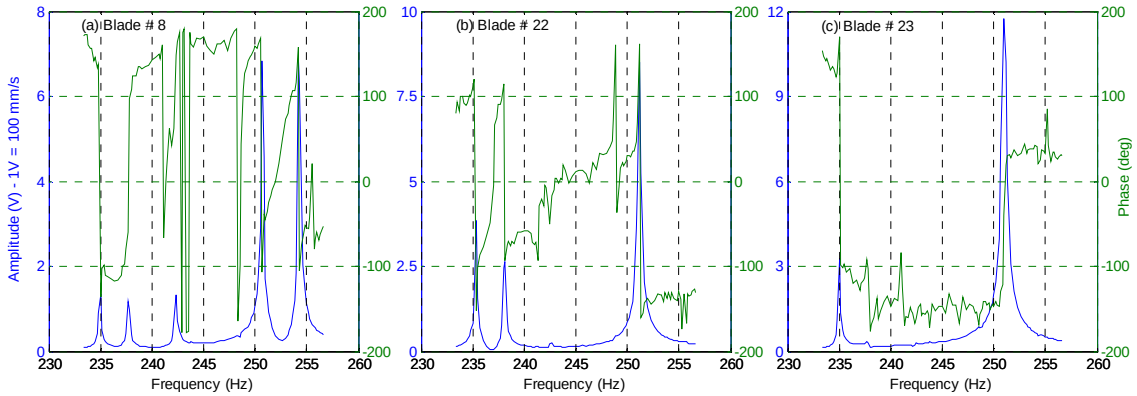

Figure 5.20 Amp. and phase measurements for blades (a) 8, (b) 22, and (c) 23.

Some of the response plots, Figure 5.19 (a)-(d), (t), (u) etc., depicted resonances at around 241, 244, 246 and 248 Hz which were not predicted by the numerical simulations for 10EO excitation. However, as it is evident from the z-mod plots given in Figure 5.18, that EOs 9 and 11, and to an extent 8, excited strong resonances in the speed range of measurements, corresponding to these frequencies for the mentioned blades. This was clearly seen from experimental response curves extracted for these EO excitations. The contribution of 10EO response was probably amplified due to large vibration amplitudes at corresponding rotation speeds and manifested itself as spurious resonances. Even so, their amplitudes were generally less than -10 dB. The response of blade 2 to 9, 10 and 11 EO excitations in the speed range of measurements is given in Figure 5.21. Predicted response curves are also given.

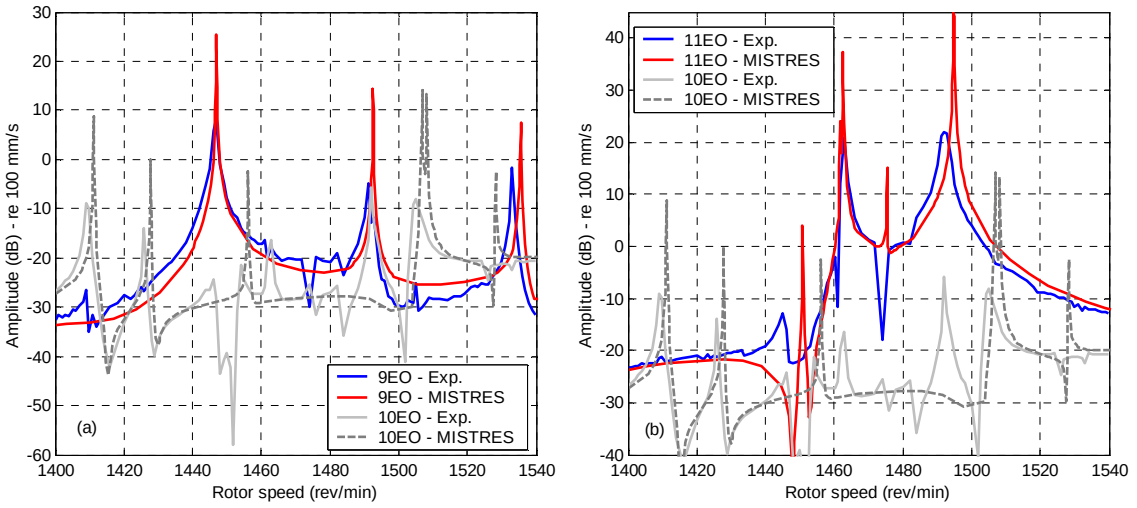

Figure 5.21 Response of blade 2 to 9, 10 and 11 EO excitations.

It is seen from the above figures that 11EO excited strong resonances at 1462 and 1492 rev/min, and 9EO at 1447 and 1490 rev/min, although not as strongly. The reflections of these resonances are clearly seen on the 10EO response curve. Close inspection of the time histories of the corresponding data showed no clear evidence of beating to suggest that two very close frequencies were excited. The time data showed a dominant single vibration frequency. It is interesting here to note that this phenomenon occurred only for the blades which were weakly excited by 10EO and at the same time strongly excited by 9 or 11EO excitations.

All blade measurements were planned for a very small rotational speed range as wider ranges demanded excessive measurement times. Although this range covered a significant amount of data to asses the quality of the predictions, it was thought appropriate to measure one particular blade with sufficiently fine speed steps and for a wider range to make sure that predictions are inline with measurements not only in a small range but also for a wider range. The best candidate for this measurement was blade 21 as in construction of the z-mod plot most of the data points were already available. For this particular measurement, intermediate speed values were added to obtain a finer resolution. The measured and predicted responses of blade 21 to 10EO excitation are given in Figure 5.22 (a). The plotted curves present a striking similarity not only at around resonances but also at around anti-resonances thus validating both the prediction tool and the measurement setup. The response curves of this blade to other EO excitations were also compared with the predictions and similar results were obtained. So far, when plotting the measured response curves, the actual measured data points were connected by solid lines visual clarity. However, the accurate representation should have plotted them as separate points, as shown in Figure 5.22 (b). This is necessary as experimental curves are not complete, particularly around resonances, simply because there are not enough measurement points to define the resonance peaks accurately (see also Chapter 4, Section 4.4.1). Thus, the apparent difference between the

measured and predicted resonance peak amplitudes seen in Figure 5.22 (a) is due to lack of measurement points and is not indicative of a genuine mismatch.

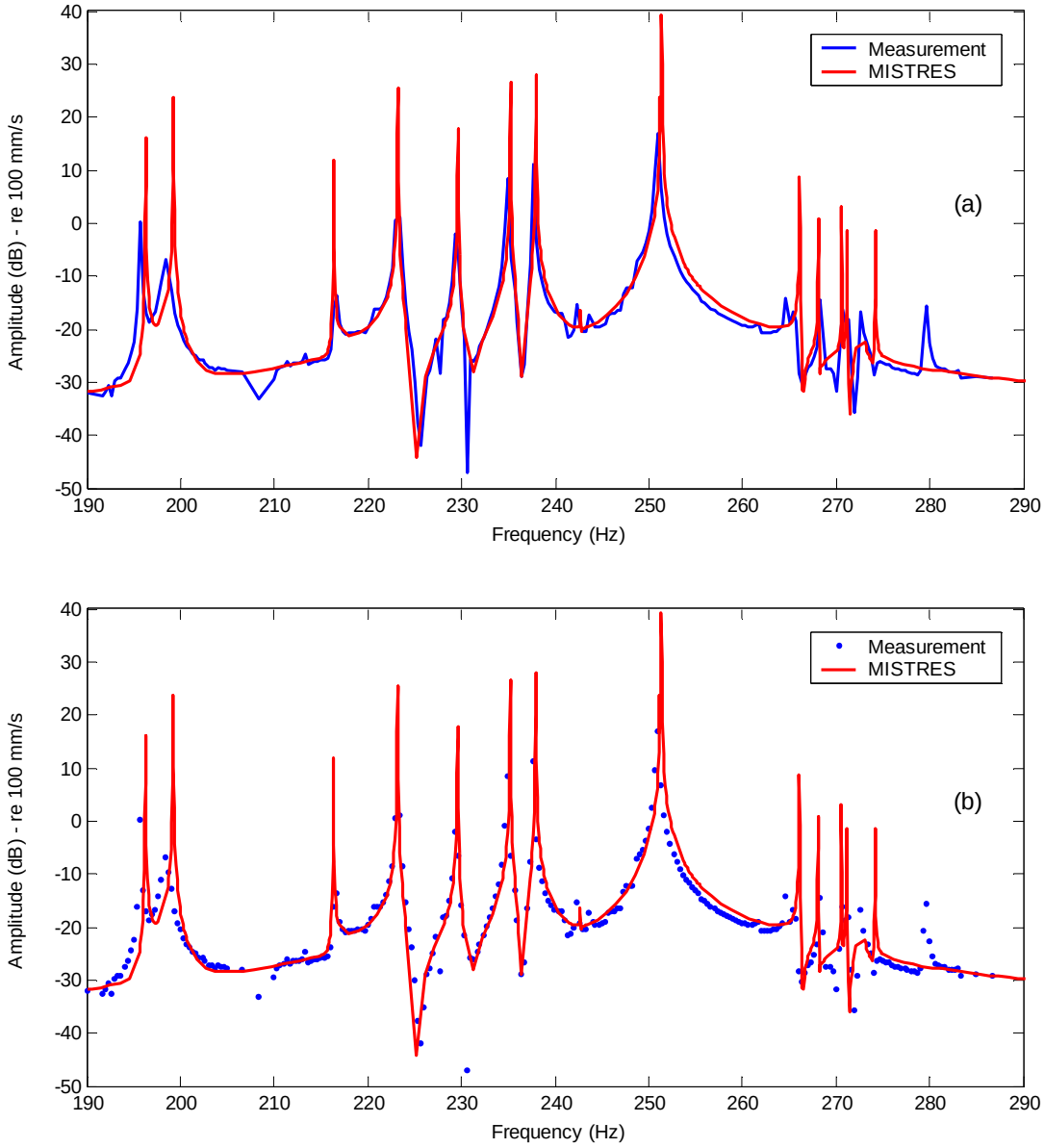

Figure 5.22 Response of Blade 21 to 10EO excitation. Measurements plotted (a) as a solid line, and (b) as points

Blade-to-blade amplitude variations were also compared for some of the excited resonances in the "all-blade measurements" speed range (i.e. 1400-1540 rev/min). The resonance amplitudes could not be used in comparisons as they could not be captured accurately in the measurements. Even then, they were demonstrated as following the same pattern, though significantly lower in

amplitude. Nevertheless, blade response patterns were compared at equal distances from corresponding measured and predicted resonances. This was necessary as resonances in measurements and predictions occurred at slightly different frequencies. As mentioned, individual blade responses also showed some variation in resonance locations, therefore, blade tip amplitudes for this comparison were measured by employing a continuous slow circular scan at the blade tips at the desired rotational speeds. Figure 5.23 shows comparisons obtained in close proximity of the first, second and last resonance peaks (approximately 1-2 rev/min away) shown in plots given in Figure 5.19, see (g). Similar to the $S8\theta$ case, predicted amplitudes were scaled to account for the uncertainties related to the location of the resonance frequency. Inter-blade vibration phase angles, Figure 5.24, indicated that the blades were either in-phase or out-of-phase with each other. Thus, the excited modes were fixed in the blisk (i.e. standing waves were excited). Predicted amplitude variations in all these cases are well correlated to measured ones both in terms of shape and magnitude.

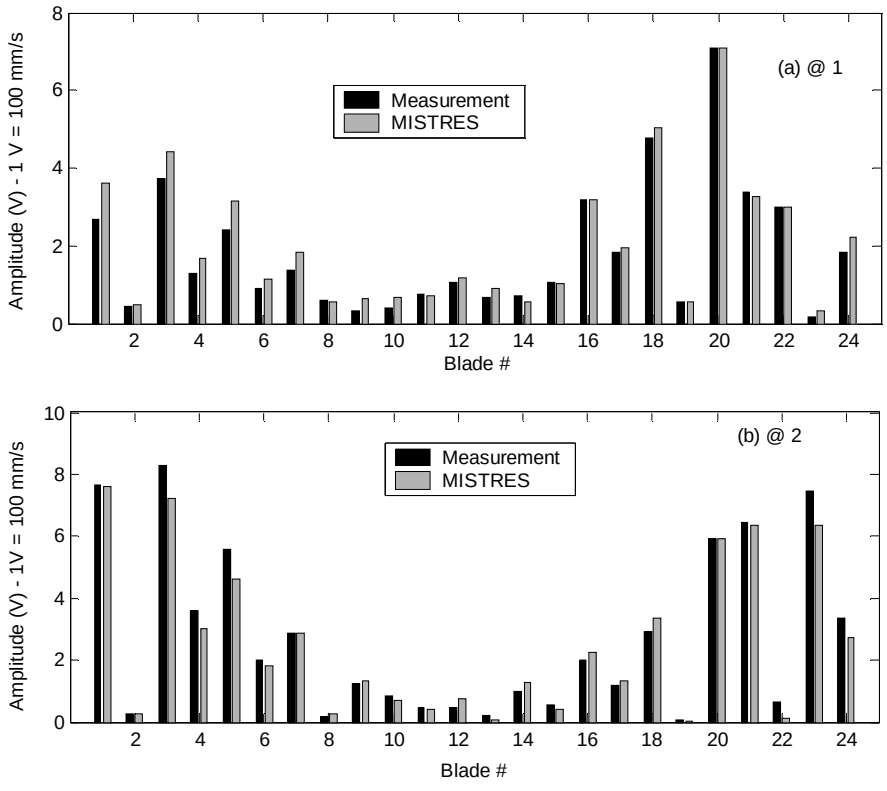

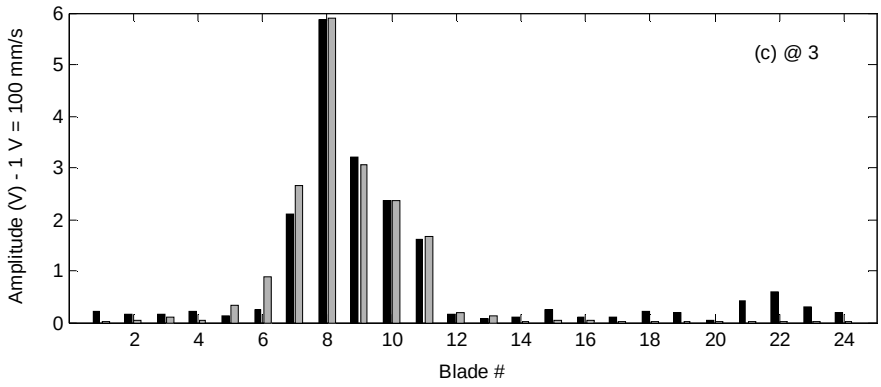

Figure 5.23 Comparison of blade-to-blade tip amplitude variations at various resonances excited by 10EO excitation.

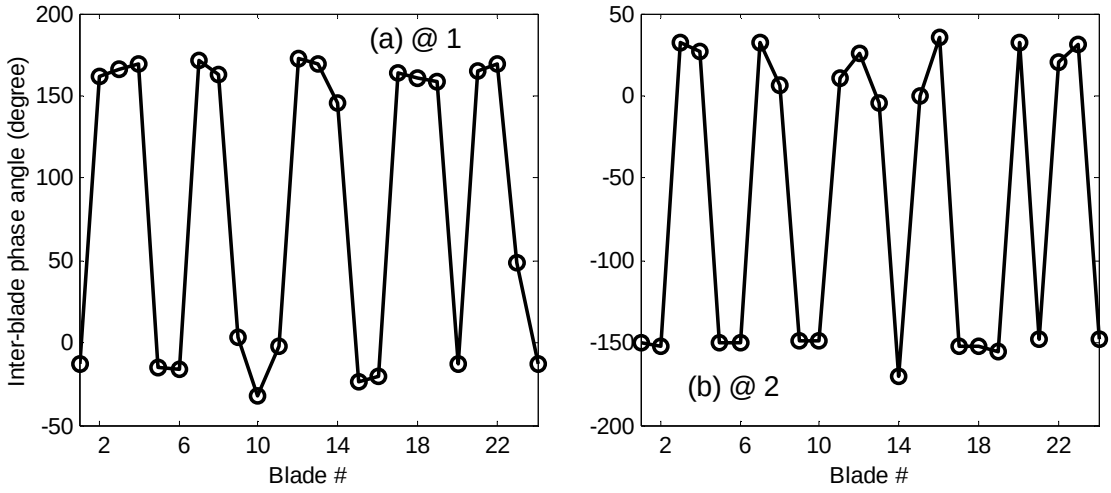

Figure 5.24 Inter-blade phase angles corresponding to amplitude plots given in Figure 5.23 (a) and (b).

5.5. Summary

In this chapter the forced response predictions of the tuned and mistuned Blisk-2, at rest and under rotating conditions have been validated through a comprehensive test campaign using the testpiece (Blisk-2) and rig whose design and development were reported earlier in the thesis. The validation strategy adopted has been one in which a step is taken at a time to make sure that all possible sources of uncertainties have been accounted for. Thus, the validation of the following have been considered: (i) natural frequencies and mode shapes in the absence of rotation, (ii) inclusion of rotational speed in the predictions, (iii) modelling of mistuning masses, (iv) repeatability of measurements and

reliability of the test setup, (v) response curves over wide speed ranges as well as short ones, and (vi) peak responses (i.e. ODSs) in the presence of uncertainty of actual damping levels.

First, the response prediction tool used in simulations was introduced. Its main advantages and the way it models mistuning were explained. Following that, the measured ODSs for the mistuned stationary blisk were compared with the predicted ones and a very good match was obtained. Then, starting with the tuned case, rotating test results with the applied regular and random mistuning patterns were presented and corresponding predictions were overlaid. The ability of the rig to reproduce the same data under the same conditions was verified through a devised method involving shifted mistuning patterns. Measured and predicted z-mod plots were demonstrated to be correlating very well although the predictions of the some of the disk-dominated lower natural frequencies were lower in measurements. In general, the predicted resonance frequencies deviated from the measured ones by 0.2%. As a result of the very low damping in the rig, the true resonance peak amplitudes could not be measured. This was because; (i) the resonance peaks were very sharp that speed increments much smaller than 1 rev/min (minimum available in the rig) were needed to capture them accurately, and (ii) the peak amplitudes were so large that the data acquisition board was overloading. However, away from the resonance peaks, an exceptionally good agreement was obtained, in general, between measured and predicted behaviour.

Blade-to-blade amplitude variations were also compared for the tuned and mistuned cases. In the tuned case, travelling waves were excited resulting in all blades having the same vibration amplitude, as predicted by theory. However, in mistuned cases the modes were grossly localised and were fixed in the blisk. Predicted patterns were illustrated to be perfectly verified in considerable detail by measurements both in terms of shape and magnitude. The quality of the match proved the vibration measurement rig as a well controlled environment

and the non-contacting self-tracking LDV technique as an accurate way of acquiring vibration response under rotation.

CHAPTER 6

VALIDATION of UNDAMPED and DAMPED BLADE RESPONSE PREDICTIONS

6.1 Overview

This chapter focuses on the evaluation of tests performed on Blisk-1 with Cottage Roof dampers and assesses the validity of the forced response predictions based on these tests. However, the undamped blisk response is considered first to measure the degree of correlation in the absence of non-linearity. The non-linear forced response prediction tool to be validated is introduced next. Mistuning of Blisk-1, identified in Chapter 4 in terms of 1F sector natural frequencies, is translated into physical mistuning and the effects of different ways of performing the translation on the forced response are analysed. Additionally, the consequences of variations in the amplitude of the forcing input are discussed and the effects are shown using the Blisk-1 FE model.

6.2 The prediction tool

The development of the non-linear forced response prediction tool, and in particular the modelling of the non-linear interfaces, to be validated in this study is given in a series of papers, [37-39]. The application of the method to bladed disks with friction and impact dampers can be found in reference [82]. Similarly, the application of the method to mistuned bladed disks (mistuned through blade properties and/or non-linear interface elements, i.e. friction dampers, gap values etc.) can also be found in [40].

The main features of the method can be summarised as follows:

- use of multi-harmonic balance method in the solution of forced response
- applicability to any structure with the option to use cyclic symmetry for structures exhibiting this property
- accurate description of friction forces in the presence of variable as well as constant normal load;
- analytical formulation of contact interface elements, thus much faster solution times, higher accuracy and rapid convergence.

Because of the above-mentioned features, the application of the method to realistic industrial models with large DOFs and heavy non-linear behaviour, resulting from under-platform and impact dampers, shroud contacts, gaps etc. has been possible. The friction interface elements are used to describe the interaction of surfaces in contact at a node; however, through use of many such elements over a given area, modelling of complex surfaces in contact is also possible. The method is coded into a computer program called FOrce Response SuitE (FORSE), [87].

Figure 6.1 shows different stages in the formation of non-linear equations and reduction process for a general, mistuned bladed disk application. System matrices for the whole tuned bladed disk are formed from a sector model using the method described in [14]. Through a multi-stage reduction technique, the size of the non-linear equations is reduced to the number of the nodes where non-linearities are applied. This enables the retained number of DOFs to be several orders of magnitude less than total number of DOFs in the model.

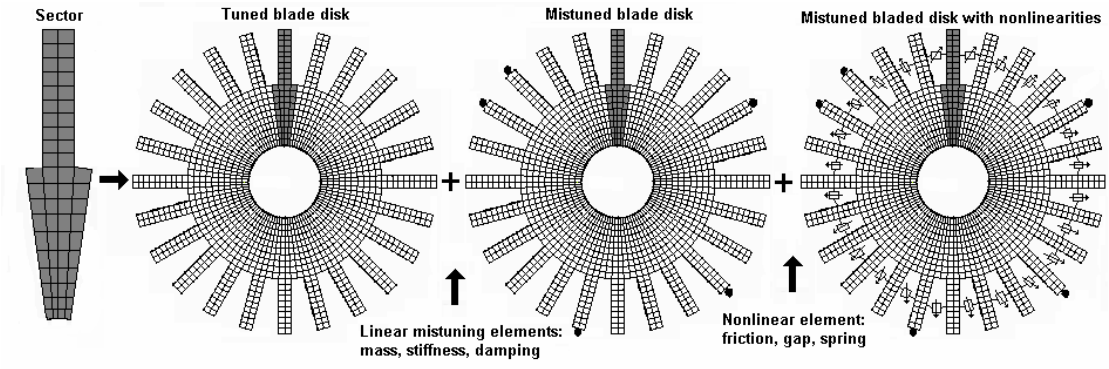

Figure 6.1 Different stages in DOF reduction and formation of non-linear equations (Adapted from [40])

6.3 Frequency mistuning to physical mistuning

When Blisk-1 was received from the manufacturer, unlike Blisk-2, it was found to be significantly mistuned. This inherent mistuning, despite some attempts, could not be removed completely. Nevertheless, it was identified to a certain degree in Chapter 4 as a sector-to-sector frequency deviation. As explained in Chapter 5, frequency mistuning can be used as a direct input to the prediction tool. However, it eventually needs to be represented by lumped mass or stiffness elements. In doing so, the prediction tool varies the values of the assigned mistuning masses or stiffnesses to adjust the natural frequencies of the first sub-model (i.e. isolated blade or sector etc.) such that the provided natural frequency mistuning is reproduced. Since only the first frequency of the sub-model is considered, depending on the selection of mistuning nodes, assembly characteristics other than the ones intended may be obtained, as discussed in Chapter 4.2.3. In order to reduce the dependency of the resulting assembly characteristics on the mistuning nodes, an isolated sector rather than a blade is used as a sub-model. This yields two main benefits. First, since a bigger model is used (a sector as opposed to a blade), matching only the first natural frequency yields closer assembly characteristics. Secondly, the disk portion as well as the blade is used to introduce mistuning and therefore a more realistic representation is obtained.

However, despite these advantages, the location of mistuning nodes still bears considerable importance. In Chapter 4, the blade-tip locations were found to be the best choices for introducing mass mistuning. This was because the characteristics of the whole assembly and sub-model were shown to be equally sensitive to the changes brought in through these locations. However, the model used in those calculations was a rather simple one. In order to analyse this effect on a realistic model, mistuning was introduced at two distinct locations using the Blisk-1 FE model. The configurations used are shown in Figure 6.2.

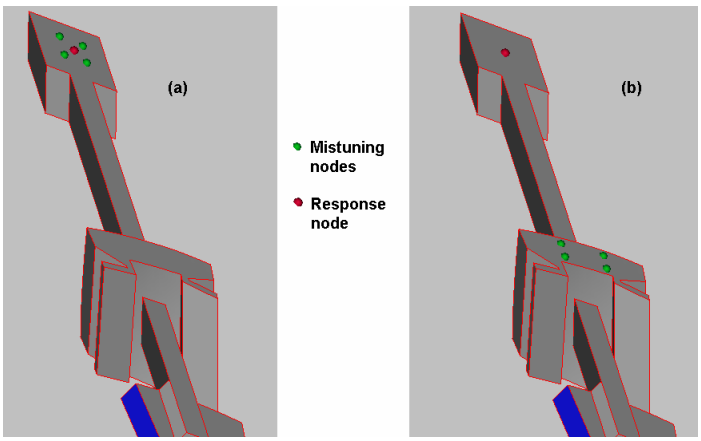

Figure 6.2 Introduction of mistuning in Blisk-1

For both configurations given in Figure 6.2, two sub-models: (i) isolated blade: where the mistuning is defined as the variation of the 1F natural frequency of a blade clamped at its root, and (ii) isolated sector: where the same variation is defined in this case in terms of a sector model clamped at its cyclic symmetry interfaces, were used. The errors introduced in the natural frequencies of the 1F blisk modes for all possible configurations are given in Figure 6.3 where the bars for each group present the deviations of obtained natural frequencies from the measured ones at rest. For a given sub-model (blade and sector), for both ways of introduction of mistuning (blade-tip and platform level), the first natural frequencies of the individual models were exactly the same. It is seen from the plot that the worst results were obtained when an isolated blade was used and the mistuning was represented by nodes at platform level. However, when the mistuning nodes were moved to the blade tip for the same sub-model, the error

was considerably reduced. This result was in line with that of the simple lumped parameter model presented in Chapter 4. In general, relatively better results were obtained for the isolated-sector/blade-tip configuration. Although comparably close natural frequencies were obtained for the isolated-sector/platform-level configuration, when applied at platform level, mistuning caused significant frequency splits, especially at lower nodal diameters.

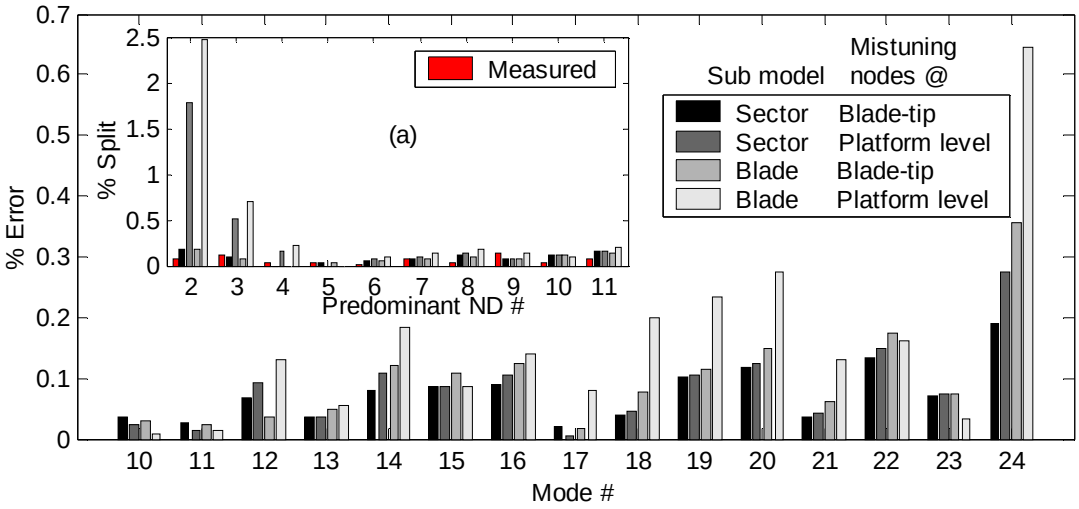

Figure 6.3 Comparison of different ways of mistuning modelling, (a) % split in ND mode pairs

In the light of the results given above, it was decided that an isolated sector should be used as the sub-model and that the mistuning should be applied at the blade tips. The number of mistuning nodes was also increased in order to assess the effect of the distribution on the forced response. For this purpose, 12 nodes were used, as shown in Figure 6.4, instead of the four shown in Figure 6.2 (a). The results of a sample forced response analysis are given in Figure 6.4. Practically no difference was observed between the two models. As the computation time increases exponentially with the increase in the number of active nodes (i.e. mistuning+force+response nodes), the model given in Figure 6.2 is used in the rest of the analyses.

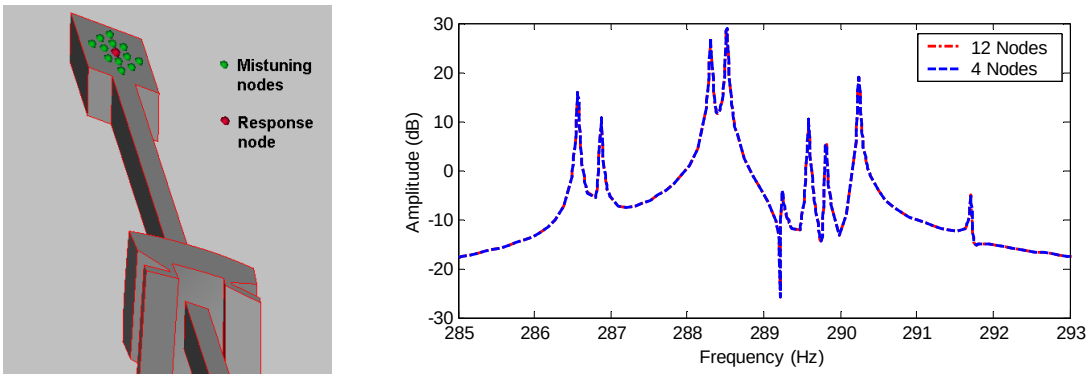

Figure 6.4 Introduction of mistuning through different number of nodes

6.4 Effects of excitation and mistuning errors on the forced response

6.4.1 Excitation errors

During the tuning process for Blisk-1, a significant amount of metal was removed from the blade tips. This implied that the magnet force applied on each blade might somehow be different, resulting in a variable amplitude forcing input around the blisk during its operation. In order to account for the effect of this variation, a recorded magnet signal was analysed to quantify the degree of variability. Such a signal is given in Figure 6.5.

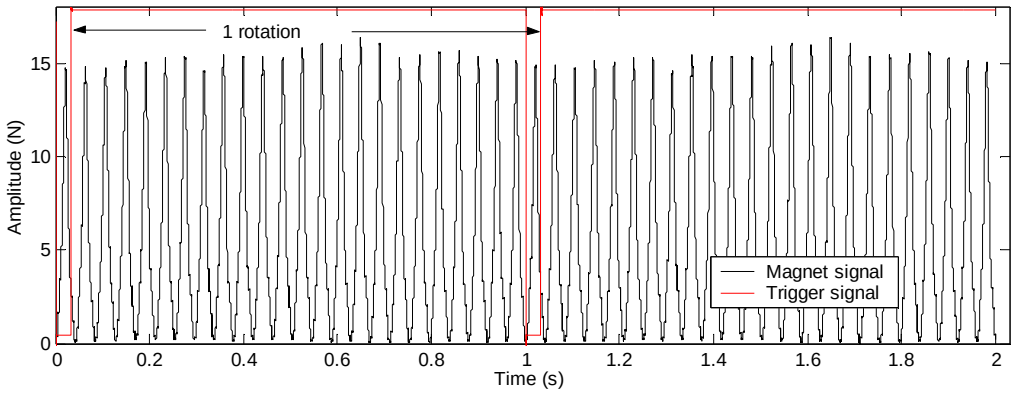

Figure 6.5 A typical magnet force signal applied to Blisk-1

Ideally, each pulse given in Figure 6.5 should have had the same amplitude. However, as expected in this case, the force signal presented a variation from

blade-to-blade (note that each pulse corresponds to a blade). It is seen that the peak amplitudes of pulses generated for each blade are slightly different and the pattern of variation repeats itself in each rotation cycle, as demonstrated in Figure 6.6 (a). In order to understand this better, these amplitudes are plotted in a circular form on a 3-D graph and given in Figure 6.6 (b).

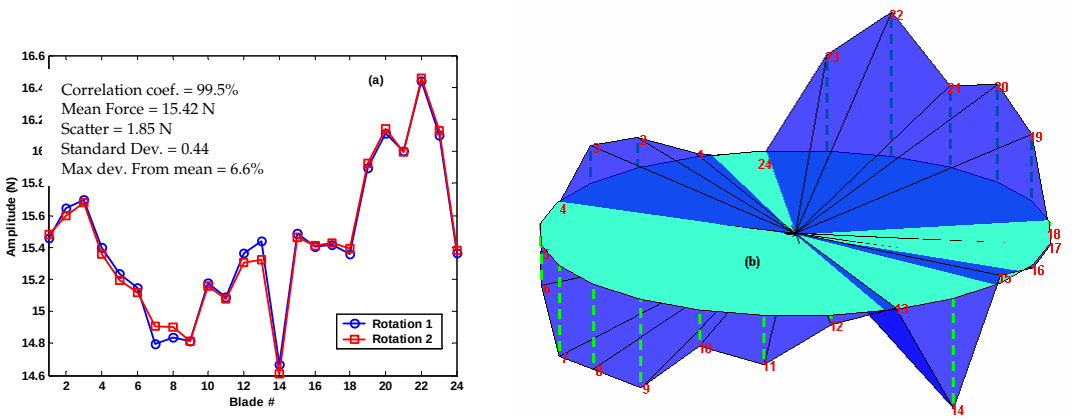

Figure 6.6. Variation of peak magnet force applied to blades of Blisk-1.

The pattern of variation given in Figure 6.6 did not correlate to the pattern formed by the amount of removed metal. The deviation of the peak amplitudes from the plane of the mean value (indicated by the flat circular area) given in Figure Figure 6.6 (b) suggested that the bladed disk was not perpendicular to the axis of rotation but tilted (i.e., swash error). Since tapered-lock devices were used to secure the bladed disk to the shaft (note that this was not the case for Blisk-2 as a different clamping mechanism was used), the degree of control on perpendicularity was somewhat limited. Additionally, it is thought that the drive shaft was slightly bent in the process of aligning the balancing disk with the identified mark on the blisk, a process which necessitated high forces to be applied to the drive shaft. In addition, it must be noted that some of the blades might have had slightly different stagger angles or bent, in a way to amplify this variation. These errors, combined with the effects due to different blade masses, are thought to have caused the presented variation.

6.4.2 Analysis of excitation errors

The effects of EO excitation errors (i.e. each blade receiving a slightly different force amplitude) was investigated on Blisk-1 FE model. For this purpose, two travelling wave excitations, one having constant amplitude (the mean value of the variation) and the other having the exact variation given in Figure 6.6, were considered. The errors in the excitation phase were neglected, based on the speed measurements given in Chapter 3, as the blade arrival times were very consistent. For both excitation patterns, the Fourier coefficients of the magnet pulses were calculated as described in Chapter 5. Note that for the second case these coefficients needed to be calculated for all 24 pulses separately. The variation of 9^{th} harmonic's amplitude is plotted in Figure 6.7 (a), as an example. The calculations were repeated both in the presence and absence of physical mistuning. The mistuned response prediction tool used in calculations, MISTRES, did not allow the amplitude of the applied EO excitation force to be different for different blades. Therefore, a commercially available FE package, in this case ANSYS, was used in calculations. This meant that a cyclic sector could not be utilised anymore. Therefore, a full blisk FE model was used. However, performing detailed forced response analyses in ANSYS proved to be extremely costly in terms of computation times. For this purpose, only the mode shapes and the natural frequencies were calculated (first 6 families of modes) using this package and the forced response was performed by a code written in Matlab. This way, the response was calculated for the nodes of interest, and much faster solution times and higher frequency resolutions were possible. The response of a particular blade obtained for both cases (i.e. tuned and mistuned) when subjected to 9EO excitation are given in Figure 6.7 (b). Although the bladed disk model used in (b-1) was perfectly tuned, the green curve exhibits response characteristics of a mistuned bladed disk. As explained earlier in Chapter 2, in order for a ND mode to be excited, the shapes of the excitation and the mode excited, as well as their frequencies should match. When the amplitude of the excitation varies, it contains some other harmonics, depending on the variation, which eventually excite corresponding ND modes. However, unlike mistuning,

the uneven distribution of the EO excitation force amplitudes does not cause double modes to split or change their natural frequencies. In the example given in Figure 6.7 (b-1), the random case excited all ND modes covered in the frequency range. Unlike physical mistuning, though, the force amplitude variation did not cause any significant change in the forced response amplitude of the main resonance (i.e. 9ND mode). For ±5% variation of the force amplitude, the maximum increase in the response amplitude was less than 0.13%. In fact, with ±5% force amplitude variation, the magnitude of the 6th harmonic did not change much, thus causing little change in the response amplitude. Similar results were obtained when a mistuned Blisk-1 model was used, as given in Figure 6.7 (b). Here the shape of the response curve for the variable-amplitude force case is not drastically different from the constant-amplitude one. This is because all the modes are already excited by the employed EO excitation, thanks to the now-finite-amplitude 9th harmonics present in their mode shapes. Even then, the effect of force amplitude variation on the response amplitude is much greater at the resonances, other than the main one, with variations up to 25%. Similar deviations are also evident away from the resonance peaks though increase in maximum amplitude for the given case is, likewise, less than 0.13%.

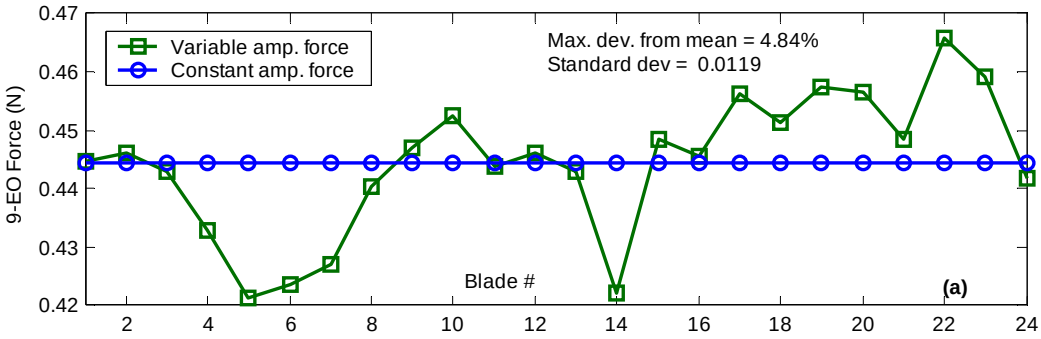

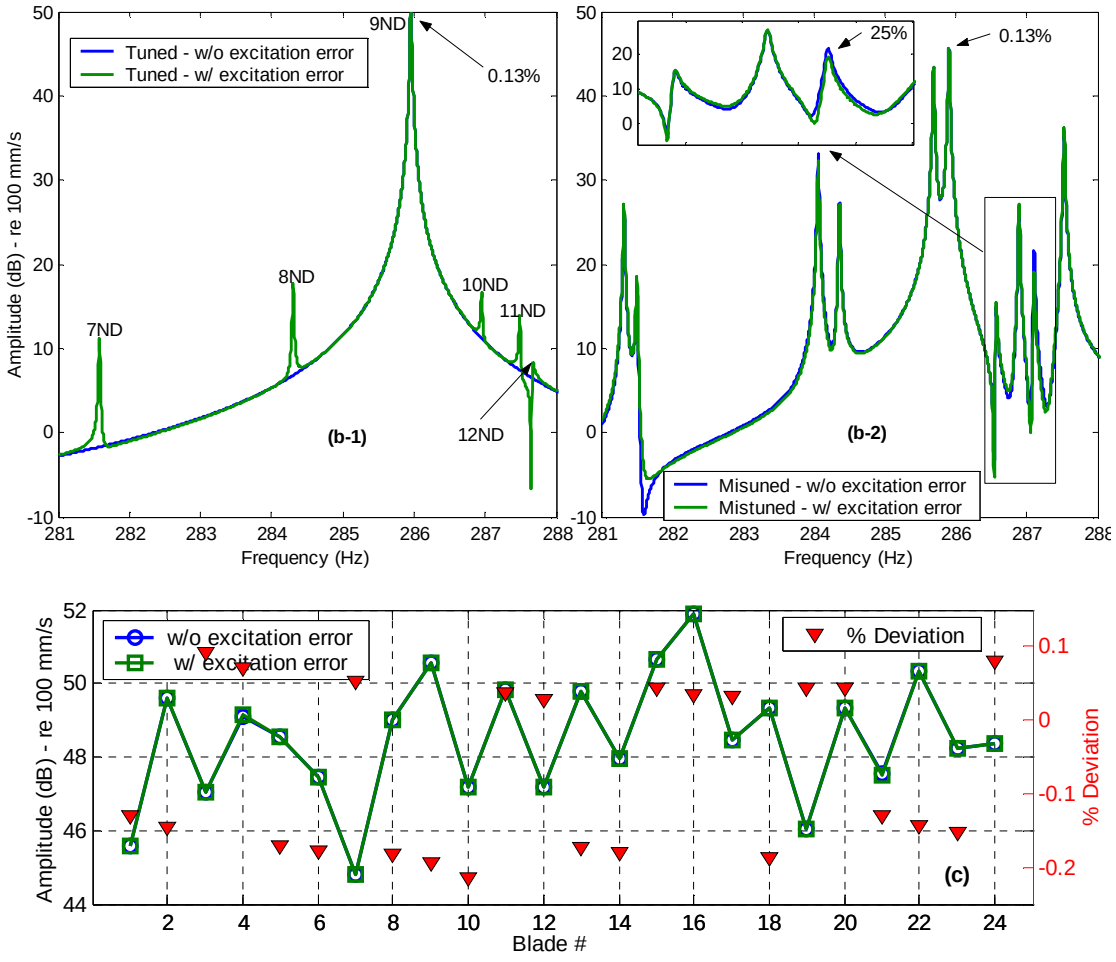

Figure 6.7(a) Applied force distributions, (b) forced response of blade 1, and (c) maximum blade-tip forced response amplitude comparison for mistuned Blisk-1.

The individual cases given in the above figure are important in providing a comparison of the overall response curves in a given frequency range. However, they alone do not present a true indication of the likely deviations the force variation might cause. In order to get a better idea about this, a large number of randomly varying force input shapes needed to be considered to form a statistical basis. To this end, 10.000 randomly generated cases were considered. Random vectors are chosen from a uniform distribution from the interval [0.0 1.0] and then shifted and scaled to provide a 5% variation on the mean value of the force variation given in Figure 6.6. The results obtained for physically tuned and mistuned bladed disk models are given in Figure 6.8. In both cases the maximum amplification due to random variations is found to be similar, and less than 3%. The maximum scatter in both cases is around 5%, although the

scatter in the mistuned case is slightly larger. The same calculations are repeated for 6 and 11EO excitations as well, and similar results obtained.

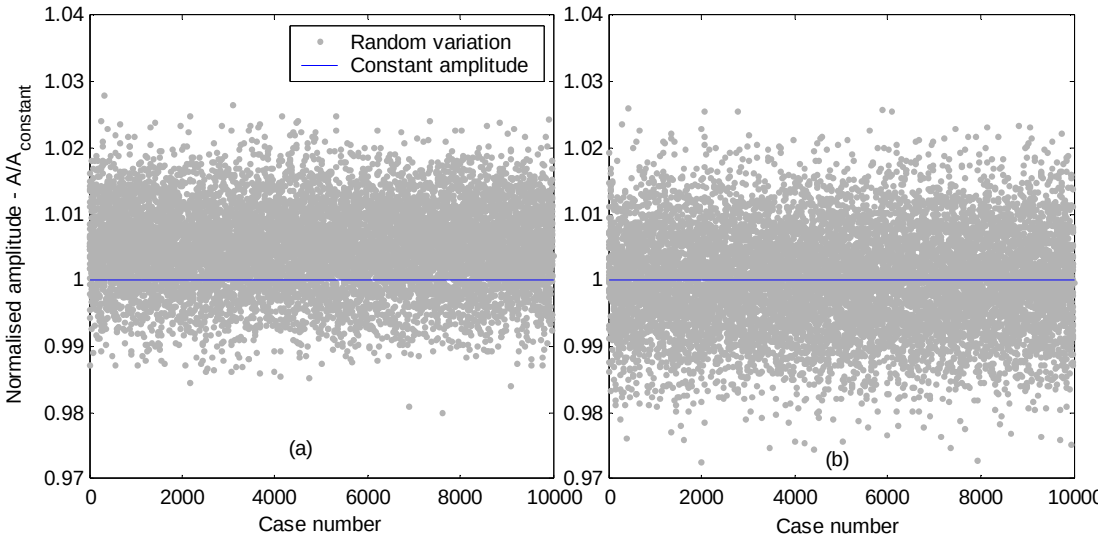

Figure 6.8 Statistical variation of maximum 9EO response amplitude due to excitation errors on the (a) tuned and (b) mistuned Blisk-1 FE model.

When blade-to-blade maximum amplitude variations or response curve comparisons at or around a given resonance are of interest, the excitation errors can be considered negligible by comparison with the uncertainties involved in the measurement system. However, for overall response curve comparisons, the variation in the force amplitudes might have a greater effect and should be remembered when assessing the correlation between predictions and measurements. Although an imperfect excitation causes several modes of a tuned system to be excited, its effects are not comparable with those of physical mistuning in any way. The latter is known to yield amplitudes which are several times larger than those of the corresponding tuned reference case. For example, the amplitudes of non-9D resonances excited in the case shown in Figure 6.7 (b-1) are much smaller than the corresponding mistuned amplitudes given in Figure 6.7 (b-2). Based on the evidence provided, the effects of excitation errors are considered insignificant and the mean value of the force was chosen for the forced response calculations of this study.

6.4.3 Mistuning errors

The effects of possible errors in the mistuning pattern (i.e. combined errors, originating from the identification process and those introduced in its modelling) on forced response levels were analysed using the discrete bladed disk model introduced in Chapter 4. This was appropriate as a qualitative indication was needed and this simple model provided computational efficiency. Here it was assumed that the overall trend of the mistuning variation was identified reasonably accurately. To this end, the mistuning pattern identified for Blisk-1 was perturbed randomly by ±10%, Figure 6.9 (a), and the variation in the maximum forced response for 6EO excitation was calculated for 10000 cases. The random variations were, again, obtained from a normal distribution. The deviations of the calculated maximum responses from the maximum response due to the original mistuning pattern are shown in Figure 6.9 (b). It is seen that the increases due to uncertainties in mistuning pattern are of the same order as those due to excitation errors. The fact that ±10% variation in the mistuning pattern caused a maximum response amplification of just 1.3% suggests that, (provided that the real error in mistuning pattern is not larger) the errors involved in the identified pattern should not have a significant effect on the correlation of the predictions and measurements.

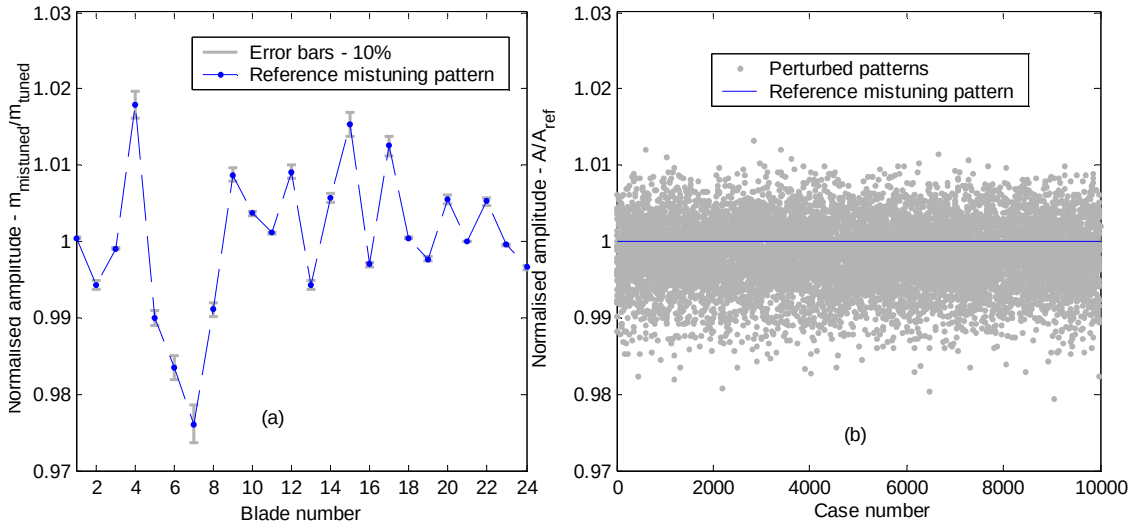

Figure 6.9 (a) Error in mistuning pattern, (b) Maximum forced response variation of a discrete bladed disk model due to errors in mistuning pattern

6.5 Undamped, rotating Blisk-1 analysis

Forced response analyses of undamped (i.e. the case of no additional damping other than material damping) Blisk-1 were particularly important for the reason that they would provide useful data to assess the suitability of the updated model prior to non-linear analyses. The mistuned forced response prediction tool was validated in Chapter 5 using measurements taken from Blisk-2. Therefore, in the case of Blisk-1, uncertainties were likely to arise due to inaccuracies in mistuning identification or in its representation, and, to an extent, due to excitation errors.

6.5.1 Comparison of overall characteristics

Similar to the Blisk-2 response measurements, the first step here was to measure the response of a particular blade over the entire speed range (i.e. 0-4000 rev/min). This, likewise, allowed the overall characteristics to be mapped out and compared with the predicted ones on a general scale, as given in Figure 6.10.

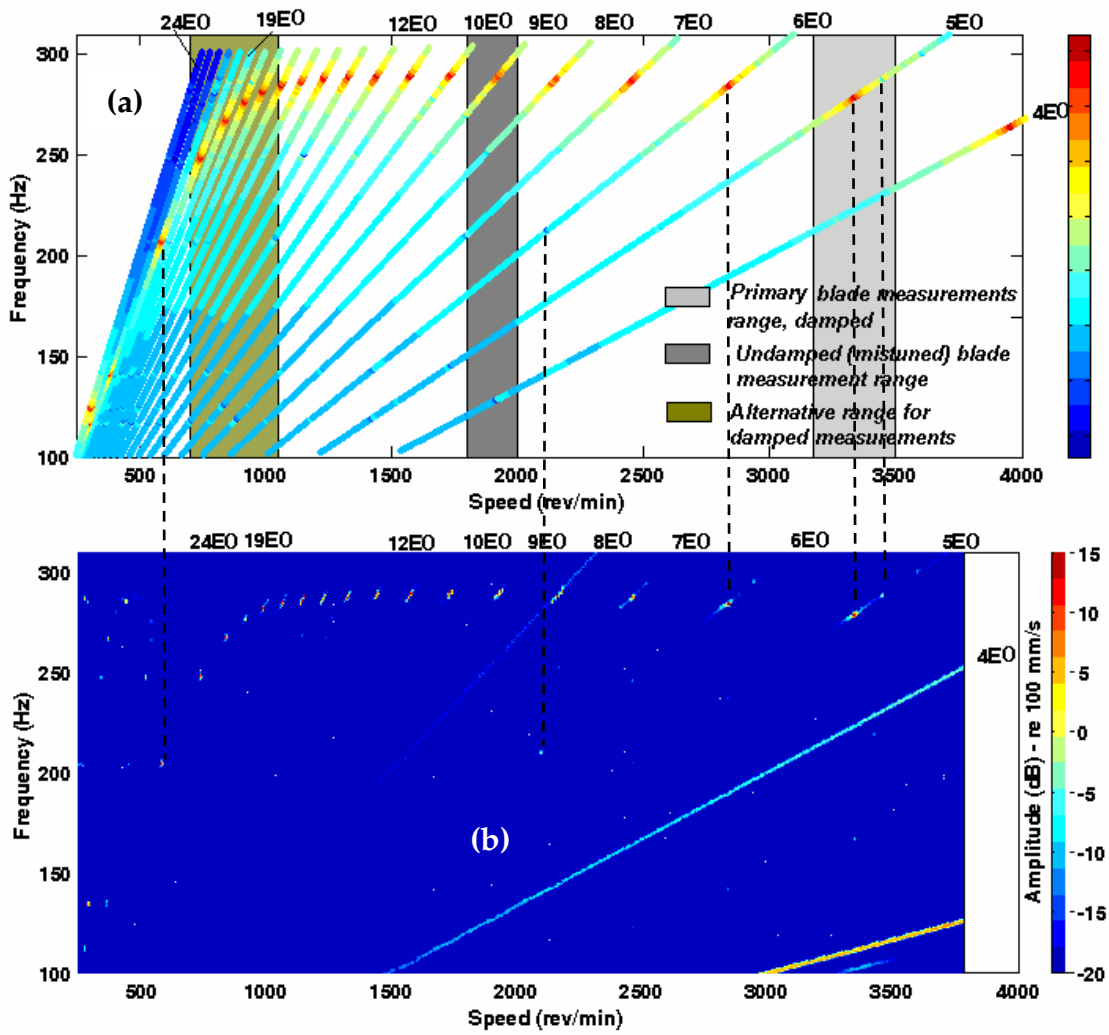

Figure 6.10 (a) Computed and (b) measured interference diagrams on blade 1 of the undamped Blisk-1

Due to the mistuned nature of Blisk-1, the *kth* EO line excited a number of modes depending on the magnitude of the *kth* harmonic in the mode shape of each. Some of the resonance spots, or groups of resonances (in general the top group of red spots contain very close many resonances), are interconnected via dashed lines, indicating a good match.

It is seen from the measured z-mod plot that the effect of misalignment between the laser beam and axis of rotation has deteriorated compared with the Blisk-2 case, as indicated by the emphasised EO lines. Most significantly, 1, 2, 4 and 8 EO responses are heavily affected. Although not on the same scale, other low EO

responses are also influenced by this effect. Individual 5, 6, 7 and 8 EO excitation responses extracted from the given z-mod plot for blade 1 are compared with the predicted ones in Figure 6.11. So far as the natural frequencies are concerned, a good correlation is obtained. The deviations are generally in line with the errors obtained for the frequencies at rest. However, some of the deviations are slightly larger than expected. This is thought to have originated from the fact that the effect of rotation has not been applied to the mistuning masses as explained in Chapter 5. As for the shapes of the response curves, the behaviour around the main resonances is well predicted in each case. However, for the lower amplitudes, the cross-talk errors introduced due to misalignment caused significant departures from the predictions.

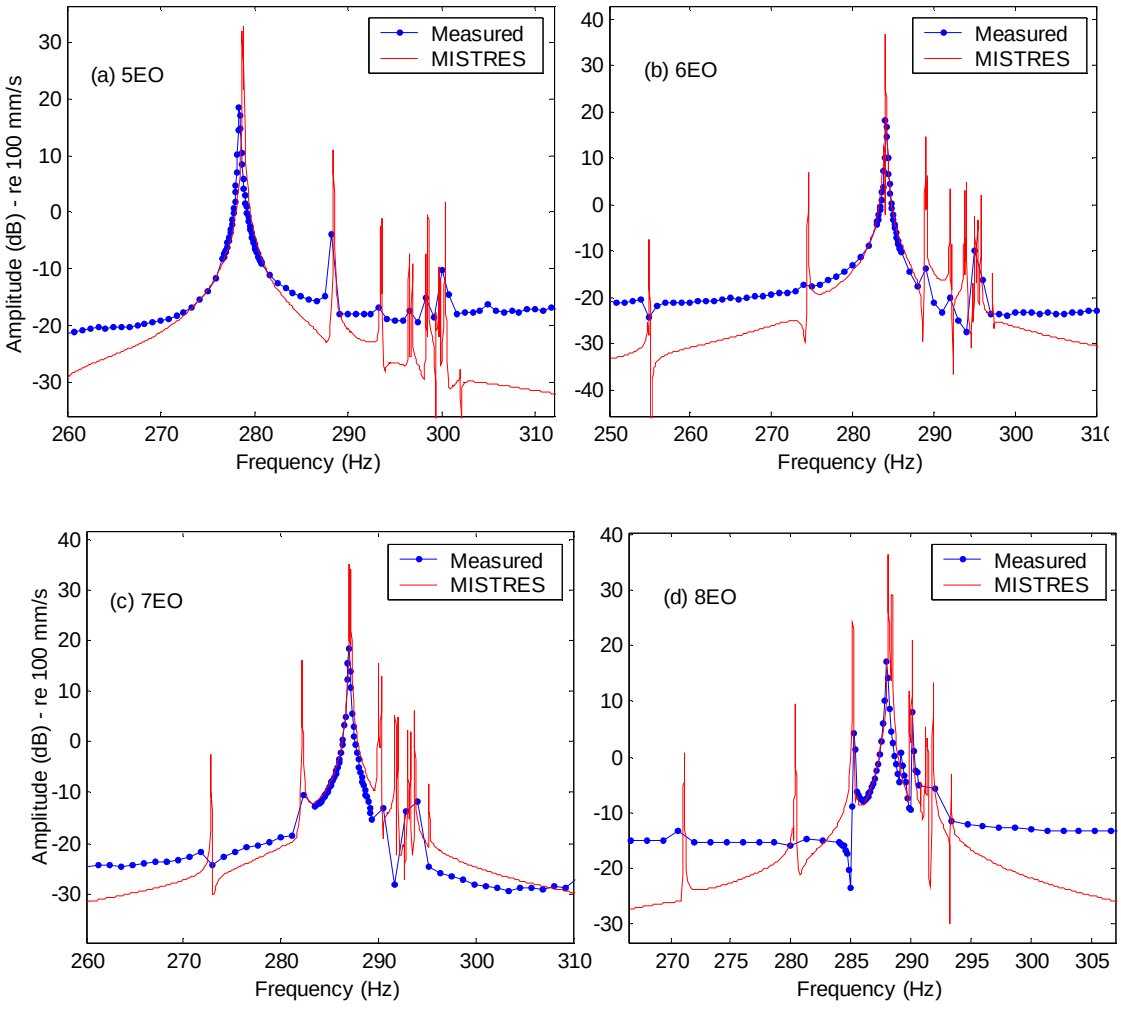

Figure 6.11 Response of blade 1 to EO excitations 5, 6, 7, and 8

The very light damping in Blisk-1 resulted in very sharp resonances peaks. Thanks to an insufficient sweep rate, some of these could not be captured. The measured amplitude and phase response curves were analysed in ICATS software to determine the structural damping. However, the obtained damping values under rotation and in vacuum were, surprisingly, significantly higher than those measured at rest, in the presence of air. It was realised that this was caused by the fact that the double ND modes were slightly split and therefore could not be accurately distinguished in the measurements. As a result, very close resonances were merged together and were processed as a single mode. Naturally, the resulting damping values were misleadingly high. Following the example of Blisk-2, and the fact that the same damping values were identified for both blisks at rest, the same damping value (i.e. 0.0075%) was chosen for Blisk-1 predictions under rotation.

6.5.2 Comparison of all blade responses

All the blades of the undamped Blisk-1 were chosen to be measured at around the 9EO-9ND resonance. This required a speed range of 1900-1950 rev/min to be covered. Despite being a very short range, it covered 9 resonances within a band of 7.5 Hz, which would provide enough data to gauge the quality of the mistuned predictions. The results of these measurements are compared to the predicted ones and given in Figure 6.12. Only the odd numbered blades are given for brevity.

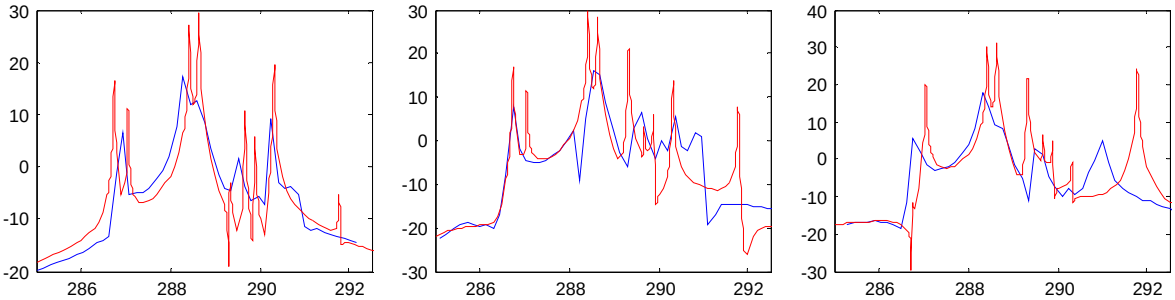

(a) Blade #1 (b) Blade #3 (c) Blade #5

(Continued over…)

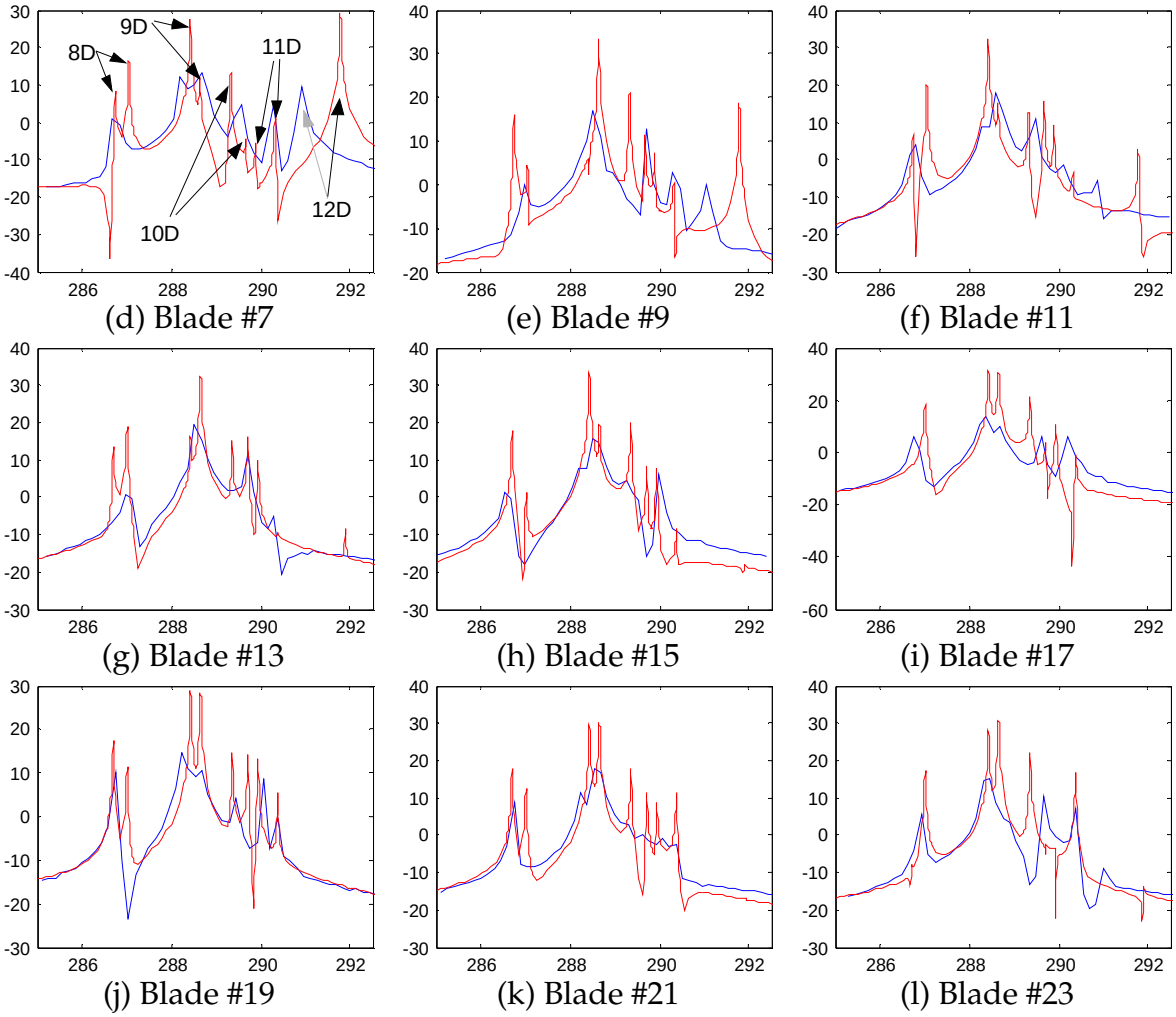

Figure 6.12 Undamped Blisk-1: Comparison of individual blade responses to 9EO excitation. —Measured, —Predicted. (x-axes: *Frequency (Hz)*, y-axes: *Amplitude (dB) – re 100 mm/s*)

Although the match between the measurements and the predictions was not as startling as the Blisk-2 results were, given the fact that a very small frequency range was considered and the knowledge that inherent mistuning was not as accurate, the overall characteristics and the general behaviour of the response curves are well predicted. The deviations in the locations of the resonances were generally around 0.1%. However, the predictions of the 12ND mode, in particular, differed by up to 0.3% from the measurements, as seen from Figure 6.12 (d). The given plots also show that the frequency splits in 8, 10 and 11ND modes were over predicted as was also evident from the inset of Figure 6.3. The actual split mode pairs corresponding to these modes were so close that they could not be measured as clearly as the 9ND mode pair. The resonance locations

obtained through measurements also showed some variability. This was probably due to changes in test conditions as the blades were, again, measured in turn, over a number of days. Thanks to the narrow frequency range, these differences are accentuated.

6.5.3 Comparison of ODSs

During the testing of Blisk-1 at rest, it was observed that the lower ND modes, although occurring in split pairs, maintained their regular sinusoidal shapes. Therefore, all blades when excited at corresponding resonances would have similar amplitudes, thus exhibiting tuned characteristics. This was also observed from the ODSs measured on the rotating blisk. Some of these measurements are compared with the predicted ones in Figure 6.13. The ODSs shown here were measured by running the rig at the corresponding resonance speeds and then measuring the blade-tip responses, either by a slow circular scan at the blade-tips or by indexing the laser beam from blade to blade. Both methods were demonstrated to have given the same results.

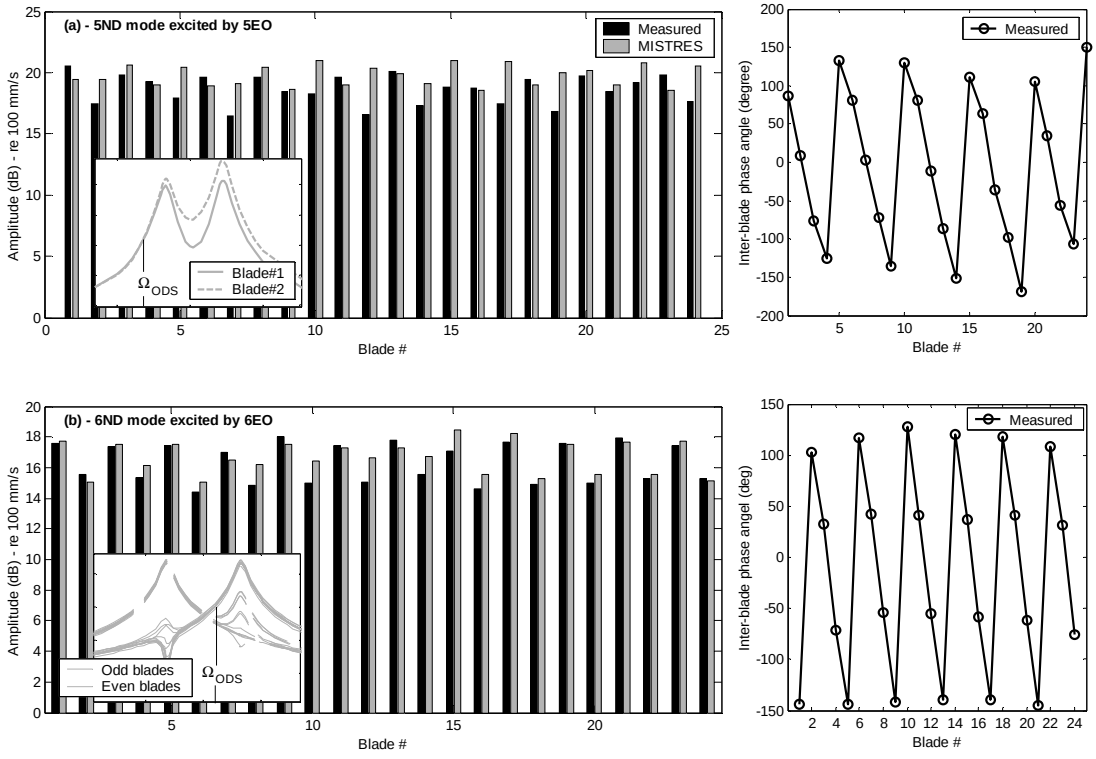

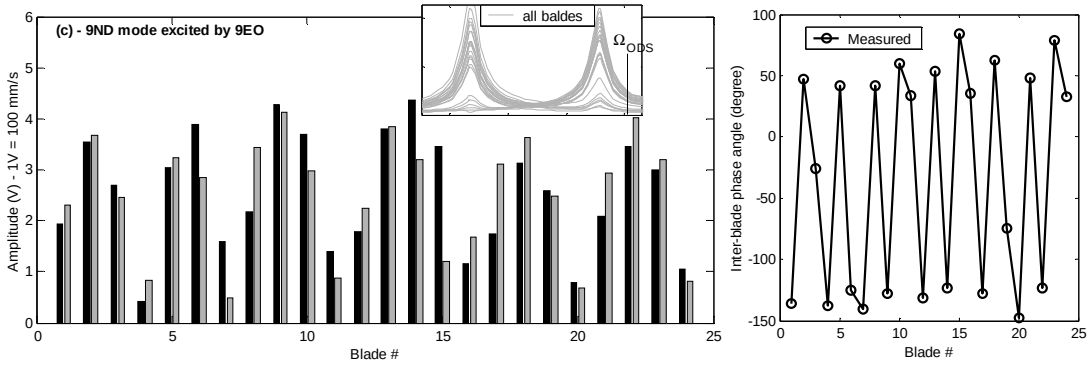

Figure 6.13 Measured and predicted ODSs for (a) 5, (b) 6, and (c) 9ND modes excited by 5, 6, and 9EOs respectively.

The frequencies at which the response amplitudes were compared in the given plots are indicated by Ω_{ODS} in the insets, which show predicted blade responses at around the corresponding ND mode pair. Inter-blade phase angle plots indicated that 5 EO and 6 EO excitations excited travelling 5 and 6 ND modes respectively, whereas 9EO excitation excited predominantly a 9ND mode with both standing and travelling wave components. Measured and predicted response patterns given in Figure 6.13 (a) and (b) correlate reasonably well. Although larger deviations in amplitude and shape are evident for the ODS corresponding to 9ND mode given in (c), in general a similar pattern is observed. As is seen from the blade amplitude variations, the 9ND mode is significantly mistuned and the errors involved in the identified mistuning and, to an extent, in its modelling, are thought to have been responsible for the deviations mentioned.

6.6 Damped, rotating Blisk-1 analyses

For the friction damped cases, Blisk-1 was fitted with Cottage-Roof (C-R) type dampers as shown in Figure 6.14. Two sets of C-R dampers, one made of steel and another from a titanium alloy were manufactured to provide a range of damper masses. The variation of individual damper masses for both sets is given in Table 6.1.

The C-R dampers are intended to reduce resonant vibration by energy dissipation via the rubbing of contact surfaces of the blisk and dampers. The contact is achieved through centrifugal force. In the case of both excitation and response amplitudes being low, the dampers will lock up and will not operate. Since, in such a situation, there is no relative motion between the dampers and the blisk, the individual blades will be coupled through the dampers, leading to substantial increases in the natural frequencies and producing little if any damping. Realistic reduction of resonance amplitudes via friction damping will be achieved if this threshold is exceeded. The threshold depends on the ratio of the excitation forces to the damper loading (centrifugal) forces, the latter being proportional to the damper mass and the square of the rotational speed. At higher amplitudes, the energy dissipation does not rise in proportion to the blisk's vibration energy, and the effective damping decreases again. The effectiveness of the dampers therefore depends, amongst other factors, on the rotational speed of the rotors, the damper masses and the strength of the exciting force. The latter two can be adjusted to make the dampers work in the speed range of interest. However, the forcing magnitude can not be increased indefinitely because of the danger of producing a fatigue failure in the test blisk.

Figure 6.14 (a) a C-R damper, and (b) its installation in Blisk-1

Blade #	Steel damper	Ti damper	Blade insert (x2)	Total –St*	Total-Ti*
1	4.57	2.58	22.73	27.82	25.83
2	4.58	2.57	22.56	27.66	25.65
3	4.56	2.57	22.61	27.69	25.7
4	4.55	2.57	22.62	27.69	25.71
5	4.54	2.57	22.63	27.69	25.72
6	4.56	2.57	22.55	27.63	25.64

7	4.58	2.58	22.66	27.76	25.76
8	4.58	2.58	22.64	27.74	25.74
9	4.56	2.57	22.63	27.71	25.72
10	4.54	2.58	22.64	27.7	25.74
11	4.51	2.57	22.95	27.98	26.04
12	4.55	2.57	22.63	27.7	25.72
13	4.57	2.58	22.62	27.71	25.72
14	4.51	2.56	22.6	27.63	25.68
15	4.55	2.58	22.64	27.71	25.74
16	4.60	2.55	22.63	27.75	25.7
17	4.55	2.58	22.56	27.63	25.66
18	4.59	2.54	22.63	27.74	25.69
19	4.56	2.56	22.64	27.72	25.72
20	4.58	2.57	22.61	27.71	25.7
21	4.61	2.56	22.64	27.77	25.72
22	4.58	2.54	22.61	27.71	25.67
23	4.68	2.56	22.60	27.8	25.68
24	4.60	2.57	22.64	27.76	25.73
Min	4.51	2.54	22.55	27.63	25.64
Max	4.68	2.58	22.95	27.98	26.04
St. Dev.	0.034	0.012	0.075	0.073	0.078
Mean	4.57	2.56	22.64	27.73	25.72

Table 6.1 Blade inserts and C-R damper masses (*: Total includes 4 retaining screws, each weighing 0.13g)

The structure of this chapter is different from that of Chapter 5 in the presentation of measurements and predictions. Here it was found more appropriate to summarise the results of the measurements first, and then to use only a selected and representative subset of them to correlate with predictions. This provides clarity at the expense of some repetition.

6.6.1 Modelling of friction dampers

Figure 6.15 shows the way the friction dampers are modelled. The forced response analyses for the whole blisk were to be performed using a cyclic sector. In this, adjacent blades were connected through friction interface elements, as shown in the figure, and cyclic boundary conditions at the disk interfaces. Friction contact surfaces were defined through the application of several friction contact elements, at nodes distributed on these faces as shown by the green points (more nodes than the ones shown were used but are not included for clarity).

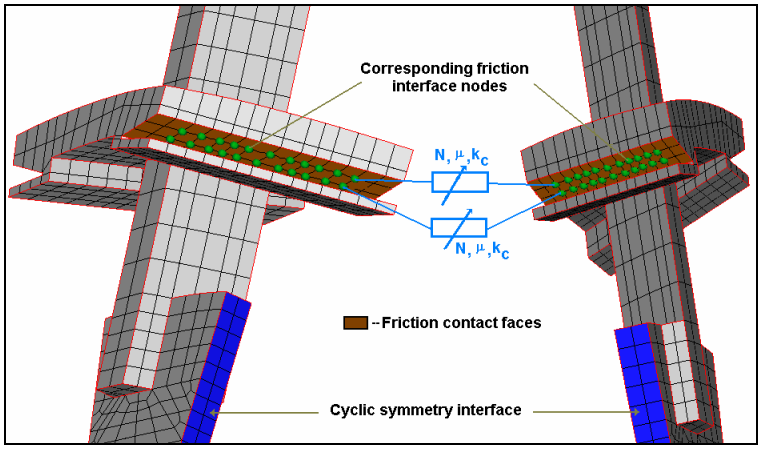

Figure 6.15 FE modelling of friction interfaces

Based on earlier tests performed at Imperial College on the same titanium alloy the coefficient of friction was taken as 0.45. The contact stiffness used in the calculations was determined by FE analysis. This was simply done by fixing a C-R damper at one of its contact faces and by applying uniform forces on the other, in horizontal and vertical directions in turn. Then the contact stiffnesses in these directions were calculated by dividing the mean displacement on the free surface by the applied total force.

6.6.2 Preliminary tests on Blisk-1 with C-R dampers

6.6.2.1 Tests with steel dampers

As stated in the test design stage, the design of friction dampers and their subsequent test plan was somewhat less certain so that some preliminary investigations were needed to identify the characteristics of the blisk with fitted dampers under rotation. The first rotating tests were carried out with steel C-R dampers, using a single magnet, rated at 245N maximum pull force (on iron, with no air gap). The centrifugal force was enough to lift off these dampers at rotor speeds above 200 rev/min. Vibration measurements indicated that the dampers did not operate above 600 rev/min as they were too heavy and locked up. Figure 6.16 (a) and (b) show two z-mod plots measured on blade 1 of the un-damped and damped Blisk-1, respectively. EO response curves extracted from

given z-mod plots showed that at lower speeds (400<Ω<600 rev/min) sharp resonances indicated by bright spots in (a) were significantly wider in (b), indicating successful operation of the dampers. However, at higher speeds no sign of resonances is seen on the damped plot. Various attempts made at increasing the magnetic force, by bringing the magnet closer to the blisk, failed to increase the operating speed range beyond 700 rev/min. At this stage it was decided to abandon the use of steel dampers and all the attention was directed to the lower-mass, titanium dampers.

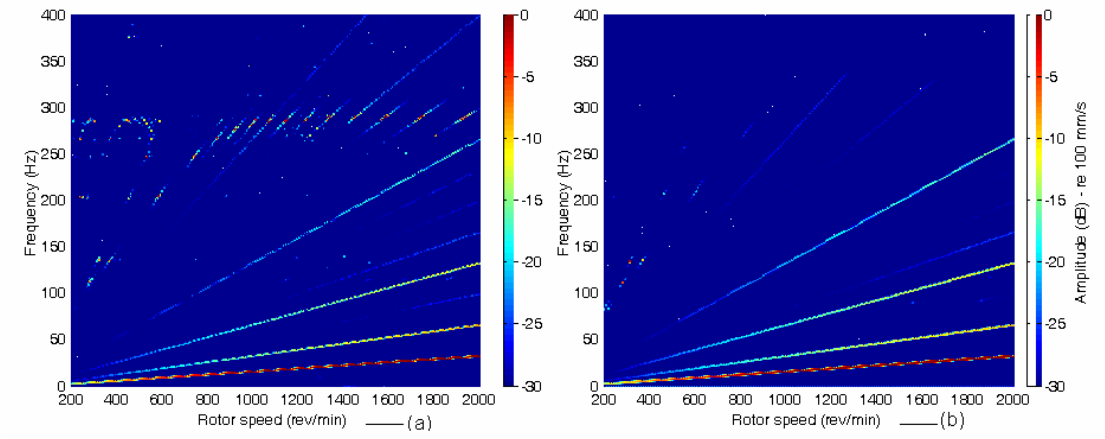

Figure 6.16 (a) Undamped and (b) Steel C-R damper fitted Blisk-1 z-mod plots

6.6.2.2 Tests with titanium dampers

Initial tests using titanium dampers and the same magnet as used in the steel damper tests, again failed to produce enough force for the dampers to work realistically. Several options were considered to make the titanium dampers work effectively: (i) to increase the magnetic force (either by using a more powerful magnet or by employing several magnets at the same time), (ii) to make the dampers lighter by removing some metal or (iii) to have new dampers made. The first option was the least complicated, least costly and involved the shortest time-scale. For this purpose a larger magnet, capable of producing a 4 times bigger pull, was purchased. This was able to exert forces of up to 20 N at the smallest safe magnet-to-blade gap. However, even with this increase, it was not possible to produce damper slip beyond about 1300 rev/min. The excitation

force was further increased by employing two magnets of the same size located diametrically at 180 degrees around the blisk. The result of this application is shown on a z-mod plot given Figure 6.17. Note that an excitation of this type will produce only even numbered EO excitations and suppress the odd ones, as is clearly seen from the given plot. In this arrangement the dampers worked more effectively, however, the operating range could not be extended to cause them to work at higher speeds so as to excite the reasonably tuned 5ND mode, as was originally chosen to be measured for damped analyses. Increasing the excitation force even further through installation of more magnets, as mentioned, would have brought about the risk of fatigue failure and therefore was not opted for.

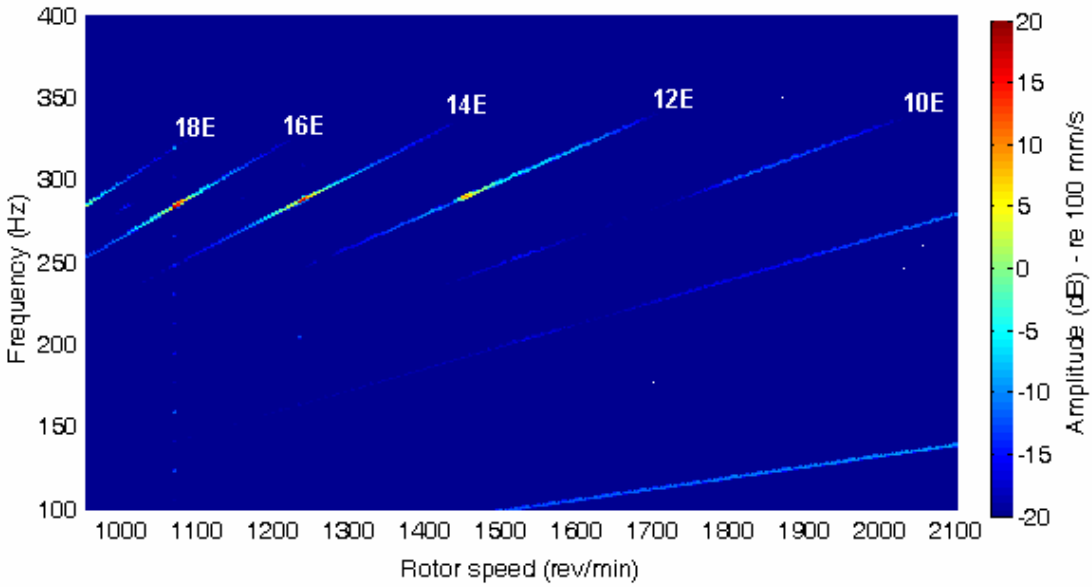

Figure 6.17 Ti C-R damper fitted Blisk-1 excited with 2 magnets

6.6.3 Measurements on Blisk-1 with C-R dampers

At the end of the preliminary investigation, it was decided to go back to the single magnet arrangement and to concentrate on the alternative damped measurements speed range identified in the test planning phase. Attention was directed, primarily, at a speed range of 700-1050 rev/min. This covered 17, 18, 19 and 20 EO lines, exciting 7, 6, 5 and 4 ND modes, respectively. The speed range could have been extended to include the 16 and 15 EO line crossings, to excite 8

and 9 ND modes, but inclusion of these would have brought additional uncertainties concerning mistuning, as these modes were significantly mistuned.

6.6.3.1 Predictions of undamped Blisk-1 response to 17-19EOs

The results of a measurement session conducted on blade 1 of un-damped Blisk-1 excited by 19 and 17 EOs are given in Figure 6.18 (a) and (b) respectively. Also given in these plots are the corresponding predictions for the tuned and mistuned Blisk-1. These results reveal several important features. First of all, a very good match is obtained between the measured and predicted response levels. Particularly for the excited main modes, the resonance frequency and the response levels are well correlated. Secondly, apart from the sharp spikes corresponding to other modes excited due to mistuning, the tuned and mistuned responses for 5ND-19EO given in (a), and particularly around the main resonance, are very similar. This finding proves that the errors in identified mistuning pattern will not be a source of uncertainty in the comparisons of damped Blisk-1 analyses in the close proximity of this resonance. The same can be said, to an extent, for the 7ND-17EO resonance given in (b). However, as the mistuned and tuned responses differ reasonably at a closer proximity of the main resonance, inclusion of mistuning for the corresponding damped predictions might yield better correlation. Another important observation from the given plots concerns the effect of misalignment of the laser beam with the axis of rotation. As mentioned, 5 and 19, and 7 and 17 EO excitations excite the same modes only at different speeds. Therefore, in theory, apart from the shift in the frequency axis due to the higher rotational speed and assuming that no significant change occurs in the mode shapes, the results given in Figure 6.11 (a) and (c) should be identical to those given in Figure 6.18 (Note that due to the steeper slope of the 19 and 17 EO lines, the frequency resolution corresponding to these curves is coarser, thus, some of the resonances are not captured in as much detail as in Figure 6.11, or are missed completely). The fact that 19 and 17 EO responses correlate much better with predictions than the 5 and 7 EO

responses given in Figure 6.11, proves that the inferior quality of match in those cases was mainly due to magnified effects of misalignment at high speeds rather than poor predictions.

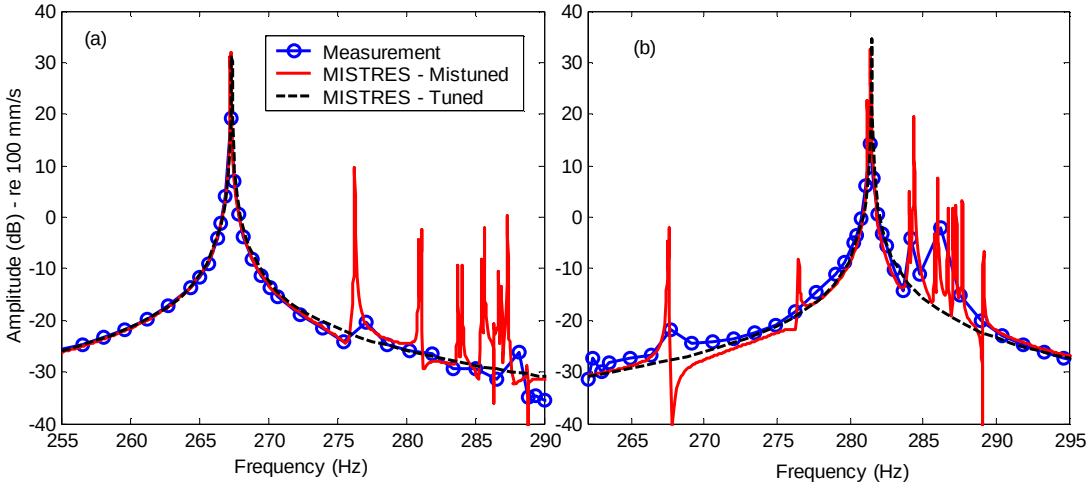

Figure 6.18 Blisk-1 –Response of blade 1 to (a) 19EO, and (b) 17EO excitations

6.6.3.2 Damped z-mod measurements

Some preliminary tests were carried out on blade #1 to obtain the overall dynamic characteristics of the blisk with fitted Ti C-R dampers. The z-plot measured is given in Figure 6.19. The bright spots, which correspond to apparent natural frequencies, indicate that the C-R dampers have not produced a large change. Examining the z-plot in detail, three groups of modes may be distinguished, (i) those excited by 20 EO and above, in which the damper forces are too small to produce significant damping, (ii) those excited by between 19 and 12 EOs, which appear to be 'spread', signifying that there is significant damping, and (iii) those excited by 13 EO and above, which have apparently disappeared from the C-R-damped z-mod picture because the dampers have 'locked up', shifting the natural frequencies out of the measured range. Strong EO lines in the z-mod picture at 4 and 8EO are probably due to misalignment in the LDV measurement laser beam, rather than to true vibration.

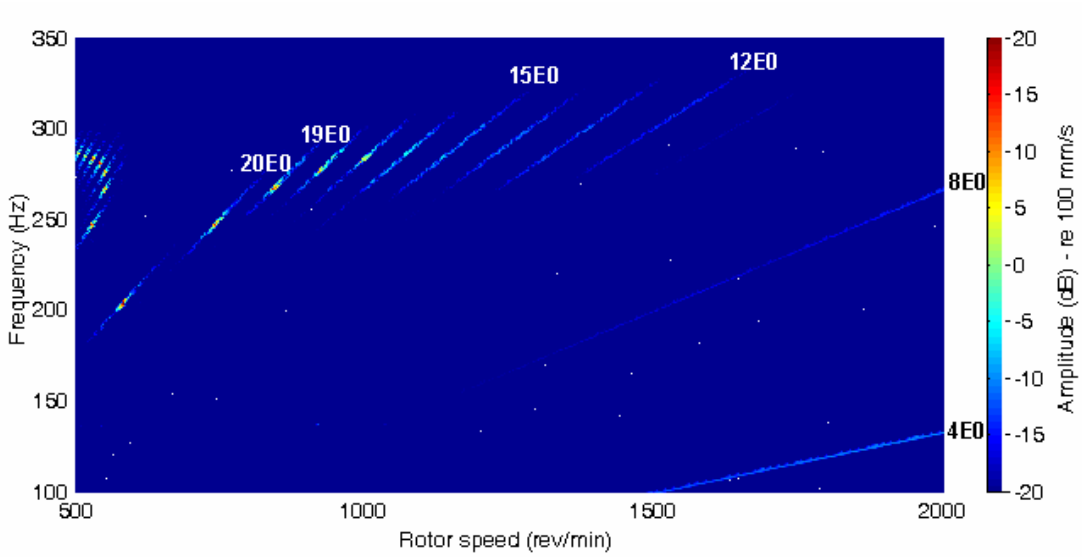

Figure 6.19 Ti C-R damper fitted Blisk-1 excited by a single magnet

6.6.3.3 Damped individual blade measurements

In order to assess the repeatability of the tests, the response of blade # 1 was measured several times, within the speed range of interest, 800-1050 rev/min. There was close agreement between the repeated response curves and it was decided to measure all blades, so that variation in blade-to-blade response could be determined. Measured 19, 18 and 17 EO amplitude response curves, blade-to-blade maximum response variations at resonances together with corresponding inter-blade phase angles are given in Figure 6.20 (a1-a3), (b1-b3) and (c1-c3), respectively. Circumferential ODSs corresponding to these (19EO-5ND, 18EO-6ND , and 17EO-7ND) resonances were also measured and are overlaid with the amplitude variations extracted from given response curves in (a-2), (b-2) and (c-2) respectively.

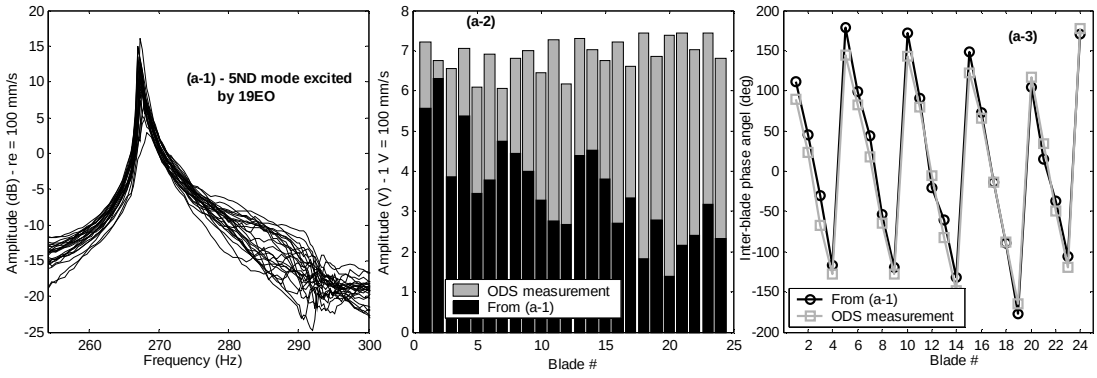

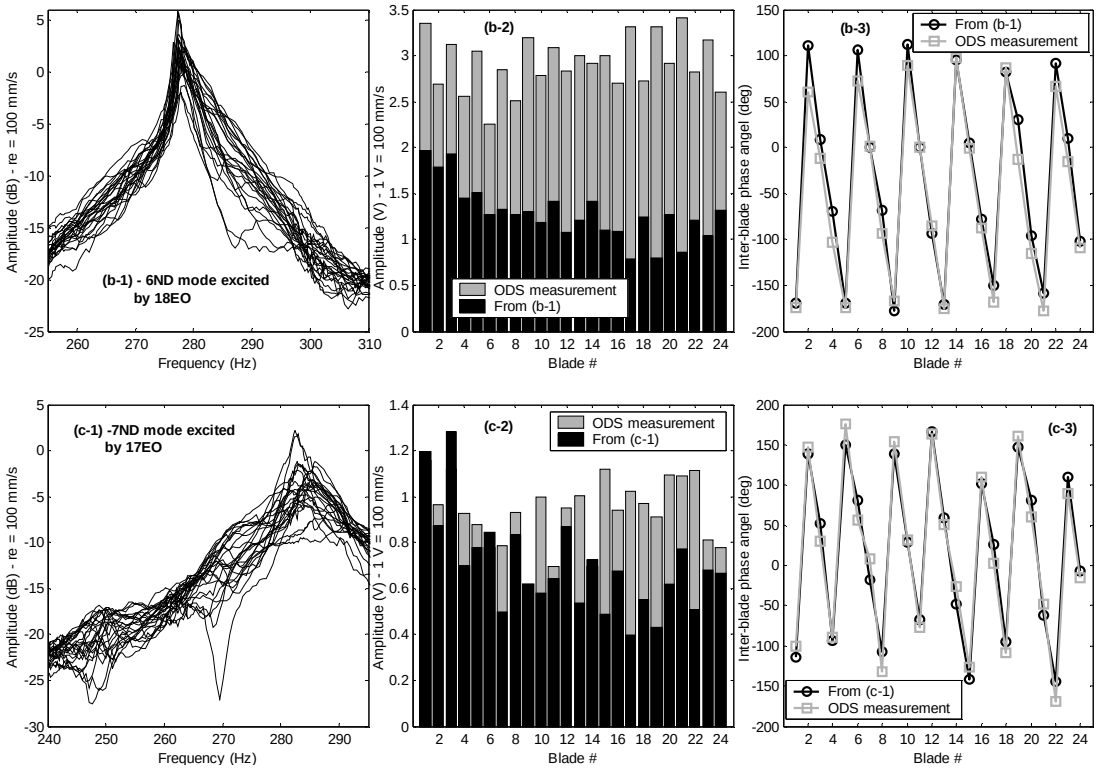

Figure 6.20. Response of Blisk-1 fitted with Ti C-R dampers excited by (a) 19, (b) 18, and (c) 17 EOs

The response curves shown in the above figure exhibit reasonable consistency, with all individual measurements (i.e. each corresponding to a blade) showing similar behaviour and yielding coherent resonance frequencies. However, the comparison of blade-to-blade amplitude variations obtained from ODS measurements and taken from measured response curves indicated a poor correlation. Although not steady, a general trend of decline in amplitudes is observed in the latter one. On the other hand, the inter-blade phase angles in both cases were in good agreement, indicating that travelling waves were excited in the blisk for all these resonances. Some of the blades were re-measured after the given set of blade measurements was completed and large variations in amplitudes from run to run were observed. To locate the source of their inconsistency, the response of blade 1 at the 19EO-5ND resonance was recorded over 20 minutes of continuous rig running and is given in Figure 6.21 (a). Despite a clear steady-state value, the vibration response presented jumps at random intervals. Thus, depending on the initial conditions, any amplitude from

2 to 5.5 V could be acquired for the given speed value. After the elimination of magnitude amplification due to misalignment, the true 19EO response amplitude for this particular measurement varied from 1.2 to 3.5 V, which presented a considerable change from the initial amplitudes of 5.5 to 7 V measured for this blade. Here it must be noted that the abscissae in Figure 6.20 (a-2), (b-2) and, (c-2) represent time as well as blade number (for the data shown in black), as the blades were measured consecutively. In fact, further investigation showed that the conditions at the damper-insert interface were changing with the time of running. Close inspection of dampers and blade inserts, after shutting down, revealed fretting debris over part of the damper contact surfaces. Some of the dampers were jammed in one side and thus unable to operate, possibly because of fretting debris which had accumulated between the contacting surfaces of inserts and dampers. This situation worsened as the operation of the rig continued, resulting in big discrepancies between blade response curves. Some photographs of the dampers after shutting down are given in Figure 6.21 (b) and (c).

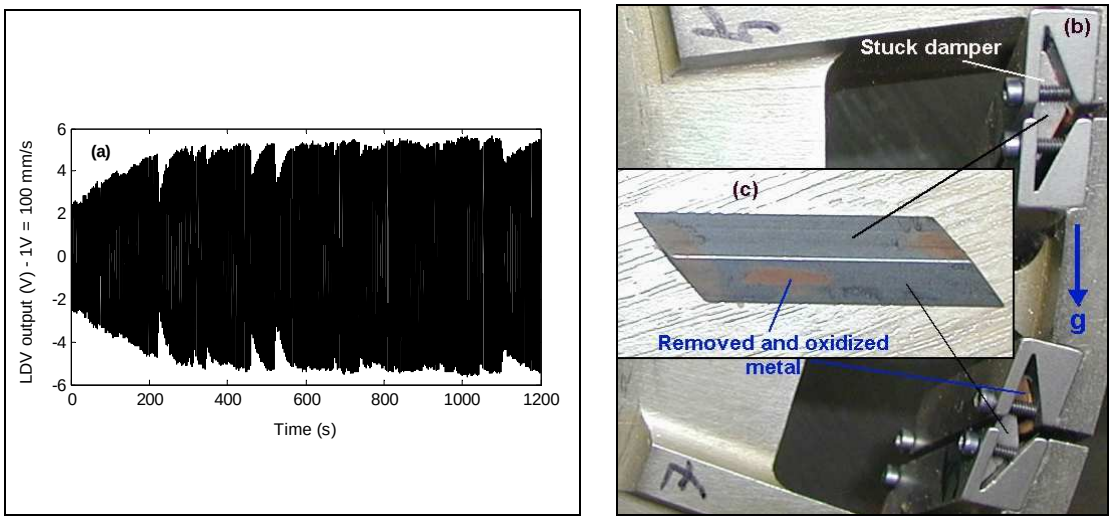

Figure 6.21 (a) Blade 1 tip response @ 19EO-5ND resonance, (b) a jammed damper, and (c) a damper surface after shutting down.

Inspection of used and unused damper contact surfaces under the microscope revealed no significant differences in surface characteristics. As mentioned, the

blade inserts accommodating the dampers were made of steel. It is believed that during the operation of the rig, when in contact, relatively soft titanium dampers were taking asperities off the harder steel surfaces of the inserts. This so-called "bedding-in" period continued until smooth insert surfaces were obtained, at the cost of the presented variability in response measurements.

6.6.3.4 Measurements with cleaned dampers

In an attempt to improve the consistency of the response amplitudes, the dampers were taken out and both steel insert and damper surfaces were cleaned thoroughly. Figure 6.22 (a), (b), and (c) show measurements taken from the first 4 blades after the dampers were re-installed. Likewise, the response curves presented similar behaviour. Note that the amplitudes measured here are slightly higher than those presented earlier. This is because the results given in Figure 6.22 were measured straight after the cleaning, while, the ones given in Figure 6.20 were measured after z-mod plot measurements were completed (i.e. several hours of rig running). Nevertheless, the amplitudes again varied as the rig running time increased. Inspection of dampers once again showed accumulation of debris (though not on the initial scale) that the cleaning operation had to be repeated. This was probably caused by the fact that attention was not paid to make sure that the original damper orientations were respected (i.e. some of them were rotated by 180° with respect to a normal in radial direction), though they were put back in between the same two blades. This is thought to have initiated a new bedding period, hence the variation in response characteristic. Larger discrepancies in (c) were probably due in-part to the mistuned nature of this mode, as well as the changes in damping effects.

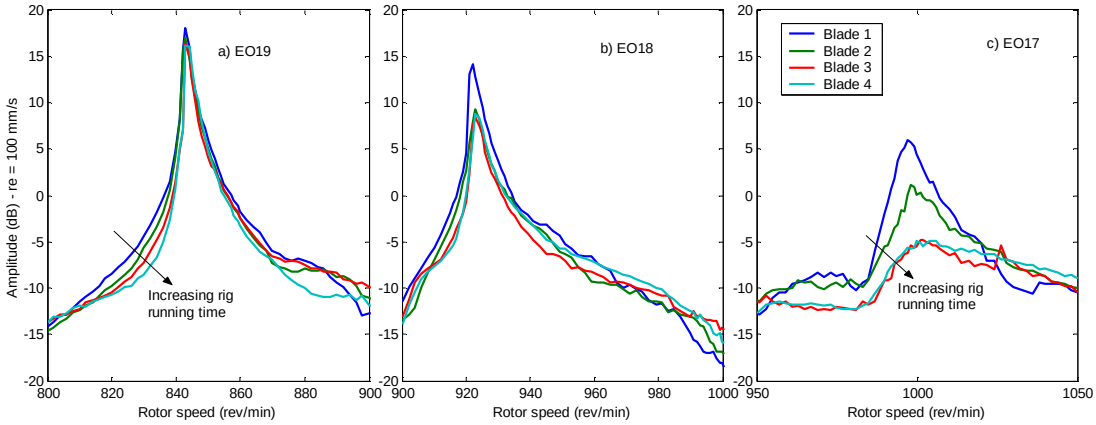

Figure 6.22 Responses of first 4 blades to EOs 19, 18 and 17 after the first cleaning of dampers and inserts

The cleaning of dampers and inserts had to be repeated 2 more times, bringing the number of installations to four. However, for the last two installations the dampers were put back in the way they were removed for cleaning. Response curves obtained after the 3rd installation were also very similar to those given for the initial and 2nd installations. The rig with the third installation was operated until consistent results were obtained. Then, the rig was stopped and the dampers were cleaned for one last time. For the measurements of the last installation, the speed range of interest was limited to an even shorter interval in an attempt to finalise measurements quickly, knowing that same/similar conditions were attained for all blade measurements. It was decided to use 800-950 rev/min speed range, which covered 19EO-5ND resonance only.

Responses of all blades to 19EO excitation, measured after the last installation of the dampers, are given in Figure 6.23 (a), maximum amplitude variation in (b) and inter-blade phase angles in (c). Here again, a travelling wave is excited and all blades exhibit the same behaviour with a more uniform amplitude variation than was observed in the previous installations. However, the response curves are significantly different from those of the first 3 installations, both in terms of amplitudes and shape characteristics.

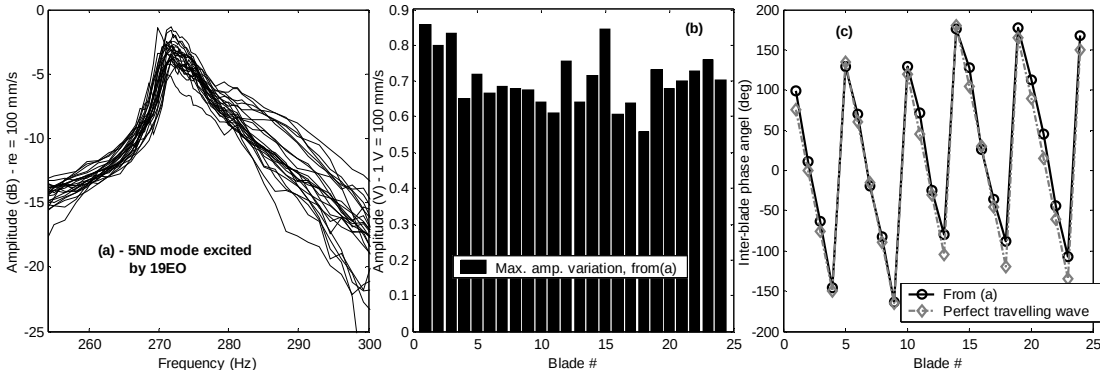

Figure 6.23 (a) 19EO response of all blades after 4th and last installation of dampers; (b) maximum amplitude, and (c) inter-blade phase angle variation.

6.6.3.5 Comparison of measurements of different installations

In order to reveal the extent of the departure in dynamic behaviour of the dampers in the last installation from that of the previous three, the responses of blade 1 to 19EO excitations for all installations are overlaid and given in Figure 6.24 (a). Also shown in this figure is the corresponding undamped response curve for the same blade. Despite the good correlation of the first three installations, the fourth one presents a substantial shift in the resonance frequency with much reduced amplitudes. Bearing in mind that the normal load (i.e. the centrifugal force acting on the dampers) and excitation forces were kept the same in all installations, the deviation can probably be attributed to a substantial change in the surface characteristics of the dampers. This might have been incurred during the process of cleaning as well as a result of the bedding period, so as to increase the friction damping and contact stiffness, thus resulting in lower amplitudes and a higher resonance frequency. However, to the best knowledge of the author, no particular action during the cleaning was taken to yield such a drastic change. Close inspection of the dampers after the tests with the final installation, once again, revealed the formation of brown patches on the damper surfaces resulting from the accumulation of debris. When compared with the undamped response curve, the first three installations yielded the same natural frequency. This was because the vibration amplitudes were higher in these installations so that the dampers were further away from the stuck

condition. Thus, although the damping in the system was increased, no additional stiffness was provided by the dampers. However, in the case of the 4th installation, the dampers were much closer to the stuck condition, and as a result they increased the stiffness of the system as well as the damping.

Short samples of time histories of the first 6 blades are given in Figure 6.24 (b) and (c), and these were measured after the first and last installations of the dampers, respectively. The lower frequency oscillations are due to laser beam-rotation axis misalignment. The fact that each blade received the magnetic force at a slightly later time was perfectly manifested by the given time histories, which exhibited larger amplitudes at magnet passing times. Although the blisk as whole was excited at all times, enough damping was produced that the vibrations on a particular blade were much reduced (in some cases completely damped out) by the next magnet passing time. However, in the close proximity of the shown resonance peak, the first three installations showed no clear sign of decay in vibration amplitudes.

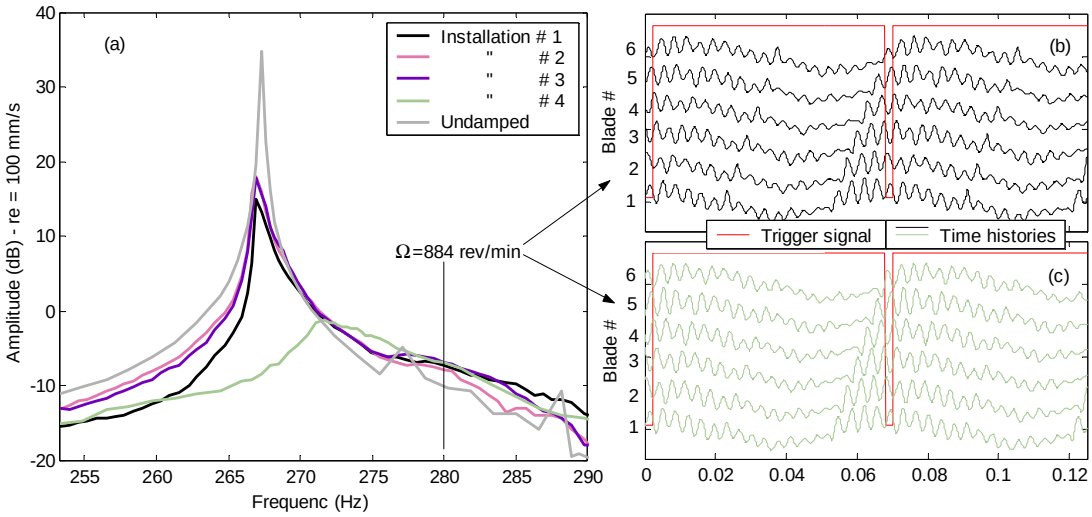

Figure 6.24 (a) Response of blade 1 to 19EO excitation for all installations, and time histories @ 884 rev min for (b) installation 1 and (c) installation 4.

6.6.3.6 Variation of response with amplitude of excitation force

Additional measurements were performed for the last installation in the 700-800 rev/min speed range, covering the 20EO-4ND mode resonance. The responses of the first 5 blades in the speed range (to check the consistency) and the circumferential ODS at the mentioned resonance were measured. Corresponding results of the latter are given in Figure 6.25 (a) and (b). The inter-blade phase angles at the identified resonance are also given in (c).

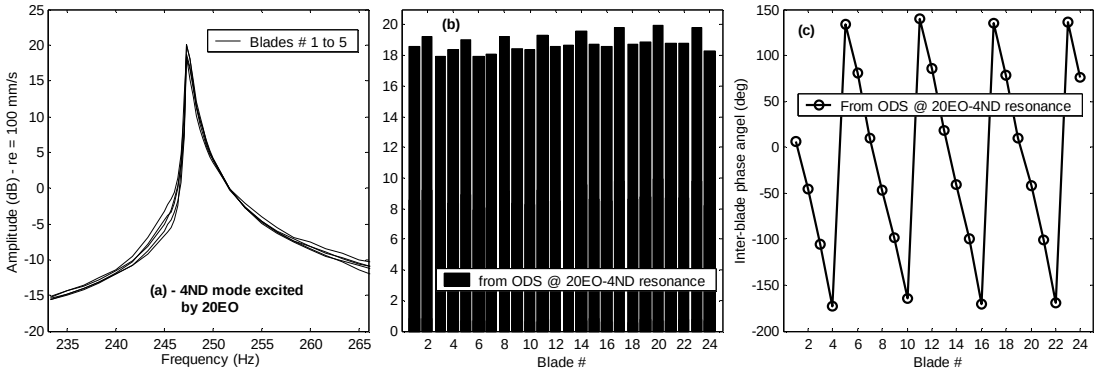

Figure 6.25 (a) Response of first 5 blades to EO20 excitation, (b) blade-to-blade amplitude variation, and (c) inter-blade phase angles @ the resonance speed.

The main goal in this last set of measurements was to measure the response of a particular blade for various magnet-blade gaps, and to observe the changes in the response characteristics as a result of different excitation levels. Figure 6.26 (a) shows the variation of the peak-to-peak amplitude of the force signal with rotational speed for 4 different magnet-blade distances. The corresponding response curves are given in (b). The black curve in (a) reveals significant force magnitude modulation around the resonance. This is because around resonance standing-wave vibration (i.e. travelling wave excitation excites a standing wave, fixed in space) causes a change in the gap between the magnet and the blades which, with a close clearance as in the black curve in (a), affected the force level considerably. As the clearance was increased, this effect became negligible.

It is clearly seen from Figure 6.26 (b) that the damping and apparent natural frequency increased with a decrease in the magnetic (excitation) force, as the dampers moved closer to the 'stuck' condition.

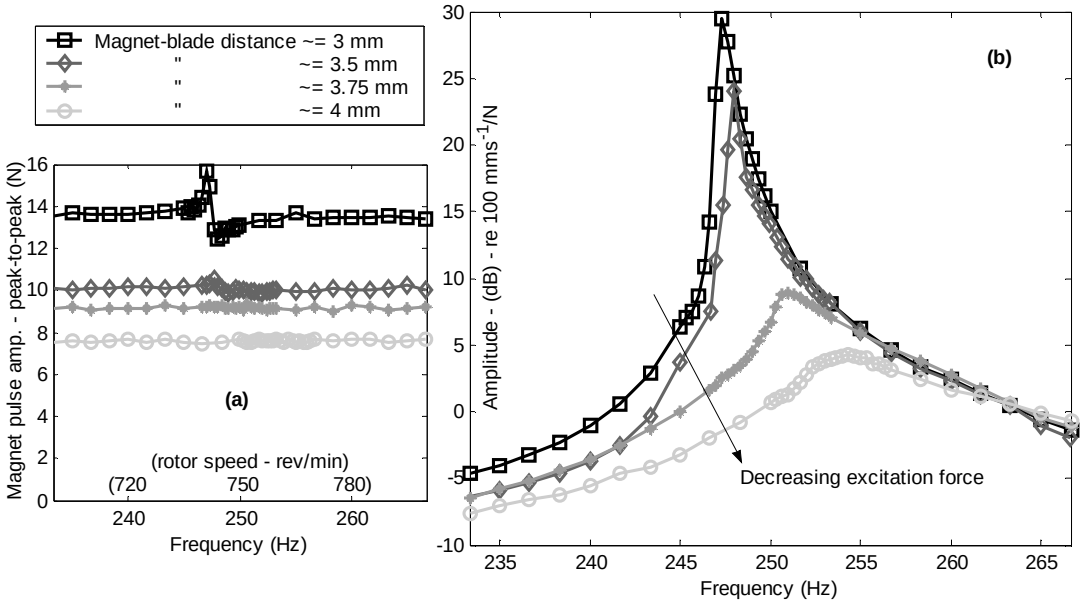

Figure 6.26 (a) variation of force signal amplitude with rotational speed, (b) response of blade 1 to EO20 excitation at various blade-magnet distances

6.6.4 Validation of damped forced response predictions

6.6.4.1 Strategy of validation process

Validation of the damped vibration response predictions was carried out by using a subset of the experimental results as presented in previous section. Owing to the variability observed in measured response characteristics between different installations, the predicted results were compared with all installations whenever the corresponding experimental data were available. These variations also necessitated that a range of contact parameter values be used in order to capture the true behaviour at different stages of the test campaign (i.e. different installations).

It was observed that the first 3 installations exhibited similar dynamic behaviour which was different from that of the last installation. In order to help explain this variation, the predictions were repeated for different contact parameter values. The results showed that the damped blisk response was insensitive to contact stiffness variations. On the other hand, the normal load and the coefficient of friction were found to be significantly affecting the response characteristics. Since the normal load was known accurately (i.e. centrifugal load acting on dampers of known masses), the observed variation between the different installations was likely to be caused by variation in the friction coefficient. The predictions were carried out first for a friction coefficient of 0.45. This figure, as mentioned, was measured earlier for the titanium alloy used and was expected to yield close predictions for the results of the first 3 installations. The preliminary predictions showed that varying the coefficient of friction from 0.45 to 0.6 allowed the variability observed in the vibration response measured to be covered. Therefore, additional predictions were performed by using a coefficient of friction of 0.6 to explain the results measured for the last installation. In following sub-sections, first the predictions obtained by using μ=0.45 (i.e. simulating the first 3 installations) are presented and then they are repeated for μ=0.6 (i.e. simulating the measurements of the last installation). In both cases, the measurement results obtained from all installations are included in the plots for the sake of comparison.

6.6.4.2 Predictions of the first 3 installations – 19EO excitation

As presented in the previous section, the main effort was directed to the measurement of the 19EO-5ND resonance though 17, 18, and, in some cases, 20 EO excitations were also considered. The 19EO response of blade 1 for all 4 installations is compared to the corresponding predictions (μ=0.45) in Figure 6.27. The predictions were repeated for two cases where mono- and multi-harmonic forcing was considered. The results of both analyses are shown in the figure. In the case of multi-harmonic force, 5 harmonics (17 to 21) were

considered. Additionally, although the normal load was taken as constant (normal load at the rotor speed exciting the 19EO-5ND resonance was applied for the frequency range used), in the mono-harmonic force case, its variation with rotational speed was taken into consideration for the multi-harmonic case. It was shown during the presentation of undamped results in this chapter (Section 6.6.2) that, in the close proximity of resonances corresponding to lower ND 1F family of modes, the response curves of the tuned and mistuned system were practically the same (see Figure 6.18). Therefore, for the computations of non-linear response of 17-20 EO excitations, the mistuning in the blisk was not taken into account. For the case of 17EO excitation, the response curves were compared for a speed range in which the undamped-tuned and -mistuned blisk responses were reasonably close, see Figure 6.18 (b).

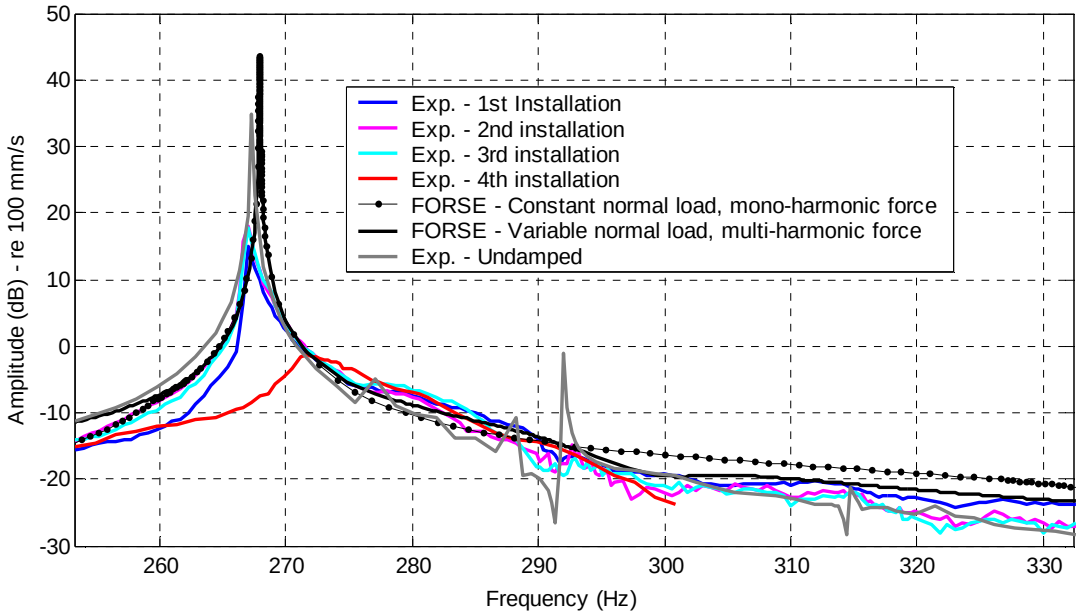

Figure 6.27 Comparison of measured and computed damped Blisk-1 response on blade # 1 to 19EO excitation; μ =0.45

It is clearly seen from the figure that the predictions correlate much better with the first 3 installations than the last one. The apparent natural frequency of the damped system obtained from the first 3 installations and the predictions was almost the same as that of the undamped system. (Note that the undamped curve given in the figure was obtained by amplitude-scaling of the original

curve, which was measured in the presence of a much smaller input force). This meant that the dampers did not increase the stiffness of the blisk. As the vibration amplitudes were sufficiently large, the dampers slid on the blade insert faces freely. Therefore, their contribution to the system stiffness was minimal. The consideration of variable normal load and of, especially, multi-harmonic vibrations, produced better predictions, particularly at positions away from the main resonance. The solid black curve in Figure 6.27 follows the measurements reasonably, both qualitatively and quantitatively. In order to verify the assumption that the blisk behaved as tuned for the results presented, the predictions were repeated by taking the mistuning in the blisk into account. However, no significant difference was observed between the tuned and mistuned cases.

Despite the mentioned similarities between the measurements of the first 3 installations and the predictions given in Figure 6.27, the resonance amplitudes predicted were much higher. In fact, close inspection of the time data measured at around the resonance revealed similar behaviour to the undamped case, where the large amplitudes led to truncation of the vibration signal. Likewise, the true resonance peak amplitude could not be measured as the speed steps were not sufficiently fine. At this stage it is necessary to note that, when no stiffness contribution is introduced, the damping introduced through friction does not limit the vibration amplitudes but lowers them by a finite amount. That is to say, when an undamped system is integrated with friction dampers which provide damping only, the resonance peak amplitudes will still be infinite. In this particular case, the resonance peak amplitude was determined mainly by the available structural damping, which was very low (η=0.000075). Nonetheless, the predictions showed that compared with the undamped case, a 70% reduction in the resonance peak amplitude was achieved by the dampers.

6.6.4.3 Predictions of the first 3 installations – 17-18EO excitations

Response curves measured for 18 and 17 EO excitations were also correlated with predictions, as shown in Figure 6.28. The speed range used for the 4th installation was smaller as it was intended to cover the 19EO-5ND resonance only. Although not completely to be compared with the other curves, the extracted response of 18EO excitation for this case was given as an indication of the departure in the behaviour of different installations. Only the predictions with variable normal load and multi-harmonic force are shown. Most of the observations noted for the 19EO excitation curves given above apply to those of the 18EO case given in Figure 6.28 (a). Despite the unavailability of the complete response curve, the behaviour of the last installation is, again, considerably different from the others. As for the 17EO excitation response, a different trend was observed between the predictions and the measurements. Here, the dampers were predicted to be working more effectively thanks to the higher normal load. In fact, the increase in the normal load (i.e. due to increasing rotation speed) was around 10%, which demonstrated that the performance of the dampers was very sensitive to the normal load. Measurement data from the last installation was not available and therefore is not given. For all other installations, the response curves obtained for blade 1 were similar and somehow dissimilar to the predicted one. Particularly near the resonance peak, the amplitudes as well as the apparent natural frequency were observed to be different. Recalling the variability encountered in the measurements of the 1st installation, the response of the minimum responding blade (blade # 18) is also given in Figure 6.28 (b) to indicate the range of variation. The amplitude response of this blade correlated well with that of the predicted curve but the frequency axis did not. As the actual dampers were working more effectively at speeds near the 17EO-7ND resonance (and in all installations) and closer to the stuck condition, their contribution to the stiffness of the system was now notable. This led to an increase in the natural frequency of the mode in question which was not predicted as accurately as the amplitudes were.

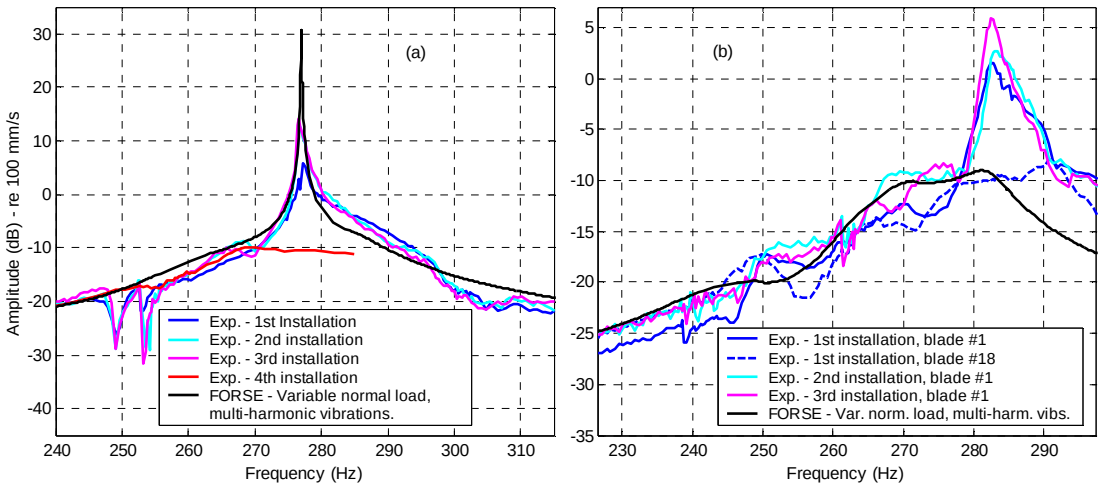

Figure 6.28 Comparison of measured and computed damped Blisk-1 response on blade # 1 to (a) 18, and (b) 17 EO excitations; μ =0.45.

6.6.4.4 Predictions of the last installation – 18-19 EO excitations

The predictions were repeated by using a friction coefficient of 0.6. In this case it was expected to simulate the measurements of the last installation. The vibration response data for the 17EO-7ND resonance was not available for the last installation and only the 18 and 19 EO excitation responses were compared. The comparisons obtained are given in Figure 6.29.

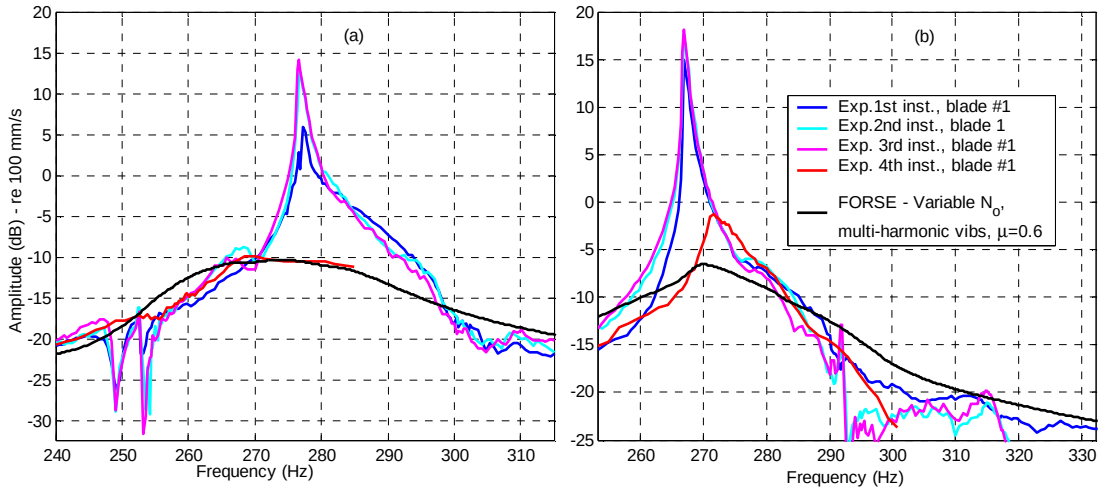

Figure 6.29 Comparison of measured and computed damped Blisk-1 response on blade # 1 to (a) 18, and (b) 19 EO excitations; μ =0.6.

The predictions obtained in this case were clearly better correlated with the measurements of the last installation, as expected. It is seen from the figure that the increase in the coefficient of friction from 0.45 to 0.6 resulted in a significant reduction in response amplitudes, covering the range of amplitude variation observed at various stages of the measurements. This finding strengthens the explanation that the mentioned response variation between the first 3 installations and the last was due to variation of coefficient of friction. Despite the incompleteness of the data, Figure 6.29 (a) shows very good agreement between the measurements of the last installation and the predictions. Although the amplitudes are not predicted as accurately in Figure 6.29 (b), a reasonable qualitative agreement is evident. However, in both Figure 6.29 (a) and (b), the apparent natural frequency is under predicted. Since the predictions for the undamped blisk for this resonance frequency were demonstrated to be closer, the discrepancy here is probably due to the modelling of the under-platform dampers.

At this stage it is worth mentioning that although the predictions are given for two extreme values of coefficient of friction, the actual values of this parameter in reality were probably changing even within the same measurement session. By giving predictions for different values of coefficient of friction, it was aimed to show that provided that the correct values of this parameter were available at corresponding stages of the measurements, reasonable predictions could be obtained. The evidence presented in this section demonstrated that the prediction tool was capable of providing reliable estimates for a blisk integrated with under-platform friction dampers once the correct input parameters were supplied.

6.7 Summary

In this chapter, the predictions of the damped and undamped vibration response of Blisk-1 have been validated against the measurements. The following steps

have been taken in achieving this: (i) translation of frequency mistuning to physical mistuning and its validation, (ii) evaluation of EO excitation errors and their effects, (iii) analysis of mistuning errors, (iv) validation of the undamped response predictions and the test setup (rig + Blisk-1), (v) identification of damper operation regions, and finally (vi) the validation of damped response predictions.

First, the principles and capabilities of the non-linear response prediction tool used were introduced. Then, the frequency mistuning identified in Chapter 4 was translated into physical mistuning. It was found that the closest results were obtained when mistuning was represented by the nodes at the blade tips as opposed to platform levels. For the family of modes of interest (1F), the nodes at a given locality underwent a similar pattern of deflection that the location of mistuning nodes was a more important factor than their number.

It was observed that the amplitude of the magnetic force experienced by each blade was slightly different, thus introducing EO excitation errors. This was expected to have been caused by a combination of possible factors including: (i) a bent shaft, (ii) swash errors, and (iii) different blade tip masses etc. The effect of excitation error was studied using the FE model of Blisk-1. The predictions on the mistuned Blisk-1 showed that the variability of the magnetic force observed in the experiments had negligible effect on the forced response. Using the same model and by applying 10000 randomly generated excitation patterns, it was shown that the variation caused in the forced response was less than the variability in the force input. It was also shown that errors in the applied EO excitation (i.e. non-uniform amplitudes) would cause several ND modes of a tuned system to be excited. However, the amplitudes of additional resonance peaks were found to be very small compared with those caused by physical mistuning. Additionally, the errors in the mistuning pattern identified were also studied using the lumped parameter model introduced in Chapter 4. This pattern was found to be robust for the variation envisaged.

The undamped Blisk-1 response predictions were compared with the measurements and good correlation was observed. Both, z-mod plots and individual blade response levels were shown to be closely predicted. The alignment of the laser beam with the rotation axis was notably worse for Blisk-1 measurements (possibly because of a bent shaft). As a result, considerable discrepancies were observed around resonances excited at high rotor speeds. However, this effect was shown to have receded for the same resonances when excited at low rotor speeds. Although the comparison of all blade response curves was not as convincing as those of Blisk-2 (see Chapter 5), they were sufficiently close to validate the mistuning pattern identified and its modelling.

In the final part of the chapter, measurements taken on the damped Blisk-1 were reported, and then a subset of these results were compared with the predictions. Preliminary investigations showed that the steel dampers were too heavy for most of the speed range and the titanium dampers did not operate adequately at high speeds. Therefore, the main effort was directed at the testing of the titanium dampers at low speeds where 17-20 EOs were exciting 7-4ND modes, respectively. It was observed that during the operation of the rig, the characteristics of the contact interfaces changed with time. This was due to the accumulation of metal debris knocked off the rubbing faces. As a result, the dampers and the blade inserts had to be cleaned and reinstalled 4 times. The results obtained for the first three installations were consistent and significantly dissimilar to those of the final installation. Nonetheless, each set of measurements was consistent in itself which proved the essential reliability of the measurement process itself.

Preliminary predictions with various values of contact stiffness, coefficient of friction and normal load showed that the blisk response was not sensitive to contact stiffness but that it varied significantly with latter two parameters. As the normal load was known fairly accurately, the predictions were repeated for two

extreme values of the coefficient of friction in an attempt to account for the variability observed during the measurements. The first value (0.45) was expected to simulate the real situation in the first three installations where the dampers were known to have slid freely at the contact interfaces. On the other hand, the second value (0.6) was used to predict the measurements of the last installation in which the dampers were closer to the stuck condition. Both cases revealed acceptably close correlation with the measured results they were expected to simulate.

CHAPTER 7

CONCLUSIONS and FUTURE WORK

7.1 Summary and Conclusions

The main goals of the presented study, as stated in Chapter 1, were to provide reliable and accurate measure of vibration data obtained under well-controlled and realistic conditions so that the forced response predictions of mistuned and friction damped blisks could be validated. An overview and conclusions drawn from the work performed towards the fulfilment of these goals are given below. However, it is appropriate to start with conclusions concerning the devised measurement technique and test setup, which were also set as major objectives of this work as means of achieving the abovementioned application aims.

7.1.1 Measurement technique and test rig

The devised self-tracking measurement technique worked successfully and proved to be an effective and reliable way of measuring response on rotating components such as bladed disks. The fact that this technique, as indeed do all other LDV measurement techniques, relied on proper alignment of the laser beam with the axis of rotation, led some of the EO excitation responses to be contaminated by the cross-talk errors. For the simpler Blisk-2, these errors have been minimised and confined to lower EO excitations (which were excluded from the measurements) through elaborate alignment measures. However, the effects of misalignment on Blisk-1 measurements have been somewhat more dominant, probably due to a bent drive shaft, and could not be improved through the same alignment measures. The measurement rig operated well under vacuum and throughout the rotating tests without any major breakdown.

The use of mechanical indexing enabled all blades to be measured sequentially and quickly without shutting the rig down. Through repeated measurements under similar conditions, it was demonstrated that the designed rig was capable of producing reliable and consistent data, which was essential since they were to be used for validation purposes.

7.1.2 Mistuning analysis

One of the main objectives of this study was to validate the models used to make forced vibration response analysis by comparing predictions of mistuned bladed disk vibration through accurate and well-controlled measurements (i.e. measurements reflecting the response due to phenomena of interest only). This was achieved via a reasonably well tuned integral bladed disk testpiece operating in a vacuum and under rotation, as well as at rest and in the presence of air. An extensive test design phase was undertaken by using an updated FE model of the blisk, which was successfully executed in the way it was planned. This enabled a very efficient test campaign, both in terms of short measurement times and in the acquisition of useful data. Through the measurements at rest with several mistuning patterns, it has been demonstrated that the calculation tool successfully predicted measured circumferential ODSs, as well as natural frequencies and the splits in double modes. Following this, the rotating measurements were carried out for three configurations on Blisk-2:

(i) *Tuned case*: The comparison of measured and predicted interference diagrams demonstrated excellent agreement. Individual blade responses were also well predicted though some variations were evident, probably due to the sensitivity of this tuned case to minor deviations in the test conditions and excitation errors. It has been demonstrated by way of rotating ODS measurements that travelling waves were excited in the blisk, with all blades experiencing the same level of vibration. This level, again, was predicted reasonably in simulations.

(ii) *Regular mistuning case,* $Sin(8\cdot\theta)$. This case was designed to display considerable modal overlap and reasonably complicated mode shapes so as to form a challenging case for predictions. The good correlation of measured and predicted natural frequencies (Table 5.1) demonstrated that the mistuning had been properly modelled. It was shown during the test design phase that the interference diagram exhibited a formation of complex resonance groups, which was backed up generously by the measurements, Figure 5.13. In this case, the modes excited at each resonance on the interference diagram were accounted for through their harmonic content, Figure 4.25. This was confirmed by the Fourier analysis performed on the measured ODSs. A mistuning pattern of this kind was expected to produce 3 different blade responses for a given EO excitation, which was gratifyingly proved by the measured response curves for 6EO excitation, Figures 5.14-15. Individual blade response curve measurements (Figure 5.15) and blade-to-blade amplitude variations (Figure 5.17) have been well predicted not only qualitatively but also quantitatively.

(iii) *Random mistuning case.* The interference diagram predicted for this case was rather complicated but compared very well with the measurements, Figure 5.18. Similarly, modes corresponding to predicted resonances were identified (Figure 4.27) and confirmed by the measured ODSs. Individual blade response curves have been measured for a limited speed range for 10EO excitation. Comparisons (Figure 5.19) demonstrated that the predictions were good not only around the resonance frequencies but also away from them, thus validating both the predictions and also the measurement technique. Comparison of measured and calculated ODSs (Figure 5.23) showed that the blade response amplitudes, as well as the pattern of variation were, well predicted.

Additional mistuning analyses were conducted on Blisk-1. Non-negligible inherent mistuning in this testpiece, which could not be removed via tuning,

was identified experimentally in terms of scatter of 1F natural frequencies of isolated sectors, Figure 4.18. This frequency mistuning was later translated into physical mistuning for forced response analyses. It was demonstrated by mode shape and natural frequency comparisons that the updated blisk model represented the real blisk accurately, Figure 4.20. Despite errors in mistuning identification, and to an extent in its representation, relatively complex response curves measured in a narrow frequency band were reasonably well predicted (Figure 6.12), with acceptable accuracy.

In forced response predictions, the effect of rotational speed was accounted for by calculating the mode shapes and frequencies at the mid-speed value of the range of interest, and then by rearranging the frequency axis of the forced response curves according to rotational speed-frequency shift relation, Figure 5.5. The good level of agreement verified that the implemented approach was appropriate. Also, the close agreement between the measured and predicted response levels confirmed that the forcing input was processed accurately.

Since the blisks used in the analyses were very lightly damped, the resonances were very sharp and produced very large vibration amplitudes when excited. As a result, in all abovementioned cases the true resonance amplitudes could not be captured accurately due to insufficient sweep rates. Also, the frequencies corresponding to lower modes were lower in measurements due to flexible disk clamping in measurements as opposed to the rigid fixing assumed in the FE models. However, in both cases the problems were related to the test setup rather than to the prediction tool. In the light of evidence presented in this study, the forced response blade vibration prediction tool has been demonstrated to be predicting the tuned and mistuned vibration response accurately, and has thus been successfully validated. Most of the experimental studies reported in the reviewed literature, which were also aimed at validation of numerical codes, dealt with stationary components. The fact that very good agreement between the measurements and the predictions was obtained under rotating conditions,

simulating a more realistic situation, stands out as an important achievement of this study.

7.1.3 Friction damping analysis

The second goal sought in this study was to validate the predictions of bladed disk forced response when under-platform friction dampers were integrated in the testpiece. This was achieved through measurements performed on Blisk-1. Two sets of dampers, one made of steel and the other made of titanium, were tested. Tests carried out on the steel dampers were not effective as they proved to be too heavy to operate as desired, Figure 6.16. These dampers were found to be locking up at relatively low rotation speeds, thus raising the natural frequencies of the bladed disk assembly through substantial stiffness increases. As a result, only the dampers made of titanium were used in the measurements reported here. Some difficulties were encountered in making these dampers function satisfactorily, too, particularly at high rotation speeds where reasonably well tuned low ND modes were excited. Testing of these modes was particularly important as the higher ND ones (7ND and higher) were significantly mistuned. Since the mistuning was not known accurately, the predictions involving these modes would have been less certain. As a result, a speed range covering resonances corresponding to the 1F family of blisk modes excited by 17, 18, 19, 20, and 21 EOs (i.e. 7, 6, 5, 4, and 3ND modes respectively) was covered. The main effort was directed towards 19 and 20 EOs so that reasonably tuned 4 and 5 ND modes were excited.

It was observed that the dynamic characteristics of the dampers changed as the rig operated, Figure 6.20. The titanium dampers were in contact with steel surfaces. As the dampers worked effectively, they removed metal from the steel surfaces they worked against. In time this removed metal accumulated in between the contact surfaces, gradually leading to rougher surfaces and higher damping, or, in some cases, even to jamming of the dampers, Figure 6.21. As a

result, it was necessary to clean the accumulated debris from the contact surfaces several times. Overall, the dampers were taken out and reinstalled 4 times over 50 hours of operating time and the measurements repeated after each installation. It was observed that the first 3 installations of the dampers yielded similar response characteristics in terms of resonance frequencies and peak amplitudes. However, the 4th one, in which the damping and stiffness contributions of the dampers were considerably higher, differed significantly from the first three, Figure 6.24. Although the resonance peak amplitudes measured in the first installation differed somehow from blade to blade, all the blade responses, in general, exhibited considerable consistency in each installation. This proved that the rig with friction damped blisks produced reliable and repeatable vibration response data.

The modelling of Blisk-1 with under-platform friction dampers was achieved by considering a single sector and making use of cyclic symmetry. Since the measurements were concentrated on the mainly tuned blisk modes, the mistuning in the blisk was assumed negligible and not considered. This assumption was verified by comparing the undamped-tuned and –mistuned response predictions (Figure 6.18) for these modes as well as the damped-tuned and -mistuned ones. The coefficient of friction used was taken from earlier measurements performed for the titanium alloy employed. However, the contact stiffness was calculated by FE analysis. Owing to the uncertainties regarding the contact parameters (i.e. contact stiffness and friction coefficient), some preliminary predictions were performed to find out the sensitivity of the system response to these parameters. The contact stiffness was found to have a less impact than the friction coefficient which, together with the normal load, was demonstrated to have played a greater role in determination of the response characteristics. Since the normal load was accurately known, the friction coefficient was varied to account for the variability observed during the measurements. By systematically changing the coefficient of friction from 0.45 to 0.6 the variation obtained between different installations of the dampers could

be accounted for. Therefore, the predictions were performed and presented for these two extreme values of the friction coefficient.

It was observed that the damped response predictions for a friction coefficient of 0.45 correlated much better with the results of the first 3 installations than the last one (Figure 6.27), as expected. The agreement was further improved by consideration of multiple harmonic vibrations and variable normal load. However, the predicted and measured peak resonance amplitudes were considerably different for some of the resonances measured (19EO-5ND and 18EO-6ND). Since the dampers in the first 3 installations slid freely along the blade insert faces, they did not cause any stiffness increase in the blisk. The comparison of the damped and undamped measurements showed little change in apparent natural frequency. In this case, although the amplitudes were reduced by a finite amount due to friction damping, the resonance peak amplitudes were mainly determined by the available structural damping, which was very low. As a result, large vibration amplitudes were created but could not be measured accurately due to insufficient sweep rate. However, for the 17EO-7ND resonance, which was excited at a relatively higher rotation speed, better estimates were obtained in terms of resonance peak amplitudes. In this case, the normal load was slightly higher due to higher rotation speeds and, the dampers were closer to the stuck condition. This meant that the damping produced was more effective and kept the resonance peak amplitude reasonably low so that it could be measured accurately, Figure 6.28.

The damped response predictions were repeated for an upper extreme value of friction coefficient of 0.6. This was done to help explain the results obtained in the last installation of the dampers. The limited range of data available allowed only 18 and 19 EO excitation responses to be compared with the predictions. Clearly, better estimates were obtained for the last installation of the dampers, Figure 6.29. The 18EO excitation response was found to be better predicted than the 19EO excitation. This was probably due to the fact that the contact conditions

were changing even within the same measurement session, at different rotation speeds. However, the same parameters were applied in a given prediction session. Some discrepancy was observed between predicted and measured resonance frequencies as well. As those of the undamped assembly were demonstrated to have correlated better, the disagreement with the damped assembly was probably due to the modelling of the friction dampers. Nonetheless, given the complicated nature of the task and based on the evidence presented, the prediction tool was demonstrated to be capable of supplying reliable estimates for blisks integrated with under-platform friction dampers provided that the correct input parameters were made available.

Most of the studies reported in the reviewed literature dealt with the problem of under-platform friction damping on simple test setups such as the ones comprising two blades and a damper in between, at rest. Even when a full assembly has been tested, the testing was performed on bladed disks having separately made blades. Thus, the effect of under-platform friction dampers alone could not be analysed as the contact at the blade roots was also non-linear and contributed to the response. To the best knowledge of the author, testing at the scale presented here, reflecting the isolated effects of friction damping, with such consistency, and under such realistic conditions has not been reported before. The fact that successful analyses have been performed with acceptable accuracy fulfils one of the main objectives of the presented work.

7.1.4 Blisk tuning and excitation errors

The attempts made at improving the symmetry of a blisk by tuning its 1F blade-alone frequencies failed to produce a reasonably well-tuned test piece. In this study the tuning was performed to obtain a better reference state with which the effectiveness of the theory could be assessed. However, in practice this is done to avoid the adverse affects (i.e. mode localisation and thus amplitude magnification) of the mistuning. It is done because the design is generally based

on the amplitudes corresponding to the tuned case. The finding here has been that, when performed through appropriate parameters, the 1F blade-alone natural frequency tuning can be successful. However, in general, an effective tuning can only be achieved if multiple frequencies of the isolated components (i.e. blades) are matched; a very difficult, long and expensive process in practice. However, it is known that only certain mistuning patterns are likely to cause critical vibration amplitudes. Thus, if the pattern of variation is known (which requires multiple frequencies of each of the blades to be measured), using the validated prediction tool, the consequences of present mistuning can be predicted and the combinations likely to cause problems can be eliminated. Therefore, it is argued that for more efficient use of resources, it is advantageous to concentrate on identification of mistuning pattern first, rather than trying to correct it no matter what it is.

The effects of EO excitation errors (i.e. all blades experiencing different force amplitudes but perfect phase shifts) were investigated through Blisk-1 FE model. The analyses showed that a *kth* EO excitation excited many of the non-*kth* ND modes of a tuned blisk (Figure 6.7), depending on the pattern of amplitude variation. However, the amplitudes of these resonances were very small compared to those caused by the physical mistuning. The deviation of maximum response (i.e. at the EO-ND resonance) was analysed by using a large number of cases and it was found that the variation of the maximum amplitude (<3%) was less than the excitation error (±5%). Thus, it is concluded that the excitation errors, unlike physical mistuning, are highly unlikely to cause excessive vibration amplitudes, and, depending on the application, can be neglected.

7.2 Recommendations for future work

The measurement technique devised in this study allowed blade tip responses to be measured using the self-tracking LDV measurement technique and circumferential ODSs through the circular scanning LDV under rotation.

However, often it is of interest to be able to measure the radial ODSs, say along the blades, or area scan measurements across the whole bladed disk under rotation. Although the latter can readily be performed on the current configuration, a precise measure of rotation speed is needed and a way of data processing needs to be developed. The former, on the other hand, cannot be performed with the current setup. However, with the aid of a dedicated research activity, either through additional optical mechanisms or new scanning techniques utilising the positioning mirrors of the laser device, the rig can still be employed in the pursuit of the technology.

Rotational speed dependency of the excitation in the rig meant that the minimum frequency resolution was limited by the precision of the motor controller. As a result, it has not been possible to perform detailed measurements around the sharp resonances which were often encountered. The use of electromagnets, instead of permanent ones used in this study, can eliminate this problem as any frequency can be input to the system. The trials conducted with available a/c magnets have been fruitless as it was not possible to exert enough force at safe stand offs. New research into development of a more powerful and compact a/c magnet, and its control to produce desired force input signals could improve the quality of measurements.

It is known that modes from different families of a bladed disk may interact strongly at regions where they get close. This phenomenon is called “curve veering” (from the fact that the families of modes approach and divert from each other as they never cross) and is particularly important under rotation when a family of bending modes is reasonably close to but lower than a family of torsion modes. What happens under rotation is that the bending natural frequencies increase more with rotational speed than the torsional ones. As a result, these two families can be brought sufficiently close at veering regions that their modes interact, producing unexpectedly high amplitudes. The fact that the designed test rig runs under rotation can be employed in pursuit of this problem by

designing a suitable new test piece. Additionally, as it is stands at the moment, the rig and the test pieces used in the analyses can be employed in quest of experimental investigation of the effects of other mistuning problems such as mode localisation, amplitude magnification and intentional mistuning.

The combination of different metals (i.e. titanium dampers operating on steel surfaces) for friction damping investigation created unexpected problems which made the characterisation and predictions of the non-linear system difficult. Now that a rig to carry out this type of experiments is available, by making both, dampers and blade inserts from the same material, a better understanding of the problem may be obtained.

REFERENCES

[1] **Ewins, D. J.**
Structural dynamics characteristics of bladed disks
AGARD Manual on aeroelasticity in axial-flow turbomachines, Vol. 2, 1988

[2] **Ewins, D.J.**
The effect of blade mistuning on vibration response – a survey
IFToMM 4th Int. Conf. on Rotordynamics, Prague, Czechoslovakia, 1991

[3] **Srinivasan, A. V.**
Flutter and Resonant Vibration Characteristics of Engine Blades
ASME Journal of Engineering for Gas Turbines and Power, Vol. 119, 1997, p. 742-775.

[4] **Slater, J.C., Minkiewicz, G. R., Blair, A. J.**
Forced response of bladed disk assemblies – A survey
The shock and vibration digest, Vol. 31, No. 1, January 1999, p.17-24

[5] **Moyroud F., Fransson T., Jacquet-Richardet G.**
A comparison of two finite element reduction techniques for mistuned bladed disks
Journal of Engineering for Gas Turbines and Power, Vol. 124, No. 4, p.942-952

[6] **Rivas-Guerra, A. J., Mignolet, M. P.**
Local/Global effects of mistuning on the forced response of bladed disks
Proceedings of ASME TURBO EXPO, 2001-GT-0289.

[7] **Judge, J., Pierre, C., Mehmed, O.**
Experimental investigation of mode localization and forced response amplitude magnification for a mistuned bladed disk
ASME Journal of Engineering for Gas Turbines and Power, Vol. 123, 2001, p. 940-950.

[8] **Myhre, M., Moyroud, F., Fransson, T. H.**
Numerical investigation of the sensitivity of forced response characteristics of bladed disks to mistuning
Proceedings of ASME Turbo Expo 2003, June 16-19, 2003, Atlanta, Georgia, USA

[9] **Kenyon, J.A., Griffin, J. H.**
Mistuned bladed disk forced response with frequency veering
Proceedings of 8th National Turbine Engine HCF conf., 14-16 April 2003, California

[10] **Bladh, R., Castanier, M. P., Pierre, C.**
Component-mode-based reduced order modeling techniques for mistuned bladed disks – Part I: Theoretical models
ASME Journal of Eng. for Gas Turbines and Power, Vol. 123, 2001a, p. 89-99.

[11] **Jacquet-Richardet, G., Ferraris, G., Rieutord, P.**
Frequencies and modes of rotating flexible blade disk-shaft assemblies: A global cyclic symmetry approach
Journal of Sound and Vibration, Vol.191 (5), 1996, p.901-915

[12] **Yang, M.-T. Griffin, J. H.**
A reduced order model of mistuning using a subset of nominal modes
ASME Journal of Engineering for Gas Turbines and Power, Vol. 123, 2001, p. 893-900.

[13] **Feiner, D. M., Griffin, J. H.**
A fundamental mode of mistuning for a single family of modes
Proceedings of ASME TURBO EXPO, 2002, GT-2002-30425.

[14] **Petrov, E. P., Sanliturk, K. Y., Ewins, D.J.**
A new method for dynamic analysis of mistuned bladed disks based on the exact relationship between tuned and mistuned systems
ASME Journal of Engineering for Gas Turbines and Power, Vol. 124, 2002, p. 586 -597.

[15] **Lim, S., Castanier, M. P., Pierre, C.**
Reduced order modelling and analysis of bladed disks with large mistuning
Proceedings of 8th National Turbine Engine HCF conf., 14-16 April 2003, California

[16] **Mignolet, M. P., Rivas-Guerra, A. J., LaBorde, B.**
Towards a comprehensive and direct prediction strategy of the effects of mistuning on the forced response of forced response of turbomachinery blades
Aircraft Engineering and Aerospace Technology, Vol. 71, 1999, No. 5, p. 462-469.

[17] **Mignolet, M. P., Lin, C.-C., LaBorde, B. H.**
A novel Limit Distribution for the analysis of randomly mistuned bladed disks
ASME Journal of Eng. for Gas Turbines and Power, Vol. 123, 2001a, p. 388 -394.

[18] **Petrov, E., Ewins, D. J.**
Analysis of the worst mistuning patterns in bladed disk assemblies
Proceedings of ASME TURBO EXPO, 2001, 2001-GT-0292, Orleans, Louisiana, USA

[19] **Rivas-Guerra, A. J., Mignolet, M. P.**
Maximum amplification of blade response due to mistuning: localization and mode shapes aspects of worst disks
Proc. of ASME TURBO EXPO, 2002, GT-2002-30323, Amsterdam, The Netherlands

[20] **Kenyon, J. A., Griffin, J. H., Feiner, D. M.**
Maximum bladed disk forced response from distortion of a structural mode
Proc. of ASME TURBO EXPO, 2002, GT-2002-30426, Amsterdam, The Netherlands

[21] **Xiao, B., Rivas-Guerra, A. J., Mignolet, A. P.**
Identification of the maximum responding blade in mistuned bladed disks
Proceedings of the Turbo Expo 2003, GT-2003-38966, Atlanta, Georgia, USA

[22] **Castanier, P. M. and Pierre, C.**
Consideration on the benefits of intentional blade mistuning for the forced response of turbomachinery rotors
ASME Int. Mech. Eng. Congress and Expo., 1997, AD-Vol. 55, pp.419-425

[23] **Kenyon, J.A., Griffin, J. H.**
Forced response of turbine engine disks and sensitivity to harmonic mistuning
Journal of Engineering for Gas Turbines and Power, January 2003, Vol. 125, p.113-120

[24] **Choi, B.-K., Lentz, J., Rivas-Guerra, A. J., Mignolet, M. P.**
Optimisation of intentional mistuning patterns for the reduction of the forced response effects of unintentional mistuning: Formulation and assessment
Journal of Eng. For Gas Turbines and Power, January 2003, Vol. 125, pp.131-140

[25] **Mignolet, M.P., Rivas-Guerra, A.J., and Delor, J.P.**
Identification of Mistuning Characteristics of Bladed Disks from Free Response Data - Part I
Journal of Engineering for Gas Turbines and Power, Vol. 123(2), 2001, pp. 395-403.

[26] **Rivas-Guerra, A.J., Mignolet, M.P., and Delor, J.P.**
Identification of Mistuning Characteristics of Bladed Disks from Free Response Data – Part II
Journal of Engineering for Gas Turbines and Power, Vol. 123(2), 2001, pp. 404-411.

[27] **Judge, J.A., Pierre, C., and Ceccio, S.L.**
Mistuning Identification in Bladed Disks
Proc. of the Int. Conf. on Structural Dynamics Modelling, 2002, Madeira, Portugal.

[28] **Feiner, D.M., and Griffin, J. H.**
Mistuning Identification of Bladed Disks Using a Fundamental Mistuning Model – Part I: Theory
ASME Paper GT2003-38648, Int. Gas Turbine Institute Turbo Expo, Atlanta, Georgia.

[29] **Feiner, D.M., and Griffin, J. H.**
Mistuning Identification of Bladed Disks Using a Fundamental Mistuning Model – Part II: Application
ASME Paper GT2003-38648, Int. Gas Turbine Institute Turbo Expo, Atlanta, Georgia.

[30] **A B Stanbridge, K Y Sanliturk & D J Ewins**
Measurement and Analysis of High-Temperature Friction Damper Properties
4th US International Turbine Engine High Cycle Fatigue (HCF) Conference, 1999

[31] **Sextro, W.**
The calculation of the forced response of shrouded blades with friction contacts and its experimental verification
Proc. Of ASME Turbo Expo, 2000, Munich Germany.

[32] **Berruti, T., Goglio, L., Filippi, S., Gola, M. M.**
A test rig for frictionally damped bladed segments
Proc. Of ASME Turbo Expo, 2000, Munich Germany.

[33] **Yang B.D., Chu M.L., Menq C.H.**
Stick-Slip-Separation analysis and nonlinear stiffness and damping characterization of friction contacts having variable normal load – a .
Journal of Sound and Vibration, 210(4), 1998, pp. 461-481.

[34] **Yang, B.D., Menq C.H.**
Characterization of 3D contact kinematics and prediction of resonant response of structures having 3D friction constraint - b.
Journal of Sound and Vibration, 217(5), 1998, pp. 909-925.

[35] **K.Y. Sanliturk, D.J. Ewins & A.B. Stanbridge**
Underplatform dampers for turbine blades: theoretical modelling, analysis and comparison with experimental data
ASME Journal of the Engineering for Gas Turbines and Power, v.123, pp.919-929

[36] **Sanliturk K.Y., Ewins D.J.**
Modeling two-dimensional friction contact and its application using harmonic balance method
J. of Sound and Vibration, 193(2), pp. 511-523.

[37] **Petrov, E., Ewins, D. J.**
Analytical formulation of friction interface elements for analysis of nonlinear multi-harmonic vibrations of bladed disks
Journal of Turbomachinery, Vol. 125, APRIL 2003, pp. 364-371

[38] **Petrov, E., Ewins, D. J.**
Generic friction models for time-domain vibration analysis of bladed discs
Proc. ASME Turbo Expo 2003, GT-2003-38475, Atlanta, Georgia.

[39] **Petrov, E.**
A method for use of cyclic symmetry properties in analysis of nonlinear multiharmonic vibrations of bladed disks
Proc. ASME Turbo Expo 2003, GT-2003-38475, Atlanta, Georgia.

[40] **Petrov, E., Ewins, D. J.**
Analysis of forced response for nonlinear vibration of mistuned bladed discs
Proceedings of 8th National Turbine Engine HCF conf., 14-16 April 2003, California

[41] **Lin, C.-C., Mignolet, M. P.**
Effects of damping and damping mistuning on the forced vibration response of bladed disks
Journal of Sound and Vibration, 1996, Vol. 193(2), pp.525-543

[42] **Griffin, J. H.**
A review of friction damping of turbine blade vibration
Int. Journal of Turbo and Jet Engines, No. 7, 1990, pp.297-307

[43] **Ewins, D. J.**
The effects of detuning upon the forced vibration of bladed-disks
Journal of Sound and Vibration, 1969, Vol. 9, No. 1, p.65-79

[44] **Ewins, D. J.**
Vibration characteristic of bladed disc assemblies
Journal of Mechanical Engineering Science, Vol. 15, No. 3, 1973, pp.165-186

[45] **Ewins, D. J.**
An experimental investigation of the forced vibration of bladed discs due to aerodynamics excitation
The winter annual meeting of ASME, New York, December 5-10, 1976

[46] **Fabunmi, J. A.**
Forced vibrations of a single stage axial compressor rotor
Transactions of ASME Journal of Eng. for Power, Vol. 102, April, 1980, p.322-328

[47] **Wei, S.-T., Pierre, C.**
Localization phenomena in mistuned assemblies with cyclic symmetry Part I: Free vibrations
ASME J. of Vib. Acoustics, Stress and Reliability in Design, Vol. 110, 1988, p. 429-438.

[48] **Wei, S.-T., Pierre, C.**
Localization phenomena in mistuned assemblies with cyclic symmetry Part II: Forced vibrations
ASME J. of Vib. Acoustics, Stress and Reliability in Design, Vol. 110, 1988, p. 439-449.

[49] **Kruse, M. J., and Pierre, C.**
An Experimental Investigation of Vibration Localization in Bladed Disks, Part I: Free Response
Proc. 42nd ASME Gas Turbine and Aeroengine Cong., 1997, Orlando, Florida, USA.

[50] **Kruse, M. J., and Pierre, C.**
An Experimental Investigation of Vibration Localization in Bladed Disks, Part II: Forced Response
Proc. 42nd ASME Gas Turbine and Aeroengine Cong., 1997, Orlando, Florida, USA.

[51] **Marugabandhu, P. and Griffin J.H.**
A Reduced Order Model for Evaluating the Effect of Rotational Speed on the Natural Frequencies and Mode Shapes of Blades,
Int. Gas Turbine and Aeroengine Con. and Expo, 2000-GT-611, Munich, Germany

[52] **Ottarson, G.S., Castanier, M. P., Pierre, C.**
A reduced order modelling technique for mistuned bladed disks
Proc. Of the 35th AIAA/ASME/EASCE/AHS/ASC Structures, Structural Dynamics and Materials Con, 1994.

[53] **Kruse, M. J., Pierre, C.**
Forced-response of mistuned bladed disks using reduced-order modeling.
Proc. of the 37th AIAA/ASME Structures, Structural Dynamics and Materials Con, Salt Lake City, Utah, 1996.

[54] **Judge, J., Pierre, C., Mehmed, O.**
Experimental investigation of mode localisation and forced response amplitude magnification for a mistuned bladed disk
Transactions of ASME, Vol. 123, October 2001, pp.940-950

[55] **Jones, K. and Cross, C.**
A travelling wave excitation system for bladed disks
43rd AIAA/ASME/EASCE/AHS/ASC Structures, Structural Dynamics and Materials Con, AIAA 2002-1531, 2002, Denver, Colorado.

[56] **Judge, A. J., Ceccio, S. L. and Pierre, C.**
Travelling wave excitation and optical measurement techniques for non-contacting investigation of bladed disk dynamics
The Shock and Vibration Digest, Vol. 34, No. 3, May 2003, pp.183-190

[57] **Kenyon, J. A. and Griffin, J. H.**
Experimental demonstration of maximum mistuned bladed disk forced response
Proceedings of ASME Turbo Expo, GT2003-38060, 2003, Georgia, USA

[58] **Shu, H. T. and Cutts, D. G.**
Methods of processing strain response signals from rotating bladed assemblies to extract modal parameters
IMAC

[59] **Hollkamp, J. J. and Gordon, R. W.**
Modal test experience with a jet engine fan model
Journal of Sound and Vibration, 2001, Vol. 248, No. 1, pp.151-165

[60] **Jaiswal, B. L. and Bhave, S. K.**
Experimental evaluation of damping in a bladed disk model
Journal of Sound and Vibration, 1994, Vol.177, No. 1, pp.111-120

[61] **Berruti, T., Filippi, S. and Gola, M. M.**
Friction damping of interlocked vane segments: experimental results
Proceedings of ASME Turbo Expo, June 2001, 2001-GT-0432

[62] **Hollkamp, J. J. and Gordon, R. W.**
An experimental investigation of non-uniform damping in bladed disks
AIAA-98-3747, 1998

[63] **Jeffers, T.R., Kielb, J.J., Abhari, R.S.**
A Novel Technique for the Measurement of Blade Damping using Piezoelectric Actuators
ASME 2000-GT-359, IGTI TURBO EXPO Conference, May 2000, Munich, Germany

[64] **Burdekin, M., Cowley, A. and Back, N.**
An elastic mechanism for the micro-sliding characteristics between contacting machined surfaces
Journal of Mechanical Engineering Science, ImechE, 1978, pp.121-132

[65] **Kulczyk, W. K and Q. V. Davis**
Laser Doppler instrument for measurement of vibration of moving turbine blade
Proceedings of the Institution of Electrical Engineers (London), 1973, Vol. 120, No. 9

[66] **Simpson, D. G. and Lamb, D. G. S.**
A laser Doppler system for the measurement of torsional vibration
NEL report No. 639, July 1977, Department of Industry, UK

[67] **Roth, H.**
Measuring vibration on turbine blades by optical means
Brown-Boveri Review, 1977, Vol. 64, No. 1

[68] **Roth, H.**
Vibration measurement on turbomachine blades with optical probes
Measurement methods in rotating components of turbomachines at Joint Fluids Engineering Gas Turbine Con. and Product Show, New Orleans, LA, March 1980

[69] **Cookson, R. A. and Bandyopadhyay, P.**
A fibre-optic laser Doppler probe for vibration analysis of rotating machines
ASME Journal of Engineering for Power, 1980, Vol. 102, No. 3.

[70] **Wlezien, R. W., Miu, D. K. and Kibens, V.**
Characteristics of rotating bladed disks using a Laser Doppler Vibrometer
Optical Engineering, 1984, Vol. 23, No. 4, pp.436-442

[71] **Reinhardt, A. K., Kadambi, J. R. and Quinn, R. D.**
Turbomachinery blade vibration and dynamic stress measurement utilising non-intrusive techniques
Transactions of ASME, Vol. 111, October 1989, pp.468-474

[72] **Rothberg, S. J. and Halliwell, N. A.**
Vibration measurement on rotating machinery using Laser Doppler Velociometer
Transactions of the ASME, 1994, Vol. 116, pp.326-331

[73] **Bucher, I., Schmiechen, P., Robb, D. A. and Ewins, D. J.**
A laser-based measurement system for measuring the vibration on rotating discs
Vibration Measurement, 1994, Vol. 2358, pp.398-408

[74] **Reinhardt, A. K., Kadambi, J. R. and Quinn, R. D.**
Laser vibrometry measurements of rotating blade vibrations
Transactions of the ASME, Vol. 117, July 1995, pp.484-488

[75] **Castellini, P. and Santolini, C.**
Vibration measurements on blades of a naval propeller rotating in water with tracking laser vibrometer
Measurement, 1998, Vol. 24, pp.43-54

[76] **R. A. Lomenzo, A. J. Barker, A. L. Wicks**
Laser Vibrometry System for Rotating Bladed Disks
1999, Proceedings of the 18th IMAC, 277-282

[77] **Stanbridge, A. B. and Ewins, D. J.**
Modal testing using scanning Laser Doppler Vibrometer
Mechanical Systems and Signal Processing 13(2), 1999, pp255-270

[78] **Stanbridge, A. B., Sever, I. A. and Ewins, D. J.**
Vibration measurements in a rotating blisk test rig using an LDV
5th Int. Con. on Vib. Measurements by Laser Techniques, Ancona, 18-21 June 2002.

[79] **Martarelli, M.**
Exploiting the laser scanning facility for vibration measurement
PhD Thesis, 2001, Imperial College London

[80] **OMETRON**
VPI Sensor Operator Manual
Issue no. 5, March 1994

[81] **Stanbridge, A. B., Martarelli, M. and Ewins, D.J.**
The scanning laser Doppler Vibrometer applied to impact modal testing
Proceedings of IMAC XVII 1999, Orlando

[82] **Petrov, E., Ewins, D. J.**
Analysis of Non-linear multi-harmonic Vibrations of Bladed Disc with Friction and Impact Dampers
7th National Turbine Engine High Cycle Fatigue (HCF) Conference, 14-17 May 2002, Florida

[83] **Ewins, D. J.**
Modal Testing: Theory, Practice and Application
Research Studies Press Ltd., 2000, Second Edition

[84] **Bucher, Izhak**
RotFE 2.1, the finite element rotor analysis package and user manual

[85] **Link, M., Rohrmann, R. G. and Pietrzko, S.**
Experience With Automated Procedures for Adjusting the Finite Element Model of a Complex Highway Bridge to Experimental Modal Data
1996, Proceedings of the 14th IMAC, 218-225

[86] **Link, M. and Zhang, L.**
Experience With Different Procedures for Updating Structural Parameters of Analytical Models Using Test Data
1992, Proceedings of the 10th IMAC,

[87] **Petrov, E.P.**
A users guide to MISTuning RESponse (MISTRES) analysis program for bladed disks (V.1)
No. VUTC/E1/99022, 21 July 1992, Imperial College London

APPENDIX A

TECHNICAL DRAWINGS

A.1 Rig drawings

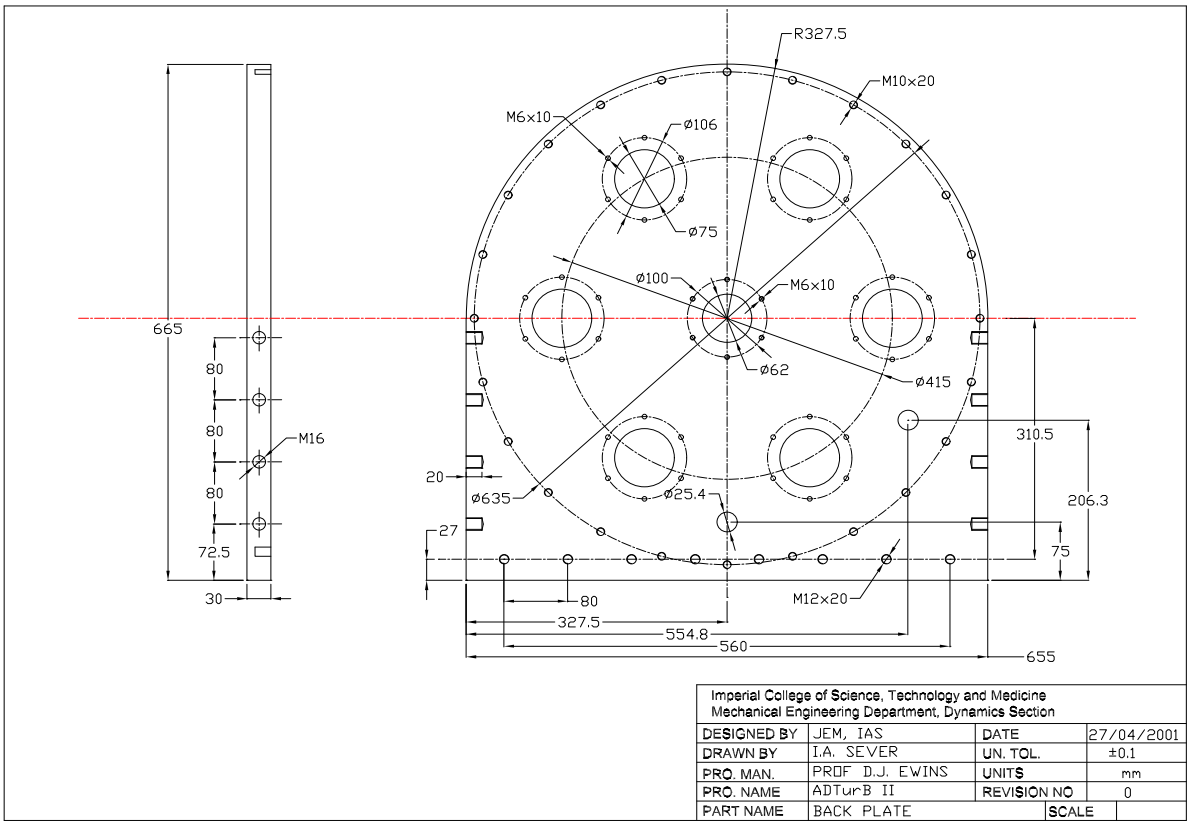

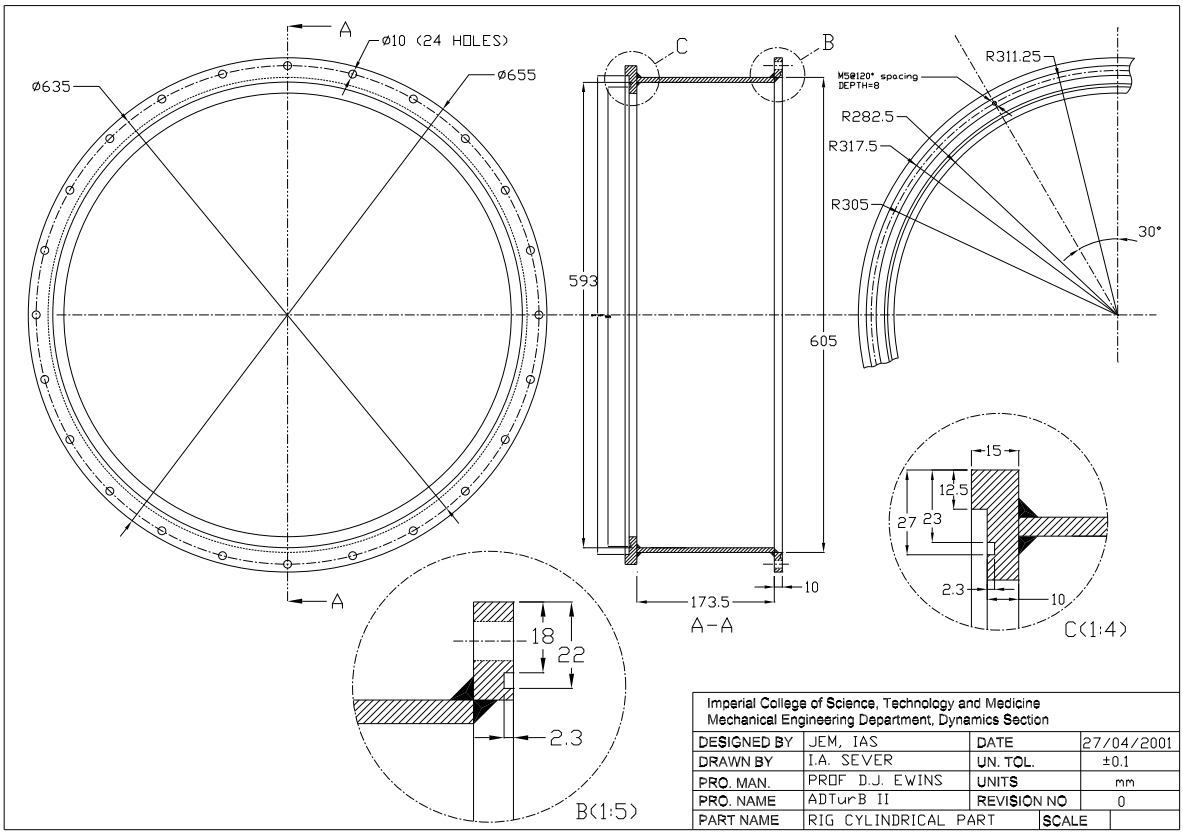

Imperial College of Science, Technology and Medicine Mechanical Engineering Department, Dynamics Section			
DESIGNED BY	JEM, IAS	DATE	27/04/2001
DRAWN BY	I.A. SEVER	UN. TOL.	±0.1
PRO. MAN.	PROF D.J. EWINS	UNITS	mm
PRO. NAME	ADTurB II	REVISION NO	0
PART NAME	RIG CYLINDRICAL PART	SCALE	

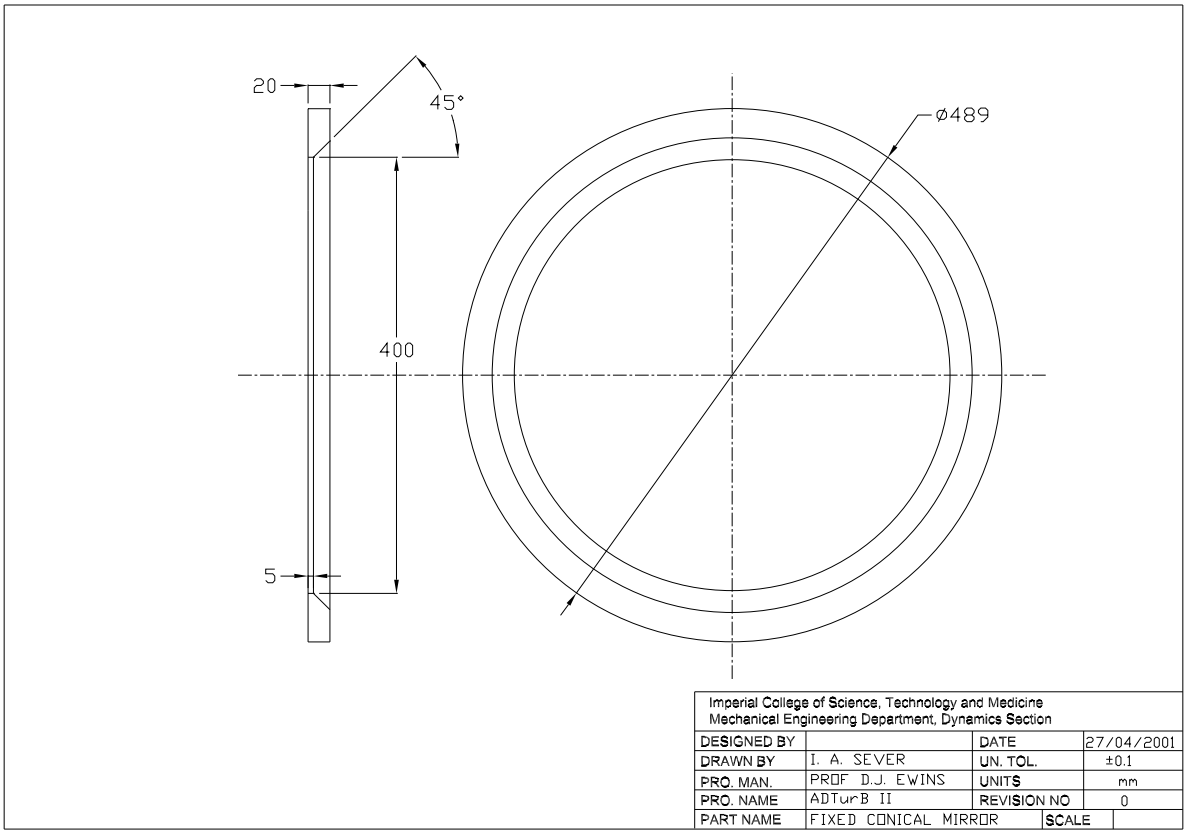

Imperial College of Science, Technology and Medicine Mechanical Engineering Department, Dynamics Section			
DESIGNED BY		DATE	27/04/2001
DRAWN BY	I. A. SEVER	UN. TOL.	±0.1
PRO. MAN.	PROF D.J. EWINS	UNITS	mm
PRO. NAME	ADTurB II	REVISION NO	0
PART NAME	FIXED CONICAL MIRROR	SCALE	

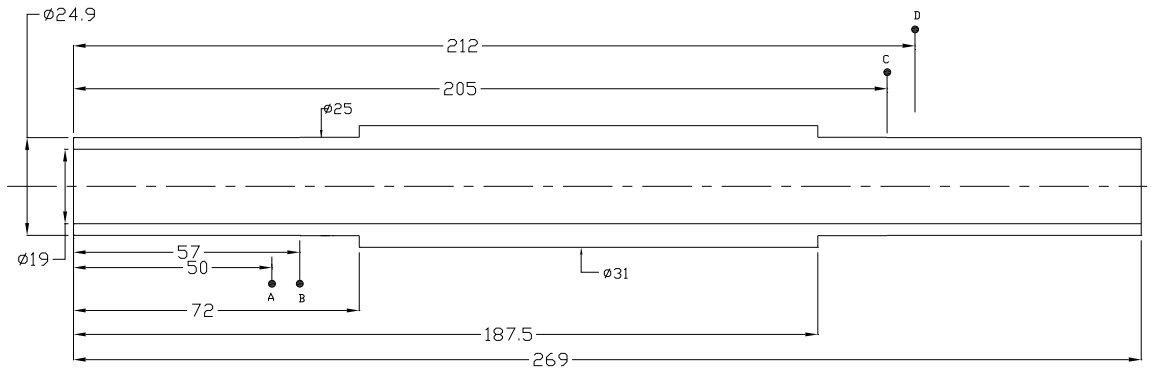

NOTE: SURFACE QUALITY FOR OUTER SURFACE OF SHAFT BETWEEN POINTS A AND B, AND BETWEEN POINTS C AND D SHOULD BE ???

Imperial College of Science, Technology and Medicine Mechanical Engineering Department, Dynamics Section			
DESIGNED BY	JEM, IAS	DATE	27/04/2001
DRAWN BY	I.A. SEVER	UN. TOL.	±0.1
PRO. MAN.	PROF D.J. EWINS	UNITS	mm
PRO. NAME	ADTurB II	REVISION NO	0
PART NAME	DRIVE SHAFT	SCALE	

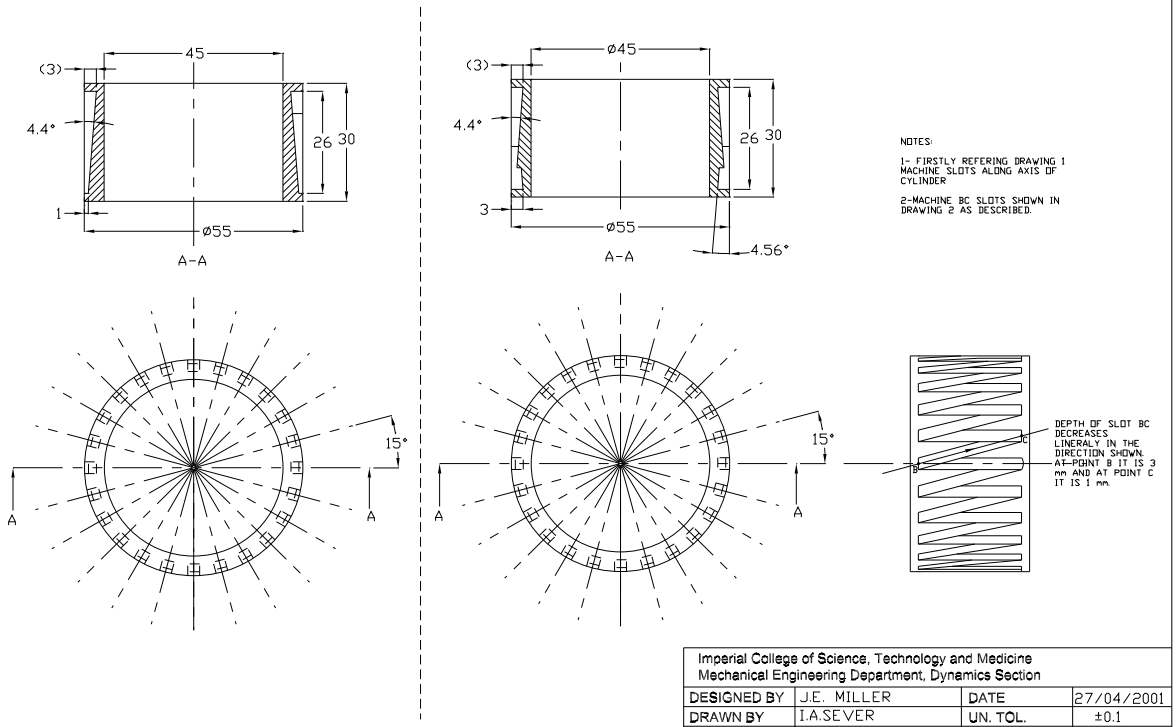

Imperial College of Science, Technology and Medicine Mechanical Engineering Department, Dynamics Section			
DESIGNED BY	J.E. MILLER	DATE	27/04/2001
DRAWN BY	I.A.SEVER	UN. TOL.	±0.1
PRO. MAN.	PROF D.J. EWINS	UNITS	mm
PRO. NAME		REVISION NO	0
PART NAME	INDEXING DRUM	SCALE	

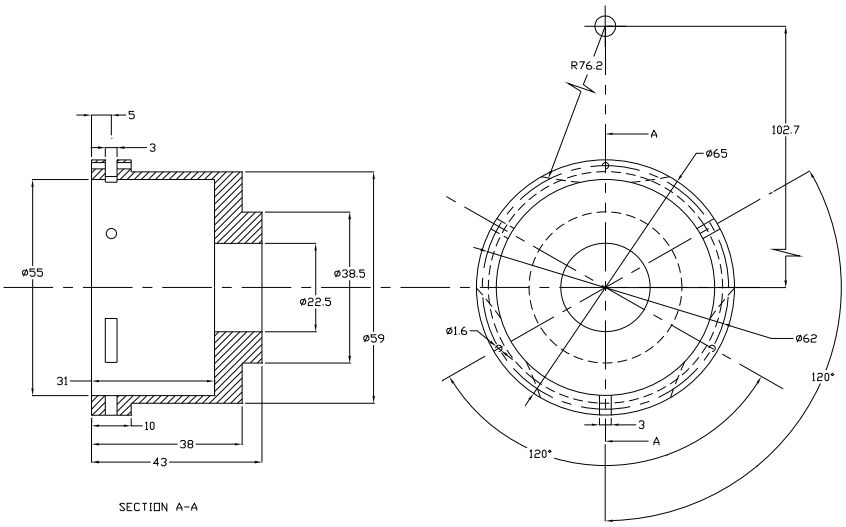

Imperial College of Science, Technology and Medicine Mechanical Engineering Department, Dynamics Section			
DESIGNED BY	J.E. MILLER	DATE	27/04/2001
DRAWN BY	I.A. SEVER	UN. TOL.	±0.1
PRO. MAN.	PROF D.J. EWINS	UNITS	mm
PRO. NAME	ADTurB II	REVISION NO	0
PART NAME	INDEXING CAB	SCALE	

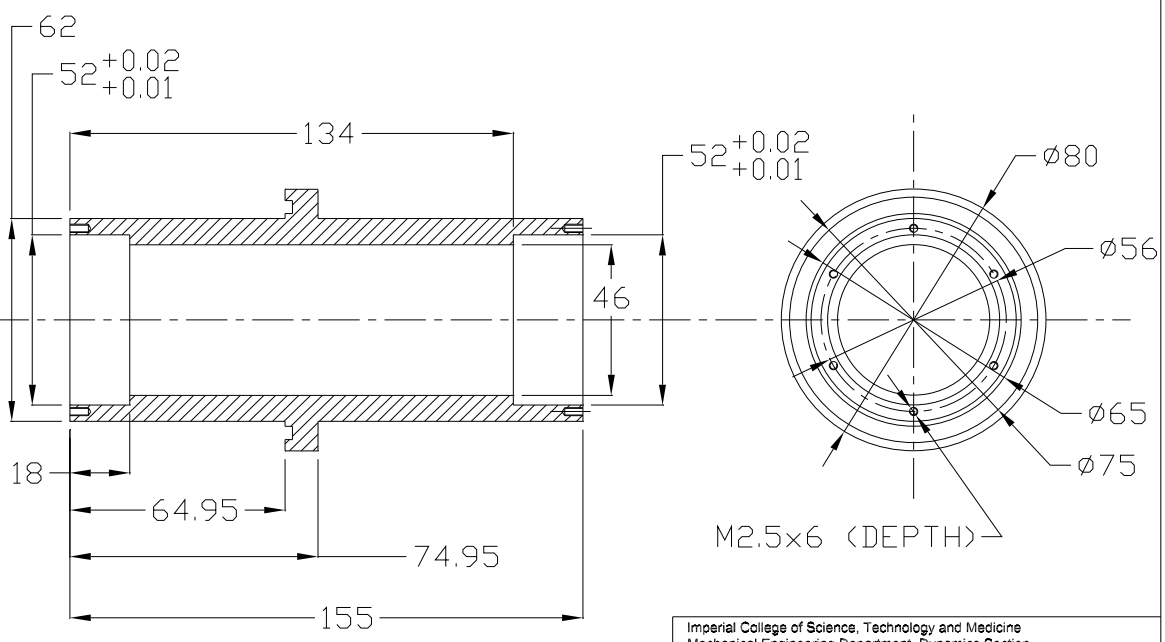

Imperial College of Science, Technology and Medicine Mechanical Engineering Department, Dynamics Section			
DESIGNED BY	JEM, IAS	DATE	27/04/2001
DRAWN BY	I.A. SEVER	UN. TOL.	±0.1
PRO. MAN.	PROF D.J. EWINS	UNITS	mm
PRO. NAME	ADTurB II	REVISION NO	0
PART NAME	BEARING HOUSING	SCALE	

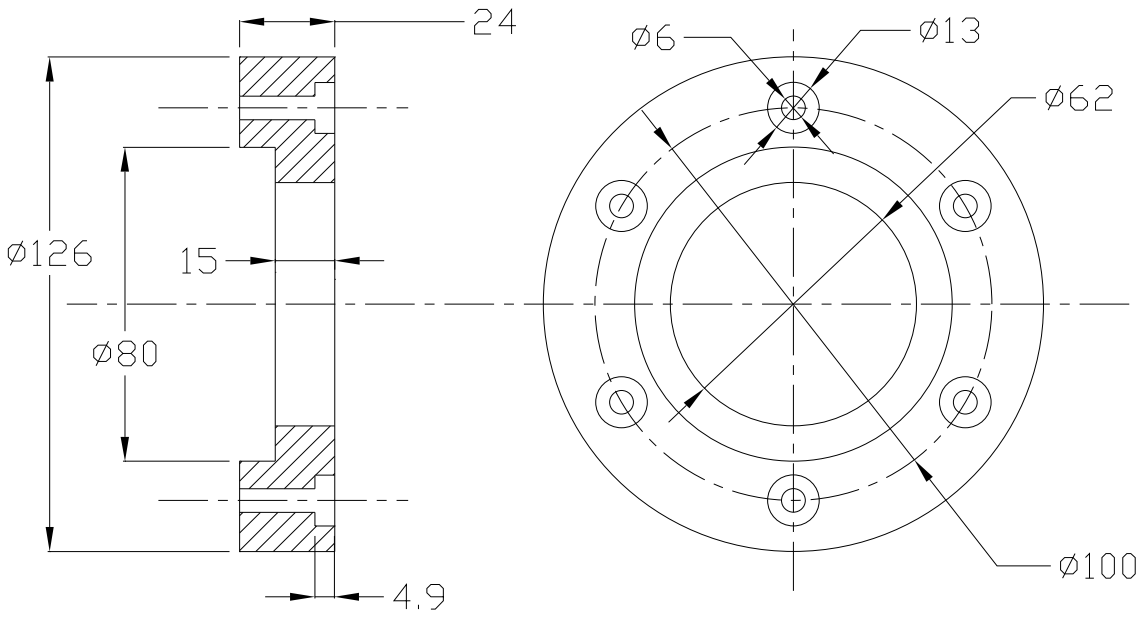

Imperial College of Science, Technology and Medicine Mechanical Engineering Department, Dynamics Section			
DESIGNED BY	JEM, IAS	DATE	27/04/2001
DRAWN BY	I.A. SEVER	UN. TOL.	±0.1
PRO. MAN.	PROF D.J. EWINS	UNITS	mm
PRO. NAME	ADTurB II	REVISION NO	0
PART NAME	MOUNTING RING	SCALE	

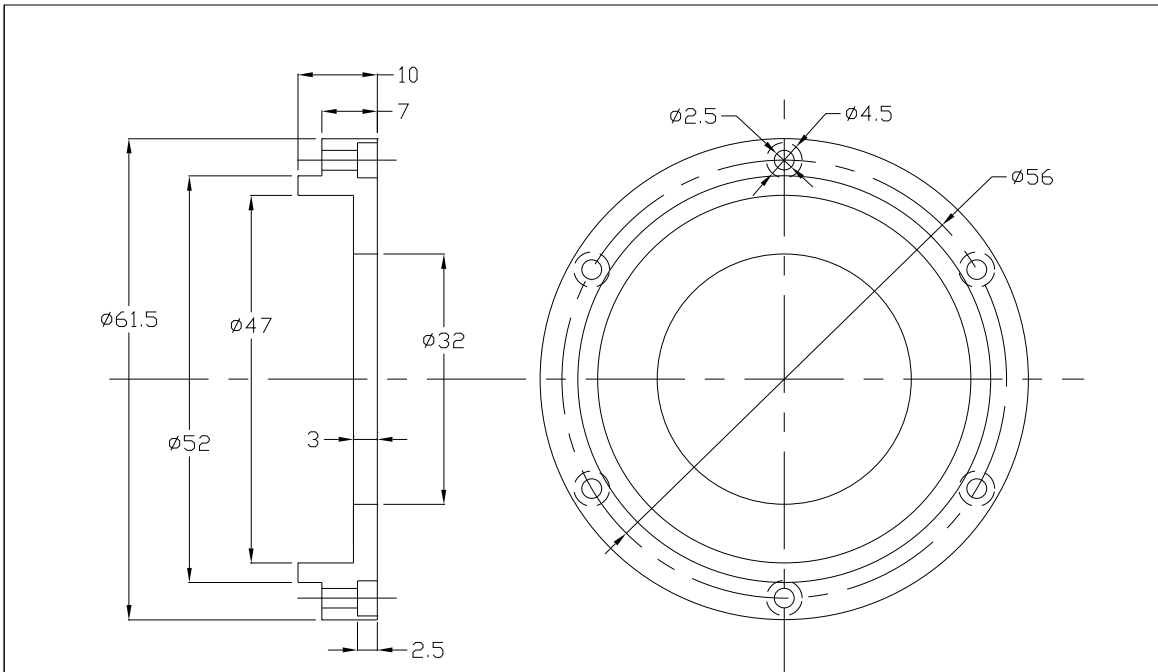

Imperial College of Science, Technology and Medicine Mechanical Engineering Department, Dynamics Section			
DESIGNED BY	JEM, IAS	DATE	27/04/2001
DRAWN BY	I.A. SEVER	UN. TOL.	±0.1
PRO. MAN.	PROF D.J. EWINS	UNITS	mm
PRO. NAME	ADTurB II	REVISION NO	0
PART NAME	RIGHT MOUNTING RING	SCALE	

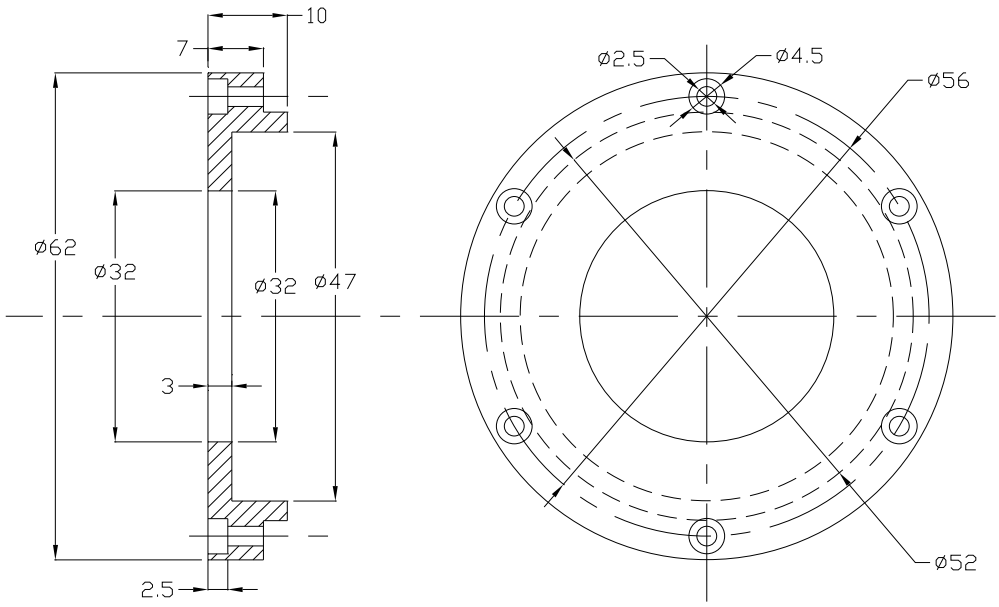

Imperial College of Science, Technology and Medicine Mechanical Engineering Department, Dynamics Section			
DESIGNED BY	JEM, IAS	DATE	27/04/2001
DRAWN BY	I.A.SEVER	UN. TOL.	±0.1
PRO. MAN.	PROF D.J. EWINS	UNITS	mm
PRO. NAME	ADTurB II	REVISION NO	0
PART NAME	LEFT MOUNTING RING	SCALE	

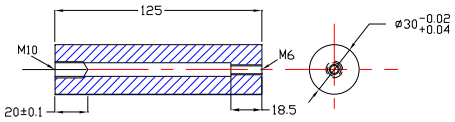

REACTION BLOCK MAGNET/FORCE GAUGE HOLDER
MATERIAL BRASS ONE OFF

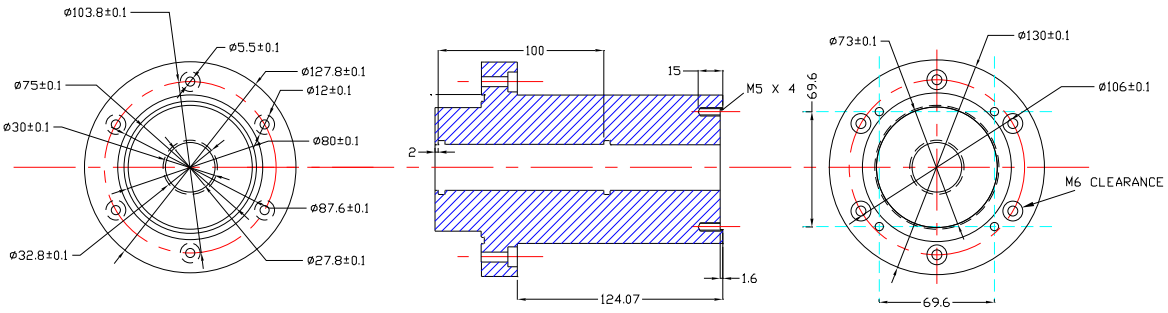

REACTION BLOCK HOLDER.
MATERIAL ALUMINIUM ONE OFF

Imperial College of Science, Technology and Medicine Mechanical Engineering Department, Dynamics Section			
DESIGNED BY	JEM, IAS	DATE	27/04/2002
DRAWN BY	I.A. SEVER	UN. TOL.	±0.1
PRO. MAN.	PROF D.J. EWINS	UNITS	mm
PRO. NAME	ADTurB II	REVISION NO	0
PART NAME	MAGNET HOLDING PARTS	SCALE	

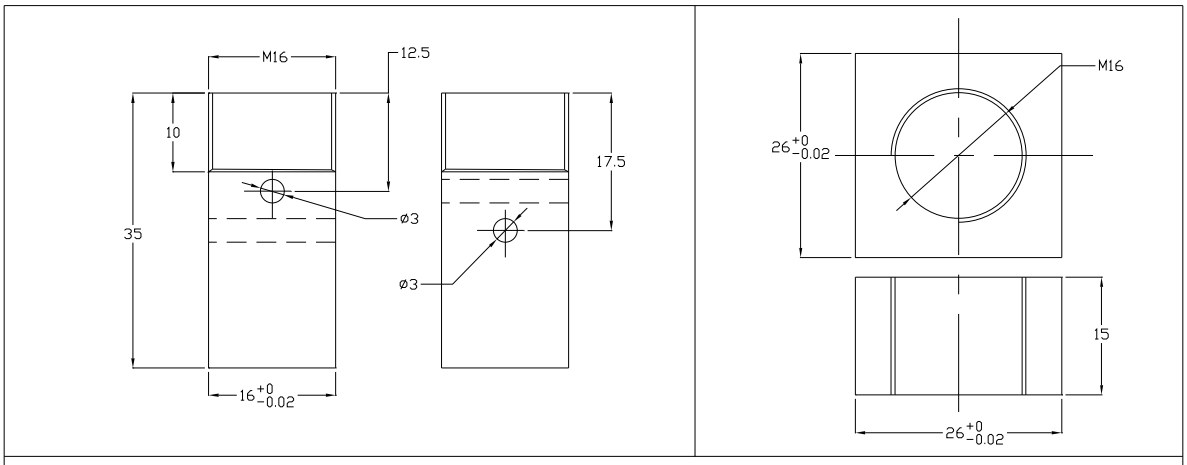

Imperial College of Science, Technology and Medicine Mechanical Engineering Department, Dynamics Section			
DESIGNED BY	JEM	DATE	27/04/2001
DRAWN BY	I.A.SEVER	UN. TOL.	±0.1
PRO. MAN.	PROF D.J. EWINS	UNITS	mm
PRO. NAME	ADTurB II	REVISION NO	0
PART NAME	MIRROR ADJUSTMENT PARTS	SCALE	

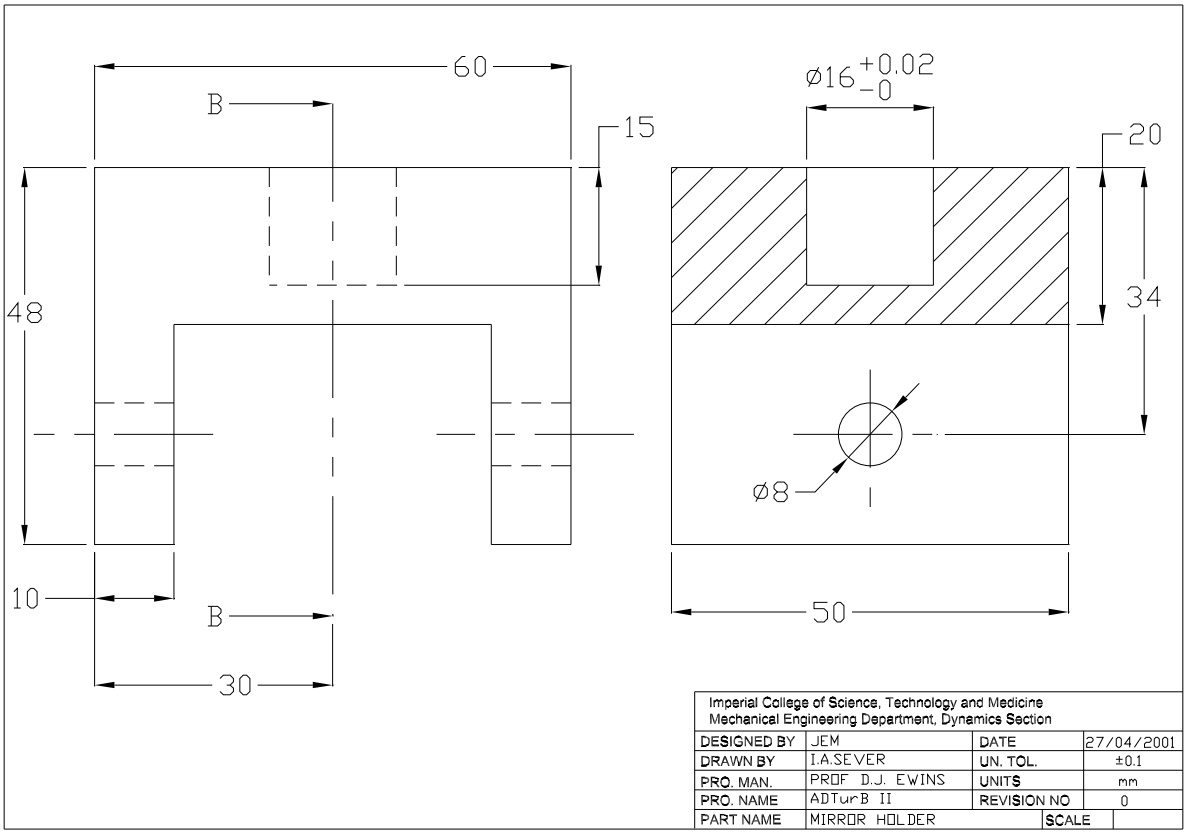

Imperial College of Science, Technology and Medicine Mechanical Engineering Department, Dynamics Section			
DESIGNED BY	JEM	DATE	27/04/2001
DRAWN BY	I.A.SEVER	UN. TOL.	±0.1
PRO. MAN.	PROF D.J. EWINS	UNITS	mm
PRO. NAME	ADTurB II	REVISION NO	0
PART NAME	MIRROR HOLDER	SCALE	

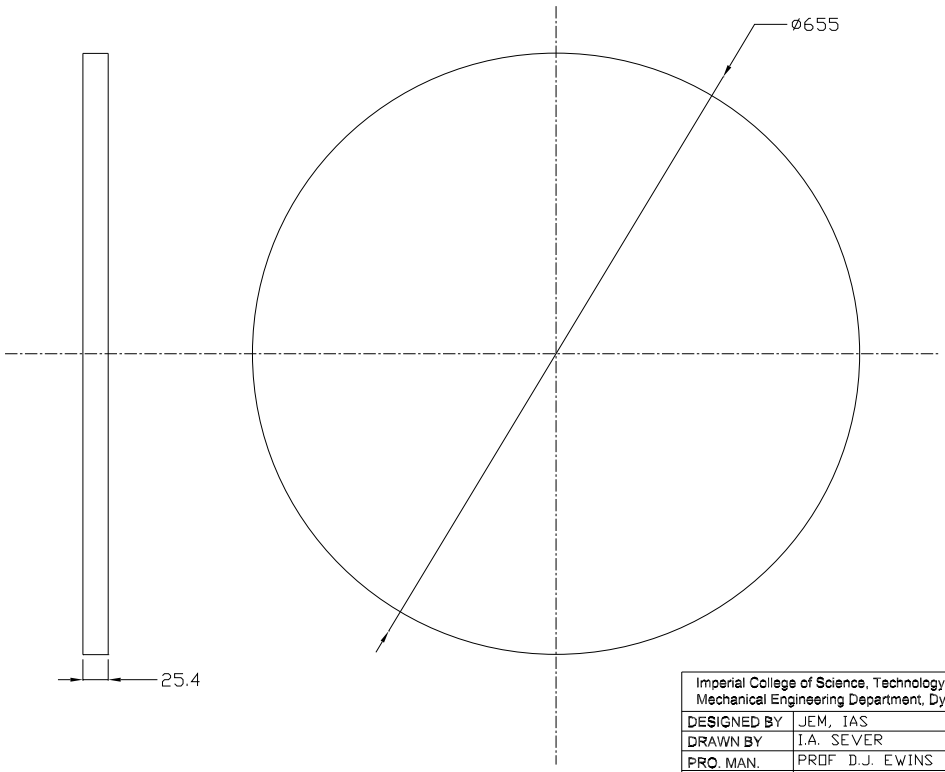

Imperial College of Science, Technology and Medicine Mechanical Engineering Department, Dynamics Section			
DESIGNED BY	JEM, IAS	DATE	27/04/2001
DRAWN BY	I.A. SEVER	UN. TOL.	±0.1
PRO. MAN.	PROF D.J. EWINS	UNITS	mm
PRO. NAME	ADTurB II	REVISION NO	0
PART NAME	FRONT POLYCARBONATE COVER	SCALE	

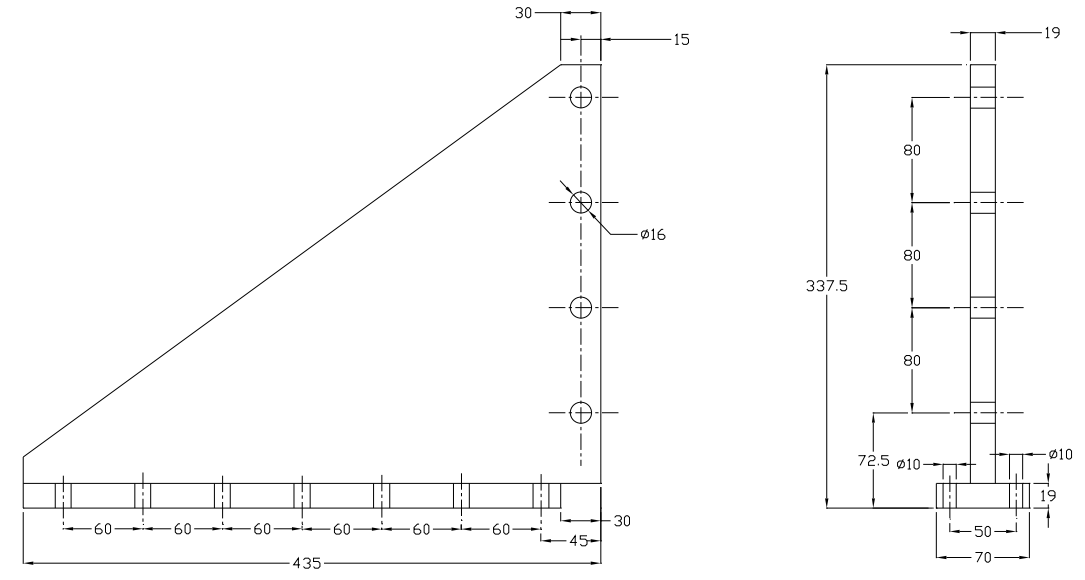

Imperial College of Science, Technology and Medicine Mechanical Engineering Department, Dynamics Section			
DESIGNED BY	JEM, IAS	DATE	27/04/2001
DRAWN BY	I.A. SEVER	UN. TOL.	±0.1
PRO. MAN.	PROF D.J. EWINS	UNITS	mm
PRO. NAME	ADTurB II	REVISION NO	0
PART NAME	RIG SUPPORT	SCALE	

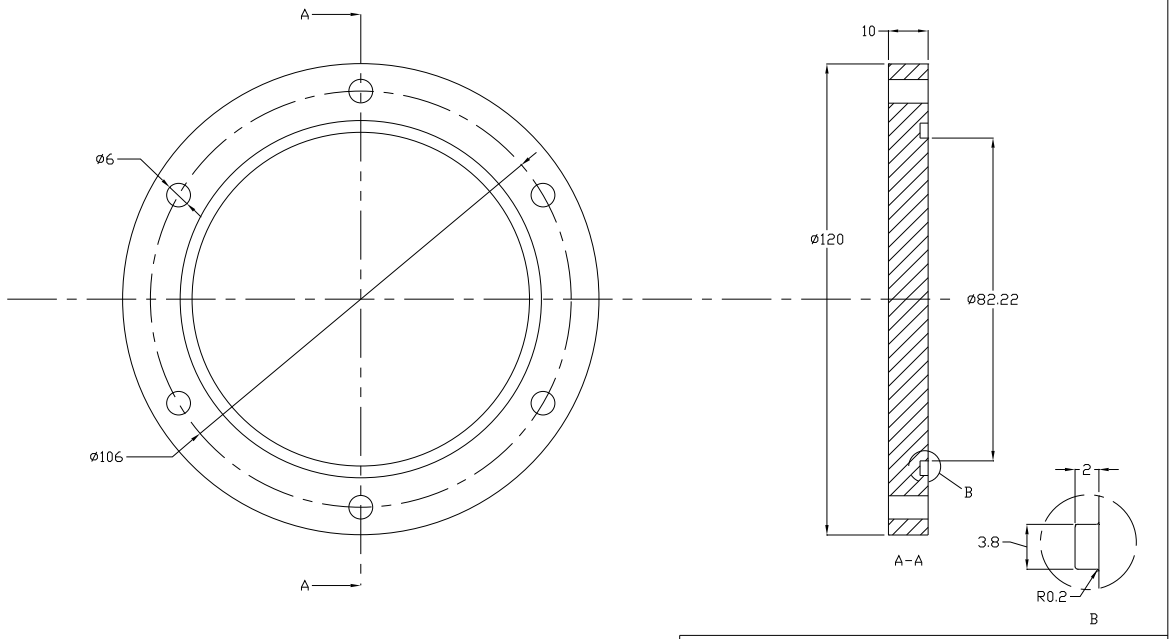

(5 OFF)

Imperial College of Science, Technology and Medicine Mechanical Engineering Department, Dynamics Section			
DESIGNED BY	JEM, IAS	DATE	27/04/2001
DRAWN BY	I.A. SEVER	UN. TOL.	±0.1
PRO. MAN.	PROF D.J. EWINS	UNITS	mm
PRO. NAME	ADTurB II	REVISION NO	0
PART NAME	MAGNET HOLE LID	SCALE	

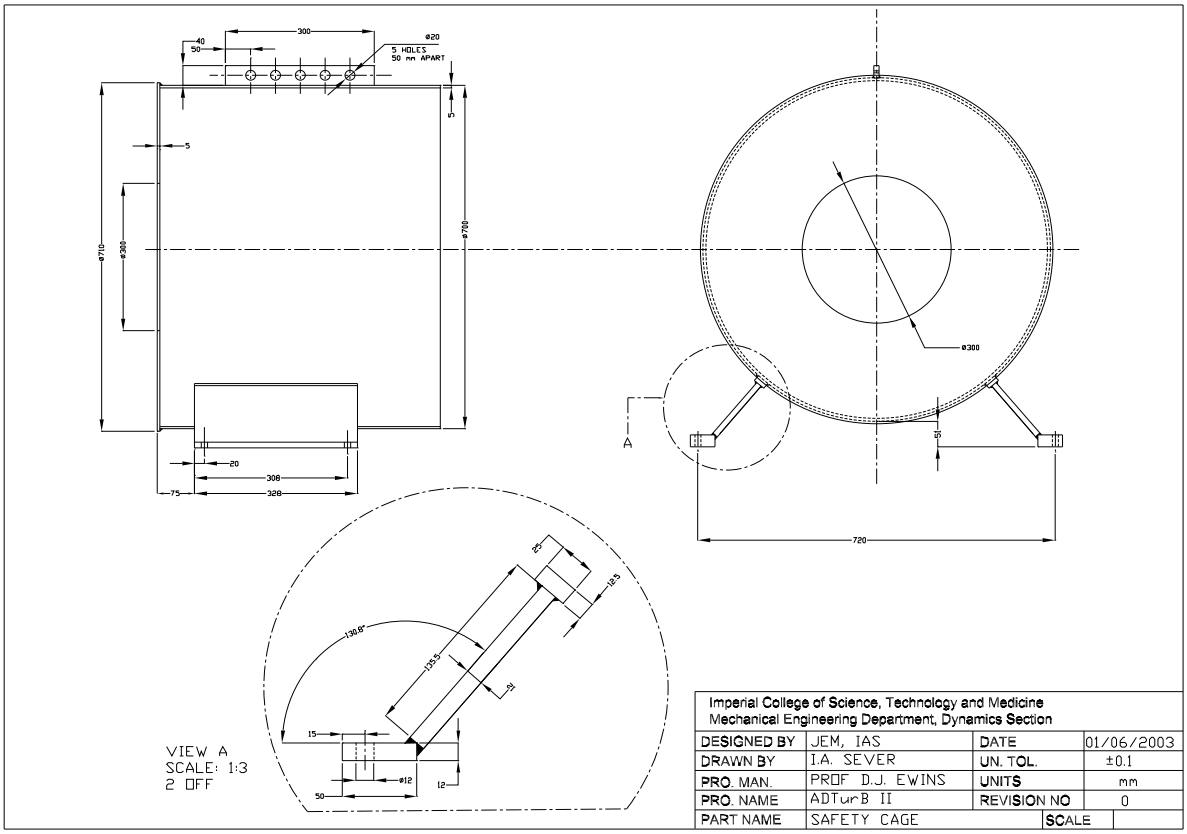

Imperial College of Science, Technology and Medicine Mechanical Engineering Department, Dynamics Section			
DESIGNED BY	JEM, IAS	DATE	01/06/2003
DRAWN BY	I.A. SEVER	UN. TOL.	±0.1
PRO. MAN.	PROF D.J. EWINS	UNITS	mm
PRO. NAME	ADTurB II	REVISION NO	0
PART NAME	SAFETY CAGE	SCALE	

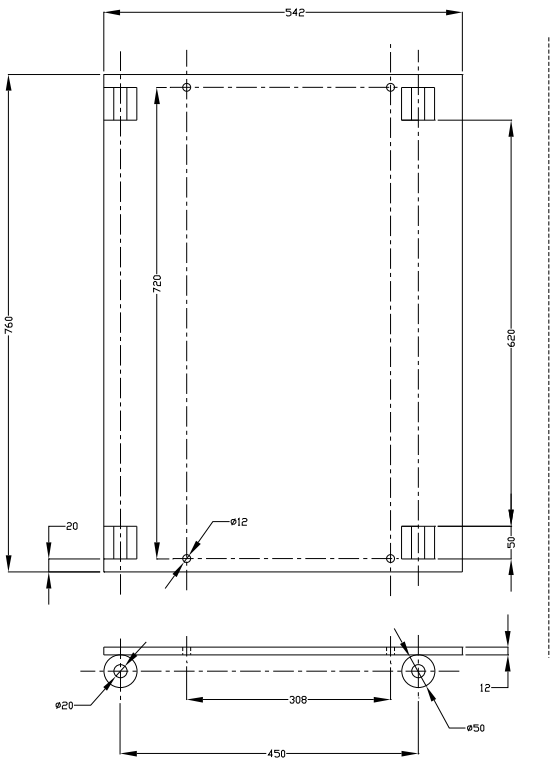

Imperial College of Science, Technology and Medicine Mechanical Engineering Department, Dynamics Section			
DESIGNED BY	JEM, IAS	DATE	01/06/2003
DRAWN BY	I.A. SEVER	UN. TOL.	±0.1
PRO. MAN.	PROF D.J. EWINS	UNITS	mm
PRO. NAME	ADTurB II	REVISION NO	0
PART NAME	SAFETY CAGE PARTS - 1	SCALE	

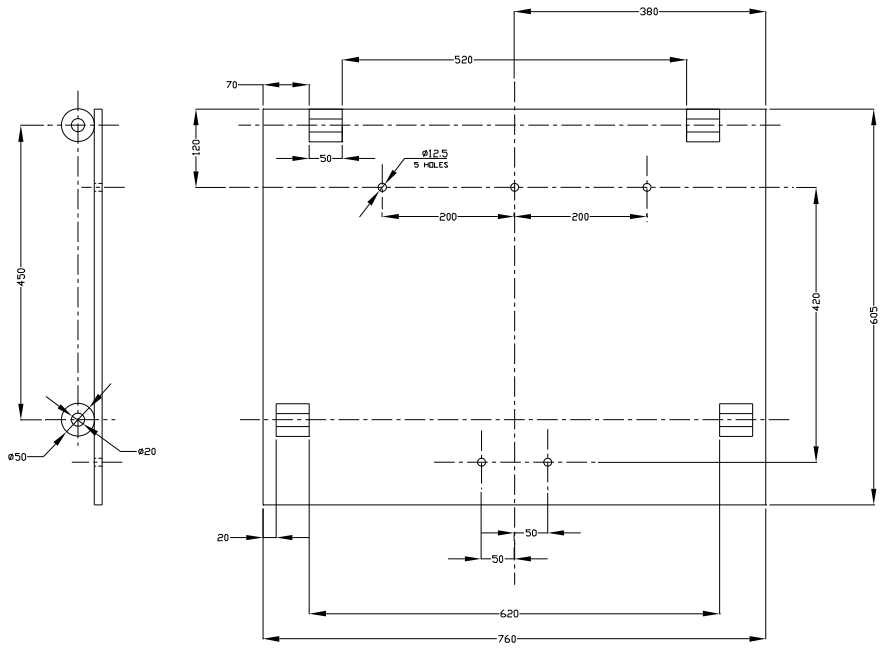

Imperial College of Science, Technology and Medicine Mechanical Engineering Department, Dynamics Section			
DESIGNED BY	JEM, IAS	DATE	01/06/2003
DRAWN BY	I.A. SEVER	UN. TOL.	±0.1
PRO. MAN.	PROF D.J. EWINS	UNITS	mm
PRO. NAME	ADTurB II	REVISION NO	0
PART NAME	SAFETY CAGE PARTS - 2	SCALE	

A.2 Blisk drawings

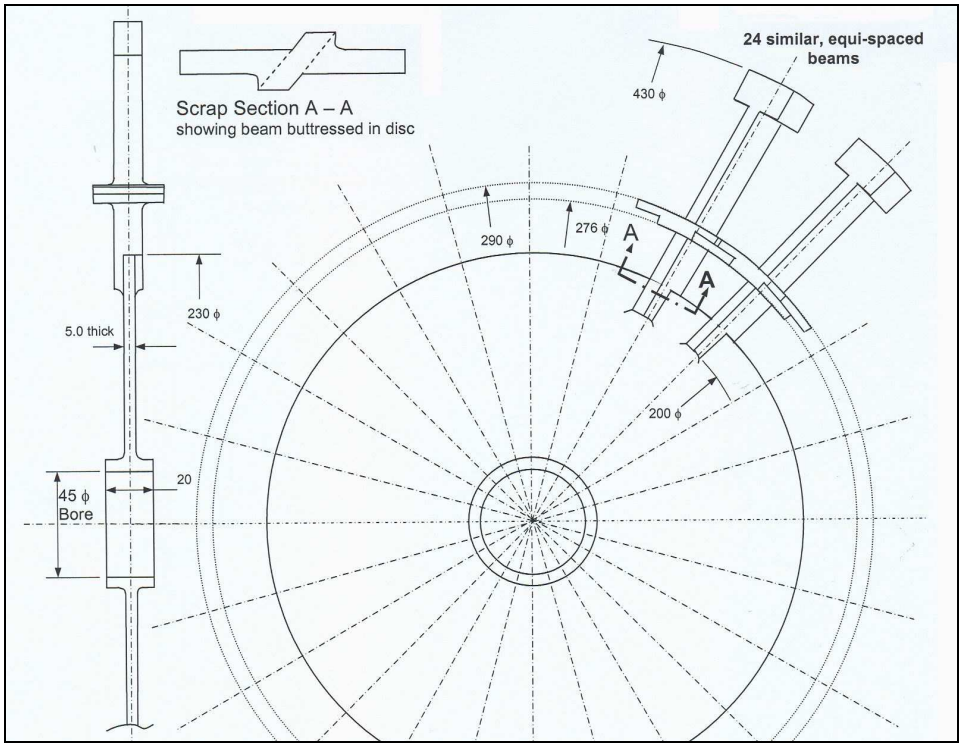

Blisk-1 - 1/2

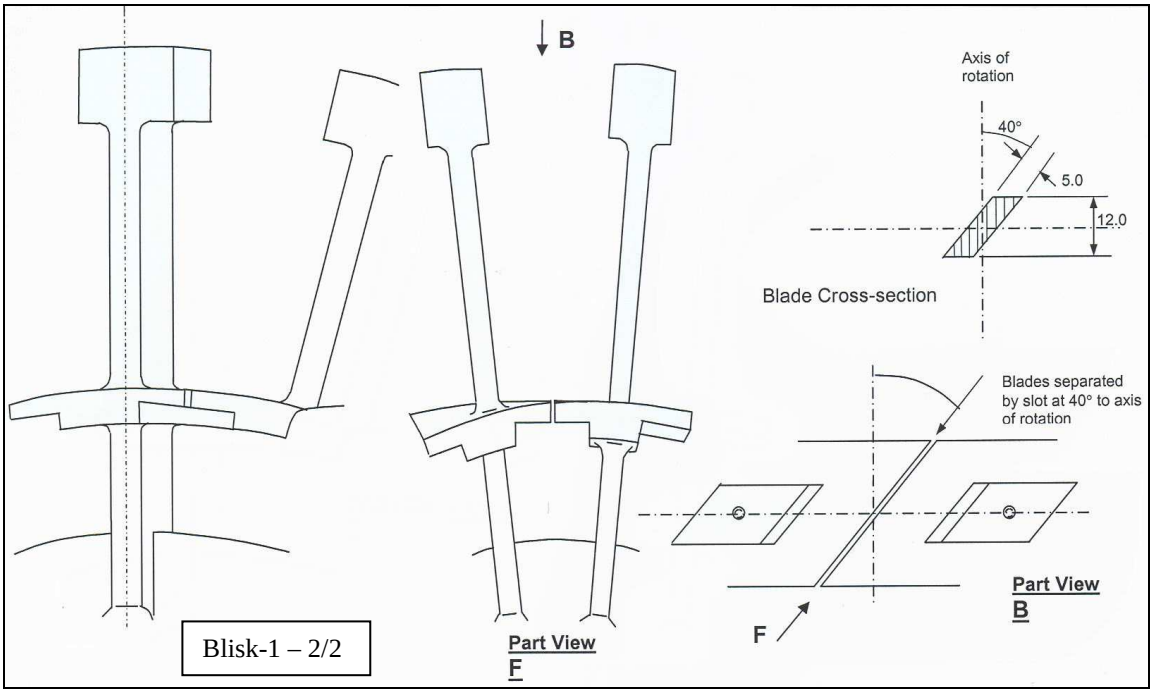

Blisk-1 – 2/2

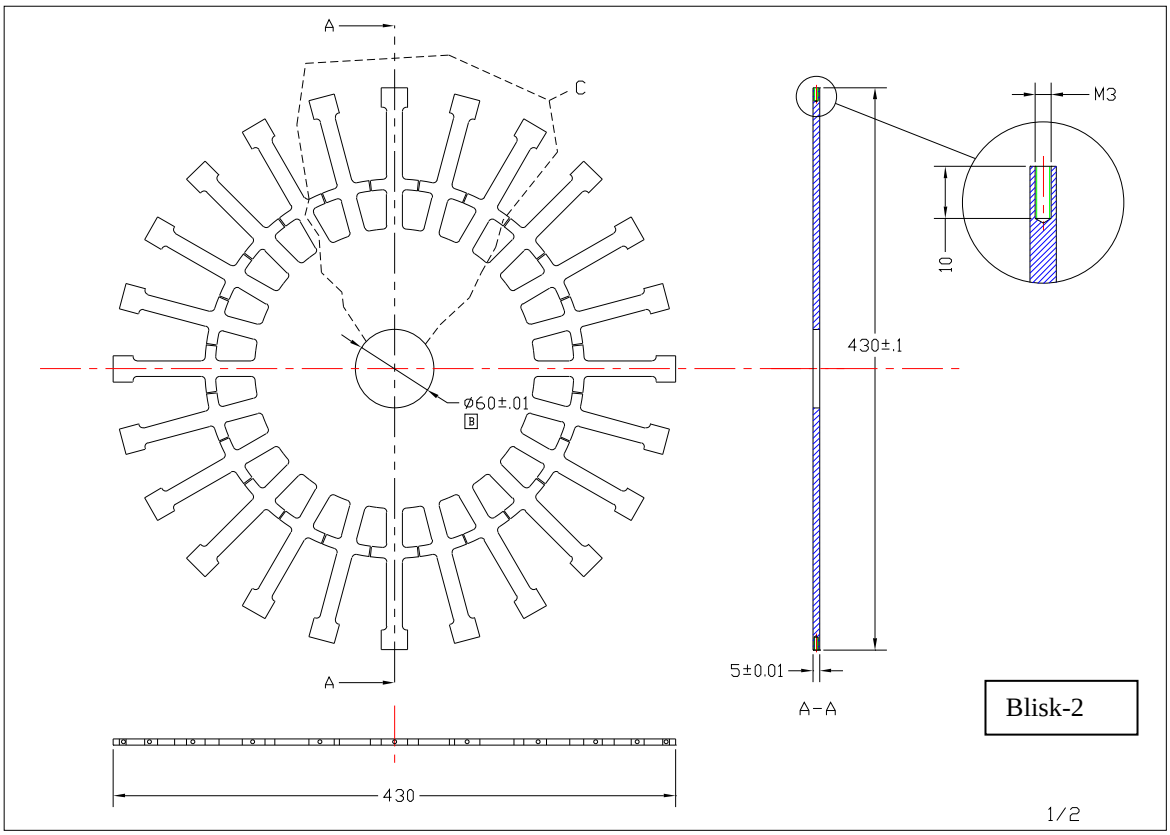
A
C
M3
10
430±.1
ø60±.01
B
A
5±0.01
A-A
430
Blisk-2
1/2

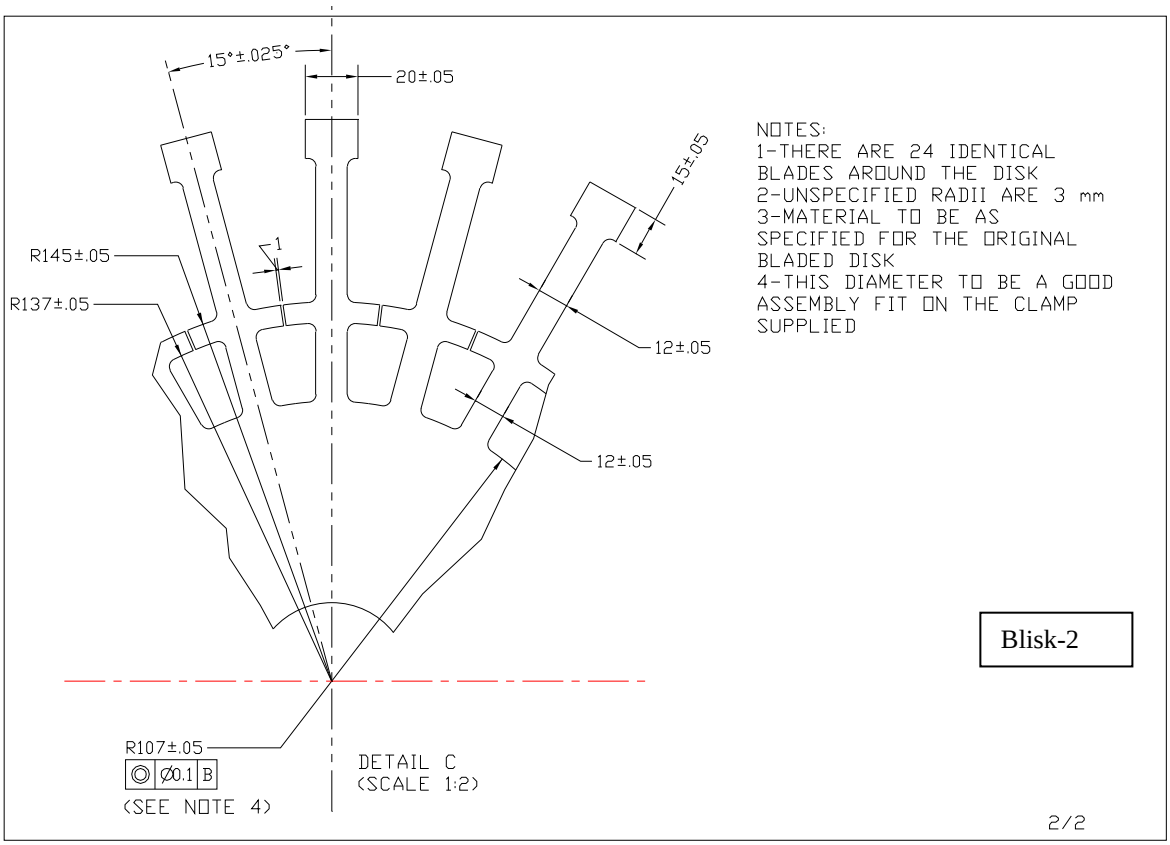
15°±.025°
20±.05
15±.05
R145±.05
R137±.05
1
12±.05
12±.05
R107±.05
⌀0.1 B
(SEE NOTE 4)
DETAIL C
(SCALE 1:2)
NOTES:
1-THERE ARE 24 IDENTICAL BLADES AROUND THE DISK
2-UNSPECIFIED RADII ARE 3 mm
3-MATERIAL TO BE AS SPECIFIED FOR THE ORIGINAL BLADED DISK
4-THIS DIAMETER TO BE A GOOD ASSEMBLY FIT ON THE CLAMP SUPPLIED
Blisk-2
2/2

A.3 Damper drawings

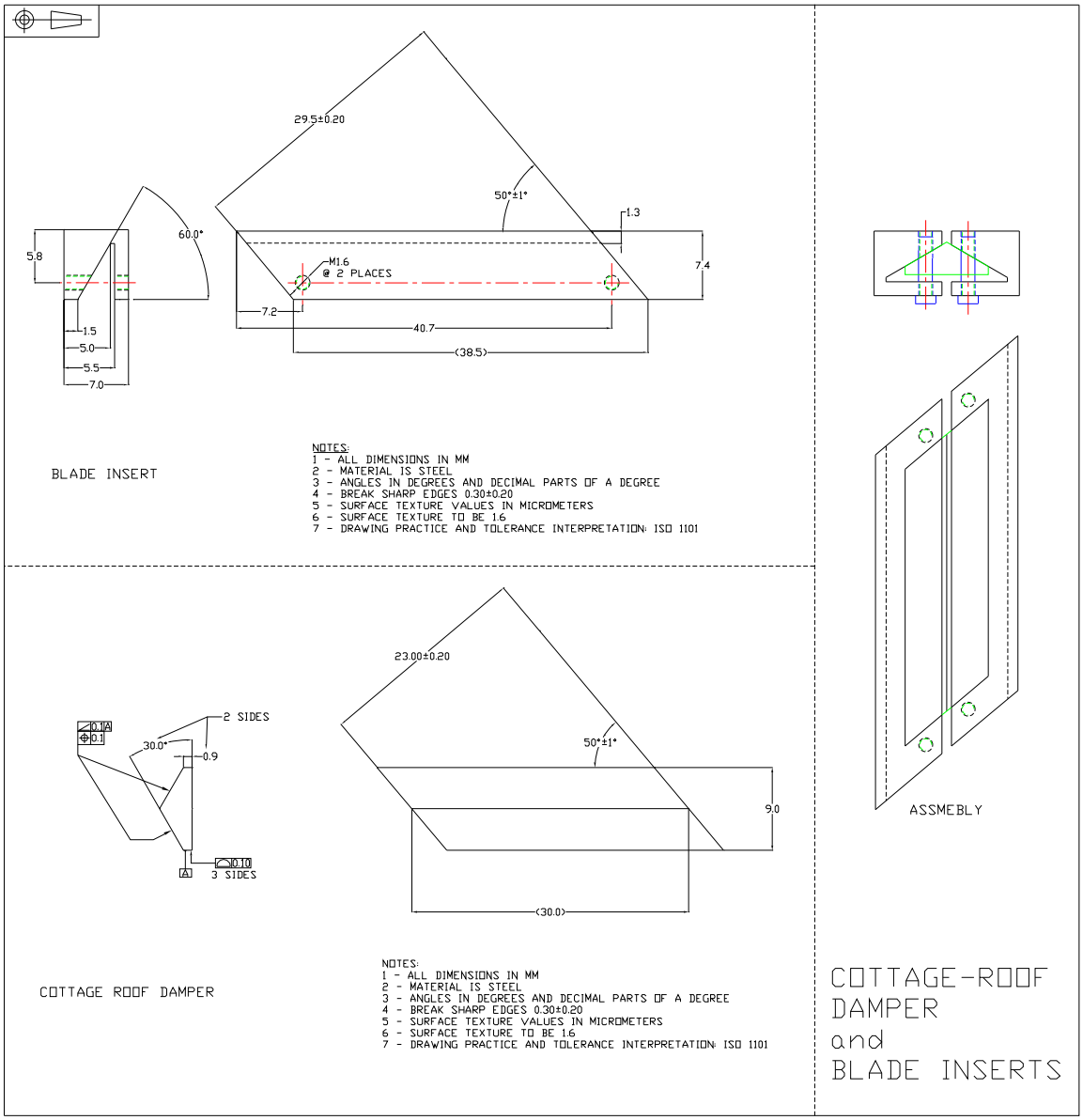

APPENDIX B

DATA ACQUISITION SOFTWARE

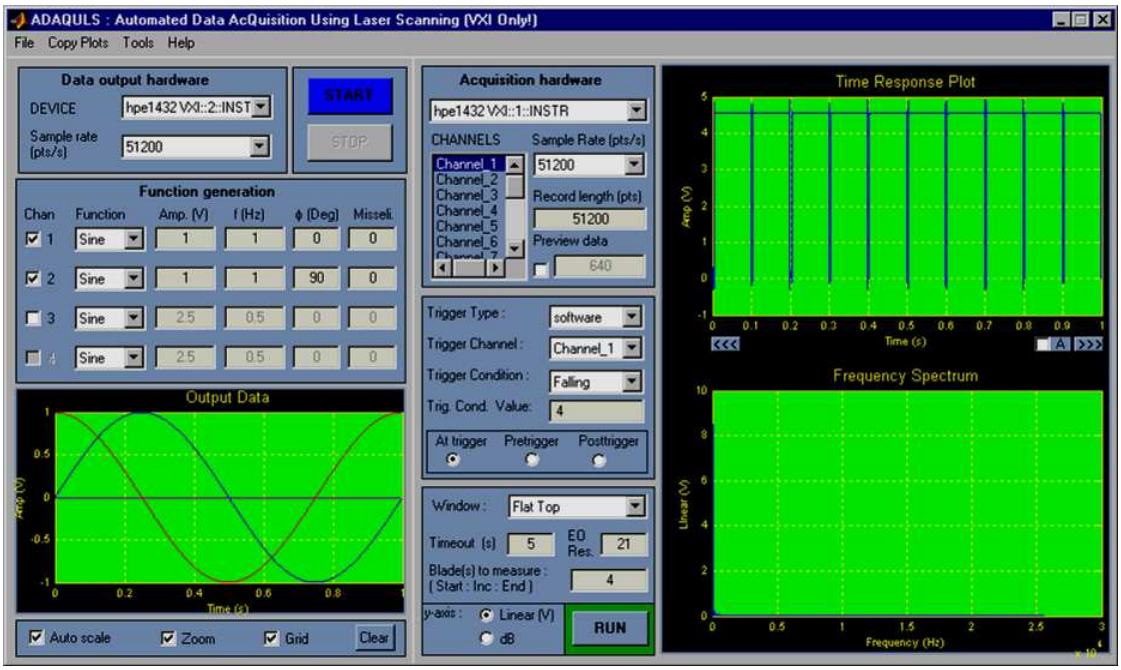

Figure B.1 The main panel of the DAQ software

The main DAQ panel of the program shown in Fig B-1 is launched from within MATLAB. Conversion of this program into a stand-alone application has not been possible as MATLAB does not allow its objects to be compiled (e.g., DAQ Toolbox objects). When launched, the program first seeks for the available DAQ boards installed on the computer. At the time of writing most of the NI cards, Computer Board cards, HP1332-4 VXI frame and Win based sound cards are recognised and can be used. Two versions of the program are available. The first one is intended to be solely used with HP VXI frame (Figure B.1 shows this version) and the other is used for all other mentioned boards. Once the boards are loaded, the user is expected to select the desired output and input cards from the pull-down menus provided. In the version shown the number of output channels is limited to 4 and the number of input channels to 16. Using the options provided the desired functions can be generated and output. A sample of these outputs will be plotted in the window below input channel section for inspection. The following are expected from the user: sampling rate, record length, input and output channels and trigger settings (channel, level, sign, etc.). Additionally if online data processing is to be carried out, window to be used and the EO excitation response to be calculated should be provided. If more than 1 blade is measured, the range of blade numbers should also be given in the corresponding input box. A "preview" option is provided (see Figure B-1) such that when selected and the "Run" button is clicked, acts as an oscilloscope and plots the streamed data in the upper right plot window. During normal run, the time data is again plotted in this window and frequency response is given in the bottom right one. For single shot measurement

individual channels can be observed separately by using direction buttons under the top-right plot window and can be copied to separate Matlab Figures using "Copy Plot" menu for further editing. For measurements performed for a range of speed values, a progress bar is displayed, as shown on the right. Via this bar the remaining measurement time, rotor speed, blade currently being measured etc. can be observed.

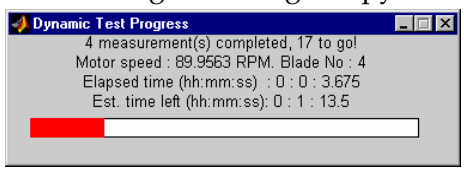

There are a number of tools provided under the "Tools" menu. These are: Motor Control, ODS, Band-Pass filter, Magnet Position tools and Preference setting window.

Motor Control Tool:

The user interface of the Motor Control Tool (MCT) is given on the right. Two test types, static and dynamic are available. When "static" option is selected the main panel does not expect any input from the MCT and all the fields seen in panel are disabled. With the selection of "Dynamic" option they are made available. When the "Run/STOP" pushbutton is clicked it initiates the communication with the motor when in "Run" state and shuts the motor down when in "STOP" state. With the use of MCT; Speed, Torque and Peak Torque can be set. The "Parameters" section is provided for speed settings via which a constant value or a range of values can be entered. When a range is entered and the EO-ND crossing speed of interest is known, providing this value in the "Crossing speed" and selecting "Cluster" option clusters the speed values around this value resulting in a more efficient test session. Settings are transferred to the main panel upon clicking the "Apply" button.

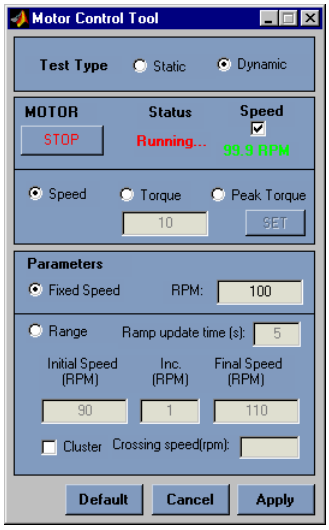

Magnet Position Tool

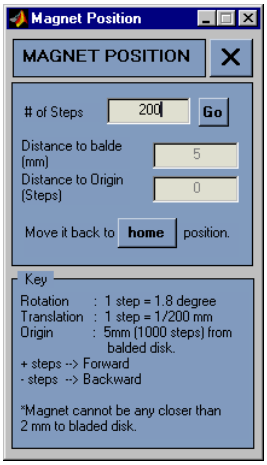

Via the Magnet Position tool shown on the left, the proximity of the magnet to the bladed disk can be adjusted. For a measurement session spanning a range of speed values, it is used internally if activated. It simply transmits the user specified "step" (i.e. distance) information through an RS232 cable to the stepper motor. "Home" is a user defined safe position for the magnet to be retracted in case of failure. Minimum distance allowed to the test piece is 2.5 mm.

ODS Tool:

The ODS tool shown on the right provides easy and quick ODS recovery and visualisation opportunity on site. Three ODS options are provided for scans of type: circular, area and line. Upon selection of a choice, the relevant input boxes are made available and the others are disabled. The excitation frequency is directly taken from the motor speed reading, however this value can be fine

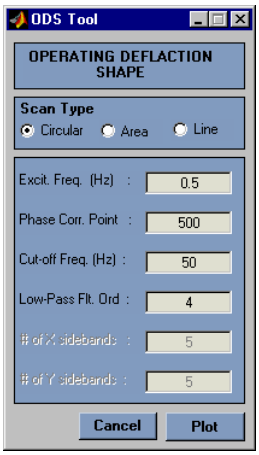

tuned if necessary. Upon the clicking on the Plot button, the recovered ODS is plotted on the lower right plot window on the main panel.

Band pass filter design

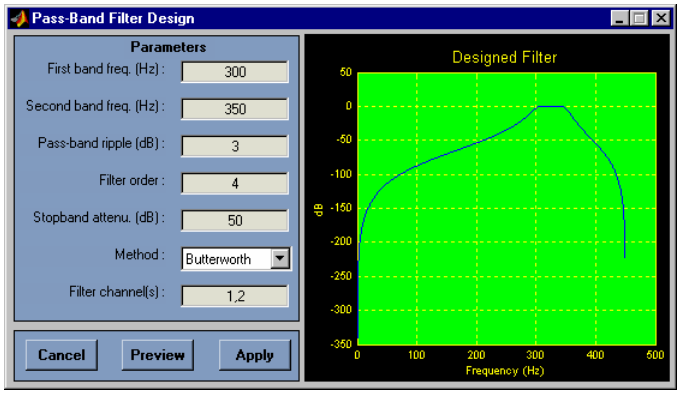

This panel provides the user with an easy and convenient way of preparing band-pass filters to be used in online EO response extraction. The filter can be applied to any number of channels and previewed before passed onto the main panel. There are a range of filters provided in the Method pull-down menu.

Preferences panel

This panel is mainly intended for variable speed measurement session settings, however channel properties such as coupling and voltage range can also be set. Using the check boxes given in the upper part, the user can indicate which data to be saved. The storage matrices for unchecked parameters are not created and therefore more memory is made available. Time settings are very important in assuring the quality of the data and are structure dependent. For a very lightly damped system, one needs to provide a long enough pause between each successive speed change to make sure the steady state vibrations are reached.